Molecular Modeling and Simulation of Real Fluids for Applications in Process Engineering

zur Erlangung des akademischen Grades eines
DOKTORS DER INGENIEURWISSENSCHAFTEN (Dr.-Ing.)
der Fakultät für Maschinenbau
der Universität Paderborn

genehmigte
DISSERTATION

von

Yow-lin Huang

aus Kaohsiung, Taiwan

Tag des Kolloquiums: 16. Dezember 2010
Referent: Prof. Dr.-Ing. habil. Jadran Vrabec
Korreferent: Prof. Dr.-Ing. Hans Hasse

Preface

This thesis is based on my work at the Institute of Thermodynamics and Thermal Process Engineering, University of Stuttgart as well as at the Chair of Thermodynamics and Energy Technology, University of Paderborn under the supervision of Prof. Dr.-Ing. Jadran Vrabec and Prof. Dr.-Ing. Hans Hasse. Without their support, this thesis would have never come into being. They and my coworkers brought me not only support but also the best working environment.

The majority of this work is part of the project Transferbereich 66 "Molekulare Modellierung und Simulation zur Vorhersage von Stoffdaten für industrielle Anwendungen" funded by Deutsche Forschungsgemeinschaft (DFG) in cooperation with BASF SE, Ludwigshafen.

The presented research was conducted under the auspices of the Boltzmann-Zuse Society of Computational Molecular Engineering (BZS), and the simulations were performed at the High Performance Computing Center Stuttgart (HLRS) and at the Steinbuch Centre for Computing, Karlsruhe.

My colleagues both in Stuttgart and Paderborn gave me an unforgettable and excellent time during this work.

If this work is worthy of something, then this honor should be given to my God, Christ Jesus and my Parents in Taiwan as well as my dearest wife, Aichen.

The last but not the least, I like to thank Jadran again. He is not only the best boss but also the best friend.

給我最摯愛的妻子，愛真
並
願主耶穌基督的恩、神的愛、
聖靈的交通，與你們眾人同在

Heidelberg, July 2010

Isaiah Huang

Abstract

The first part of this work is on molecular modeling and simulation of 12 industrially relevant pure fluids as well as 12 binary mixtures of these components. Their economical importance and hazardous nature is a strong incentive for computer simulations. The investigation of these substances is separated into two groups. The Phosgene group includes Hydrogen chloride, Phosgene, Benzene, Chlorobenzene, Ortho-Dichlorobenzene and Toluene. The Ethylene oxide group contains Ethylene oxide, Ethylene glycol and Water. The underlying force fields for these 12 pure substances are developed in this work on the basis of quantum chemical information on molecular geometry and electrostatics. The molecular models are individually optimized to experimental pure fluid data for vapor pressure and saturated liquid density. A comparison to other molecular models from the literature is given. The unlike dispersive interaction is optimized for ten of the 12 studied binary mixtures. Previously unpublished experimental VLE data, measured by BASF in the vicinity of ambient temperature, are predominantly used for these fits. VLE data, including dew point composition, saturated densities and enthalpy of vaporization, are predicted for a wide range of temperatures and compositions. The predictions are compared to additional experimental binary VLE data that was not considered in the model development. The good agreement shows the reliability of the molecular approach for predicting thermophysical properties of hazardous fluid mixtures.

In the second part of this work, by assessing a large number of binary systems, it is shown on a large scale that molecular modeling is a reliable and robust route to VLE of mixtures. A set of simple molecular models for 78 pure substances from the literature is taken to systematically describe all 366 binary and ternary mixtures of these components for which relevant experimental VLE data are available. Among them, 267 binary mixtures and 33 ternary mixtures were investigated with respect to VLE data at finite mole fractions and 95 binary mixtures with respect to the Henry's law constant. The mixture models are based on the modified Lorentz-Berthelot combining rule. Per binary system, one state independent interaction parameter from the unlike dispersive energy is adjusted to a single experimental vapor pressure or a Henry's law constant. The mixture models are validated regarding the vapor pressure at other state points and also regarding the dew point composition, which is a fully predictive property in this work. Subsequently, these binary interaction parameters are applied for ternary mixtures without any further adjustment. The predictions from the molecular models of the 366 mixtures are extensively compared to available experimental data. In almost all cases, the the molecular models give excellent predictions of the mixture properties.

The following publications contribute to the present work:

Vrabec J., Huang Y. L. and Hasse H.,
"Molecular models for 267 binary mixtures validated by vapor-liquid equilibr.: A systematic approach",
Fluid Phase Equilib. **279**, 120-135 (2009).

Huang Y. L., Vrabec J. and Hasse H.,
"Prediction of ternary vapor-liquid equilibria for 33 systems by molecular simulation",
Fluid Phase Equilib. **287**, 62-69 (2009).

Huang Y. L., Miroshnichenko S., Hasse H. and Vrabec J.,
"Henrys law constant from molecular simulation: a systematic study of 95 systems",
Int. J. Thermophys. **30**, 1791-1810 (2009).

Huang Y. L., Heilig M., Hasse H. and Vrabec J.,
"Molecular Modeling and Simulation of Vapor-Liquid Equilibria of Hydrogen Chloride, Phosgene, Benzene, Chlorobenzene, Ortho-Dichlorobenzene, Toluene and Their Binary Mixtures."
AIChE J., in press (2010).

Zusammenfassung

Für die Auslegung und Optimierung verfahrenstechnischer Prozesse ist die Kenntnis thermophysikalischer Stoffdaten, insbesondere Dampf-Flüssigkeits Gleichgewichte von Mischungen, unerlässlich. Da häufig nur sehr wenige experimentelle Daten vorliegen, werden Methoden benötigt, die eine quantitative Stoffdatenvorhersage ermöglichen. Hierfür werden üblicherweise Zustandsgleichungen oder G^{E}-Modelle verwendet, die zwar sehr gute Korrelationswerkzeuge sind, aber erhebliche Schwächen bei der Stoffdatenvorhersage haben. Das Entwicklungspotenzial dieser Ansätze ist zudem weitgehend ausgereizt. Die vorliegende Arbeit ist in zwei Teile gegliedert.

Der erste Teil diskutiert die molekulare Modellierung und Simulation von zwölf industriell wichtigen Reinstoffen sowie zwölf binären Mischungen dieser Komponenten. Deren wirtschaftliche Bedeutung und sicherheitsrelevante Eigenschaften sind eine starke Motivation für numerische Simulationsmethoden. Diese Untersuchung ist in zwei Stoffgruppen aufgeteilt. Die erste Gruppe beinhaltet Wasserstoffchlorid, Phosgen, Benzol, Monochlorbenzol, Ortho-Dichlorbenzol und Toluol, die zweite Gruppe enthält Ethylenoxid, Ethylenglykol und Wasser. Modelle für diese Reinstoffe werden in dieser Arbeit auf der Grundlage von quantenchemischen Rechnungen zur molekularen Geometrie und Elektrostatik entwickelt. Die Parameter der molekularen Modelle werden anschließend an experimentelle Reinstoffdaten von Dampfdruck und Siededichte optimiert. Ein Vergleich zu anderen molekularen Modellen aus der Literatur wird gegeben. Die ungleiche Dispersionswechselwirkung wird für zehn der zwölf untersuchten binären Mischungen angepasst. Dampf-Flüssigkeits Gleichgewichte, insbesondere Dampfzusammensetzung, Sättigungsdichten und Verdampfungsenthalpie, werden für verschiedene Temperaturen und Zusammensetzungen vorhergesagt und mit experimentellen Daten verglichen, die nicht in die Modellentwicklung eingeflossen sind.

Im zweiten Teil dieser Arbeit wird durch eine Untersuchung einer sehr großen Zahl von Systemen gezeigt, dass die molekulare Modellierung und Simulation ein zuverlässiges und robustes Werkzeug für VLE von Mischungen ist. Molekulare Modelle für 78 Reinstoffe wurden der Literatur entnommen, um alle 366 binären und ternären Mischungen dieser Komponenten systematisch zu untersuchen, für die entsprechende experimentelle Daten verfügbar sind. Dabei werden 267 binäre Mischungen und 33 ternäre Mischungen in Bezug auf Phasengleichgewichte bei endlicher Verdünnung sowie 95 binäre Mischungen in Bezug auf die Henrykonstante untersucht. Die Vorhersagen auf der Basis der 366 molekularen Modelle werden extensiv mit verfügbaren experimentellen Daten verglichen. In fast allen Fällen werden ausgezeichneten Vorhersagen der Mischungseigenschaften erzielt.

Contents

List of Symbols

Latin Letters

a	component index
B	second virial coefficient
b	component index
b	binary vapor-liquid equilibrium
f	force
H_i	Henry's law constant of solute i
h	intramolecular site-site distance
h	Henrys law constant
Δh_v	heat of vaporization
i	molecule index
i	solute
j	molecule index
k_B	Boltzmann's constant, $k_B = 1.38066{\cdot}10^{23}$ J/K
k_{ij}	binary parameter of the Peng-Robinson equation of state
L	elongation
l	distance
N	number of molecules
N	number of pure fluid models
P	polarity representing a point dipole or a point quadrupole
p	pressure
Q	quadrupolar moment
q	point charge
R	ideal gas constant
S	solvent
r	distance
r_c	cut-off radius
T	temperature
t	ternary vapor-liquid equilibrium
t	time
U	intermolecular interaction energy
u	pair potential
V	volume
v_i	partial molar volume of the solute
x	mole fraction in the liquid phase
x	space coordinate
y	mole fraction in the vapor phase
y	space coordinate
z	space coordinate

Greek Letters

α	angle between sites
γ	activity coefficient
ϵ	Lennard-Jones energy parameter
ϵ_0	permittivity of vacuum: $\epsilon_0 = 8.8541\ldots\cdot 10^{-12}$ $\mathrm{C^2J^{-1}m^{-1}}$
μ	dipolar moment
ξ	binary interaction parameter
ρ	molar density
θ	dihedral angle between the orientation vectors of two molecules
σ	Lennard-Jones size parameter
ψ_i	potential energy of test particle i
ϕ	azimuthal angle between the orientation vectors of two molecules
ϕ	fugacity coefficient

Subscripts

A	related to component A
a	count variable for molecule sites
a	constant
B	related to component B
b	count variable for molecule sites
b	constant
C	related to component C
c	critical value
cor	correlation value
D	dipole
H	Henry's law constant
i	related to component i
i	solute
ij	related to components i and j
j	related to component j
m	mixture
Q	quadrupole
q	point charge
S	saturated liquid state
S	solvent
μ	dipole

Superscripts

exp	experimental data
sim	simulation data
$'$	property of saturated liquid phase
$''$	property of saturated vapor phase

Abbreviations

1CLJ	one-center Lennard-Jones
1CLJD	one-center Lennard-Jones plus point dipole
2CLJ	two-center Lennard-Jones
2CLJD	two-center Lennard-Jones plus point dipole
2CLJQ	two-center Lennard-Jones plus point quadrupole
DDB	Dortmunder Datenbank
EOS	equation of state
QC	quantum chemical
VLE	vapor-liquid equilibrium

Vector properties

$\boldsymbol{r}_{ij}$	center-center distance vector between two molecules i and j
$\boldsymbol{\mu}$	dipole vector
$\boldsymbol{\omega}$	orientation vector of a molecule

1 Introduction

Obtaining data on thermophysical properties of fluids is an indispensable task for developing and designing industrial processes and products. Accurate thermophysical data are the basis of quality, efficiency and sustainability. Usually, these data are obtained by experiments and are subsequently aggregated in correlations. However, they are needed in many cases for inconvenient conditions, e.g. at high temperatures, or for toxic fluids. Correlations are in many cases excellent descriptive tools, but often lack in predictive power, especially when the available experimental database for their adjustment is narrow.

Due to the advances in methodology and computer technology, an alternative approach became feasible, namely molecular simulation. Fluids consist of molecules and their thermophysical properties are determined by the molecular interactions. Molecular models describe these molecular interactions by means of parameterized potential functions.

The development of a molecular model usually starts with the geometry of the molecule. Ab initio quantum chemical (QC) calculations may precisely yield bond lengths and angles as well as intermolecular electrostatic interactions [1]. Dispersion and repulsion can only be obtained with computationally very expensive QC methods, thus parameters for these interactions are initially taken from similar sites of other molecular models. Some of these parameters are subsequently fitted to yield the correct vapor-liquid equilibrium (VLE) behavior of the regarded pure substance [2].

Predicting data which cannot be easily obtained by experiments is a great advantage of molecular simulation. Therefore, an essential question is whether molecular models, which were optimized to experimental VLE data, can accurately yield other thermophysical properties. Furthermore, these pure fluid models should be compatible with each other and allow for predictions of mixture properties.

Backed by the chemical industry, substantial efforts were made in recent years by the molecular simulation community to tackle thermophysical properties of technically relevant fluid systems [3, 4, 5, 6, 7]. This is particularly rewarding for substances which have inconvenient properties, like being toxic or explosive, that render experimental studies difficult.

The results from a co-operation with BASF SE, Ludwigshafen, are presented in the first part of this work. There, the fluid phase behavior of hazardous chemicals which are produced on a large scale was studied. Two groups of molecules were investigated. First, the Phosgene group which includes Hydrogen chloride, Phosgene, Benzene, Chlorobenzene, Ortho-Dichlorobenzene and Toluene and second, the Ethylene oxide group which contains Ethylene oxide, Ethylene glycol and Water was studied.

Hydrogen chloride and Phosgene are key components in the production of Isocyanates which are important intermediates in the Polyurethane production. The Isocyanate synthesis is a phosgenation in which Phosgene and Hydrogen chloride are present in mixtures with organic solvents, where Benzene, Chlorobenzene, Ortho-Dichlorobenzene and Toluene are of special interest. Therefore, the binary mixtures of Hydrogen chloride or Phosgene with these four solvents were systematically studied together with the mixture Hydrogen chloride + Phosgene.

Polyethylene glycol (PEG) is a polyether compound with many applications from industrial manufacturing to medicine. The main components in its production are Ethylene oxide, Water and Ethylene glycol. Ethylene oxide is highly explosive and thus very little experimental data are available. Water is a particularly difficult substance for developing a molecular model, e.g. due to its strong hydrogen bonding behavior.

In the second part of this work, a large systematic study on VLE of mixtures is presented. 366 binary and ternary mixtures were investigated. Through an extensive comparison of simulation results and experimental data, a conclusive statistics as the reliability of the molecular modeling and simulation was generated. In this study, 78 real pure fluids using the dipolar or quadrupolar two-center Lennard-Jones (2CLJD and 2CLJQ) potential were taken from prior work [8, 9]. This model type has been proposed more than three decades ago [10], however, it is far from being fully exploited. Polar 2CLJ models consider the basic molecular interactions repulsion and dispersive attraction and also feature anisotropy and polarity in a simple way. 78 small molecules consisting of up to nine atoms that belong to different classes of real fluids, including noble gases, alkanes, halogens and numerous refrigerants. For many of the 78 molecules, the polar 2CLJ model strongly simplifies the intermolecular interactions. E.g., the asymmetry of the molecules is neglected and the polar interaction is always aligned along the main molecular axis. Also the polarizability, which is often assumed to be a crucial molecular property for thermodynamics, is only implicitly considered by Lennard-Jones interaction sites. Furthermore, the internal degrees of freedom are neglected as the polar 2CLJ models are rigid. The aim of this study was to investigate whether these crude assumptions for pure substance models have an impact on mixture properties, in particular on binary and ternary VLE. It can be argued that oversimplified molecular models can be adjusted to a few experimental pure substance properties, but major deficiencies should be visible when applied to mixtures.

Molecular simulations on binary VLE containing some of the 78 components, but using other models or parameter sets, are available from different authors: Potoff and Siepmann [11] (N_2, CO_2 and alkanes), de Pablo et al. [12] (hydrocarbons), Gao et al. [13]

(hydrofluorocarbon and hydrochlorofluorocarbon mixtures), Kronome et al. [14] (N_2 + C_2H_6), Nath et al. [15] (alkane mixtures), Cui et al. [16] (CO_2 + perfluoroalkanes), Potoff et al. [17] (mixtures of various polar and non-polar components), Delhommelle and Millié [18] (Ne, Ar and Kr), Liu and Beck [19] as well as Vrabec and Fischer [20, 21] (CH_4, C_2H_6 and CO_2). However, each of these publications is restricted to a few mixtures only.

Some of the above-mentioned 78 pure substance models have successfully been used in simulation studies by others: Several authors used them as solute models for predictions of the Henry's law constant: Boutard et al. [22] for O_2 in Ethanol, Krishnamurthy et al. [23] for N_2 and O_2 in Ethylene oxide and Shah and Maginn [24] for C_2H_6 and C_2H_4 in an ionic liquid. Grimm et al. [25] used the CH_2I_2 model to investigate local density effects on photoinduced isomerization kinetics of this substance in supercritical CO_2. Müller et al. [26, 27] used several models (C_2H_6, C_2H_4, N_2 and C_2F_6) for simulations on adsorption regarding micro-porous carbon. Jia and Murad [28, 29] took the N_2 and O_2 models to simulate zeolite membrane separations of gas mixtures. The same models were taken by Chialvo and Horita [30] for a study on vapor-liquid fractionation factors. Schumacher et al. [31] used the N_2, O_2 and CO_2 models for investigations on the optimization of organic/inorganic adsorbents. Carrero-Mantilla and Llano-Restrepo [32] used them to predict VLE of binary mixtures containing CH_4, C_2H_6, C_2H_4 and Propylene, they also regarded reactive systems [33]. Furthermore, Smith and Lísal [34, 35] used the N_2 model for non-reacting and reacting systems regarding ammonia synthesis.

Based on the 78 pure substance models, the unlike energy parameter was adjusted in previous work [36, 37, 38] to the experimental binary vapor pressure for 44 systems in order to very accurately describe their VLE. The viability of this approach was also shown with VLE predictions of five ternary mixtures [36, 37, 38]. Galbraith and Hall [39] took some of those adjusted mixture models and calculated VLE of four binaries containing N_2, O_2, CO_2 and C_2H_6 by Gibbs-Duhem integration and obtained an excellent agreement with experimental data.

A few publications on molecular simulation results for ternary VLE are available from different authors: Carrero-Mantilla and Llano-Restrepo [40] (N_2 + CH_4 + C_2H_6), Potoff and Siepmann [11] (N_2 + CO_2 + propane), Kamath and Potoff [41] (CH_4 + H_2S + CO_2), Hansen et al. [42] (N_2 + O_2 + CO_2), Liu and Beck [19] (CH_4 + CO_2 + C_2H_6), Nath et al. [43] (C_2H_4 + 1-hexene + polyethylene), Lísal et al. [44] (isobutene + methanol + MTBE) and Van't Hof [45] (CH_4 + CO_2 + C_2H_6 and CH_4 + CO_2 + propane). However, each of these publications is restricted to one or two ternary mixtures only. Note that there are additional works on ternary VLE by simulation [46, 47, 48, 49, 50, 51], but they deal exclusively with model systems.

Thermodynamic data on the distribution of the components in coexisting vapor and liquid phases are essential for a wide range of technical applications. A common classification distinguishes between mixtures in which the components have a similar volatility and mixtures in which the components have a strongly differing volatility. In the first case, for binary mixtures, considerable amounts of both components can be found in the coexisting phases and the characterization of the equilibrium requires for a given pair of temperature and pressure both the liquid composition and the vapor composition. Depending on the mixture, a large variation in the distribution of the components is found, leading to qualitatively different forms of the two-phase envelope, such as for zeotropic or azeotropic systems. In the second case, the liquid overwhelmingly contains the component with low volatility (i.e. solvent), while the vapor is composed mainly out of the volatile component (i.e. solute). The two-phase envelope is thus wide and has a characteristic shape. E.g., it is observed at constant temperature that the solute mole fraction in the liquid increases approximately linearly with the pressure. This has given rise to a condensed characterization of the phase equilibrium in such cases through the Henry's law constant.

Molecular modeling and simulation is used for more than two decades for calculating the Henry's law constant. In the early works [52, 53, 54, 55], usually model mixtures of Lennard-Jones spheres without reference to real fluids were regarded. Lotfi and Fischer [56] also simulated mixtures of Lennard-Jones spheres, however, they applied them to real fluid systems, like He in liquid CH_4 or Ne in liquid Kr. The influence of the unlike interaction between the two molecule species was also investigated by applying different combining rules [56].

Mixtures of real components became better accessible through the development of simulation methodology and computing infrastructure. E.g., Boulougouris et al. [57] calculated the solubility of CH_4 in liquid C_2H_6 and of the same solute in liquid water. Due to their technical importance also the solubility of larger hydrocarbons, like n-butane, n-hexane, cyclohexane or benzene in liquid water, was studied [58, 59]. Other systems, like CO_2 in liquid water [60] or O_2 in liquid benzene [61], were tackled as well.

The Industrial Fluid Property Simulation Collective [4] has challenged the molecular simulation community in 2004 to predict the Henry's law constant for Ar, N_2, CH_4 and C_2H_6 in liquid ethanol. The submitted contributions have shown the capability of the molecular approach to determine this thermodynamic property [22, 62, 63, 64, 65].

In terms of simulation methodology, there is a variety of possibilities for determining the Henry's law constant. The most straightforward route is to sample the phase space of the solvent either by molecular dynamics or Monte-Carlo and to calculate the chemical

potential of the solute at infinite dilution through insertions of test molecules by Widom's method [66]. However, if the density of the solvent is very high, e.g. in case of liquid water around ambient conditions, successful test molecule insertions become highly unlikely which deteriorates the statistics. Solutions to this problem are e.g. staged particle insertions/deletions [58] or expanded ensemble methods [57, 59, 60]. Alternatively, Murad and Gupta [55, 61] proposed a molecular dynamics scheme with a semi-permeable membrane that can only be permeated by the solute. In equilibrium, a part of the simulation volume contains only the gaseous solute and the remaining part of the simulation volume contains the liquid solvent that is saturated with the solute. A recent overview on molecular simulation methodology can be found in [67].

The theoretical background of the molecular simulation methods applied in the present work is described in Chapter 2. Chapter 3 covers the co-operation work with industry on hazardous fluids and Chapter 4 includes the large systematic study on mixture models. Finally, Chapter 5 gives a summary.

2 Fundamentals

Classical thermodynamics was developed to understand the relationship between work and heat, with the transformations of heat into mechanical work and the opposite transformations of mechanical work into heat. In the middle of 17th century, with the invention of the first vacuum pump, a correlation between pressure, temperature and volume was developed. Afterwards, in the 19th century, the technical interest in the steam engine fostered a profound scientific description of processes that transform heat into work. Sadi Carnot pioneered in the theoretical explanation of thermodynamics. The works of James Joule and Robert von Mayer manifested the equivalence of heat and work in physics. After many scientists devoted themselves to the field of thermodynamics, it quickly became a complex field of physics, linked with and influenced by other sciences. In the field of biology, Hermann von Helmholtz discovered the conservation of energy in his experiments on fermentation, a holistic formulation of the first law of thermodynamics. Alongside these discoveries, the second law of thermodynamics, introduced by Rudolf Clausius, complemented the theoretical framework of classical thermodynamics. It gives an answer to the question why some processes cannot be reversed, even though the reversion complies with the first law. Subsequently, the development of physics initialized an explanation of thermodynamic phenomena with a molecular argumentation. Ludwig Boltzmann, Josiah Willard Gibbs and James Clerk Maxwell founded the fields of statistical mechanics (or statistical thermodynamics), the groundwork of molecular thermodynamics.

Classical thermodynamics gives a comprehensive relation between macroscopic properties, but it does not cover the quantitative prediction of these properties. On the contrary, statistical mechanics relates the microscopic properties of individual atoms and molecules to the macroscopic properties of materials. It connects the macroscopic properties to intermolecular interactions through the partition functions. In the field of statistical thermodynamics, fluid systems are not regarded as a continuum, but their particulate nature is considered. In brief, statistical mechanics is able to rigorously yield macroscopic properties based on microscopic properties, which can not be achieved by classical thermodynamics.

Making use of the highly progressive development of computer technology, nowadays molecular simulation has allowed for considerable contributions to the fields of chemistry, material science, biology and engineering. High performance computers facilitate molecular simulation studies for systems that were not accessible a couple of decades ago. Thus molecular simulation has evolved into an own subject in engineering and the natural sciences, closely related to computer sciences, dedicating itself to the analysis, development and improvement of numerical methods to perform simulations of molecular systems and

to depict the molecular characteristics of real substances in a physically sound way.

Some theoretical background, principles and methods applied in the present study are briefly described in the following sections.

2.1 Molecular Modeling

Molecular simulation forges a link between microscopic configurations and the macroscopic state of a system. Once the motions and positions of all molecules in a system are determined according to the interactions between the molecules, the state of this system, e.g. temperature, pressure or any other thermophysical property can be calculated. Even rather abstract or tediously measurable properties, such as surface tension or diffusion coefficients, can be obtained. This leads inevitably to the question on how the molecular interactions are specified.

In the world of atoms and molecules, different physical effects cause several types of interactions between molecules. Repulsion plays a central role when the molecules come close to each other. Dispersive interactions cause attraction among molecules at intermediate and greater distances [68]. Electrostatic interactions also have a notable effect on the molecular behavior. Moreover, for some substances, like Water, hydrogen bonding is a dominant interaction that has to be taken into account.

2.1.1 Lennard-Jones Potential

Figure 1 shows the Lennard-Jones 12-6 function, which is the most well-known model for the Van der Waals interactions, i.e. repulsion and dispersion. The interaction potential u_{ij} is given by

$$u_{ij}(r_{ij}) = 4\epsilon \left[\left(\frac{\sigma}{r_{ij}} \right)^{12} - \left(\frac{\sigma}{r_{ij}} \right)^{6} \right], \tag{1}$$

with r_{ij} being the distance between two Lennard-Jones sites i and j. The Lennard-Jones potential has two adjustable parameters, the size parameter σ and the energy parameter ϵ. It is widely used for its effective modeling and numerical efficiency.

Due to the generally high computational effort associated with molecular simulations, the widespread use of Lennard-Jones potential roots in its computing convenience. The term $(\sigma/r_{ij})^6$ describing the dispersive interaction on a sound physical basis, merely has to be multiplied with itself to give the repulsive term $(\sigma/r_{ij})^{12}$.

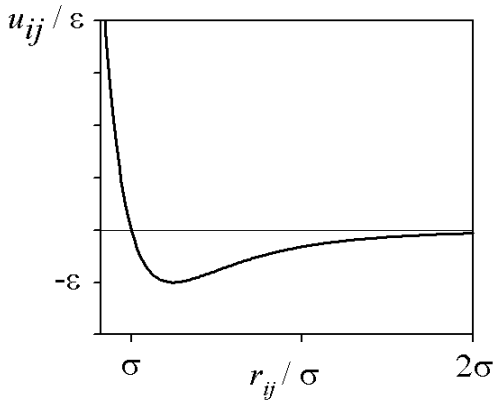

Figure 1: The Lennard-Jones 12-6 potential.

2.1.2 Electrostatic Interactions

In addition to the dispersive and repulsive interactions, molecular models describe electrostatic interactions with point charges, dipoles or quadrupoles [69]. Polarities which are of higher order than quadrupoles are usually not taken into account, as they have a short interaction range, scaling with $\sim r^{-7}$ or less.

The Coulomb interaction, i.e. attraction or repulsion of two charges i and j, is described by

$$u_{qq}(r_{ij}) = \frac{1}{4\pi\epsilon_0}\frac{q_i q_j}{r_{ij}}, \tag{2}$$

where r_{ij} is the distance between the point charges with the magnitude q_i and q_i. And ϵ_0 denotes the permittivity of the vacuum, $\epsilon_0 = 8.8541 \cdot 10^{-12}$ $\mathrm{C^2J^{-1}m^{-1}}$. Point charges are often applied to describe ions, but also polar molecules composed of atoms with significant by different electronegativity. Furthermore, they are used to model hydrogen bonding as well.

In molecules that have covalent bonds, differences in electronegativity yield an uneven distribution of the electrons and protons. A positive and a negative charge q, separated by a distance l, generate an electrostatic dipole with the permanent dipole moment $\mu = ql$, cf. Figure 2.

If l is much smaller than the typical distance r between two molecules, a dipole can be idealized by a single interaction site, i.e. a point dipole. The interaction potential between two point dipoles is [69]

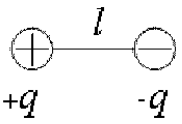

Figure 2: Two opposite charges q at a distance l generating a dipole.

$$u_{\mu\mu}(r_{ij}, \boldsymbol{\omega_i}, \boldsymbol{\omega_j}) = -\frac{1}{4\pi\epsilon_0}\frac{\mu_i\mu_j}{r_{ij}^3}\left(2\cos\vartheta_i\cos\vartheta_j - \sin\vartheta_i\sin\vartheta_j\cos\varphi_{ij}\right), \tag{3}$$

with r_{ij} being the distance between two interacting dipoles, which have the dipole moments μ_i and μ_j. The orientation vectors $\boldsymbol{\omega_i}$ and $\boldsymbol{\omega_j}$ of the dipoles boil down to three relevant mutual angles ϑ_i, ϑ_j and φ_{ij}, cf. Figure 3.

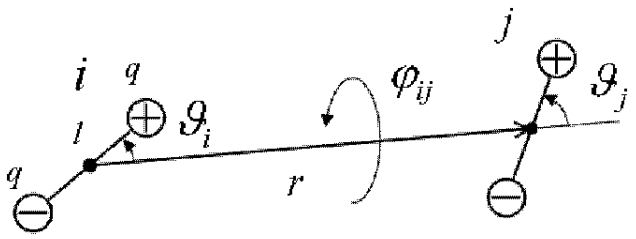

Figure 3: The orientation of two dipoles.

The polarity of the next higher order is the quadrupole. A quadrupole is a linear alignment of two opposite dipoles or three point charges, respectively, cf. Figure 4. The quadrupole moment is given by

$$Q = 2ql^2. \tag{4}$$

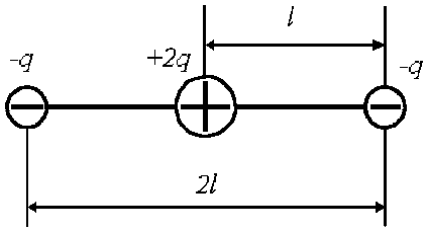

Figure 4: Linear alignment of three charges forming a quadrupole.

According to the multipole expansion, the quadrupolar interaction is [69]

$$u_{QQ}(r_{ij}, \boldsymbol{\omega_i}, \boldsymbol{\omega_j}) = \frac{3}{64\pi\epsilon_0}\frac{Q_i Q_j}{r^5}[1 - 5(\cos^2\vartheta_i + \cos^2\vartheta_j) - 15\cos^2\vartheta_i\cos^2\vartheta_j + 2(\sin\vartheta_i\sin\vartheta_j\cos\varphi_{ij} - 4\cos\vartheta_i\cos\vartheta_j)^2]. \quad (5)$$

The interaction is determined by the distance between two quadrupoles r_{ij}, their moments by Q_i and Q_j as well as their orientations depending on the angles ϑ_i, ϑ_j and φ_{ij}, cf. Figure 3.

2.1.3 Pairwise Additivity

For the potential energy U of an entire system containing N molecules, the assumption of pairwise additivity for the interaction potential u_{ij} between two molecules yields

$$U = \sum_{i=1}^{N}\sum_{j>i}^{N} u_{ij} = \frac{1}{2}\sum_{i=1}^{N}\sum_{j=1}^{N} u_{ij}. \quad (6)$$

In fact, the presence of other molecules alters the intermolecular energy between two molecules. The extent to which these three-body interactions are affecting the thermodynamic properties was studied, e.g. by Sadus and Prausnitz [70]. However, this issue still requires significant research effort in the future to really be resolved. The pairwise additivity assumption complies with the requirement of reducing computation time. So the effects of the multi-body interactions have to be compensated by the optimization for the molecular models at hand. Hence, the average three-body effect can be seen as included in "effective" pair potentials, which were employed throughout of this work.

2.1.4 Pure Fluid Models

Interaction energies between molecules stem from electrostatic and magnetic interactions of the molecular charge clouds and nuclei. Usually, models of molecular interactions only describe interactions resulting from electrostatics, as they are about four orders of magnitude higher than the magnetic interactions [69].

For the present modeling approach based on additive semiempirical potential functions, the molecular interactions can be separated into different contributions. At large intermolecular distances, dispersive and electrostatic interactions can be distinguished. The latter ones are caused by permanent molecular charge distributions. At small distances, repulsive interactions due to electronic cloud overlaps come into play. Furthermore, strong

and highly directional short-ranged interactions occur when hydrogen bonding molecules are studied.

To describe the intermolecular interactions, a varying number of Lennard-Jones sites and superimposed point charges, point dipoles and linear point quadrupoles was used. Point dipoles and quadrupoles were employed for the description of the electrostatic interactions to reduce the computational effort during simulation.

However, as described in Section 2.1.2, a point dipole may, e.g. when a simulation program does not support this interaction site type, be approximated by two point charges $\pm q$ separated by a distance l. Limited to small l, one is free to choose this distance as long as $\mu = ql$ holds. Analogously, a linear point quadrupole can be approximated by three collinear point charges q, $-2q$ and q, separated by l each, where $Q = 2ql^2$ [71].

The total intermolecular interaction energy thus writes as

$$
\begin{aligned}
U = \sum_{i=1}^{N-1} \sum_{j=i+1}^{N} \Bigg\{ & \sum_{a=1}^{S_i^{\mathrm{LJ}}} \sum_{b=1}^{S_j^{\mathrm{LJ}}} 4\epsilon_{ijab} \left[\left(\frac{\sigma_{ijab}}{r_{ijab}} \right)^{12} - \left(\frac{\sigma_{ijab}}{r_{ijab}} \right)^{6} \right] + \\
& \sum_{c=1}^{S_i^{\mathrm{e}}} \sum_{d=1}^{S_j^{\mathrm{e}}} \frac{1}{4\pi\epsilon_0} \Bigg[\frac{q_{ic} q_{jd}}{r_{ijcd}} + \frac{q_{ic}\mu_{jd} + \mu_{ic} q_{jd}}{r_{ijcd}^2} \cdot f_1(\boldsymbol{\omega}_i, \boldsymbol{\omega}_j) + \frac{q_{ic} Q_{jd} + Q_{ic} q_{jd}}{r_{ijcd}^3} \cdot f_2(\boldsymbol{\omega}_i, \boldsymbol{\omega}_j) + \\
& \frac{\mu_{ic}\mu_{jd}}{r_{ijcd}^3} \cdot f_3(\boldsymbol{\omega}_i, \boldsymbol{\omega}_j) + \frac{\mu_{ic} Q_{jd} + Q_{ic}\mu_{jd}}{r_{ijcd}^4} \cdot f_4(\boldsymbol{\omega}_i, \boldsymbol{\omega}_j) + \frac{Q_{ic} Q_{jd}}{r_{ijcd}^5} \cdot f_5(\boldsymbol{\omega}_i, \boldsymbol{\omega}_j) \Bigg] \Bigg\}, \quad (7)
\end{aligned}
$$

where r_{ijab}, ϵ_{ijab}, σ_{ijab} are the distance, the Lennard-Jones energy parameter and the Lennard-Jones size parameter, respectively, for the pair-wise interaction between Lennard-Jones site a on molecule i and Lennard-Jones site b on molecule j. ϵ_0 is the permittivity of vacuum, whereas q_{ic}, μ_{ic} and Q_{ic} denote the point charge magnitude, the dipole moment and the quadrupole moment of the electrostatic interaction site c on molecule i and so forth. The expressions $f_x(\boldsymbol{\omega}_i, \boldsymbol{\omega}_j)$ stand for the dependency of the electrostatic interactions on the orientations $\boldsymbol{\omega}_i$ and $\boldsymbol{\omega}_j$ of the molecules i and j, cf. [69, 72]. Finally, the summation limits N, S_x^{LJ} and S_x^{e} denote the number of molecules, the number of Lennard-Jones sites and the number of electrostatic sites, respectively.

For a given molecule, the interactions between Lennard-Jones sites of different type were defined by applying the standard Lorentz-Berthelot combining rules [73, 74]

$$
\sigma_{ijab} = \frac{\sigma_{iiaa} + \sigma_{jjbb}}{2}, \quad (8)
$$

and

$$\epsilon_{ijab} = \sqrt{\epsilon_{iiaa}\epsilon_{jjbb}}. \tag{9}$$

2.1.5 Mixture Models

On the basis of defined pairwise additive pure fluid models, molecular modeling of mixtures reduces to modeling the interactions between unlike molecules. Unlike interactions consist of two different types here. The electrostatic interactions, e.g. between dipole and dipole, dipole and quadrupole, as well as quadrupole and quadrupole, belong to one type. These interactions are treated here in a physically straightforward way, simply using the laws of electrostatics.

Repulsion and dispersive attraction are other interaction types and are present between all molecules. If a mixture A + B is modeled on the basis of Lennard-Jones potentials, the knowledge of the unlike Lennard-Jones parameters σ_{AB} and ϵ_{AB} is required. For their determination, the broadly used Lorentz-Berthelot combining rule is a good starting point [75]

$$\sigma_{\mathrm{AB}} = (\sigma_{\mathrm{A}}+\sigma_{\mathrm{B}})/2, \tag{10}$$

and

$$\epsilon_{\mathrm{AB}} = \sqrt{\epsilon_{\mathrm{A}}\epsilon_{\mathrm{B}}}. \tag{11}$$

Applying σ_{AB} and ϵ_{AB}, as given by equations (10) and (11), allows the prediction of mixture properties from pure fluid data alone [32, 36, 37, 38, 75]. But as shown in there, a significant improvement can be achieved by introducing one state independent binary interaction parameter ξ to adjust the unlike energy parameter

$$\epsilon_{\mathrm{AB}} = \xi\sqrt{\epsilon_{\mathrm{A}}\epsilon_{\mathrm{B}}}. \tag{12}$$

It should be pointed out that A and B are molecule species that may each be described by several LJ sites with different energy parameters ξ. Thus ξ is a single overall parameter that acts consistently on all individual unlike LJ interactions of the pair A + B.

2.2 Molecular Properties from Quantum Chemistry

Molecular models that were developed on the basis of QC calculations stand between *ab initio* models and empirical models. The present strategy is based on the idea to include *ab initio* information without giving up the freedom to reasonably optimize the model to important macroscopic thermodynamic properties. Thus, for the modeling process some

experimental data are needed for optimization. The chosen properties, vapor pressure and saturated liquid density, have the advantage to be well available for numerous engineering fluids and to represent dominant features of the fluid state.

The parameters of the present molecular models can be separated into three groups. First, the geometric parameters specify the positions of the different interaction sites of the molecular model. Second, the electrostatic parameters define the polar interactions in terms of point charges, dipoles and quadrupoles. And finally, the dispersive and repulsive parameters determine attraction by London forces and repulsion by overlaps of the electronic orbitals. Here, the Lennard-Jones 12-6 potential [76, 77] can be used to allow for a straightforward compatibility with the overwhelming majority of the molecular models in the literature.

In a recent publication, Sandler and Castier [78] gave a brief overview on the use of QC in thermodynamics. By numerically solving Schrödinger's equation, different molecular properties of technically relevant components can be calculated in a quite standardized way. Many different QC codes are available for this task. For license reasons, the open source code GAMESS(US) [1] was used in the present work.

2.2.1 Geometry

All geometric data of the molecular models, i.e. bond lengths, angles and dihedrals, were determined based on QC calculations. Therefore, a geometry optimization, i.e. an energy minimization, was initially performed using GAMESS(US) [1]. The Hartree-Fock level of theory was applied with a relatively small (6-31G) basis set.

The resulting configuration of the atoms was taken to specify the spatial distribution of the Lennard-Jones sites, except for the sites that represent groups containing Hydrogen atoms. As the united atom approach was used to obtain computationally efficient molecular models, the dispersive and repulsive interactions of the Hydrogen atoms were modeled together with the atom they are bonded to. For the methyl (CH_3) united atom site, the Lennard-Jones potential was located at the geometric mean of the nuclei, while the methine (CH) united atom site was located at 0.4 of the distance between carbon and hydrogen atom. These empirical offsets are in good agreement with the results of Ungerer et al. [79], which were found by optimization of transferable molecular models for n-Alkanes.

2.2.2 Electrostatics

Intermolecular electrostatic interactions mainly occur due to static polarities of single molecules that can well be obtained by QC. Here, the Møller-Plesset 2 level was used that considers electron correlation in combination with the polarizable 6-311G(d,p) basis set.

The purpose of the present work was the development of effective pair potentials with state-independent model parameters. Obviously, the electrostatic interactions are stronger in the liquid state than in the gaseous state due to the higher density. Furthermore, the mutual polarization raises their magnitude in the liquid. Thus, for the calculation of the electrostatic moments by QC a liquid-like state should be considered. This was done here by placing one molecule into a dielectric continuum and assigning the experimental dielectric constant of the liquid to it, as in the COSMO method.

From the resulting electron density distribution for the small symmetric molecules studied here, the dipole and quadrupole moments were estimated by simple integration over the orbitals. Thus magnitudes and orientations of these electrostatic interaction sites were derived from QC calculations.

2.2.3 Dispersion and Repulsion

It would be highly desirable to also calculate the dispersive and repulsive interactions using *ab initio* methods as well. This approach was followed by different authors in the past, e.g. for Neon [80, 81, 82, 83], Argon [81, 83, 84], Krypton [85], Nitrogen [86], Carbon dioxide [87], Hydrogen chloride [88], Acetonitrile [89], Methanol [89], Acetylene [90] or Methanethiol [91]. However, from an engineering point of view, this leads to difficulties.

For an estimation of dispersive and repulsive interactions at least two molecules must be taken into account. To properly scan the energy hyper surface, many QC calculations at different distances and orientations of the molecules have to be performed. As the dispersive, and partly also the repulsive, interactions are usually only a very small fraction of the total energy calculated by QC, highly accurate methods like coupled cluster (CC) with large basis sets or even extrapolations to the basis set limit must be used for this task [78].

Due to the fact that this is computationally too expensive for engineering purposes, Lennard-Jones parameters for a given atom or molecular group were passed on from other molecular models. Some of these parameters were subsequently fitted in the optimization process to yield an accurate VLE behavior of the modeled pure substance.

2.3 Simulation Methods

2.3.1 Molecular Dynamics

Molecular dynamics is an approach to mimic the movement of molecules in an ensemble [92, 93]. The molecules are regarded as mechanical bodies which move according to Newton's laws of motion. The intermolecular potential yields the force f_{ij} between two molecules by deriving the potential with respect to the distance between the interaction partners i and j

$$f_{ij} = -\frac{\partial u_{ij}}{\partial r_{ij}}. \tag{13}$$

According to Newton's law, the sum of all forces acting on a mass is equal to the acceleration multiplied with it. Thus, the motion is governed by the interactions between the molecules. A numerical integration is required to compute the specific trajectory of all molecules during simulation. The knowledge of the position and velocity as well as the interactions of all molecules allows the evaluation of macroscopic observables of the system. Averaging over the macroscopic observables at each time step yields the macroscopic properties [94].

The numerical integration is performed by time discretization methods, where the trajectories of the molecules are computed over a large number of time steps δt in the order of 1 fs. The position, velocity and acceleration of each molecule at a later time $t+\delta t$ are calculated considering the forces afflicted on the molecules by its surrounding molecules at the time t, while these forces are regarded constant throughout the time interval δt. A variety of algorithms exist for this integration, the Velocity-Verlet or the Gear predictor-corrector algorithm being two popular and effective algorithms today. A concern in the application of these algorithms is the approximation that the forces between the interaction sites are constant throughout the time step despite the fact that the forces change as the molecules move during the time interval δt. To generate a more accurate trajectory of the molecules, more sophisticated algorithms employ a cascaded computation [72]. In the case of the Gear predictor-corrector algorithm, a predicted position of the molecule, based on its velocity and acceleration, helps to calculate the new forces, and therefore the acceleration at the new position. The difference between the former acceleration and the new acceleration is used to correct the new position, velocity and acceleration of the molecule. These corrected values are regarded as the state of the molecule at $t + \delta t$. However, it should be noted that the thermodynamic properties are not significantly influenced by the choice of the integrator.

2.3.2 Periodic Boundary Condition

The aim of molecular simulation in the present work is to compute the thermodynamic properties of a substance on the macroscopic scale by taking exclusively its molecular behavior into account. The number of atoms in a molecular simulation is still extremely small compared to the number of atoms in real systems on the macroscopic level. Therefore, periodic boundary conditions are applied to mimic a quasi-infinite bulk medium [95]. The simulation volume V is treated as a single cell in the center of an infinite periodic lattice of identical cells. Once a molecule moves out of the simulation volume on one side, an identical molecule moves into the volume from the opposite site. By this technique, the simulation volume has effectively no walls and the fluid has no boundaries.

By applying the periodic boundary conditions, the amount of interaction partners of a molecule in a simulation theoretically rises to infinity. The minimum image convention is a solution to resolve this problem. The interactions to molecules outside of a cubic volume V centered on the regarded molecule are not considered explicitly in the calculation of the intermolecular forces [72]. The undesired periodicity evoked by the periodic boundary conditions is thereby eliminated. Due to the limited extent to which the molecular interactions thus are considered, correction terms have to account for the truncation. These correction terms are typically deduced for a spherical volume. Hence, around the molecule of interest, a sphere with the radius r_c, called the cut-off radius [94], is defined within which the interactions are evaluated explicitly. The cut-off radius has to be less than half of the length of the cubic simulation volume. If the center of mass of a molecule lies outside of this sphere, it is not included in the explicit calculation of the intermolecular forces. Instead, it is assumed that the volume outside of the sphere is a homogeneous fluid of constant density. The correction term added to the potential is then given by

$$\Delta u_i = 2\pi\rho \int_{r_c}^{\infty} u(r) r^2 dr. \tag{14}$$

2.4 Determination of Thermodynamic Properties with Molecular Simulation

2.4.1 Vapor-Liquid Coexistence Curves

The Grand Equilibrium method [96], which was used in this work to determine the VLE of properties for both pure fluids and mixtures, is based on the separate simulation of the vapor and the liquid phase. With the Grand Equilibrium method, the vapor pressure

and dew point composition of mixtures can be determined at specified temperature and bubble point composition.

The first step of the Grand Equilibrium method is the simulation of the liquid phase. Therein, the chemical potential and the partial molar volume of all components are determined at specified bubble point temperature and composition as well as an estimated pressure. For smaller non-associating components, Widom's test particle method [66] was used to obtain reasonable statistics. For larger or associating components, the gradual insertion method [97, 98, 99] was applied to obtain accurate results.

In the second step of the Grand Equilibrium method, the dew point composition and the vapor pressure related to the specified temperature and bubble point composition are determined in a pseudo grand canonical (pseudo-μVT) ensemble. In this ensemble, the chemical potentials are not constant, but continuously updated according to the results for the chemical potential as a function of pressure which is known from the liquid phase simulation. The vapor phase simulation converges quickly to the equilibrium pressure and composition. Only a reasonably large volume has to be chosen as a starting point of the vapor simulation. Simulation details on the Grand Equilibrium method can be found in Appendix B.

2.4.2 Henry's Law Constant

Several approaches have been proposed in the literature to obtain the Henry's law constant on the basis of molecular models. Here, a straightforward route was followed. The Henry's law constant H_i is related to the residual chemical potential of the solute i at infinite dilution in the solvent ${\mu_i}^\infty$ [52, 62] by

$$H_i = \rho_\mathrm{S} k_\mathrm{B} T \exp\left({\mu_i}^\infty/(k_\mathrm{B}T)\right), \tag{15}$$

where ρ_S is the density of the solvent in its saturated liquid state.

In order to evaluate ${\mu_i}^\infty$, molecular dynamics simulation applying Widom's test particle method [66] was used here. Therefore, test molecules representing the solute i were inserted into the pure saturated liquid solvent after each time step at random spatial coordinates, and the potential energy ψ_i between the solute test molecule i and all solvent molecules was calculated within the cut-off radius by

$${\mu_i}^\infty = -k_\mathrm{B}T \ln \langle V \exp(-\psi_i/(k_\mathrm{B}T))\rangle / \langle V \rangle, \tag{16}$$

where V is the volume and the brackets represent the NpT ensemble average.

The residual chemical potential at infinite dilution μ_i^{∞} and hence the Henry's law constant H_i is directly related to the unlike solvent-solute interaction and indirectly to the like solvent-solvent interaction which yields the configurations of the solvent molecules. In these configurations, the solute test molecules are inserted. The mole fraction of the solute in the solvent is exactly zero, as required for infinite dilution, since the test molecules are ghost particles that are removed after the potential energy calculation and thus do not affect the solvent molecules. Simulations were performed in the liquid state at a specified temperature, and the pressure was set to the pure substance vapor pressure of the solvent, as described by the molecular model.

Based on pairwise additive molecular models, the Henry's law constant is determined by two different interactions: first, the like interaction between solvent molecules and, second, the unlike interaction between solvent and solute molecules. While the like interaction is fully defined by the solvent model, the unlike interaction requires some discussion: the unlike polar contribution is defined in a physically straightforward manner, simply using the laws of electrostatics. To define the unlike Lennard-Jones contribution between solute i and solvent S molecules, the modified Lorentz-Berthelot combining rule [75] was used.

$$\sigma_{i\mathrm{S}} = \frac{\sigma_i + \sigma_{\mathrm{S}}}{2}, \tag{17}$$

and

$$\epsilon_{i\mathrm{S}} = \xi \cdot \sqrt{\epsilon_i \epsilon_{\mathrm{S}}}\,, \tag{18}$$

where ξ is the binary interaction parameter that mainly accounts for the unlike dispersion. The Henry's law constant is sensitive to ξ, i.e., it decreases with increasing ξ [62]. This is physically reasonable, as a higher solubility due to stronger unlike dispersive attraction is expected. Note that Equations (10) and (12) are discussed in Section 2.1.5 with a somewhat different focus.

2.4.3 Second Virial Coefficient

The virial expansion gives an equation of state (EOS) for low density gases. It has been shown that the virial coefficient can easily be derived from the intermolecular potential [100, 101, 102]. The second virial coefficient is related to the molecular model by [69]

$$B = -2\pi \int_0^\infty \left\langle \exp\left(-\frac{u_{ij}(r_{ij}, \boldsymbol{\omega}_i, \boldsymbol{\omega}_j)}{k_\mathrm{B}T}\right) - 1 \right\rangle_{\boldsymbol{\omega}_i, \boldsymbol{\omega}_j} r_{ij}^2 \mathrm{d}r_{ij}, \tag{19}$$

where $u_{ij}(r_{ij}, \boldsymbol{\omega}_i, \boldsymbol{\omega}_j)$ is the interaction energy between two molecules i and j, cf. Equation (19). k_B denotes Boltzmann's constant and the $\langle\rangle$ brackets indicate an average over the orientations $\boldsymbol{\omega}_i$ and $\boldsymbol{\omega}_j$ of the two molecules separated by the center of mass distance r_{ij}.

The second virial coefficient was calculated here by evaluating Mayer's f-function at 363 radii from 2.4 to 8 Å, averaging over 500^2 random orientations at each radius. The random orientations were generated using a modified Monte Carlo scheme [103]. A cut-off correction was applied for distances larger than 8 Å for the Lennard-Jones potential [72]. The electrostatic interactions need no long-range correction as they vanish by angle averaging.

3 Toxic Fluids for Process Engineering Applications

Based on mathematical representations of the intermolecular interactions, molecular simulation has strong predictive capabilities as it adequately represents structure, energetics and dynamics on the microscopic scale that govern the fluid behavior on the macroscopic scale.

In this chapter, the fluid phase behavior of hazardous chemicals which are produced on a large scale is studied. Two groups of molecules are investigated. One is the Phosgene group which includes Hydrogen chloride, Phosgene, Benzene, Chlorobenzene, Ortho-Dichlorobenzene and Toluene. The other is the Ethylene oxide group which covers Ethylene oxide, Ethylene glycol and Water.

3.1 Phosgene Group

For seven binary mixtures studied in the present work, i.e. Hydrogen chloride + Phosgene, Hydrogen chloride + Benzene, Hydrogen chloride + Chlorobenzene, Hydrogen chloride + Toluene, Phosgene + Chlorobenzene, Phosgene + Ortho-Dichlorobenzne and Phosgene + Toluene, BASF supplied a narrow base of predominantly non-public experimental data points on the bubble line. These data, typically a single point per binary system measured around ambient temperature and for compositions that are rich in the high boiling component, were used as a basis to predict the binary VLE at higher temperatures and at other compositions. Subsequently to the computations by molecular simulation, additional, also predominantly non-public experimental VLE data were supplied by BASF to assess the present predictions.

For an eighth mixture, i.e. Hydrogen chloride + Ortho-Dichlorobenzene, a strictly predictive approach was chosen. Binary VLE data for that mixture were generated here on the basis of pure substance properties alone and later on assessed by non-public experimental BASF data.

Finally, for a ninth mixture, i.e. Phosgene + Benzene, it was tested for one given temperature whether a known, but rather unusual slope of the bubble line can be predicted.

3.1.1 Pure Fluid Models

None of the molecules studied in the present work exhibits significant conformational changes. Their internal degrees of freedom were thus neglected and the molecular models were chosen to be rigid, using the most stable configuration as determined by QC.

The optimization was performed using a Newton scheme following Stoll [38, 104]. The applied method has many similarities with the one published by Bourasseau et al. [105]. It relies on a least-square minimization of a weighted fitness function that quantifies the deviations of simulation results for a given molecular model compared to reference data.

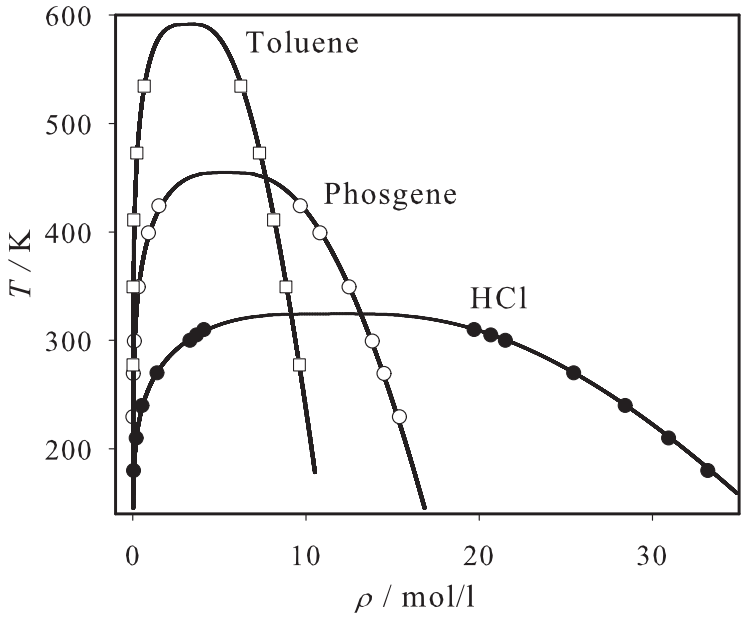

Figure 5: Saturated densities; present simulation data: ● Hydrogen chloride, ○ Phosgene, □ Toluene; correlations of experimental data [106]: —.

Correlations for vapor pressure, saturated liquid density and enthalpy of vaporization, taken from the DIPPR database [106], were used as reference data for model adjustment and evaluation. This was done even in cases where the correlations are based only on few true experimental data points, as they were regarded as best practice. The quantitative comparison between simulation results and correlations was done by applying fits to the simulation data according to Lotfi et al. [2]. The relative deviation between fit and correlation was calculated in steps of 1 K in the temperature range where simulations were performed and is denoted by "mean unsigned error" in the following.

VLE were simulated with the Grand Equilibrium method [96], the technical details are given in Appendix B. The optimized parameter sets of the new molecular models are summarized in Table 13, Appendix A.

The pure substance VLE simulation results on the basis of these optimized models are shown in absolute terms in Figures 5 to 8, where they are compared to the DIPPR correlations. Numerical simulation results for vapor pressure, saturated densities and

enthalpy of vaporization are given in Table 14, Appendix A.

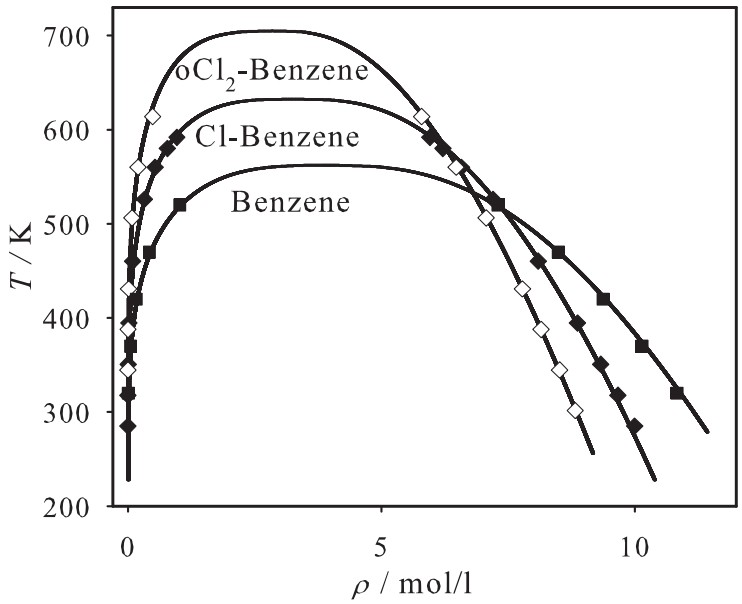

Figure 6: Saturated densities; present simulation data: ■ Benzene, ♦ Chlorobenzene, ◇ Ortho-Dichlorobenzene; correlations of experimental data [106]: —.

Figure 6 illustrates the influence of molecular size and polarity on the phase envelope in a systematic manner. Both size and polarity increase in the sequence Benzene, Chlorobenzene, Ortho-Dichlorobenzene, which is reflected by a decreasing average saturated liquid density and an increasing critical temperature.

The critical properties were determined through fits to the present VLE simulation results as suggested by Lotfi et al. [2]. The estimated uncertainties of critical temperature, critical density and critical pressure from simulation are 1, 3 and 3 %, respectively. Table 1 compares these critical properties to experimental data [107, 108, 109, 110, 111]. An excellent agreement was achieved, being almost throughout within the combined error bars.

For Hydrogen chloride, Phosgene and Benzene experimental data on the second virial coefficient are available [112, 113, 114, 115]. Figure 9 compares the predictions based on the present molecular models with these data. The agreement is very good, only at low temperatures noticeable deviations are present for the smaller two molecules.

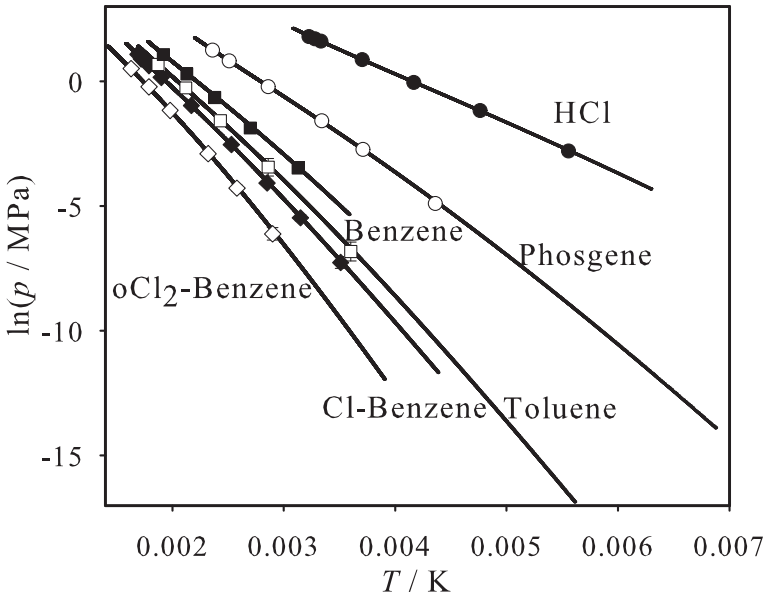

Figure 7: Vapor pressure; present simulation data: ● Hydrogen chloride, ○ Phosgene, ■ Benzene, □ Toluene, ♦ Chlorobenzene, ◇ Ortho-Dichlorobenzene; correlations of experimental data [106]: —.

Table 1: Critical properties of the pure substances on the basis of the new molecular models in comparison to recommended experimental data. The number in parentheses indicates the experimental uncertainty in the last digit.

	T_c^{sim} K	T_c^{exp} K	ρ_c^{sim} mol/l	ρ_c^{exp} mol/l	p_c^{sim} MPa	p_c^{exp} MPa	Ref.
Hydrogen chloride	324	324.65 (5)	12.2	12.34 (3)	8.3	8.31 (5)	[107]
Phosgene	454	455.0 (7)	5.1	5.40 (6)	5.7	5.35 (4)	[108]
Benzene	563	562.15 (6)	3.9	3.88 (2)	4.9	4.9 (1)	[109]
Chlorobenzene	631	632.35 (8)	3.2	3.24 (7)	4.6	4.52 (8)	[110]
Ortho-Dichlorobenzene	705	705.0 (9)	2.8	2.77 (6)	4.0	4.1 (3)	[111]
Toluene	592	591.75 (8)	3.4	3.20 (4)	4.1	4.08 (3)	[109]

In the following sections, substance specific details are discussed and the model optimization results are assessed by means of deviation plots. Thereby, models from the literature are compared to the present models as far as available.

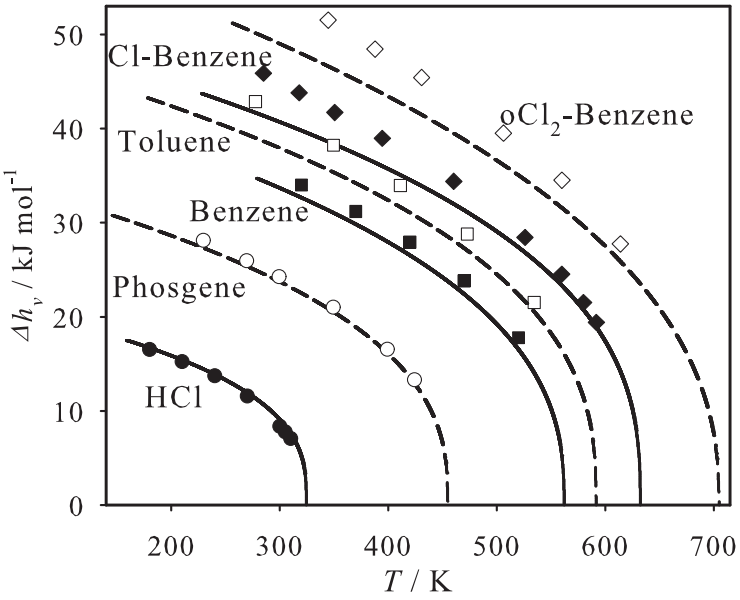

Figure 8: Enthalpy of vaporization; present simulation data: ● Hydrogen chloride, ○ Phosgene, ■ Benzene, □ Toluene, ♦ Chlorobenzene, ◇ Ortho-Dichlorobenzene; correlations of experimental data [106]: —, - -. Note that the empty symbols correspond to the dashed lines.

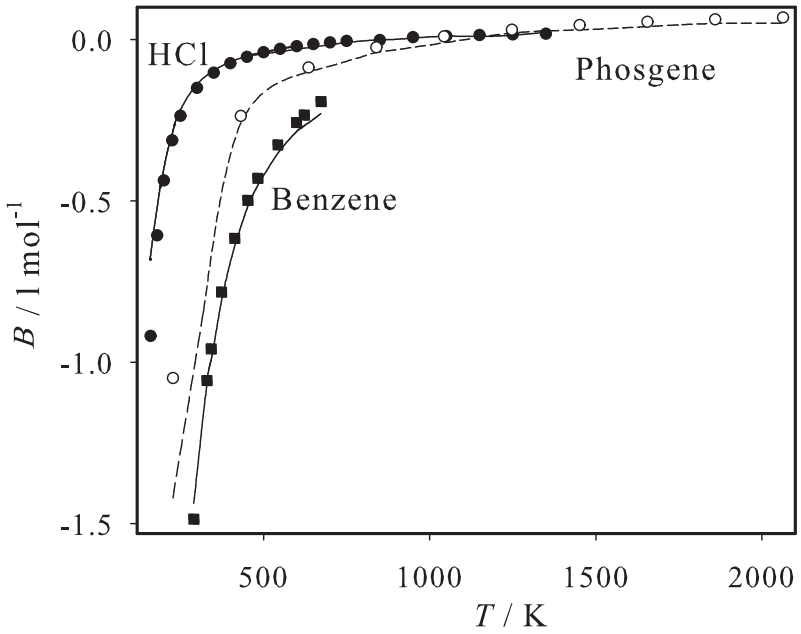

Figure 9: Second virial coefficient; present simulation data: ● Hydrogen chloride, ○ Phosgene, ■ Benzene; correlations of experimental data [112, 113, 114, 115]: —, - -.

3.1.1.1 Hydrogen Chloride

The intermolecular interactions of Hydrogen chloride were described by one Lennard-Jones site plus two point charges, being located exactly at the positions of the hydrogen atom and the chlorine atom as determined by QC. During the optimization of the model parameters to vapor pressure and saturated liquid density, the magnitude of the point charges was altered only by 3.5 %, leading to a dipole moment of 1.679 D which is thus close to the one determined by QC (1.622 D). The experimental dipole moment of Hydrogen chlorideis 1.108 D [116]. It can be argued that this elevated polar moment is necessary as the model's point charges have to cover both polarity and hydrogen bonding [117].

Figure 10 shows deviation plots between simulation and correlations, where also simulation results from Meredith et al. [118] and experimental data [107, 119] are included. A very good agreement was obtained for the present model yielding mean unsigned errors in vapor pressure, saturated liquid density and enthalpy of vaporization of 2.0, 0.4 and 4.4 %, respectively, in the temperature range from 180 to 310 K, which is about 55 to 96 % of the critical temperature. It should be pointed out that the DIPPR correlations deviate from the actual experimental data roughly to the same extent as the present simulation results. Data by Meredith et al. show a significant scatter, particularly for the saturated liquid density. The deviations are approximately one order of magnitude larger than those of this work. Note that Meredith et al. did not publish data on the enthalpy of vaporization.

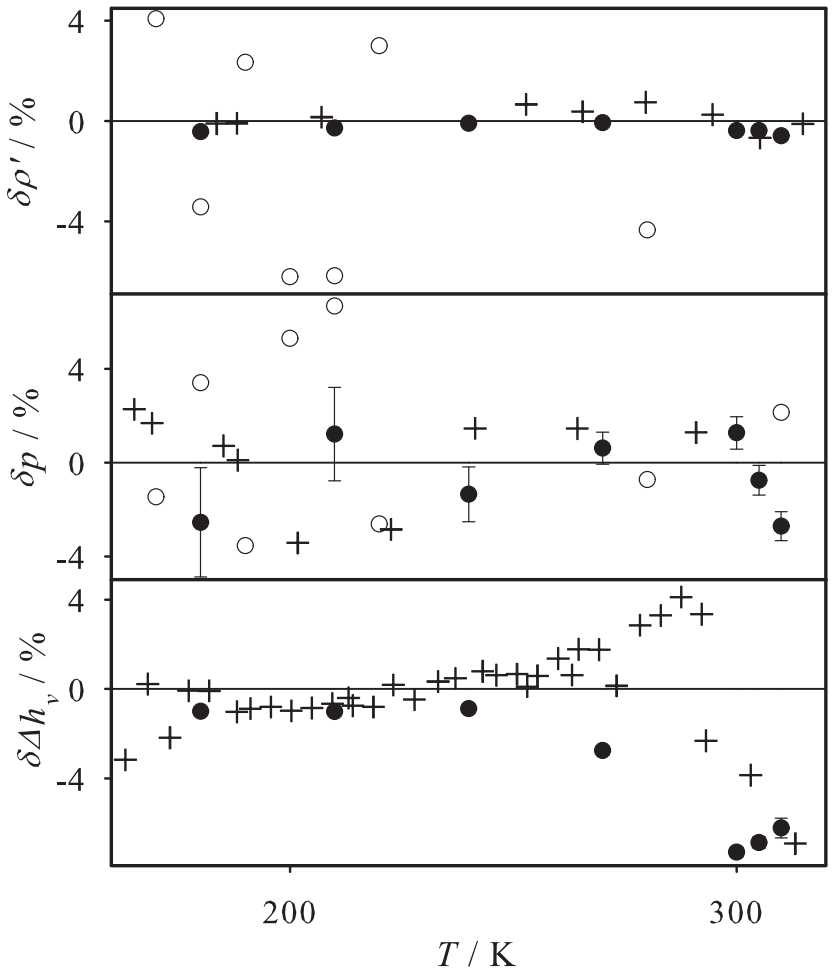

Figure 10: Relative deviations of vapor-liquid equilibrium properties from correlations of experimental data [106] ($\delta z = (z_\mathrm{i} - z_\mathrm{cor})/z_\mathrm{cor}$) for Hydrogen chloride: ● present simulation data, ○ Meredith et al. [118], + experimental data [107, 119]. Top: saturated liquid density, center: vapor pressure, bottom: enthalpy of vaporization.

3.1.1.2 Phosgene

The present Phosgene model consists of four Lennard-Jones sites, i.e. one for every atom, plus one relatively weak dipole (1.002 D) and one relatively strong quadrupole (-3.627 DÅ). Compared to the QC results, the geometry of that molecular model was slightly scaled by 0.2 %, i.e. the bond lengths were increased by that fraction. However, the polar moments had to be reduced more significantly, i.e. by -32 % and -17 % for the dipole and quadrupole moment, respectively, to achieve the optimization result. The experimental dipole moment, being 1.170 D [120], is closer to the molecular model than to the QC result..

Figure 11 presents deviation plots between simulation and correlations, including simulation results from Wu et al. [121] and experimental data [108, 122]. Again, a very good agreement was obtained for the present model, yielding mean unsigned errors in vapor pressure, saturated liquid density and enthalpy of vaporization of 2.1, 0.5 and 3.0 %, respectively, in the temperature range from 230 to 424 K, which is about 50 to 93 % of the critical temperature. There is only a single experimental data point for the saturated liquid density. This point is fully in line with the present molecular model. The experimental data for the vapor pressure deviate from the correlation in a sinusoidal fashion with extremal values of around ± 3 %, which indicates questionable fitting by DIPPR. With respect to the enthalpy of vaporization, the present simulation data exhibit an almost constant positive offset. The present model shows more reliable results than the one by Wu et al. for both saturated liquid density and vapor pressure, particularly due to lower statistical noise. No comparison between the models was possible for the enthalpy of vaporization as numerical data were not published by Wu et al.

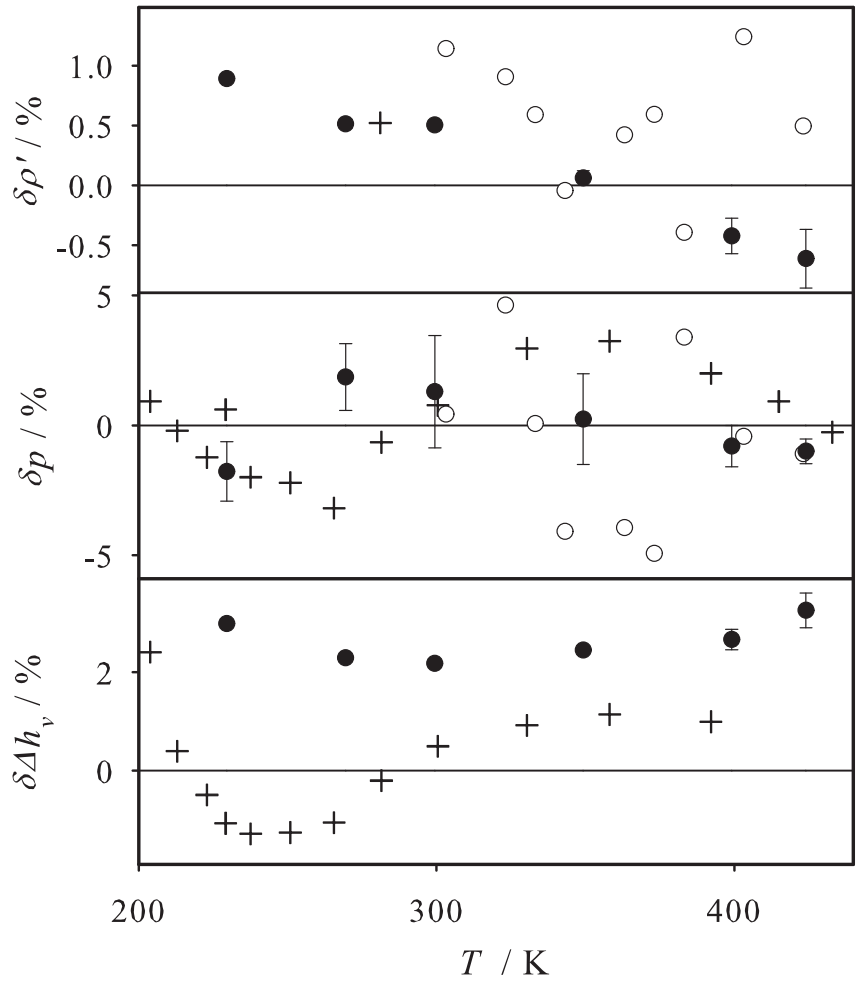

Figure 11: Relative deviations of vapor-liquid equilibrium properties from correlations of experimental data [106] ($\delta z = (z_\mathrm{i} - z_\mathrm{cor})/z_\mathrm{cor}$) for Phosgene: ● present simulation data, ○ Wu et al. [121], + experimental data [108, 122]. Top: saturated liquid density, center: vapor pressure, bottom: enthalpy of vaporization.

3.1.1.3 Benzene

Different molecular models for Benzene can be found in the literature, which are mostly based on six Lennard-Jones sites plus one quadrupole in the center of the molecule that is oriented perpendicular to the molecular plane. Initially, the same model type was chosen for this study, however, it was found to be incompatible with the Hydrogen chloride model to describe mixtures with this component. The central quadrupole of the benzene model is hardly shielded by Lennard-Jones sites so that the Hydrogen point charge of Hydrogen chloride, which is strongly attracted to it, enters into the central cavity. Eventually, this leads to an extreme pairwise electrostatic energy minimum and to the breakdown of simulation. Therefore, the quadrupole was equally divided into six parts and located on the six Lennard-Jones sites representing the methine groups, cf. Figure 12 for a graphical schematic.

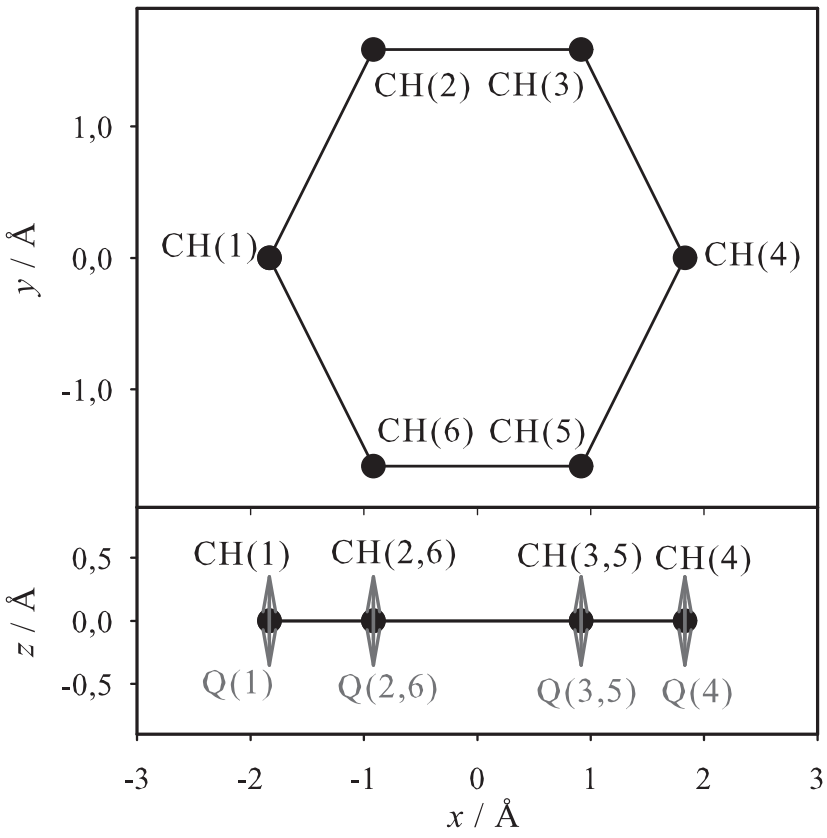

Figure 12: Coordinates of the Lennard-Jones sites for the present Benzene model.

That arrangement is also physically more sound than the initial one. Again, during the optimization process, the geometry was slightly scaled down (-0.1 %), while the total quadrupolar moment was reduced more significantly (-31 %).

Figure 13 shows the deviation plots, where also simulation results from Bonnaud et al. [123], Carrero-Mantilla [124] and Errington and Panagiotopoulos [125], Contreras-Camacho et al. [126], Wick et al. [127] as well as several sets of experimental data [109, 128, 129] are included. A very good agreement was obtained for the present model, yielding mean unsigned errors in vapor pressure, saturated liquid density and enthalpy of vaporization of 3.4, 0.4 and 5.2 %, respectively, in the temperature range from 320 to 520 K, which is about 57 to 92 % of the critical temperature.

Among the six molecular models, the one by Bonnaud et al. has the best performance for both saturated liquid density (mean unsigned error lower than 0.1 %) and enthalpy of vaporization (lower than 2 %), however, it performs poorly for the vapor pressure (about 18 %). Similarly, saturated density and enthalpy of vaporization are quite well represented by the model of Contreras-Camacho, but more significant deviations are present for the vapor pressure. The model of Errington and Panagiotopoulos performs well for both saturated liquid density (about 0.4 %) and vapor pressure (about 3 %), but its description of the enthalpy of vaporization is very poor. The model of Carrero-Mantilla describes the vapor pressure well (about 5 %), but large deviations are present for the remaining two properties. Finally, the model by Wick et al. shows an offset of about 9 % in vapor pressure and enthalpy of vaporization, whereas for the saturated liquid density a different temperature trend is present, where the two points at 500 and 525 K deviate by more than 1.5 %. Note that in the deviation plot 13 a substantial number of VLE simulation data points by the other authors is out of scale.

The present modeling approach was independent on the work by Contreras-Camacho et al. [126], nonetheless the resulting model parameters for geometry and Lennard-Jones sites are very similar. The difference is less than 0.02 Å for the site positions and the Lennard-Jones size parameter σ as well as less than 2 % for the Lennard-Jones energy parameter ϵ. The difference between the two models thus mainly lies in the different treatment of the electrostatics, which was not explicitly modeled by Contreras-Camacho et al.

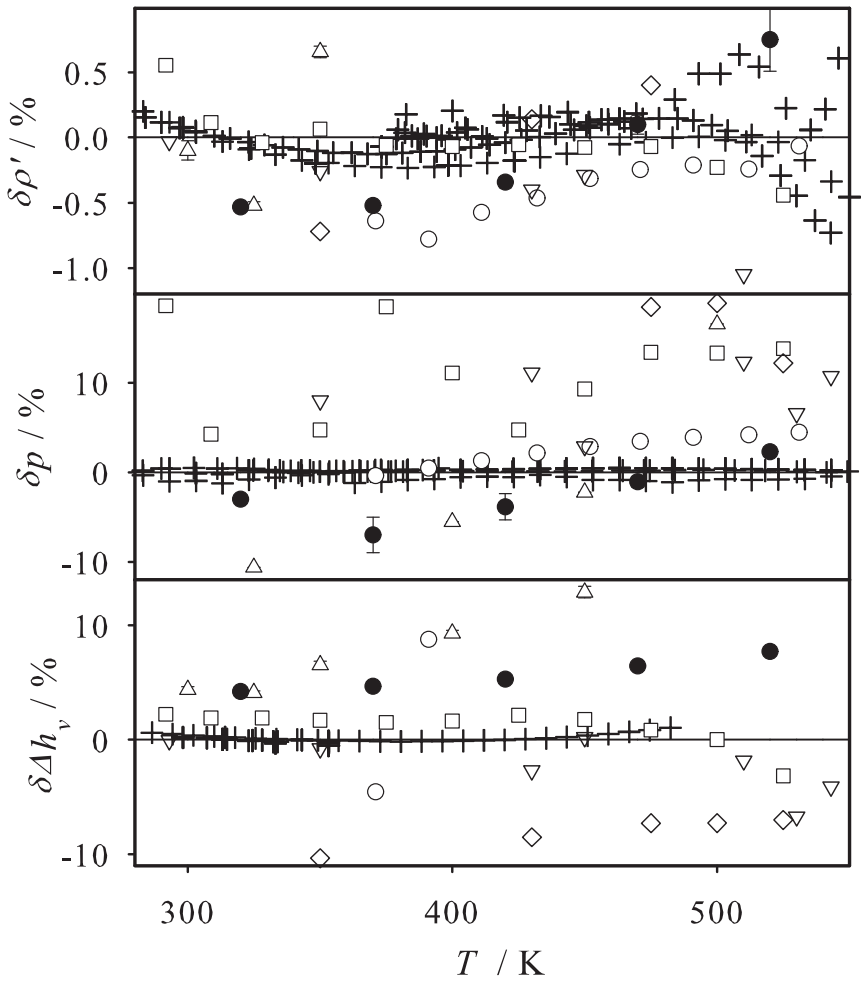

Figure 13: Relative deviations of vapor-liquid equilibrium properties from correlations of experimental data [106] ($\delta z = (z_\mathrm{i} - z_\mathrm{cor})/z_\mathrm{cor}$) for Benzene: ● present simulation data, □ Bonnaud et al. [123], △ Carrero-Mantilla [124], ○ Errington and Panagiotopoulos [125], ▽ Contreras-Camacho et al. [126], ◇ Wick et al. [127], + experimental data [109, 128, 129]. Top: saturated liquid density, center: vapor pressure, bottom: enthalpy of vaporization.

3.1.1.4 Chlorobenzene

For Chlorobenzene, seven Lennard-Jones sites plus one dipole in the molecular plane and five quadrupoles perpendicular to it were chosen. Due to the high electronegativity of the Chlorine atom, the dipole moment is quite strong (2.170 D), whereas the total quadrupole moment amounts to -9.096 DÅ. The quadrupole was again equally distributed onto the methine groups to allow for a compatibility with Hydrogen chloride in the mixture. Compared to the QC results, the geometry was scaled down by -0.8 %, whereas the polar moments were increased by 3.4 % (dipole) and 6.5 % (quadrupole), respectively. In this case, the experimental dipole moment is 1.782 D [130].

Figure 14 shows the deviation plots between simulation and correlations including experimental data [110, 131, 132]. A good agreement was obtained, yielding mean unsigned errors in vapor pressure, saturated liquid density and enthalpy of vaporization of 5.0, 0.9 and 7.9 %, respectively, in the temperature range from 285 to 592 K, which is about 45 to 94 % of the critical temperature. While the vapor pressure agrees with the experiment almost throughout within its statistical uncertainty, particularly the enthalpy of vaporization shows a significant positive offset.

No VLE data based on molecular models were found in the literature for this substance.

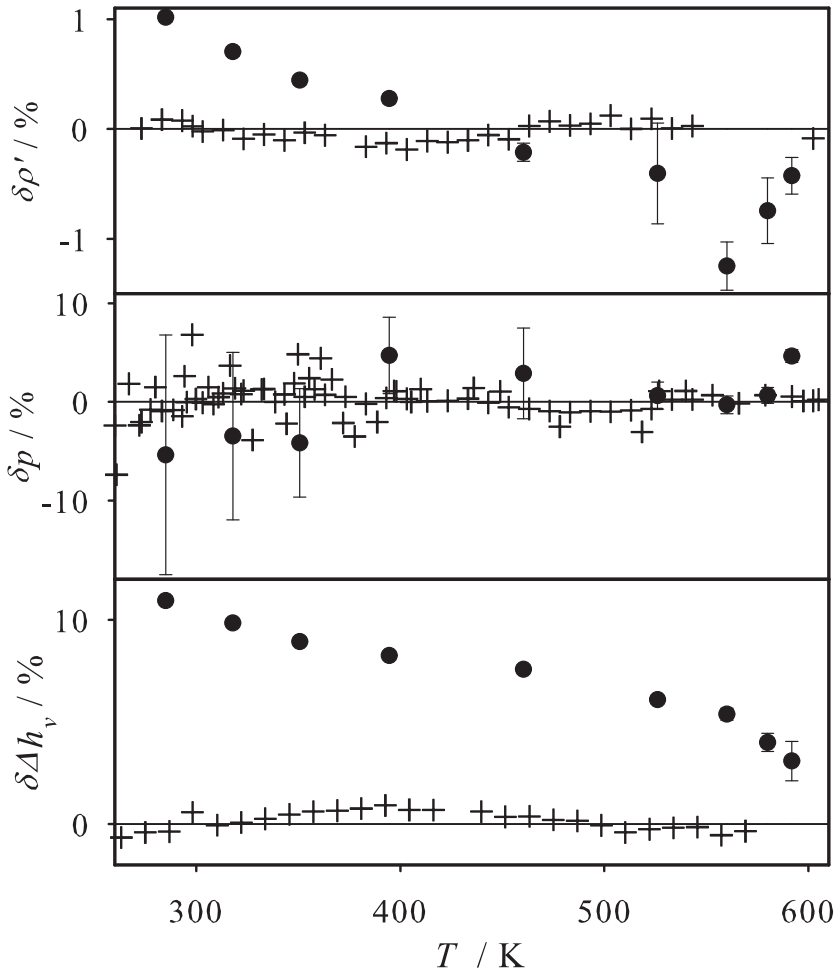

Figure 14: Relative deviations of vapor-liquid equilibrium properties from correlations of experimental data [106] ($\delta z = (z_\mathrm{i} - z_\mathrm{cor})/z_\mathrm{cor}$) for Chlorobenzene: ● present simulation data, + experimental data [110, 131, 132]. Top: saturated liquid density, center: vapor pressure, bottom: enthalpy of vaporization.

3.1.1.5 Ortho-Dichlorobenzene

Eight Lennard-Jones sites plus four quadrupoles and one strong dipole (3.249 D) were used to describe the intermolecular interactions of Ortho-Dichlorobenzene. The total quadrupole moment of 8.788 DÅ was equally distributed onto the four methine groups due to the reasons mentioned above. Compared to the QC results, geometry, dipole and quadrupole moments of the present Ortho-Dichlorobenzene model were slightly scaled by -1.4, 1.6 and 0.2 %, respectively. The experimental dipole moment of 2.51 D [133] compares well with the model value.

Figure 15 shows the deviation plots between simulation and correlations, where two sets of experimental data [111, 134] are included. A good agreement was obtained, yielding mean unsigned errors in vapor pressure, saturated liquid density and enthalpy of vaporization of 6.4, 0.5 and 9.5 %, respectively, in the temperature range from 345 to 614 K, which is about 50 to 87 % of the critical temperature. Both for vapor pressure and saturated liquid density, the simulation data agree well with the experiment in the range where measurements were made. However, for the enthalpy of vaporization, a significant and almost constant offset is present.

No VLE data based on molecular models were found in the literature for this substance.

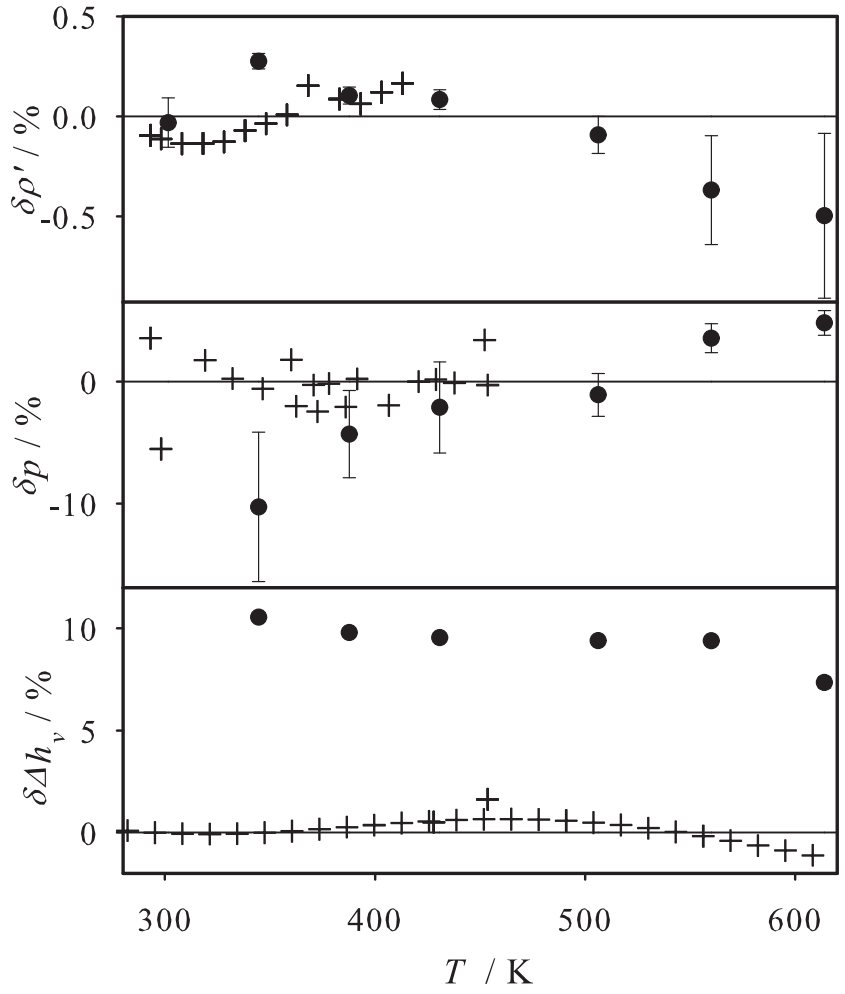

Figure 15: Relative deviations of vapor-liquid equilibrium properties from correlations of experimental data [106] ($\delta z = (z_\mathrm{i} - z_\mathrm{cor})/z_\mathrm{cor}$) for Ortho-Dichlorobenzene: ● present simulation data, + experimental data [111, 134]. Top: saturated liquid density, center: vapor pressure, bottom: enthalpy of vaporization.

3.1.1.6 Toluene

The present Toluene model is composed of seven Lennard-Jones sites plus five quadrupoles and one weak dipole (0.440 D). In contrast to Chlorobenzene and Ortho-Dichlorobenzene, the dipole is oriented from the methyl group towards the center of the molecule. Compared to the QC results, geometry, dipole and quadrupole moments were marginally scaled by -0.6, 0.5 and 0.3 %, respectively. The experimental dipole moment is 0.375 D [135].

Figure 16 shows deviation plots between simulation and correlations. The deviation plots include simulation results from Nieto-Draghi et al. [136] and Contreras-Camacho et al. [137] as well as two sets of experimental data [109, 128]. A good agreement was obtained for the present model, yielding mean unsigned errors in vapor pressure, saturated liquid density and enthalpy of vaporization of 3.9, 0.3 and 7.3 %, respectively, in the temperature range from 278 to 534 K, which is about 47 to 90 % of the critical temperature. The present model leads to more accurate results than the model by Nieto-Draghi et al. for both saturated liquid density and vapor pressure. Nevertheless, the model from Nieto-Draghi et al. shows a much better performance for the enthalpy of vaporization. The model of Contreras-Camacho et al. is of comparable quality, saturated liquid density and enthalpy of vaporization are well represented, whereas significant deviations are present for the vapor pressure.

The geometry of the present toluene model is very similar to the one by Contreras-Camacho et al. [137] (the difference is less than 0.02 Å), which can well be understood as both are based on QC results. Note that the model by Contreras-Camacho et al. does not consider the electrostatic interactions explicitly.

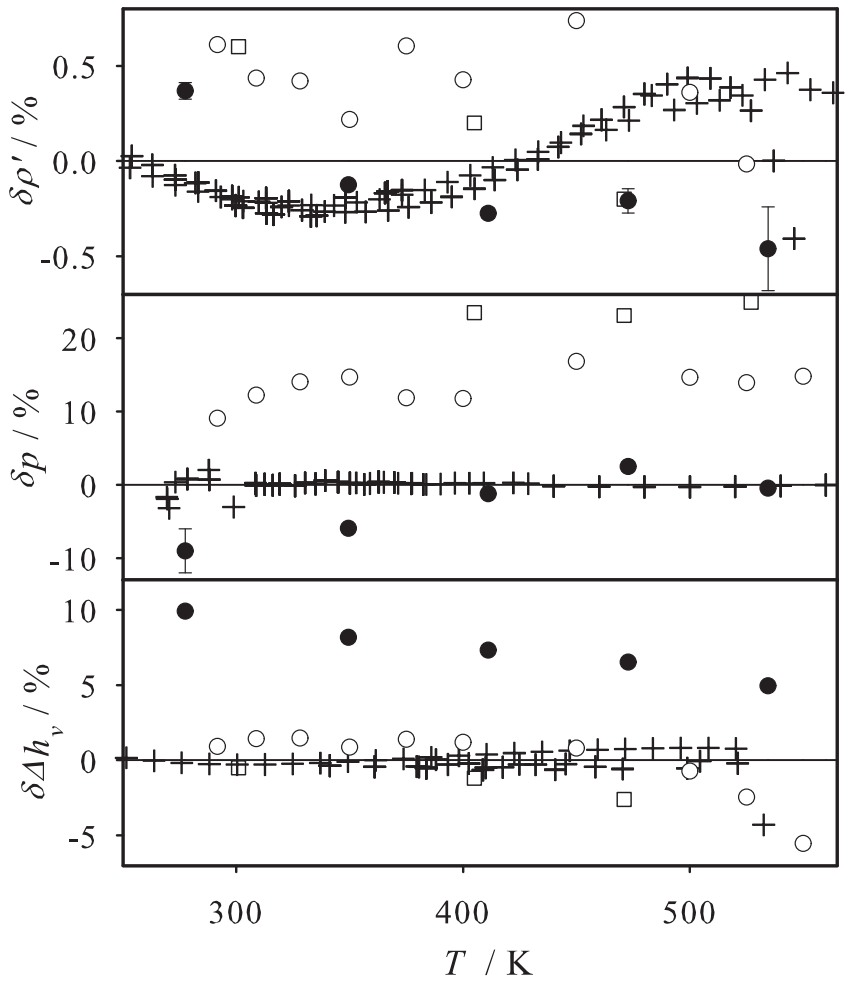

Figure 16: Relative deviations of vapor-liquid equilibrium properties from correlations of experimental data [106] ($\delta z = (z_\mathrm{i} - z_\mathrm{cor})/z_\mathrm{cor}$) for Toluene: ● present simulation data, ○ Nieto-Draghi et al. [136], □ Contreras-Camacho et al. [137], + experimental data [109, 128]. Top: saturated liquid density, center: vapor pressure, bottom: enthalpy of vaporization.

3.1.2 Binary Vapor-Liquid Equilibria

Based on the six pure substance models developed in this study, the VLE of nine zeotropic binary mixtures were simulated. These are Hydrogen chloride + (Benzene, Chlorobenzene, Ortho-Dichlorobenzene and Toluene) and Phosgene with the same four solvents as well as Hydrogen chloride + Phosgene.

The results are presented here in pressure vs. mole fraction phase diagrams, cf. Figures 17 to 25, where the pure substance vapor pressure of the molecular models is indicated as well. Full numerical VLE simulation data are given in Table 15, Appendix A, which also contains the saturated densities and the heat of vaporization from simulation. Because such data from experiment are not available for comparison, they are not discussed here.

For all studied mixtures, experimental bubble point data are available for adjustment or comparison. Only for the mixture Hydrogen chloride + Phosgene, VLE data were measured in the full composition range, while for the remaining mixtures, experimental data are available only for compositions which are rich of the high boiling substance. To our knowledge, experimental dew point data were not published at all for any of the studied mixtures.

The experimental approach followed at BASF in this project was the following: In the pressure range below 0.5 MPa Hydrogene chloride or Phosgene were transferred into the solvent and the mass was determined volumetrically or by weighing. The composition of the liquid mixture was corrected by the calculated amounts of the components in the vapor phase. In the pressure range above 0.5 MPa, Hydrogene chloride was filled into a visual cell and the mass was also determined volumetrically or by weighing. The amount of solvent, added into the cell in order to measure a bubble point, was calculated form the volume displacement in a calibrated spindle press. The experimental uncertainty of the equilibrium data is estimated to be 0.1 K and 2 % relative error in composition and vapor pressure.

For orientation and comparison, the results of the Peng-Robinson EOS [138] with adjusted binary parameter k_{ij} are also shown. The EOS was optimized to the same state point as the molecular model.

Table 2: Binary interaction parameter ξ, experimental bubble point used for the adjustment with reference, simulation results with adjusted binary parameter ξ of the molecular model and binary parameter k_{ij} of the Peng-Robinson EOS. The number in parentheses indicates the statistical uncertainty in the last digit.

Mixture (A + B)	ξ	T	x_A	p^{exp}	p^{sim}	y_A^{sim}	k_{ij}
		K	mol/mol	MPa	MPa	mol/mol	
Hydrogen chloride + Phosgene							
	0.751	266.15	0.39	0.84 [139]	0.84 (9)	0.95 (1)	0.020
Hydrogen chloride + Benzene							
	1.112	293.15	0.043	0.101 [140]	0.104 (2)	0.93 (1)	-0.077
Hydrogen chloride + Chlorobenzene							
	1.020	283.15	0.094	0.267 [140]	0.266 (9)	1.000 (0)	0.000
Hydrogen chloride + Ortho-Dichlorobenzene							
	1	393.15	0.133		1.84 (2)	0.9920 (8)	0.000
Hydrogen chloride + Toluene							
	0.981	293.15	0.048	0.101 [140]	0.103 (2)	0.983 (4)	-0.075
Phosgene + Benzene							
	0.960	293.15	0.370	0.086 [141]	0.085 (3)	0.935 (7)	0.050
Phosgene + Chlorobenzene							
	0.990	323.15	0.142	0.065 [140]	0.067 (3)	0.94 (1)	0.006
Phosgene + Ortho-Dichlorobenzene							
	1.000	363.15	0.080	0.103 [140]	0.105 (5)	0.97 (1)	0.020
Phosgene + Toluene							
	0.990	308.15	0.242	0.072 [140]	0.069 (3)	0.952 (5)	0.010

3.1.2.1 Hydrogen Chloride + Phosgene

Figure 17 shows the VLE of Hydrogen chloride + Phosgene at 266.15 and 423.15 K from experiment, simulation and Peng-Robinson EOS. At 266.15 K, the mixture is sub-critical, the phase envelope is wide with a straight bubble line and a concave dew line. Hydrogen chloride is supercritical at 423.15 K. No experimental data are available for the high temperature so that the simulation data can only be compared to the Peng-Robinson EOS.

The binary parameters $\xi = 0.751$ and $k_{ij} = 0.02$ were adjusted to the vapor pressure measured by Gillespie et al. [139] at 266.15 K for a liquid mole fraction $x_\mathrm{HCl} = 0.39$ mol/mol. In the Phosgene-rich region at 266.15 K, the simulation results agree well with both the experimental data and the Peng-Robinson EOS. However, with increasing mole fraction of Hydrogen chloride, the statistical uncertainty strongly increases so that predictions from simulation in the Hydrogen chloride-rich region were technically not feasible.

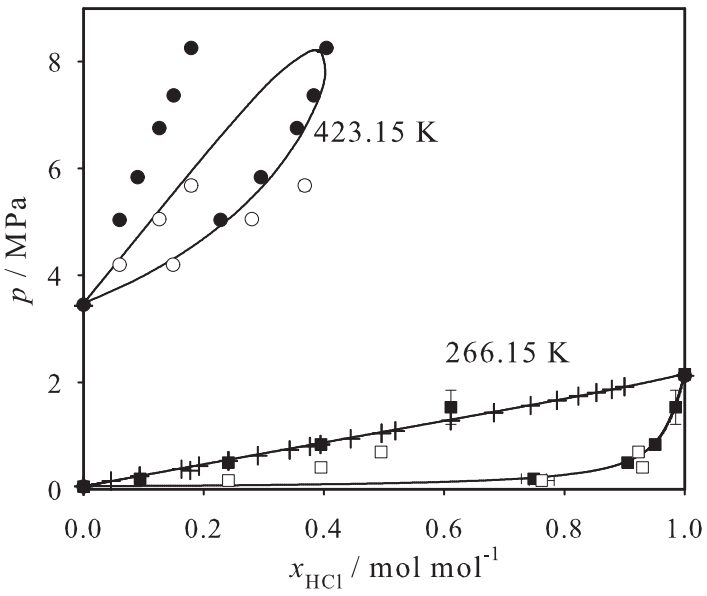

Figure 17: Vapor-liquid phase diagram of Hydrogen chloride + Phosgene at 266.15 and 423.15 K: + experimental data [139]; ■, ● present simulation data with ξ=0.751; □, ○ present simulation data with ξ=1; — Peng-Robinson EOS with k_{ij}=0.02.

It can be seen in Figure 17 that the predictions at 423.15 K obtained by molecular simulation and those from the Peng-Robinson EOS do not agree, although for the binary parameter adjustment in both cases the same low temperature data point was used. As there are no high temperature experimental data for this system, no ranking of the methods is possible. For comparison, also a prediction by molecular simulation with $\xi = 1$ is included in Figure 17, which is assumed to be less reliable than that with the adjusted ξ. For $\xi = 1$ the results obtained with molecular simulation are close to those from the Peng-Robinson EOS on the bubble line, but not on the dew line. Note also that the simulation results for $\xi = 1$ strongly deviate from the experimental bubble points at the low temperature.

3.1.2.2 Hydrogen Chloride + Benzene

Figure 18 depicts the VLE of Hydrogen chloride + Benzene at 293.15 and 393.15 K. The bubble point vapor pressure supplied by BASF at ambient temperature (293.15 K) in the Benzene-rich region (x_{HCl} = 0.043 mol/mol) was taken to adjust the binary parameter of the molecular model ξ = 1.112 and of the Peng-Robinson EOS k_{ij} = -0.077.

The simulation results are in very good agreement with the Peng-Robinson EOS for both temperatures, some deviations are present in the extended critical region at 393.15 K. The models consistently predict a concave bubble line. These data sets are supported by the experimental bubble point at 393.15 K, cf. Figure 18. Please note that this experimental bubble point was not considered in the fitting procedure, it was supplied after the calculations.

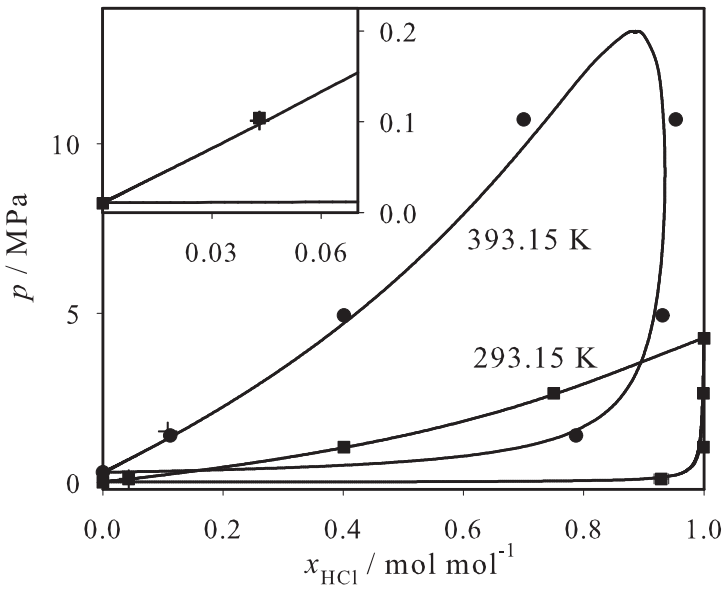

Figure 18: Vapor-liquid phase diagram of Hydrogen chloride + Benzene at 293.15 and 393.15 K: + experimental data [140]; ■, ● present simulation data with ξ=1.112; — Peng-Robinson EOS with k_{ij}=-0.077. Inset: magnified view at the Benzene-rich region at 293.15 K.

3.1.2.3 Hydrogen Chloride + Chlorobenzene

In Figure 19, the VLE of Hydrogen chloride + Chlorobenzene at 283.15, 393.15 and 423.15 K is presented. Here, the 283.15 K isotherm is sub-critical, for the other two temperatures Hydrogen chloride is supercritical.

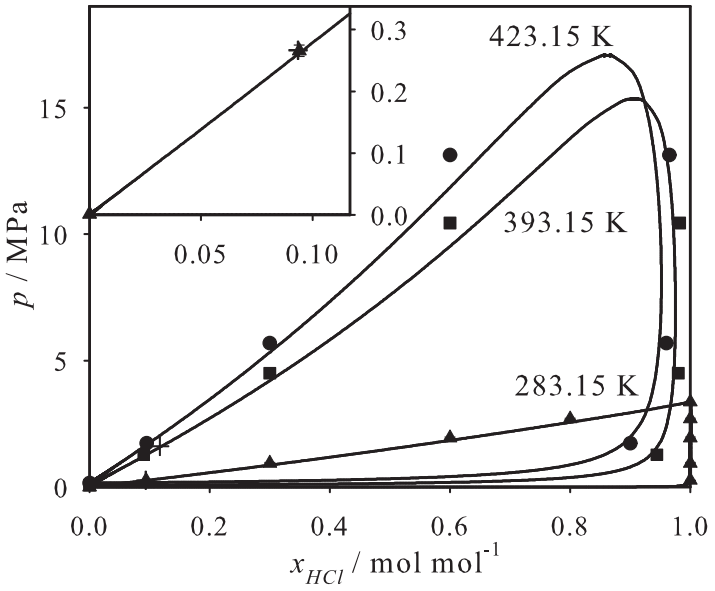

Figure 19: Vapor-liquid phase diagram of Hydrogen chloride + Chlorobenzene at 283.15, 393.15 and 423.15 K: + experimental data [140]; ▲, ■, ● present simulation data with ξ=1.020; — Peng-Robinson EOS with k_{ij}=0. Inset: magnified view at the Chlorobenzene-rich region at 283.15 K.

Both ξ and k_{ij} were adjusted in the Chlorobenzene-rich composition range (x_{HCl} = 0.094 mol/mol) at 283.15 K, where one experimental bubble point was made available by BASF. The binary parameter of the molecular mixture model is ξ = 1.020 and the one of the Peng-Robinson EOS is zero. The simulation results and those from the Peng-Robinson EOS are consistent, except in the extended critical region of the mixture, where some deviations occur. Again, both models predict a concave bubble line at elevated temperatures. Furthermore, the dew line at 283.15 K indicates that the saturated vapor contains almost exclusively Hydrogen chloride. The subsequently supplied experimental bubble point at 393.15 K, cf. Figure 19, supports again both models.

3.1.2.4 Hydrogen Chloride + Ortho-Dichlorobenzene

The mixture Hydrogen chloride + Ortho-Dichlorobenzene is a unique case in this study, as no experimental VLE data were available during the model development. Figure 20 shows the isotherm 393.15 K. Hydrogen chloride is supercritical at this temperature and the dew line is very close to pure Hydrogen chloride. Without experimental data for adjustment, $\xi = 1$ and $k_{ij} = 0$ were adopted for the molecular model and the Peng-Robinson EOS, respectively.

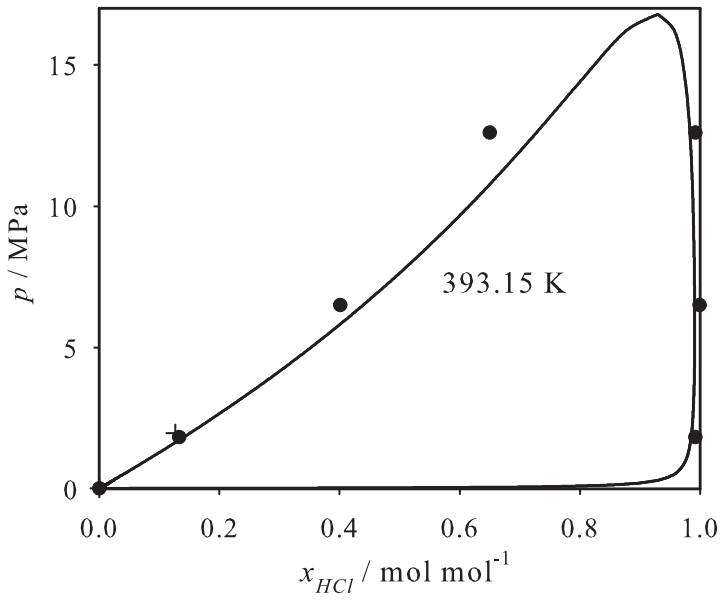

Figure 20: Vapor-liquid phase diagram of Hydrogen chloride + Ortho-Dichlorobenzene at 393.15 K: + experimental data [140]; ● present simulation data with ξ=1; — Peng-Robinson EOS with k_{ij}=0.

The results of the two models are generally in good agreement, however, with increasing deviations in the extended critical region. Again, both models predict a concave bubble line. The subsequently supplied experimental bubble point is in very good agreement, cf. Figure 20, particularly with the simulation data.

3.1.2.5 Hydrogen Chloride + Toluene

Figure 21 shows the VLE of Hydrogen chloride + Toluene for 293.15 and 393.15 K. For this mixture a single experimental bubble point at ambient temperature (x_{HCl} = 0.048 mol/mol) was made available by BASF for the adjustment of the binary parameters (ξ = 0.981 and k_{ij} = -0.075).

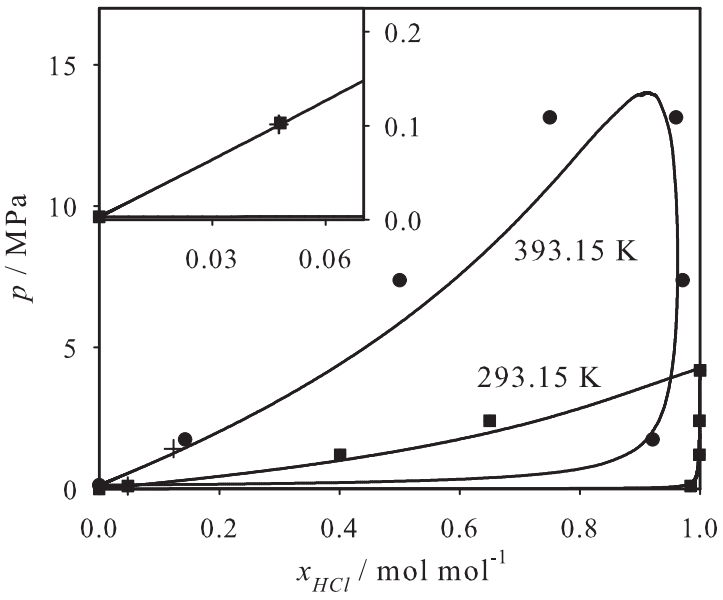

Figure 21: Vapor-liquid phase diagram of Hydrogen chloride + Toluene at 293.15 and 393.15 K: + experimental data [140]; ■, ● present simulation data with ξ=0.981; — Peng-Robinson EOS with k_{ij}=-0.075. Inset: magnified view at the Toluene-rich region at 293.15 K.

Simulation results and Peng-Robinson EOS show similar trends, significant deviations are present for the higher temperature, especially on the bubble line approaching the critical region. The bubble line is again concave, as for all mixtures containing Hydrogen chloride studied in this work. Figure 21 presents one additional subsequently supplied bubble point at 393.15 K that supports the results of both models.

3.1.2.6 Phosgene + Benzene

In Figure 22, another topology of the two-phase envelope can be seen for the mixture Phosgene + Benzene. At ambient temperature (293.15 K), Phosgene + Benzene has a binary vapor pressure which is close to ambient conditions, both components are sub-critical and the bubble line is S-shaped.

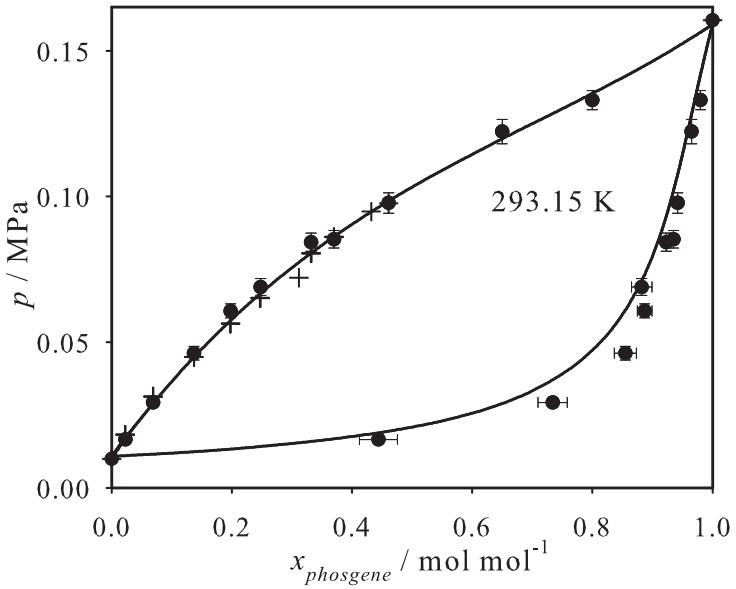

Figure 22: Vapor-liquid phase diagram of Phosgene + Benzene at 293.15 K: + experimental data [141]; ● present simulation data with ξ=0.960; — Peng-Robinson EOS with k_{ij}=0.05.

The publicly available experimental data at this temperature by Kireev et al. [141] are ten bubble points in the Benzene-rich region. The binary parameters $\xi = 0.960$ and $k_{ij} = 0.05$ were adjusted at 293.15 K and $x_{\text{Phosgene}} = 0.37$ mol/mol. Both the simulation results and the Peng-Robinson EOS match almost perfectly with the experimental data, but the phase envelope from simulation is a little wider than the one from the EOS.

3.1.2.7 Phosgene + Chlorobenzene

The VLE of Phosgene + Chlorobenzene is presented in Figure 23 at 323.15, 423.15 and 448.15 K. Experimental data on the bubble line supplied by BASF at 323.15 K in the Chlorobenzene-rich region ($x_{\text{Phosgene}} = 0.234$ mol/mol) were taken for the optimization of the models, yielding $\xi = 0.990$ and $k_{ij} = 0.006$.

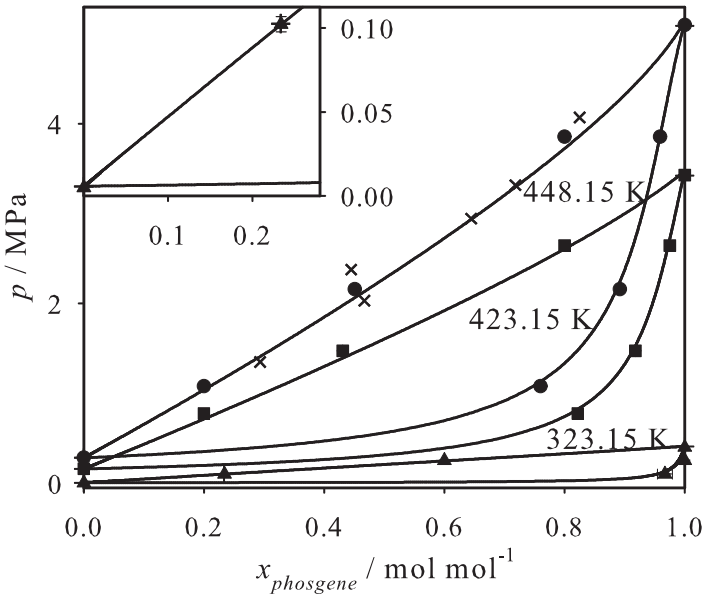

Figure 23: Vapor-liquid phase diagram of Phosgene + Chlorobenzene at 323.15, 423.15 and 448.15 K: + experimental data [140]; × experimental data [142]; ▲, ■, ● present simulation data with ξ=0.990; —Peng-Robinson EOS with k_{ij}=0.006. Inset: magnified view at the Chlorobenzene-rich region at 323.15 K.

For this mixture, Peng-Robinson EOS and simulation results agree very well for all three temperatures on the bubble line as well as on the dew line. Both models predict a concave bubble line. Audette et al. [142] determined the bubble line at 448 K, cf. Figure 23. Considering the obvious scatter of that experimental data, the results of both models studied here are well supported.

3.1.2.8 Phosgene + Ortho-Dichlorobenzene

Figure 24 shows the wide VLE envelope of the mixture Phosgene + Ortho-Dichlorobenzene at 343.15 and 363.15 K. The dew lines are very close to the low boiling pure substance (Phosgene) in this case. One experimental bubble point at 363.15 K and $x_{\text{Phosgene}} = 0.080$ mol/mol was made available by BASF for this mixture. No adjustment was necessary for the molecular model as the vapor pressure predicted with $\xi = 1$ matches the experimental number well. The adjustment of the binary parameter of the EOS yielded $k_{ij} = 0.02$.

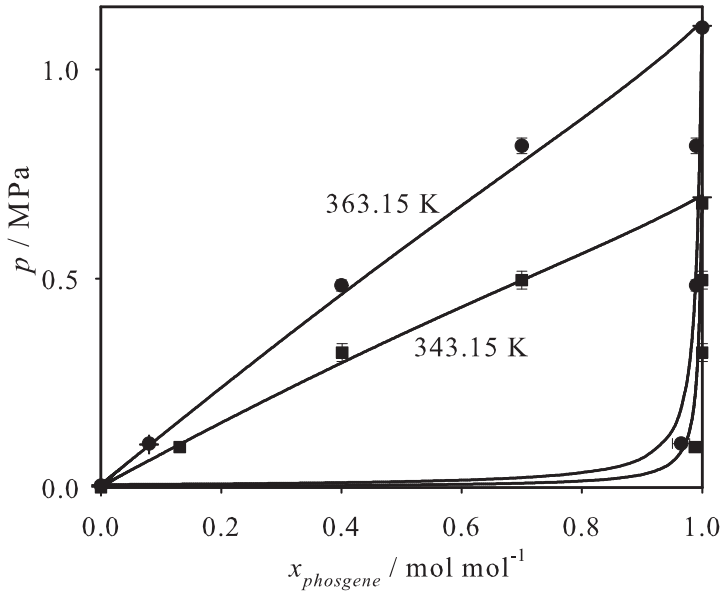

Figure 24: Vapor-liquid phase diagram of Phosgene + Ortho-Dichlorobenzene at 343.15 and 363.15 K: + experimental data [140]; ■, ● present simulation data with ξ=1; — Peng-Robinson EOS with k_{ij}=0.02.

A very good agreement between simulation results and Peng-Robinson EOS on both the bubble line and the dew line was found throughout. However, no additional experimental VLE data are available for this mixture for an assessment, but based on the results discussed above, it can be expected that the predictions for this mixture are reliable. The fact that the predictions from the EOS and those from molecular simulation, hence from two structurally different methods, agree well gives additional confidence.

3.1.2.9 Phosgene + Toluene

The VLE of Phosgene + Toluene is presented at 308.15, 423.15 and 448.15 K in Figure 25. One experimental bubble point was made available by BASF at 308.15 K in the Toluene-rich region. The binary parameters $\xi = 0.990$ and $k_{ij} = 0.01$ were adjusted at this temperature and $x_{\mathrm{Phosgene}} = 0.102$ mol/mol.

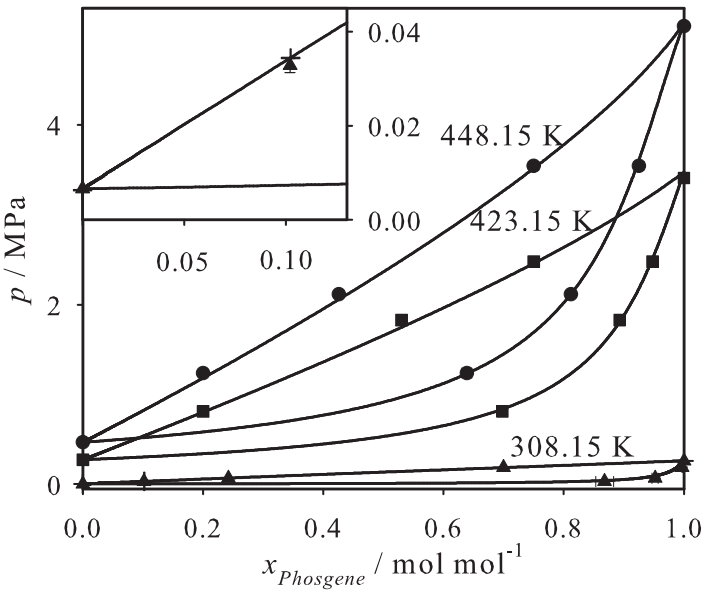

Figure 25: Vapor-liquid phase diagram of Phosgene + Toluene at 308.15, 423.15 and 448.15 K: + experimental data [140]; ▲, ■, ● present simulation data with ξ=0.990; — Peng-Robinson EOS with k_{ij}=0.01. Inset: magnified view at the Toluene-rich region at 308.15 K.

Here, throughout an almost perfect agreement between the simulation results and the Peng-Robinson EOS was found on the bubble line and on the dew line. As before, unfortunately no additional VLE data are available for a further assessment but it can be expected that the results are reliable.

3.2 Ethylene Oxide Group

Key components in the production of Polyethylene glycol (PEG) are Ethylene oxide, Ethylene glycol and Water. Knowledge on VLE of binary mixtures of those compounds is crucial for the design and optimization of thermal separation operations. In this section, the models of three pure substances are presented here as well as their binary VLE mixtures. Furthermore, the gas solubility of Ethylene oxide in Water was also predicted here.

3.2.1 Pure Fluid Models

Molecular models for Ethylene oxide, Ethylene glycol and Water are presented here. The latter two models were newly developed, whereas the one for Ethylene oxide was taken from Eckl et al. [143]. The optimization strategy of the two new models was analogous to the one presented in Section 3.1.1. The pure substance VLE simulation results on the basis of these optimized models are shown in absolute terms in Figures 26 to 28, where they are compared to the DIPPR correlations [106].

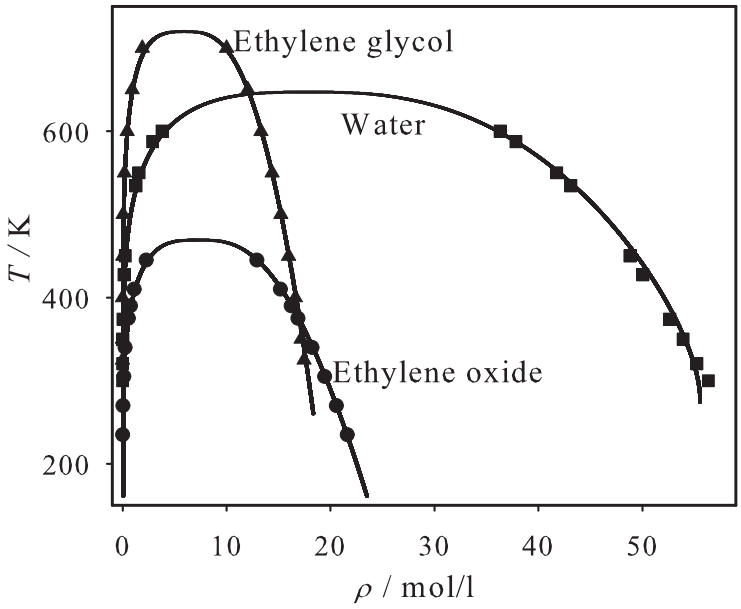

Figure 26: Saturated densities; present simulation data: ● Ethylene oxide, ▲ Ethylene glycol, ■ Water; — correlations of experimental data [106].

Numerical simulation results for vapor pressure, saturated densities and enthalpy of vaporization are given in Table 17, Appendix A. The critical properties were determined

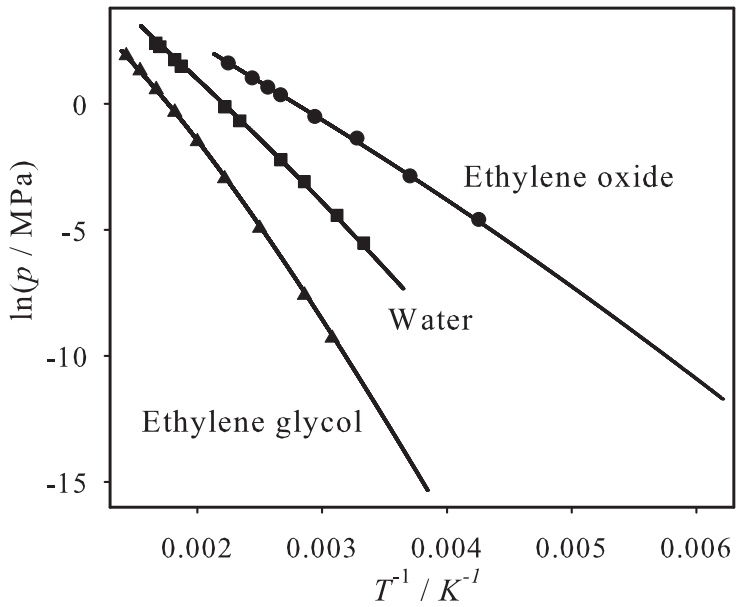

Figure 27: Vapor pressure; present simulation data: ● Ethylene oxide, ▲ Ethylene glycol, ■ Water; — correlations of experimental data [106].

through fits to the present VLE simulation results as suggested by Lotfi et al. [2]. The estimated uncertainties of critical temperature, critical density and critical pressure from simulation are 1, 3 and 3 %, respectively. Table 3 compares these critical properties to experimental data [143, 144, 145, 146, 147, 148, 149, 150]. An excellent agreement was achieved, being almost throughout within the combined error bars.

Table 3: Critical properties of the pure substances on the basis of the present molecular models in comparison to recommended experimental data.

	T_c^{sim} K	T_c^{exp} K	ρ_c^{sim} mol/l	ρ_c^{exp} mol/l	p_c^{sim} MPa	p_c^{exp} MPa	Ref.
Ethylene oxide	469.55	469.15	7.1840	7.1278	7.211	7.190	[143]
Ethylene glycol	722.00	720.00	5.87	5.92	8.3	8.257	[144, 145, 146, 147]
Water	649.30	647.10	17.474	17.874	21.975	22.064	[148, 149, 150]

For Ethylene glycol and Water experimental data on the second virial coefficient are available [149, 151]. Figure 29 compares the predictions based on the present molecular models with these data. The agreement is very good for the Water model, but the Ethylene glycol model shows significant deviations at high temperatures. These can be attributed to the rigid nature of the molecular model, which does not cover any conformational changes

that play an increasing role under these conditions.

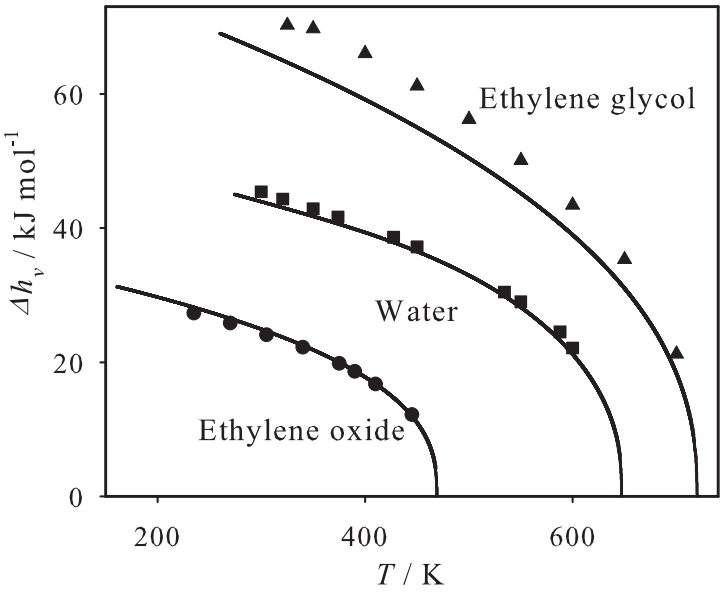

Figure 28: Enthalpy of vaporization; present simulation data: ● Ethylene oxide, ▲ Ethylene glycol, ■ Water; — correlations of experimental data [106].

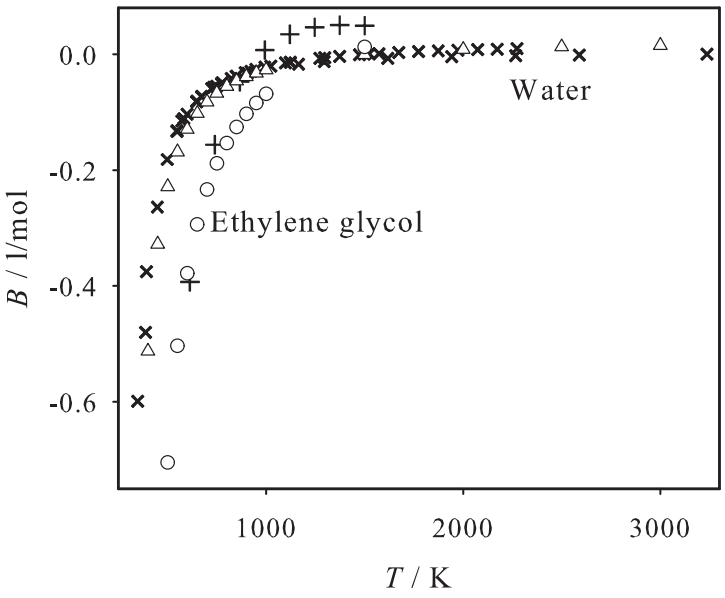

Figure 29: Second virial coefficient; Ethylene glycol: ○ present model, + experimental data [152]; Water: △ present model, × experimental data [149, 151].

3.2.1.1 Ethylene Oxide

The employed Ethylene oxide model consists of three Lennard-Jones sites (one for each methylene (CH_2) group and one for the oxygen atom) plus one dipole. It was taken from previous work of our group [143] that was the first entry in the 2007 Industrial Fluid Properties Simulation Challenge [6]. This model yields mean unsigned errors in vapor pressure, saturated liquid density and enthalpy of vaporization of 1.5 %, 0.4 % and 1.8 %, respectively. For further details the reader is referred to the original publication [143].

3.2.1.2 Ethylene Glycol

Ethylene glycol is an organic compound widely used as an automotive antifreeze agent and as a precursor to polymers. In its pure form, it is an odorless, colorless, syrupy, liquid which is toxic such that ingestion can be lethal. An important factor in modeling Ethylene glycol is its strong hydrogen bonding due to the two hydroxyl groups. The intermolecular interactions were described by four Lennard-Jones sites plus six point charges, being located exactly at the positions of the Hydrogen atoms, Oxygen atoms and methyl groups, where all sites are situated in a plane, cf. Figure 30. The geometric structure was calculated by QC and the initial magnitudes of the six point charges were taken from the Ethanol model of Schnabel et al. [153].

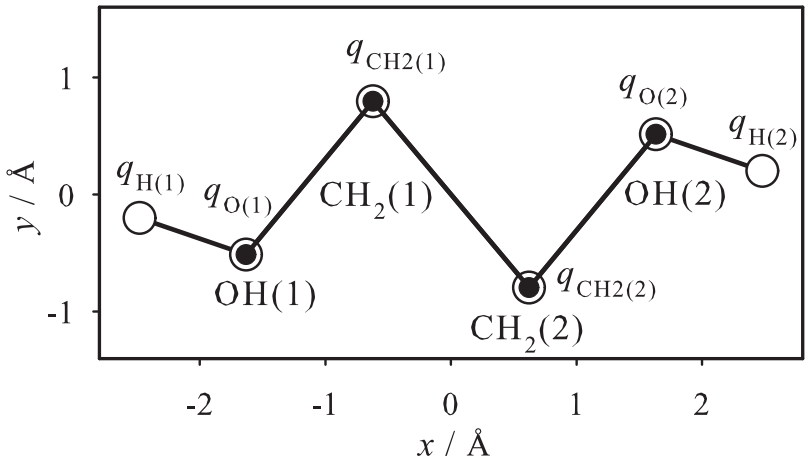

Figure 30: Geometry of the present Ethylene glycol model. Note that all sites are situated in a plane. Lennard-Jones sites are indicated by ●, point charges by ○.

The geometric data of the molecular Ethylene glycol model, i.e. bond lengths, angles and dihedrals, were derived from QC calculations. The details of the calculation of geom-

etry and the electrostatic interactions are given in Section 2.2. VLE were simulated with the Grand Equilibrium method [96], the technical details are given in Appendix B. The optimized parameter set of the new Ethylene glycol model is summarized in Table 16, Appendix A.

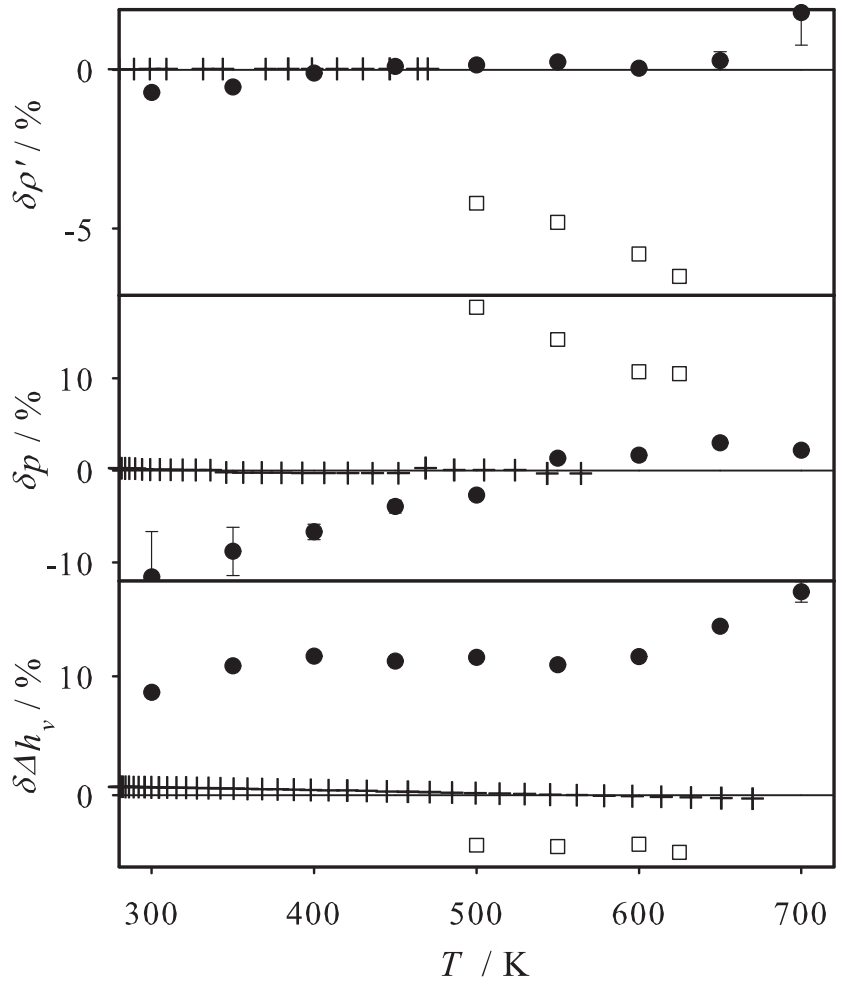

Figure 31: Relative deviations of vapor-liquid equilibrium properties from correlations of experimental data [106] ($\delta z = (z_\mathrm{i} - z_\mathrm{cor})/z_\mathrm{cor}$) for Ethylene glycol: ● present simulation data, □ Ferrando et al. [154], + experimental data [144, 145, 146, 147]. Top: saturated liquid density, center: vapor pressure, bottom: enthalpy of vaporization.

Figure 31 shows the deviation plots between simulation and correlations, where also simulation results from Ferrando et al. [154] and four sets of experimental data [144, 145, 146, 147] are included. A good agreement was obtained for the present model, yielding mean unsigned errors in saturated liquid density, vapor pressure and enthalpy of vaporization of 0.8, 8.8 and 13.4 %, respectively, in the temperature range from 300 to 700

K, which is about 42 to 97 % of the critical temperature. For both vapor pressure and saturated liquid density, the simulation data show larger deviations at low temperatures than at high temperatures. The vapor pressure from simulation shows larger statistical uncertainties at low temperatures. For the enthalpy of vaporization, a significant and almost constant offset is present. The present model leads to more accurate results than the model by Ferrando et al. for both saturated liquid density and vapor pressure. Nevertheless, the model from Ferrando et al. shows a much better performance for the enthalpy of vaporization.

3.2.1.3 Water

Since the early nineteen sixties, numerous force fields for Water were developed and investigated regarding their capability to describe thermopyhsical and structural fluid properties qualitatively and quantitatively. The number of underlying potential functions is vast and the number of Water models is even more comprehensive. Guillot [155] reported a survey on Water models which contain rigid, flexible, dissociable and polarizable interaction sites. Further reviews on Water models are given by Brodsky [156], Wallqvist and Mountain [157] and Finney [158].

None of the force fields reviewed by these authors [155, 156, 157, 158] is appropriate for describing the fluid properties of Water over the complete fluid state range with a high precision. Most of them favorably describe thermophysical properties only close to the state points at which they were adjusted, some of them yield fair predictions at best for state points far away from the adjustment region.

Recently, Paricaud et al. [159] proposed a rather complex force field which covers Water properties from dimer to condensed phases at extreme conditions accurately. It describes bubble density, vapor pressure and heat of vaporization for temperatures between 331 and 610 K with mean unsigned errors of 1.4 %, 11.3 % and 3.9 %, respectively. To our knowledge, this is the most accurate representation of the VLE properties on the basis of a molecular model with state-independent parameters so far.

The model of Paricaud et al. [159] is based on Gaussian charge polarizable interaction sites, i.e. smeared charges to describe electrostatics and hydrogen bonding. Additionally, it uses one Buckingham exponential-6 site [160] to consider repulsion and dispersion. Thus, this Water model is not straightforwardly compatible with the overwhelming majority of Lennard-Jones based force fields from the literature for simulations of mixtures.

To investigate whether a much simpler molecular model can describe the VLE properties of Water with similar quality of the complex model of Paricaud et al. [159], the

rigid four-site TIP4P model type as proposed by Jorgensen et al. [161] was studied. This model type consists of three point charges, excentrically superimposed on one Lennard-Jones site, cf. Figure 32. The two positive point charges represent the Hydrogen atoms, cf. Figure 32. The negative point charge is located in the bisection of the Hydrogen sites. The Lennard-Jones site is located at the Oxygen site such that all sites are situated in a plane.

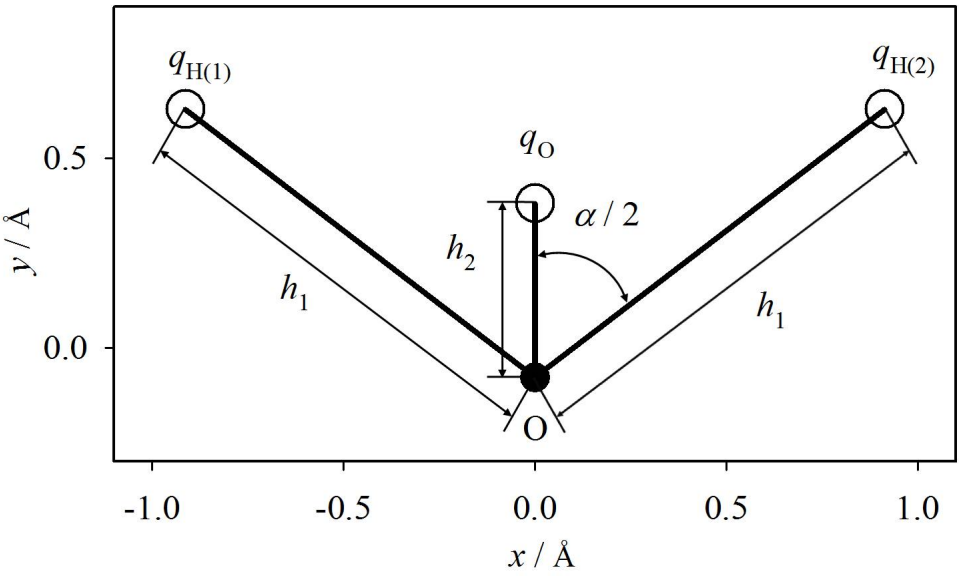

Figure 32: Geometry of TIP4P type Water models, cf. Table 4. Note that all sites are situated in a plane. Lennard-Jones sites are indicated by ●, point charges by ○.

Recently, the TIP4P model was re-parameterized by Horn et al. [162] (TIP4P-Ew). Two further optimizations for the TIP4P model type were recently suggested by Abascal and Vega [163] (TIP4P/2005) and Abascal et al. [164] (TIP4P/Ice). Furthermore, a TIP4P-like model was developed by Guissani and Guillot [165] (SPC/E). Among these models, for TIP4P/Ice no VLE data are available, thus, it is not discussed in the following.

The parameters of the TIP4P, TIP4P-Ew, TIP4P/2005, TIP4P/Ice, SPC/E as well as of the present model, labeled TIP4P/2010, are given in Table 4. The distance between the Oxygen atom and the Hydrogen atoms in a water molecule is 0.95718 Å [166]. Thus most of the TIP4P type models adopt the value 0.9572 Å. However, this distance is 40 % larger for the present TIP4P/2010 model to achieve a more directional interaction covering hydrogen bonding. The magnitude of the point charges of the present model is smaller than for any other TIP4P type model and the attractive force is compensated by a relatively high Lennard-Jones energy parameter ϵ.

Table 4: Geometry, Lennard-Jones and point charge parameters for molecular Water models of TIP4P type, cf. Figure 32.

Model	h_1 Å	h_2 Å	α °	σ_O Å	ϵ_O/k_B K	q_O e	q_H e
TIP4P [161]	0.9572	0.15000	104.52	3.15365	78.020	-1.04000	+0.52000
TIP4P-Ew [162]	0.9572	0.12500	104.52	3.16435	81.921	-1.04844	+0.52422
TIP4P/2005 [163]	0.9572	0.15460	104.52	3.15890	93.200	-1.11280	+0.55640
TIP4P/Ice [164]	0.9572	0.15770	104.52	3.16680	106.100	-1.17940	+0.58970
SPC/E [170]	1	0	109.47	3.16600	78.178	-0.84760	+0.42380
TIP4P/2010	1.1549	0.20482	104.52	3.11831	208.080	-0.83910	+0.41955

Figure 33 shows the deviation plots for the VLE data, where also simulation results of the TIP4P model by Lísal et al. [167], the SPC/E model by Guissani and Guillot [165], the TIP4P/2005 model by Vega et al. [168], the TIP4P-Ew model by Baranyai et al. [169], as well as several sets of experimental data [148, 149, 150] are included. A very good agreement was obtained for the present model, yielding mean unsigned errors in vapor pressure, saturated liquid density and enthalpy of vaporization of 7.2, 1.1 and 2.8 %, respectively, in the temperature range from 300 to 600 K, which is about 46 to 93 % of the critical temperature. Among the five molecular models, TIP4P/2005 has the best performance for saturated liquid density at very low temperatures, but at higher temperatures, the deviations increase. However, it performs poorest for the vapor pressure (from 25 up to 80 %). TIP4P shows the largest deviations for both saturated liquid density and enthalpy of vaporization. TIP4P-Ew and SPC/E have an average performance for all three properties. Note that there are no simulation data available for the enthalpy of vaporization based on the TIP4P/2005 and SPC/E models.

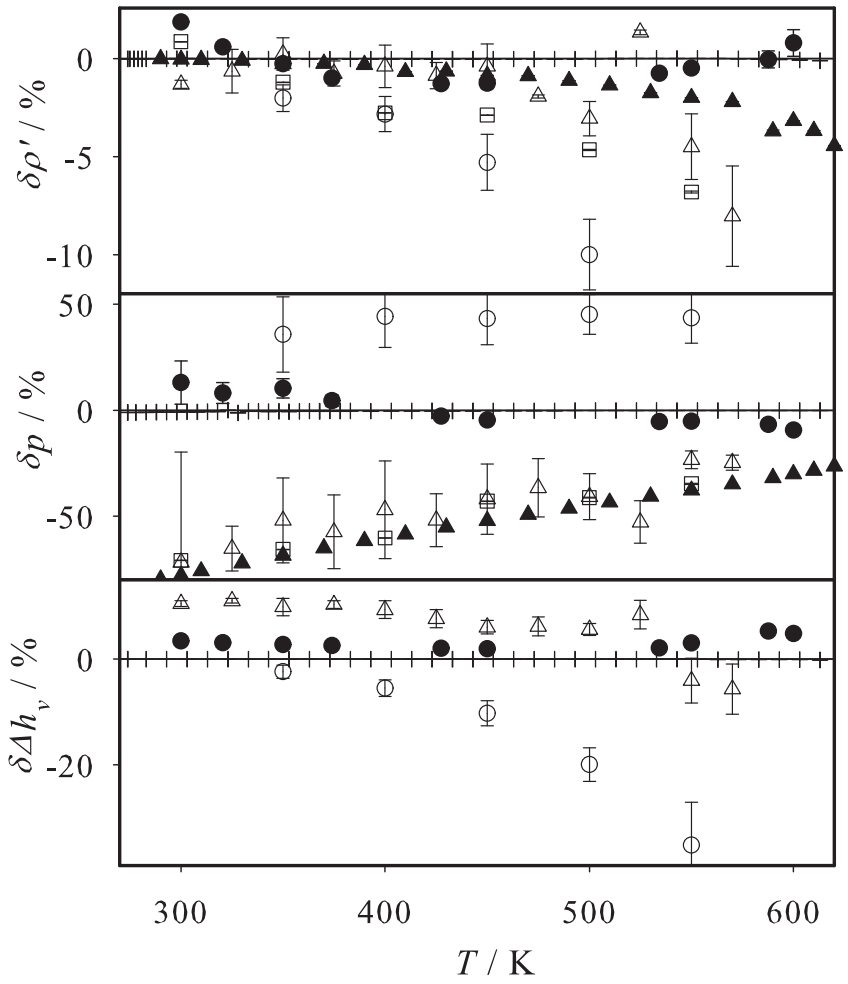

Figure 33: Relative deviations of vapor-liquid equilibrium properties from correlations of experimental data [106] ($\delta z = (z_\mathrm{i} - z_\mathrm{cor})/z_\mathrm{cor}$) for Water: ● present TIP4P/2010 simulation data; ○ TIP4P simulation data of Lísal et al. [167]; □ SPC/E simulation data of Guissani and Guillot [165]; ▲ TIP4P/2005 simulation data of Vega et al. [168]; △ TIP4P-Ew simulation data of Baranyai et al. [169]; + experimental data [148, 149, 150]. Top: saturated liquid density, center: vapor pressure, bottom: enthalpy of vaporization. Note that data for the enthalpy of vaporization are not available for the TIP4P/2005 and the SPC/E model.

3.2.2 Binary Vapor-Liquid Equilibria

Table 5 gives the state point (i.e. temperature T and bubble point mole fraction of the lower boiling component x_A) and the experimental vapor pressure p^{exp} which was used for the adjustment as well as the resulting binary parameter ξ. A first validating VLE simulation at this state point with the adjusted mixture model was performed. The resulting vapor pressure p and dew point composition y_A from simulation are also listed in Table 5 and can numerically be compared to experimental vapor pressure data there.

Table 5: Binary interaction parameter ξ, experimental bubble point used for the adjustment with reference, simulation results with adjusted parameter ξ of the molecular model and binary parameter k_{ij} of the Peng-Robinson EOS. The number in parentheses indicates the statistical uncertainty in the last digit.

Mixture (A + B)	ξ	T	x_A	p^{exp}	p^{sim}	y_A^{sim}	k_{ij}
		K	mol/mol	MPa	MPa	mol/mol	
Ethylene oxide + Water							
	1.126	370.00	0.03	0.31 [171]	0.31 (3)	0.701 (8)	0.01
Ethylene oxide + Ethylene glycol							
	1.016	378.15	0.1	0.38 [172]	0.38 (1)	0.999 (1)	-0.1
Water + Ethylene glycol							
	0.790	395.15	0.466	0.084 [173]	0.082 (2)	0.965 (4)	-0.066

Based on the discussed three pure substance models, VLE data were predicted for all three binary combinations. The phase behavior is throughout zeotropic. Full numerical VLE simulation data are given in Table 18, Appendix A, which also contains the saturated densities and the heat of vaporization from simulation. Because such data from experiment are not available for comparison, they are not further discussed here.

For orientation and comparison, the results of the Peng-Robinson EOS [138] with adjusted binary parameter k_{ij} are also shown. Generally, the EOS was optimized to the experimental vapor pressure at the same state point as the molecular mixture model.

3.2.2.1 Ethylene Oxide + Water

Figure 34 shows the isobaric VLE of Ethylene oxide + Water at 0.4428 MPa from experiment, simulation and Peng-Robinson EOS. Figures 35 and 36 show isothermal VLE at temperatures from 350 to 500 K. The binary parameters ξ = 1.2 and k_{ij} = -0.1 were adjusted to the vapor pressure measured by Schilk and Hurd [171] at 370 K for a liquid mole fraction x_{EO} = 0.03 mol/mol. Both ξ = 1.2 and k_{ij} = -0.1 exhibit quite large absolute values, yet this may be due to the strong hydrogen bonding of Water.

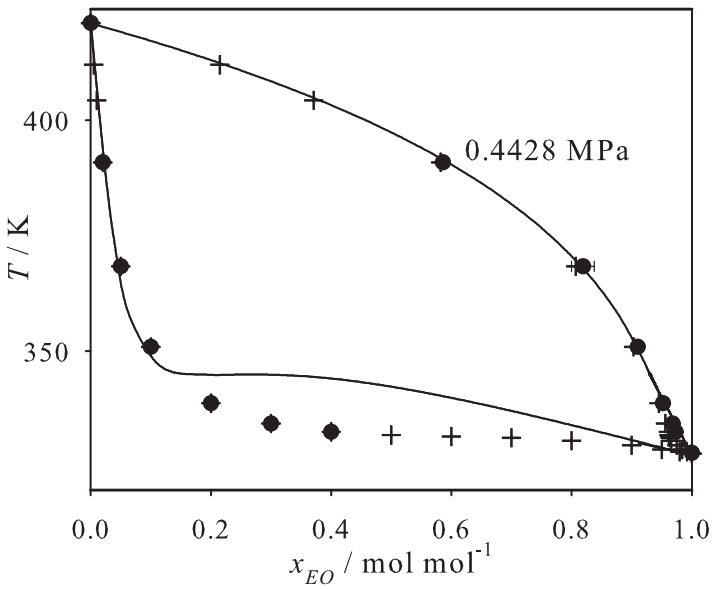

Figure 34: Isobaric vapor-liquid phase diagram of Ethylene oxide + Water at 0.4428 MPa: + experimental data [171]; ● present simulation data with ξ = 1.126; — Peng-Robinson EOS with k_{ij} = -0.1.

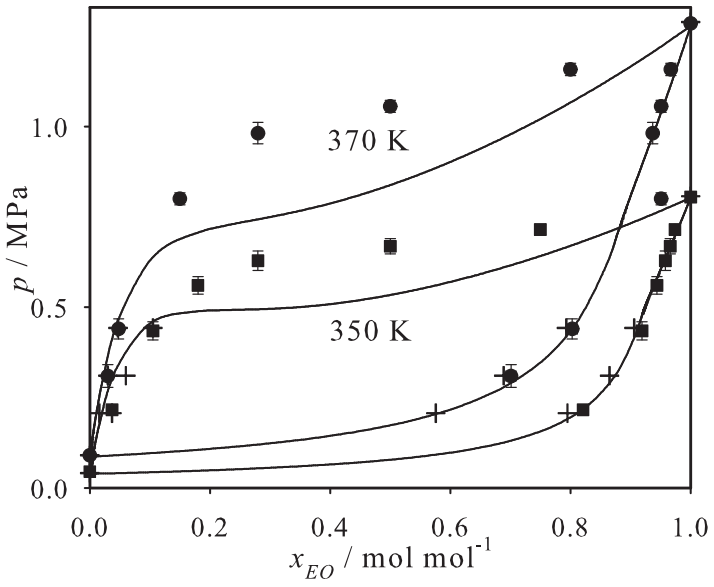

Figure 35: Isothermal vapor-liquid phase diagram of Ethylene oxide + Water at 350 and 370 K: + experimental data [171]; ■, ● present simulation data with ξ = 1.126; — Peng-Robinson EOS with k_{ij} = -0.1.

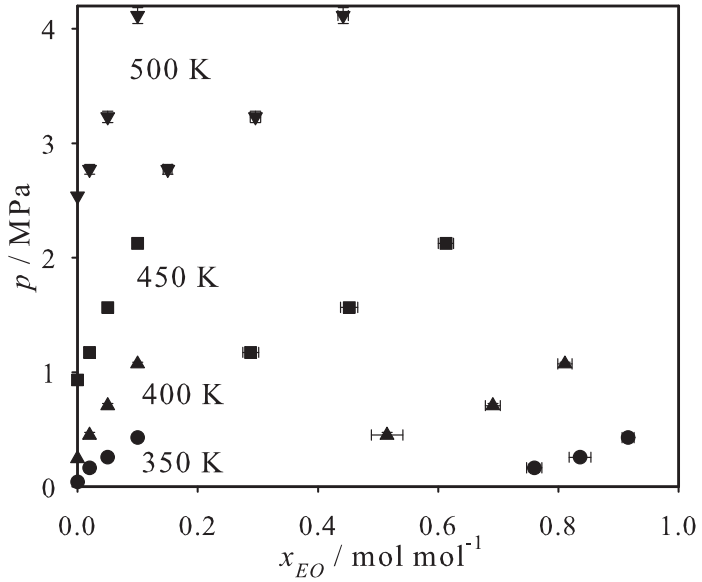

Figure 36: Isothermal vapor-liquid phase diagram of Ethylene oxide + Water at 350, 400, 450 and 500 K: ●, ▲, ■ and ▼ present simulation data with $\xi = 1.126$.

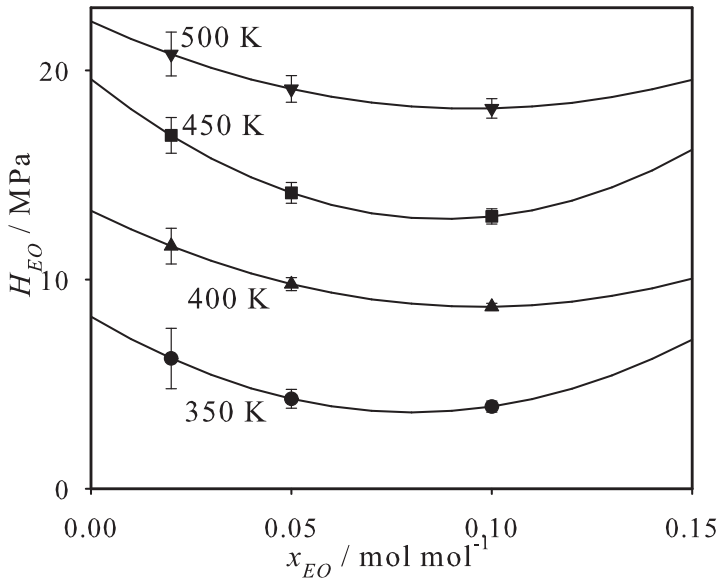

Figure 37: Approximation of the Henry's law constant of Ethylene oxide in Water: ●, ▲, ■ and ▼ present simulation data with $\xi = 1.126$; — guide to the eye.

In Figure 34, at 0.4428 MPa the mixture is sub-critical, the phase envelope is wide with a concave bubble line and a slightly convex dew line. The simulation data show a good agreement with the experimental data, but the Peng-Robinson EOS only matches

with the dew line, but fails to describe the bubble line, especially outside the Water-rich area. Due to the shortage of isothermal experimental data, six points were interpolated from [171] to form two isothermal data sets in Figure 35. There, the Peng-Robinson EOS outside of Water-rich region qualitatively deviates on the bubble line from the present simulation data, yet the dew line is accurate.

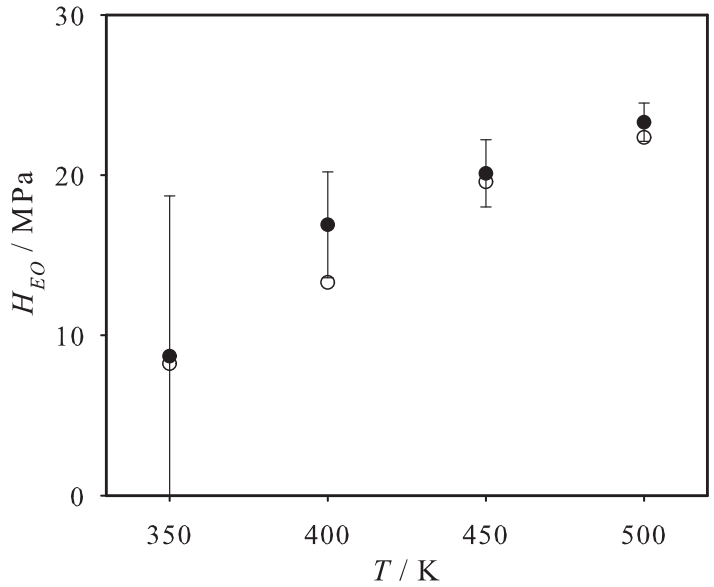

Figure 38: Henry's law constant of Ethylene oxide in Water: ○ extrapolation of simulation results with $\xi = 1.126$ at finite mole fractions to the limit of infinite dilution; ● direct simulation data with $\xi = 1.126$.

Based on this molecular model, the Henry's law constant was predicted. In Figure 36, simulations were performed at temperatures of 350, 400, 450 and 500 K and Ethylene oxide liquid mole fractions x_{EO} of 0.05, 0.10 and 0.15 mol/mol. With these results, the Henry's law constant was calculated by

$$H_i \ \exp\left\{\frac{1}{k_{\mathrm{B}}T}\int_{p_{\mathrm{S}}^{\mathrm{s}}}^{p} v_i^{\infty}\mathrm{d}p\right\} x_i\ \gamma_i^* = p\ y_i\ \phi_i, \tag{20}$$

where x_i and y_i are the solute mole fractions in the saturated liquid and vapor phases, respectively, v_i^{∞} is the partial molar volume of the solute at infinite dilution in the liquid, and k_{B} is the Boltzmann constant. Non-idealities of the liquid phase were considered by the activity coefficient normalized according to Henry's law γ_i^*, and of the vapor phase by the fugacity coefficient ϕ_i. The exponential term, known as the Krichevski-Kasarnovski

correction [174], accounts for the dependence of the chemical potential of the solute on the pressure p, where p_S^s stands for the pure solvent vapor pressure.

In Figure 37, the curves were correlated to $H(x_{EO})$ and extrapolated to $H(x_{EO} = 0 \text{ mol/mol})$. The results of this extrapolation are plotted as circles in Figure 38 comparing with the direct results obtained with the Gradual insertion method. The simulation results have large error bars, especially at low temperatures. However, the trends of the two data sets support each other.

3.2.2.2 Ethylene Oxide + Ethylene Glycol

Figure 39 shows isothermal VLE data of Ethylene oxide + Ethylene glycol at 378.15 and 360.15 K. The mixture is sub-critical for these temperatures and the phase envelope is very wide with a convex bubble line and a slightly concave dew line.

The binary parameters $\xi = 1.016$ and $k_{ij} = 0.01$ were adjusted to the vapor pressure measured by Di Serio et al. [172] at 378.15 K and $x_{EO} = 0.1$ mol/mol. Both ξ and k_{ij} exhibit typical values. A strong disagreement between the simulation data and the Peng-Robinson EOS was found on the bubble line outside of the Ethylene glycol-rich region.

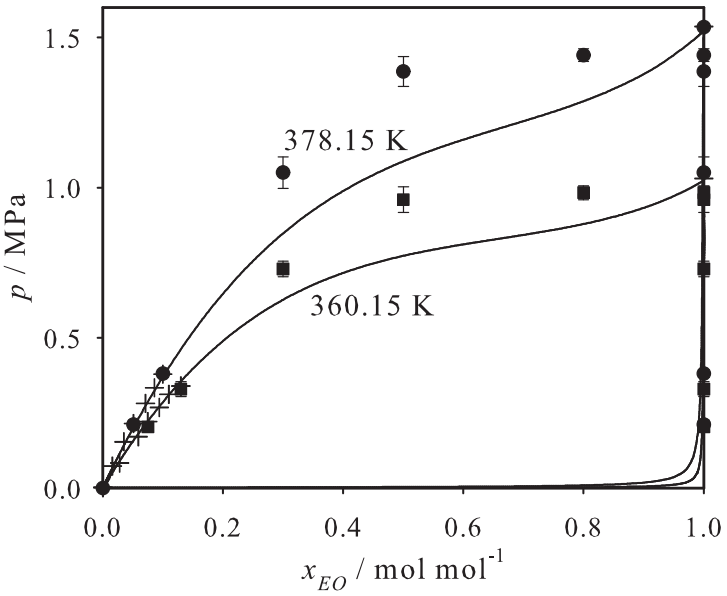

Figure 39: Isothermal vapor-liquid phase diagram of Ethylene oxide + Ethylene glycol at 360.15 and 378.15 K: + experimental data [172]; ■, ● present simulation data with $\xi = 1.016$; — Peng-Robinson EOS with $k_{ij} = 0.01$.

3.2.2.3 Water + Ethylene Glycol

Isothermal VLE data of Water + Ethylene glycol are presented in Figure 40 at 383.15 and 395.15 K. For both temperatures, the mixture is sub-critical and the phase envelope is wide with a slightly concave bubble line and dew line. Experimental data on the bubble line measured by Lancia et al. [173] at 395.15 K in the Water-rich region (x_W = 0.466 mol/mol) were taken for the optimization of the mixture models, yielding ξ = 0.790 and k_{ij} = -0.066.

At 395.15 K, the Peng-Robinson EOS fails to describe the bubble line in the Ethylene glycol-rich region and it does not match well with the experimental dew line either. The simulation results show a good agreement with the experimental data outside of the Ethylene glycol-rich region for both temperatures. Nevertheless, the experimental data show significant scatter.

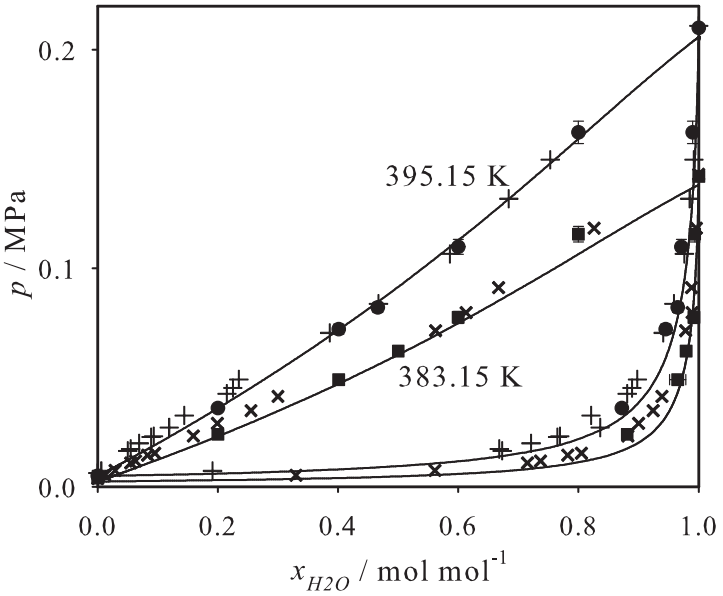

Figure 40: Isothermal vapor-liquid phase diagram of Water + Ethylene glycol at 383.15 and 395.15 K: + experimental data [173]; ■, ● present simulation data with ξ = 0.790; — Peng-Robinson EOS with k_{ij} = -0.066.

4 Large Systematic Study on Vapor-Liquid Equilibria of Mixtures

Molecular simulation has been applied in the past decades to various systems. However, so far there is no large scale investigation to prove statistically that molecular modeling and simulation can be relied upon as a main instrument beside experiment or EOS. In this chapter, a large systematic study on VLE of mixtures is presented. The predictions from molecular models of 366 mixtures are extensively compared to experimental data.

4.1 Models for 78 Pure Fluids

78 real pure fluids were studied on the basis of the dipolar or quadrupolar two-center Lennard-Jones (2CLJD and 2CLJQ) potential with parameters taken from prior work of our group [8, 9]. This model type has been proposed more than three decades ago [10], however, it is far from being fully exploited. Polar 2CLJ models consider the basic molecular interactions repulsion and dispersive attraction and also feature anisotropy and polarity in a simple way. For many of the 78 molecules, the polar 2CLJ model strongly simplifies the intermolecular interactions. E.g., the asymmetry of the molecules is neglected and the polar interaction is always aligned along the main molecular axis. Also the polarizability, which is often assumed to be a crucial molecular property for thermodynamics, is only implicitly considered by Lennard-Jones interaction sites. Furthermore, the internal degrees of freedom are neglected as the polar 2CLJ models are rigid.

The aim here was to investigate whether these crude assumptions for pure substance models have an impact on mixture properties, in particular on binary VLE. It can be argued that oversimplified molecular models can be adjusted to a few experimental pure substance properties, but major deficiencies should be visible when applied to mixtures.

It should be noted that polar 2CLJ models are not suited for hydrogen bonding molecules, as they cannot mimic their very strong short-range interaction. However, it was shown for 35 binaries [175, 176] that they are, e.g. for CO_2, compatible with appropriate molecular models, e.g. for Methanol, for hydrogen bonding fluids.

These 78 models include five spherical non-polar (LJ) models for noble gases and CH_4, four spherical dipolar (Stockmayer) models for CH_2I_2, R30, R32 and R30B2, furthermore 42 elongated dipolar (2CLJD) models which include carbon monoxide and numerous refrigerants, and finally 27 elongated quadrupolar (2CLJQ) models which include halogens, alkanes, refrigerants and CO_2.

Most polar 2CLJ models have four parameters: size σ, energy ϵ, elongation L and dipolar moment μ or quadrupolar moment Q; Stockmayer models have a vanishing elongation, while the non-polar spherical Lennard-Jones models have only two parameters: σ and ϵ. Both their elongation and polarity are zero. Model parameters were adjusted in [8, 9] to experimental pure fluid VLE data using global correlations of critical temperature, saturated liquid density and vapor pressure as functions of these molecular parameters [177, 178]. These pure substance model parameters are not repeated here. It should be noted that a wide range of polar momenta are covered by the 78 pure substance models. Starting from a non-existent polar moment in case of the noble gases and methane, it ranges to up to 4.7919 D for the dipolar R130a and up to 16.143 DÅ for the quadrupolar R1110.

The advantage of these molecular models is their simplicity, which reduces simulation time considerably, and their accuracy: typically, the relative deviations between simulation and experiment are below 1 % for the saturated liquid density, below 3 % for the vapor pressure, and below 3 % for the enthalpy of vaporization. They also have shown to predict reliably Joule-Thomson inversion curves for pure fluids and mixtures [179, 180], covering a wide range of state points, but also transport properties [181, 182, 183, 184, 185].

In Table 6, the 78 pure substances are listed. There, the letters b/t/h indicate if that pure fluid was included in the study on the binary VLE, the ternary VLE or the Henry's law constant.

Table 6: List of the 78 components included in the present work, where b, t, h stand for binary VLE, ternary VLE or Henry's law constant, respectively. For the mixtures regarded with respect to the Henry's law constants, i indicates solutes and S solvents.

Fluid	CAS RN	Type	Fluid	CAS RN	Type
Non-polar, 1CLJ			R143a (CH_3–CF_3)	420-46-2	b/t
Ne	7440-37-1	b/h(i)	R150a ($CHCl_2$–CH_3)	75-34-3	b/h(S)
Ar	13965-95-2	b/t/h(i)	R152a (CH_3–CHF_2)	75-37-6	b/t
Kr	7439-90-9	b/h(i)	R160B1 (CH_2Br–CH_3)	74-96-4	b
Xe	7440-63-3	b/h(i)	R161 (CH_2F–CH_3)	353-36-3	t/h(i)
CH_4	74-82-8	b/t/h(i)	R1122 (CHCl=CF_2)	359-10-4	b
Dipolar, 1CLJD			R1132 (CF_2=CH_2)	75-38-7	h(i)
CH_2I_2	75-11-6		R1140 (CHCl=CH_2)	75-01-4	b/h(i, S)
R30 (CH_2Cl_2)	75-09-2	b/t/h(S)	$CHBr_2$–CH_3	557-91-5	
R30B2 (CH_2Br_2)	74-95-3	b/t	CH_2F–CCl_3	27154-33-2	
R32 (CH_2F_2)	75-10-5	b/t	CHF=CH_2	75-02-5	
Dipolar, 2CLJD			CFCl=CF_2	79-38-9	
CO	630-08-0	b/t/h(i)	CFBr=CF_2	598-73-2	
CH_3I	74-88-4	b	**Quadrupolar, 2CLJQ**		
R10B1 ($CBrCl_3$)	75-62-7		F_2	7782-41-4	
R11 ($CFCl_3$)	75-69-4	b/t/h(S)	N_2	7727-37-9	b/t/h(i)
R12 (CF_2Cl_2)	75-71-8	b/t/h(i)	O_2	7782-44-7	b/t/h(i)
R12B1 ($CBrClF_2$)	353-59-3	b	Cl_2	7782-50-5	b/h(i, S)
R12B2 (CBr_2F_2)	75-61-6	b	Br_2	7726-95-6	b
R13 (CF_3Cl)	75-72-9	b/t/h(i)	I_2	7553-56-2	b
R13B1 ($CBrF_3$)	75-63-8	b	CO_2	124-38-9	b/t/h(i, S)
R20 ($CHCl_3$)	67-66-3	b/t/h(S)	CS_2	75-15-0	b/h(S)
R20B3 ($CHBr_3$)	75-25-2	h(S)	C_2H_2	74-86-2	b/t/h(i)
R21 ($CHFCl_2$)	75-43-4	b	C_2H_4	74-85-1	b/t/h(i)
R22 (CHF_2Cl)	75-45-6	b/t/h(i)	C_2H_6	74-84-0	b/t/h(i)
R23 (CHF_3)	75-46-7	b/t/h(i)	Propadiene (CH_2=C=CH_2)	463-49-0	b
R30B1 (CH_2BrCl)	74-97-5	b/t	Propyne (CH_3–C≡CH)	74-99-7	b
R40 (CH_3Cl)	74-87-3	b/h(i, S)	Propylene (CH_3–CH=CH_2)	115-07-1	b/h(i, S)
R40B1 (CH_3Br)	74-83-9		SF_6	2551-62-4	b/h(i, S)
R41 (CH_3F)	593-53-3	b	R10 (CCl_4)	56-23-5	b/t/h(S)
R112a (CCl_3–CF_2Cl)	76-11-9	b	R14 (CF_4)	75-73-0	b/t/h(i)
R123 ($CHCl_2$–CF_3)	306-83-2	b	R113 ($CFCl_2$–CF_2Cl)	76-13-1	b/t/h(S)
R123B1 (CHClBr–CF_3)	151-67-7	b	R114 (CF_2Cl–CF_2Cl)	76-14-2	b/t/h(S)
R124 (CHFCl–CF_3)	2837-89-0	b/t	R114B2 ($CBrF_2$–$CBrF_2$)	124-73-2	b
R125 (CHF_2–CF_3)	354-33-6	b/t	R115 (CF_3–CF_2Cl)	76-15-3	b
R130a (CH_2Cl–CCl_3)	630-20-6	b/h(S)	R116 (C_2F_6)	76-16-4	b/h(i)
R134a (CH_2F–CF_3)	811-97-2	b/t	R134 (CHF_2–CHF_2)	359-35-3	b
R140 ($CHCl_2$–CH_2Cl)	79-00-5	b/h(S)	R150B2 (CH_2Br–CH_2Br)	106-93-4	b/t/h(S)
R140a (CCl_3–CH_3)	71-55-6	b/t/h(S)	R1110 (C_2Cl_4)	127-18-4	b/t/h(S)
R141b (CH_3–$CFCl_2$)	1717-00-6	b/t	R1114 (C_2F_4)	116-14-3	b/h(i)
R142b (CH_3–CF_2Cl)	75-68-3	b/t	R1120 (CHCl=CCl_2)	79-01-6	b/t/h(S)

4.2 Binary Vapor-Liquid Equilibria

Reasonable molecular modeling of mixtures requires the definition of the unlike interactions only. While unlike polar interactions are straightforwardly known on a sound physical basis, i.e. by using the laws of electrostatics, there is still no such framework for the unlike dispersive interactions [186]. Therefore, combining rules have been proposed that determine the parameters of that unlike interaction, where, among many others, the most well-known is the Lorentz-Berthelot rule. Regarding binary VLE of 44 systems it has recently shown in [75] that *(a)* the Lorentz rule is excellent, *(b)* the unlike dispersion energy parameter is crucial for accurate predictions of the pressure, *(c)* none of a set of eleven investigated combination rules yields really optimal values for it and *(d)* it should be adjusted to one experimental vapor pressure of the mixture.

In most fields of science, there is a danger that results are biased by a selection of the studied subjects. Moreover, successful approaches are generally more likely to be published than failures. To counter this, a combinatorial approach was used here. Theoretically, out of the $N = 78$ components $N(N-1)/2 = 3\ 003$ binary mixtures can be formed, but of course, not all of these systems have been studied experimentally. To our knowledge, the VLE was measured for a subset of 267 out of the 3 003 binaries. In the present work, *all* those 267 binary mixtures were studied. This is by far the largest set of binaries that was used to probe the application of molecular modeling and simulation to mixtures.

The presented simulation results are compared to experimental data and in most cases to the Peng-Robinson EOS. For parameter adjustments of the molecular models and the Peng-Robinson EOS always the same experimental data were used to achieve a fair comparison.

4.2.1 Experimental Database

Experimental data in this study were predominately retrieved using Dortmunder Datenbank (DDB) [187], which collects *all* publicly available mixture VLE data sets, covering more than a century of experimental work. For a subset of 286 of the potential 3 003 binary mixtures experimental VLE data is available. That data is contained in 201 publications [188]-[388]. These 286 binaries include 66 of the 78 pure components, i.e. for 12 substances no mixture data was found with any of the other 77 components. A list of these 66 components, including their CAS RN number for proper identification, is given in Table 6. Please note that the ASHRAE nomenclature is preferred in the following due to its brevity, despite its deficiencies [389].

Of those 286 binary mixtures, 44 have been modeled in previous work of our group [36, 37, 38], but the resulting VLE data were published only partly.

The term VLE data is used here for information on vapor-liquid coexistence at finite mole fractions, i.e. not for properties at infinite dilution like the Henry's law constant. For an additional 66 binary mixtures experimental Henry's law constant data were found, which are discussed in Section 4.4.

Table 7 gives the state point (i.e. temperature T and bubble point mole fraction of the lower boiling component x_1) and the experimental vapor pressure p^{exp} which was used for the adjustment as well as the resulting binary interaction parameter ξ. A first validating VLE simulation at this state point with the adjusted mixture model was performed. The resulting vapor pressure p^{sim} and dew point composition from simulation are also listed in Table 7 and can numerically be compared to experimental data there. Note that for 80 binaries no experimental dew point composition is available.

For 55 of the 286 systems, experimental data are available only from a single source. Among them are 8 binaries, where exclusively data on the dew line were published. Such cases, cf. Table 8, are of little use for the present modeling and validation procedure so that these mixtures were excluded here. For 11 binaries VLE data are available only for very dilute state points, i.e. the bubble point mole fraction of the low boiling component is $x_1 < 0.02$ mol/mol, cf. Table 9. Such data rather present gas solubilities which are related to the Henry's law constant. For direct VLE simulations they are not well suited so that they were excluded as well. The total number of investigated systems is therefore 286-8-11=267 binaries.

Table 7: List of 259 binary mixtures. Binary interaction parameter ξ, experimental bubble point used for the adjustment with reference, simulation results with adjusted ξ, and binary parameter of the Peng-Robinson EOS k_{ij}.

Mixture (1+2)	ξ	T	x_1	p^{exp}	p^{sim}	y_1^{exp}	y_1^{sim}	k_{ij}	Ref.
		K	mol/mol	MPa	MPa	mol/mol	mol/mol		
Ne + Ar	0.826	110.78	0.024	2.734	2.78 (7)	0.670	0.69 (1)	0.203	[188]
Ne + Kr	0.733	178.15	0.072	10.12	9.8 (2)	0.638	0.666(7)	0.035	[189]
Ne + N_2	0.928	82.70	0.089	3.04	3.02 (2)	0.906	0.904(3)	0.111	[190]
Ne + O_2	0.921	110.39	0.252	20.94	20.5 (3)	0.808	0.844(4)	0.139	[191]
Ne + CO_2	1.124	273.15	0.038	8.84	8.84 (1)	0.445	0.466(1)	0.100	[192]
Ar + Kr	0.989	138.15	0.176	0.772	0.766(7)	0.583	0.590(3)	0.010	[193]
Ar + CH_4	0.964	123.05	0.541	0.912	0.915(8)	0.848	0.839(3)	0.037	[194]
Ar + O_2	0.988	104.51	0.148	0.386	0.389(5)	0.190	0.178(4)	0.015	[195]
Ar + CO_2	0.999	288.15	0.099	8.754	8.48 (8)	–	0.243(4)	0.170	[196]
Ar + C_2H_6	0.978	115.50	0.505	0.68	0.65 (4)	–	0.995(1)	0.050	[197]
Ar + Propylene	1.019	150.00	0.328	4.374	4.3 (2)	–	0.910(8)	–	[198]
Ar + R10	0.964	348.15	0.292	27.86	26.0 (1)	–	0.980(8)	0.130	[199]
Ar + R14	1.024	203.68	0.179	3.65	3.67 (5)	0.431	0.436(5)	0.010	[200]
Ar + R22	0.989	323.15	0.227	10.13	10.1 (2)	0.596	0.60 (1)	0.104	[201]
Kr + Xe	0.989	200.64	0.463	2.07	2.09 (2)	0.787	0.805(2)	0.010	[202]
Kr + C_2H_4	1.020	115.77	0.492	0.048	0.050(4)	0.990	0.998(1)	0.050	[203]
Kr + C_2H_6	1.023	278.98	0.225	4.751	4.82 (5)	0.424	0.398(1)	0.033	[204]
Kr + Propylene	1.001	200.00	0.333	1.648	1.65 (4)	–	0.980(5)	0.050	[198]
Xe + C_2H_6	0.984	292.00	0.528	4.737	4.80 (5)	0.561	0.579(2)	0.010	[205]
Xe + R40	0.973	182.32	0.478	0.18	0.18 (2)	0.993	0.990(6)	0.074	[206]
Xe + R41	0.928	182.33	0.472	0.235	0.23 (2)	0.831	0.91 (4)	0.120	[207]
Xe + R116	1.010	173.11	0.552	0.153	0.154(3)	0.857	0.877(6)	0.120	[208]
CH_4 + Kr	0.998	174.55	0.455	2.268	2.284(1)	0.516	0.516(3)	0.005	[209]
CH_4 + CO_2	0.962	230.00	0.318	5.57	5.61 (4)	0.764	0.766(3)	0.084	[210]
CH_4 + C_2H_4	1.022	223.15	0.398	4.053	4.09 (4)	0.734	0.696(5)	0.034	[211]
CH_4 + C_2H_6	0.997	172.04	0.504	1.24	1.21 (1)	0.966	0.969(3)	0.001	[212]
CH_4 + Propylene	1.032	190.00	0.667	2.815	2.80 (2)	0.992	0.997(1)	0.010	[213]
CH_4 + R12	1.052	298.20	0.431	7.4	7.28 (7)	0.829	0.827(4)	0.030	[214]
CH_4 + R14	1.030	98.00	0.688	0.026	0.023(2)	0.982	0.998(1)	0.115	[215]
CH_4 + R22	1.021	263.20	0.540	9.80	9.2 (2)	0.844	0.884(5)	0.055	[214]
N_2 + Ar	1.010	122.89	0.390	2.006	1.999(9)	0.495	0.501(2)	-0.015	[216]
N_2 + Kr	0.989	125.00	0.247	1.044	1.02 (3)	0.852	0.855(6)	0.008	[217]
N_2 + CH_4	0.958	140.00	0.519	3.080	3.07 (2)	0.777	0.785(2)	0.026	[218]
N_2 + O_2	1.007	105.00	0.500	0.743	0.734(9)	0.702	0.709(4)	0.012	[219]

Table 7: continued.

N_2 + CO	1.007	83.82	0.445	0.167	0.174(1)	0.56	0.544(1)	0.028	[220]
N_2 + CO_2	1.041	270.00	0.132	9.290	9.2 (4)	0.417	0.43 (2)	0.017	[221]
N_2 + C_2H_4	0.926	200.00	0.181	6.033	6.9 (2)	0.829	0.849(6)	0.065	[222]
N_2 + C_2H_6	0.974	200.00	0.026	1.043	1.07 (1)	0.753	0.766(1)	0.052	[222]
N_2 + Propylene	0.959	290.00	0.203	11.138	10.5 (1)	0.751	0.766(6)	0.088	[222]
N_2 + R12	1.000	295.15	0.370	15.199	14.8 (4)	0.830	0.850(5)	0.002	[223]
N_2 + R12B1	0.942	313.20	0.106	7.0	6.85 (8)	0.882	0.884(2)	0.054	[224]
N_2 + R13	1.045	253.15	0.285	7.0	6.92 (4)	0.680	0.677(5)	0.060	[225]
N_2 + R13B1	1.022	313.20	0.200	7.4	7.5 (2)	0.385	0.371(9)	0.076	[224]
N_2 + R22	1.000	348.15	0.145	8.26	8.3 (1)	0.380	0.36 (1)	0.000	[201]
N_2 + R23	1.042	179.80	0.450	15.8	15.8 (6)	–	0.852(9)	0.030	[226]
O_2 + Kr	1.050	100.00	0.536	0.162	0.163(6)	0.944	0.946(3)	0.030	[227]
O_2 + CO_2	0.979	253.15	0.092	6.079	6.68 (9)	0.537	0.556(7)	0.048	[228]
Cl_2 + R12	0.975	298.15	0.532	0.805	0.81 (3)	0.571	0.59 (2)	0.026	[229]
Cl_2 + R140	0.948	313.00	0.083	0.101	0.100(6)	–	0.91 (5)	0.010	[230]
Cl_2 + R140a	0.930	313.00	0.063	0.101	0.102(4)	–	0.72 (2)	0.020	[230]
Cl_2 + R150a	0.967	293.00	0.104	0.101	0.099(3)	–	0.78 (1)	0.030	[230]
Br_2 + R10	0.995	336.25	0.342	0.098	0.098(3)	0.536	0.55 (1)	0.020	[231]
Br_2 + R112a	0.967	344.15	0.238	0.101	0.101(2)	0.600	0.60 (1)	0.030	[232]
CO + Ar	0.992	83.00	0.534	0.108	0.108(5)	–	0.65 (2)	0.040	[233]
CO + CH_4	1.003	123.40	0.360	0.988	1.07 (1)	0.800	0.796(3)	0.026	[234]
CO + CO_2	1.080	263.15	0.210	10.32	11.2 (2)	0.496	0.392(9)	0.034	[235]
CO + C_2H_6	1.000	248.15	0.056	2.758	3.15 (3)	0.452	0.487(7)	0.020	[236]
CO + R30	0.816	333.15	0.014	2.45	2.37 (4)	0.885	0.91 (1)	0.050	[237]
CO_2 + Cl_2	0.936	243.15	0.140	0.507	0.57 (1)	0.800	0.778(8)	0.093	[238]
CO_2 + CS_2	0.918	360.00	0.354	11.5	11.6 (1)	0.875	0.914(3)	0.002	[239]
CO_2 + C_2H_2	1.000	297.90	0.500	5.5	5.50 (1)	–	0.520(5)	0.007	[240]
CO_2 + C_2H_6	0.954	263.15	0.425	2.9	2.98 (3)	0.514	0.524(3)	0.132	[241]
CO_2 + Propylene	0.915	273.15	0.231	1.51	1.52 (1)	0.630	0.631(5)	0.095	[242]
CO_2 + R12	0.927	273.00	0.714	2.65	2.67 (2)	–	0.932(4)	0.069	[243]
CO_2 + R20	0.945	333.15	0.569	6.45	6.3 (1)	0.962	0.972(4)	0.032	[244]
CO_2 + R22	1.006	273.15	0.560	1.99	2.07 (2)	0.848	0.853(3)	0.007	[245]
CO_2 + R23	0.997	263.35	0.417	2.292	2.34 (2)	0.482	0.503(5)	0.011	[245]
CO_2 + R30	0.923	326.95	0.550	6.246	6.3 (1)	–	0.970(7)	0.063	[246]
CO_2 + R32	1.050	280.00	0.486	2.51	2.48 (2)	0.724	0.732(4)	0.033	[247]
CO_2 + R40	0.990	282.65	0.534	2.53	2.45 (7)	0.861	0.90 (1)	0.001	[248]
CO_2 + R41	1.024	290.00	0.662	4.53	4.42 (8)	0.720	0.720(8)	0.010	[249]
CO_2 + R125	1.021	304.60	0.450	3.34	3.31 (4)	0.630	0.640(7)	0.050	[250]
CO_2 + R134a	0.982	329.60	0.510	5.37	5.43 (9)	0.707	0.710(8)	0.010	[251]
CO_2 + R140	0.902	323.20	0.662	6.89	7.26 (7)	0.995	0.990(1)	0.092	[252]
CO_2 + R140a	0.889	323.17	0.462	4.88	4.85 (6)	0.983	0.983(5)	0.080	[253]
CO_2 + R142b	0.952	318.30	0.551	4.71	4.73 (5)	0.848	0.873(4)	0.200	[254]
CO_2 + R152a	1.004	347.70	0.392	5.53	5.58 (7)	0.580	0.610(7)	0.005	[254]
CS_2 + R10	1.029	318.15	0.468	0.069	0.069(2)	0.717	0.72 (1)	0.002	[255]
CS_2 + R20	1.007	353.15	0.500	0.247	0.23 (4)	–	0.7 (1)	0.020	[256]
CS_2 + R1110	1.025	318.15	0.298	0.04	0.041(2)	0.880	0.89 (1)	0.020	[257]
CH_3I + CS_2	1.000	317.15	0.122	0.101	0.102(4)	–	0.16 (1)	0.040	[258]

Table 7: continued.

CH_3I + R10	0.971	298.15	0.558	0.04	0.038(1)	0.811	0.80 (1)	0.010	[259]
CH_3I + R20	0.994	308.15	0.492	0.06	0.059(2)	–	0.68 (2)	0.010	[260]
C_2H_2 + R10	0.890	393.15	0.480	9.11	9.1 (2)	–	0.895(8)	0.080	[261]
C_2H_2 + R152a	1.090	303.20	0.569	2.5	2.45 (8)	0.837	0.87 (2)	0.085	[262]
C_2H_4 + Xe	1.010	269.54	0.499	3.98	4.00 (3)	0.502	0.499(4)	0.020	[263]
C_2H_4 + CO_2	0.944	243.15	0.087	1.588	1.51 (2)	0.156	0.162(5)	0.055	[264]
C_2H_4 + C_2H_2	0.975	255.37	0.980	2.682	2.72 (2)	0.979	0.994(2)	0.064	[265]
C_2H_4 + C_2H_6	1.037	233.15	0.500	1.132	1.151(9)	0.622	0.622(4)	0.040	[266]
C_2H_4 + Propylene	0.996	263.07	0.625	2.067	2.08 (1)	0.884	0.882(2)	0.021	[267]
C_2H_4 + R10	1.003	323.15	0.473	4.37	4.33 (7)	0.981	0.985(3)	-0.010	[268]
C_2H_4 + R20	1.001	323.15	0.539	5.066	4.9 (1)	0.976	0.93 (2)	0.030	[269]
C_2H_4 + R22	1.026	213.15	0.030	0.062	0.063(2)	–	0.29 (1)	0.022	[270]
C_2H_4 + R30	1.070	423.15	0.250	6.03	6.20 (8)	0.60	0.647(8)	0.080	[271]
C_2H_4 + R30B1	0.946	373.15	0.210	6.08	6.02 (6)	0.905	0.915(5)	0.050	[272]
C_2H_4 + R1140	0.945	313.15	0.539	4.9	4.94 (4)	0.902	0.856(2)	0.100	[273]
C_2H_6 + C_2H_2	0.968	277.59	0.180	3.544	3.89 (2)	0.243	0.262(3)	0.156	[274]
C_2H_6 + Propylene	1.015	310.93	0.260	2.41	2.51 (2)	0.447	0.438(4)	0.007	[275]
C_2H_6 + R22	0.981	293.24	0.551	2.76	2.78 (3)	0.762	0.753(3)	0.090	[276]
Propylene + Propadiene	0.991	293.15	0.464	0.852	0.88 (2)	0.545	0.56 (1)	0.020	[277]
Propylene + Propyne	1.003	313.15	0.566	1.442	1.46 (2)	–	0.639(6)	0.050	[278]
Propylene + R10	1.005	333.15	0.282	0.766	0.79 (4)	–	0.90 (2)	0.020	[279]
Propylene + R12	0.998	283.00	0.529	0.63	0.62 (1)	0.654	0.66 (1)	0.026	[280]
Propylene + R20	0.975	293.15	0.361	0.455	0.46 (3)	–	0.950(1)	0.010	[279]
Propylene + R22	0.982	283.00	0.147	0.73	0.71 (2)	0.187	0.171(6)	0.036	[280]
Propylene + R114	0.966	298.00	0.514	0.745	0.72 (2)	0.807	0.810(7)	0.050	[280]
Propylene + R115	0.948	298.00	0.549	1.244	1.24 (2)	0.607	0.59 (1)	0.080	[280]
Propylene + R134a	0.924	298.00	0.204	0.95	0.95 (2)	0.399	0.383(8)	0.105	[280]
Propylene + R142b	0.987	298.00	0.443	0.73	0.71 (1)	0.701	0.705(9)	0.035	[280]
Propylene + R152a	0.933	298.15	0.281	0.94	0.95 (1)	0.431	0.483(6)	0.100	[281]
Propylene + R1110	1.008	293.15	0.441	0.534	0.49 (6)	–	0.998(5)	0.010	[279]
Propylene + R1120	0.983	303.15	0.275	0.507	0.55 (4)	–	0.94 (3)	0.050	[282]
Propylene + R1140	1.029	293.15	0.542	0.687	0.69 (1)	0.781	0.775(5)	0.050	[283]
SF_6 + R12	0.984	319.78	0.330	2.1	2.10 (3)	0.534	0.540(5)	0.050	[284]
SF_6 + R13B1	0.999	296.70	0.339	1.93	1.94 (4)	0.407	0.410(7)	0.035	[284]
SF_6 + R22	0.915	318.58	0.154	2.406	2.42 (4)	0.307	0.300(8)	0.100	[284]
SF_6 + R32	0.790	310.00	0.480	4.041	4.07 (7)	0.523	0.517(8)	0.190	[247]
SF_6 + R114	1.050	270.80	0.011	0.087	0.088(4)	–	0.065(4)	0.070	[285]
R10 + R140	0.955	360.05	0.490	0.099	0.097(3)	0.750	0.74 (1)	0.120	[286]
R10 + R150B2	0.987	323.15	0.533	0.028	0.027(2)	–	0.88 (1)	0.000	[287]
R10 + R1110	0.967	343.15	0.488	0.05	0.05 (2)	0.808	0.81 (1)	0.005	[288]
R10 + R1120	0.998	354.64	0.506	0.101	0.097(3)	0.577	0.588(1)	0.010	[289]
R12 + R10	0.991	297.75	0.090	0.101	0.101(3)	–	0.877(5)	0.040	[383]
R12 + R11	1.001	343.00	0.439	1.025	0.99 (1)	0.739	0.721(5)	0.010	[290]
R12 + R113	1.014	293.15	0.513	0.27	0.28 (2)	0.936	0.94 (2)	0.030	[291]
R12 + R114	0.989	313.15	0.523	0.668	0.69 (2)	0.727	0.70 (2)	0.010	[292]
R12 + R142b	0.960	303.00	0.414	0.583	0.59 (4)	–	0.58 (3)	0.040	[293]
R12 + R152a	0.936	323.01	0.269	1.39	1.40 (3)	–	0.320(5)	0.060	[294]

Table 7: continued.

R12B2 + R114B2	1.030	306.70	0.500	0.101	0.099(3)	0.670	0.70 (1)	0.010	[295]
R13 + Propylene	0.970	273.00	0.568	1.5	1.48 (2)	0.738	0.743(4)	0.059	[280]
R13 + R11	0.975	253.15	0.568	0.73	0.73 (2)	–	0.986(2)	0.030	[296]
R13 + R12	0.971	290.00	0.549	1.836	1.80 (3)	0.809	0.800(6)	0.030	[297]
R13 + R13B1	0.992	273.00	0.566	1.46	1.42 (2)	0.712	0.699(6)	0.010	[298]
R13 + R113	0.980	348.15	0.499	3.55	3.54 (6)	–	0.890(6)	0.010	[299]
R13 + R134a	0.955	273.00	0.464	1.28	1.27 (1)	0.809	0.806(5)	0.090	[298]
R13B1 + Propylene	0.998	298.00	0.545	1.5	1.49 (1)	0.591	0.607(5)	0.032	[280]
R13B1 + R12	1.002	364.36	0.214	3.42	3.42 (3)	–	0.270(4)	0.003	[300]
R13B1 + R22	0.975	328.15	0.635	2.95	2.99 (4)	–	0.674(4)	0.031	[301]
R13B1 + R114	1.038	343.15	0.534	2.09	2.07 (3)	–	0.777(6)	0.030	[302]
R13B1 + R115	1.018	343.15	0.509	3.24	3.20 (3)	–	0.554(4)	0.015	[302]
R13B1 + R125	0.969	298.15	0.514	1.682	1.68 (1)	0.538	0.548(4)	0.063	[303]
R14 + Propylene	0.872	210.00	0.479	1.75	1.73 (4)	0.970	0.968(4)	0.050	[304]
R14 + SF_6	0.978	273.00	0.388	3.83	3.75 (5)	0.618	0.619(6)	0.010	[305]
R14 + R12	0.893	174.60	0.133	0.32	0.32 (4)	0.992	0.987(6)	0.130	[306]
R14 + R13	0.972	288.70	0.108	3.699	3.59 (6)	0.175	0.190(5)	0.050	[307]
R14 + R22	0.895	289.65	0.285	5.287	5.30 (8)	–	0.720(7)	0.105	[200]
R14 + R23	0.876	224.82	0.435	2.29	2.26 (4)	0.776	0.790(5)	0.115	[308]
R14 + R41	0.920	130.00	0.061	0.03	0.03 (1)	0.990	0.998(1)	–	[309]
R14 + R152a	0.982	174.91	0.550	0.459	0.45 (7)	0.998	0.998(1)	0.100	[306]
R20 + R10	0.958	328.15	0.499	0.068	0.068(2)	0.618	0.61 (1)	0.005	[310]
R20 + R1110	0.931	356.95	0.358	0.101	0.10 (1)	0.805	0.80 (5)	0.023	[311]
R22 + Cl_2	0.955	283.15	0.100	0.59	0.58 (1)	–	0.22 (1)	0.061	[312]
R22 + CS_2	0.950	323.15	0.509	1.448	1.47 (2)	0.923	0.928(2)	0.092	[245]
R22 + R10	0.929	383.00	0.524	3.097	3.08 (3)	0.907	0.916(3)	0.003	[313]
R22 + R11	0.956	348.15	0.543	1.98	2.00 (2)	–	0.827(4)	0.045	[314]
R22 + R12	0.974	343.81	0.498	2.61	2.61 (3)	0.574	0.570(5)	0.034	[315]
R22 + R21	0.982	293.33	0.536	0.585	0.59 (2)	0.891	0.87 (2)	0.010	[316]
R22 + R113	0.929	372.20	0.506	2.5	2.55 (4)	–	0.833(7)	0.040	[317]
R22 + R114	0.924	338.15	0.487	1.732	1.73 (3)	0.722	0.73 (1)	0.060	[292]
R22 + R115	0.931	336.75	0.518	2.781	2.75 (4)	0.546	0.549(7)	0.055	[318]
R22 + R123	0.976	383.15	0.374	2.52	2.50 (3)	0.642	0.645(7)	0.010	[315]
R22 + R124	0.999	283.15	0.500	0.444	0.428(4)	0.706	0.700(1)	-0.005	[319]
R22 + R134a	0.988	343.81	0.506	2.66	2.65 (2)	0.550	0.563(5)	0.010	[320]
R22 + R142b	0.985	328.15	0.560	1.52	1.50 (3)	0.732	0.730(8)	0.010	[321]
R22 + R152a	1.019	313.15	0.519	1.19	1.20 (3)	0.624	0.61 (3)	0.000	[321]
R23 + CS_2	0.852	398.15	0.191	14.07	13.6 (5)	0.774	0.790(8)	0.150	[245]
R23 + Propylene	0.891	265.00	0.189	1.0	1.00 (2)	0.552	0.580(6)	0.115	[298]
R23 + SF_6	0.849	295.00	0.476	3.905	3.84 (4)	0.542	0.548(4)	0.120	[247]
R23 + R11	0.849	348.10	0.400	5.23	5.15 (7)	–	0.847(5)	0.130	[233]
R23 + R12	0.883	243.00	0.600	0.774	0.74 (3)	–	0.897(6)	0.100	[322]
R23 + R13	0.902	273.15	0.538	2.732	2.75 (3)	0.564	0.562(6)	0.101	[323]
R23 + R13B1	0.906	268.15	0.415	1.619	1.57 (3)	0.600	0.629(9)	0.100	[303]
R23 + R22	0.962	323.15	0.524	4.575	4.55 (3)	0.644	0.646(4)	0.025	[245]
R23 + R113	0.812	348.10	0.415	4.72	4.65 (5)	–	0.910(5)	0.100	[324]
R23 + R114	0.836	348.00	0.300	3.54	3.55 (3)	–	0.680(6)	0.120	[325]

Table 7: continued.

R23 + R115	0.880	330.14	0.202	3.253	3.29 (4)	0.349	0.342(6)	0.120	[284]
R23 + R116	0.840	280.15	0.299	3.04	2.92 (3)	–	0.370(5)	0.120	[326]
R23 + R134a	0.956	293.15	0.401	1.75	1.79 (2)	0.750	0.715(7)	0.001	[327]
R23 + R142b	0.930	273.11	0.362	0.99	1.00 (2)	0.861	0.873(7)	0.050	[306]
R23 + R143a	0.956	293.15	0.550	2.52	2.54 (2)	0.727	0.719(3)	0.000	[328]
R23 + R152a	0.982	293.15	0.550	2.11	2.12 (3)	0.835	0.828(7)	0.000	[328]
R30 + CH_3I	1.040	298.15	0.498	0.058	0.058(1)	0.516	0.54 (1)	0.001	[259]
R30 + R10	0.979	318.15	0.450	0.082	0.081(2)	0.753	0.741(9)	0.001	[329]
R30 + R20	1.014	318.15	0.500	0.090	0.091(2)	0.676	0.709(9)	-0.010	[329]
R30 + R30B1	0.990	322.35	0.502	0.101	0.102(2)	0.717	0.745(7)	0.005	[330]
R30 + R30B2	1.000	331.25	0.436	0.101	0.101(2)	0.775	0.800(1)	0.010	[330]
R30 + R140a	0.994	432.40	0.500	1.36	1.36 (1)	–	0.660(4)	0.001	[331]
R30 + R1110	0.950	333.00	0.350	0.101	0.102(2)	0.907	0.908(6)	0.010	[332]
R30B1 + R10	0.921	313.15	0.242	0.034	0.035(2)	0.340	0.37 (2)	0.010	[333]
R30B1 + R30B2	0.972	355.08	0.372	0.101	0.102(2)	0.599	0.527(9)	0.010	[330]
R32 + Cl_2	0.965	283.15	0.352	1.111	1.12 (2)	–	0.595(8)	0.148	[312]
R32 + R12	0.941	283.15	0.180	0.783	0.782(9)	0.502	0.488(6)	0.013	[334]
R32 + R22	1.052	283.15	0.502	0.908	0.92 (1)	0.604	0.567(7)	0.130	[334]
R32 + R30	0.812	313.20	0.440	1.372	1.39 (2)	0.912	0.917(2)	0.055	[335]
R32 + R40	1.012	283.15	0.392	0.777	0.772(9)	0.663	0.649(6)	0.061	[334]
R32 + R115	0.827	298.15	0.736	1.92	1.93 (2)	–	0.724(5)	0.130	[336]
R32 + R123	0.982	313.95	0.478	1.29	1.303(1)	0.909	0.894(3)	0.045	[337]
R32 + R125	0.910	308.15	0.495	2.066	2.150(8)	0.53	0.54 (1)	0.015	[338]
R32 + R134a	1.109	289.99	0.566	1.005	0.994(2)	–	0.709(6)	0.001	[339]
R32 + R142b	0.955	314.95	0.435	1.45	1.50 (1)	0.725	0.730(4)	0.035	[328]
R32 + R143a	0.883	313.15	0.439	2.22	2.30 (4)	0.491	0.490(6)	0.015	[340]
R32 + R152a	0.995	323.15	0.260	1.775	1.76 (2)	0.463	0.419(5)	0.041	[341]
R40 + R30	0.964	278.15	0.476	0.151	0.145(3)	–	0.900(6)	0.020	[335]
R41 + R40	0.982	182.33	0.584	0.032	0.031(2)	0.975	0.974(4)	0.020	[342]
R113 + Br_2	0.940	319.25	0.820	0.101	0.103(9)	0.370	0.33 (6)	0.001	[232]
R113 + R123B1	0.998	308.15	0.103	0.06	0.059(2)	–	0.130(8)	0.006	[343]
R114 + R21	0.950	338.37	0.404	0.695	0.71 (1)	0.479	0.440(7)	0.030	[344]
R114 + R113	1.019	294.15	0.442	0.101	0.101(3)	0.770	0.79 (1)	0.010	[345]
R115 + R114	1.000	369.50	0.269	1.98	1.99 (2)	–	0.428(4)	0.010	[346]
R116 + CO_2	0.867	227.60	0.583	0.88	0.964(1)	0.380	0.382(1)	0.028	[347]
R116 + Propylene	0.888	275.00	0.563	1.8	1.82 (3)	0.687	0.702(6)	0.150	[280]
R116 + R22	0.878	288.15	0.560	2.325	2.30 (5)	0.741	0.688(4)	0.100	[348]
R116 + R32	0.768	253.55	0.385	1.20	1.21 (2)	–	0.624(3)	0.180	[347]
R116 + R41	0.775	225.45	0.529	0.69	0.68 (1)	–	0.44 (2)	0.170	[349]
R116 + R115	1.000	285.10	0.500	1.52	1.48 (1)	0.682	0.716(3)	0.020	[350]
R116 + R134a	0.881	275.00	0.300	1.17	1.17 (3)	0.730	0.72 (1)	0.095	[280]
R123B1 + R10	1.002	318.15	0.431	0.06	0.057(2)	0.651	0.64 (1)	0.010	[343]
R123B1 + R20	0.978	318.15	0.452	0.074	0.074(2)	0.544	0.55 (1)	0.001	[343]
R123B1 + R140a	1.006	318.15	0.456	0.059	0.058(1)	0.646	0.63 (1)	-0.007	[343]
R124 + R142b	0.990	312.15	0.508	0.536	0.536(8)	0.536	0.530(7)	0.000	[293]
R125 + R115	0.927	298.15	0.821	1.369	1.33 (5)	0.836	0.815(7)	0.070	[351]
R125 + R134a	0.999	323.00	0.484	1.9	1.85 (2)	0.590	0.588(4)	0.009	[352]

Table 7: continued.

R125 + R143a	0.987	264.01	0.503	0.466	0.504(5)	0.516	0.526(6)	–	[353]
R125 + R152a	0.989	333.02	0.551	2.35	2.35 (3)	0.674	0.641(6)	0.000	[354]
R134 + R142b	0.998	254.95	0.596	0.101	0.103(3)	–	0.72 (1)	0.010	[280]
R134 + R152a	1.075	253.45	0.278	0.101	0.101(3)	–	0.167(7)	0.070	[355]
R134a + R12	0.943	298.00	0.219	0.772	0.74 (2)	0.302	0.30 (1)	0.090	[280]
R134a + R114	0.899	298.00	0.534	0.538	0.54 (1)	0.746	0.76 (1)	0.080	[298]
R134a + R123	0.940	332.74	0.489	0.99	0.99 (2)	0.791	0.81 (1)	0.045	[356]
R134a + R124	0.971	307.25	0.486	0.707	0.72 (2)	0.605	0.59 (1)	0.030	[293]
R134a + R141b	0.935	333.15	0.520	1.07	1.08 (2)	0.822	0.840(6)	0.052	[357]
R134a + R142b	0.960	298.00	0.451	0.51	0.51 (3)	0.600	0.60 (3)	0.025	[280]
R134a + R152a	1.003	323.08	0.485	1.226	1.22 (3)	0.505	0.50 (1)	0.001	[358]
R140 + R130a	1.003	399.75	0.186	0.101	0.100(2)	0.260	0.262(8)	0.020	[359]
R140 + R1110	0.974	390.50	0.232	0.101	0.100(3)	0.308	0.289(1)	0.010	[360]
R140a + R10	1.010	298.15	0.506	0.017	0.016(1)	–	0.53 (2)	-0.001	[361]
R141b + R140a	0.996	323.25	0.200	0.076	0.075(2)	0.502	0.50 (1)	0.010	[334]
R142b + R113	0.952	373.00	0.502	1.25	1.27 (4)	–	0.77 (2)	0.030	[325]
R142b + R140a	0.945	323.25	0.481	0.383	0.42 (4)	0.931	0.94 (2)	0.030	[334]
R142b + R141b	0.994	323.25	0.490	0.433	0.44 (2)	0.749	0.74 (2)	0.010	[334]
R143a + R12	0.936	313.00	0.600	1.71	1.65 (4)	–	0.675(8)	0.080	[322]
R143a + R22	1.023	275.00	0.500	0.589	0.58 (3)	0.546	0.54 (3)	0.000	[362]
R143a + R134a	0.994	293.15	0.442	0.798	0.816(7)	0.567	0.570(5)	0.013	[363]
R143a + R152a	0.977	313.15	0.447	1.34	1.40 (1)	0.571	0.570(4)	0.001	[363]
R143a + R1122	0.958	313.50	0.708	1.57	1.56 (2)	–	0.800(4)	0.030	[270]
R150a + R10	0.937	335.63	0.506	0.101	0.104(3)	0.661	0.65 (1)	0.030	[364]
R150a + R20	1.000	302.86	0.456	0.033	0.032(1)	0.494	0.51 (2)	–	[365]
R150a + R140	1.010	349.15	0.500	0.101	0.09 (2)	0.853	0.87 (5)	0.015	[359]
R152a + R12B1	0.921	293.15	0.385	0.44	0.44 (2)	–	0.63 (2)	0.085	[366]
R152a + R113	0.883	348.20	0.462	1.246	1.24 (3)	–	0.85 (1)	0.080	[324]
R152a + R114	0.897	345.50	0.392	1.53	1.471(2)	–	0.592(5)	0.110	[367]
R152a + R142b	0.963	347.60	0.461	1.72	1.74 (2)	0.544	0.550(5)	0.045	[368]
R152a + R150a	0.963	323.20	0.488	0.67	0.64 (7)	0.900	0.91 (2)	0.030	[262]
R152a + R1140	0.975	323.20	0.505	1.05	1.06 (1)	0.578	0.600(4)	0.030	[335]
R160B1 + CS_2	1.018	286.15	0.074	0.032	0.032(2)	0.145	0.10 (1)	0.040	[369]
R1114 + R32	0.932	253.15	0.391	0.885	0.88 (4)	0.607	0.64 (3)	0.130	[370]
R1120 + R1110	0.954	380.85	0.262	0.101	0.102(3)	0.512	0.50 (2)	0.010	[371]
R1140 + R140	0.980	346.15	0.517	0.703	0.72 (5)	–	0.95 (1)	0.010	[372]
R1140 + R1120	1.037	298.15	0.180	0.067	0.065(2)	–	0.886(9)	-0.030	[373]

Table 8: List of the 8 binary mixtures for which experimental VLE data is available on the dew line only, including reference.

Ne + C_2H_6	[374]	Xe + I_2	[375]	N_2 + R10	[377]	CO_2 + R10	[377]
Ne + C_2H_4	[374]	I_2 + CO_2	[376]	CO_2 + Kr	[378]	R143a + R12B1	[379]

Table 9: List of the 11 binary mixtures for which experimental VLE data is available for dilute state points only.

Ar + R113	[380]	Cl_2 + R130a	[230]	CO_2 + SF_6	[382]	SF_6 + R113	[285]
CH_4 + CS_2	[381]	N_2 + CS_2	[381]	CO_2 + R113	[380]	R13 + R10	[383]
CH_4 + R113	[380]	N_2 + R113	[380]	SF_6 + CS_2	[381]		

4.2.2 Results and Discussion

The results are presented here in pressure vs. mole fraction phase diagrams, cf. Figures 41 to 60 and the supplementary material of [390]. Full numerical VLE simulation data are given in the supplementary material of [390] as well, which also contains the saturated densities and the heat of vaporization from simulation. Due to the fact that such data is rarely available from experiment for comparison, they are not discussed here.

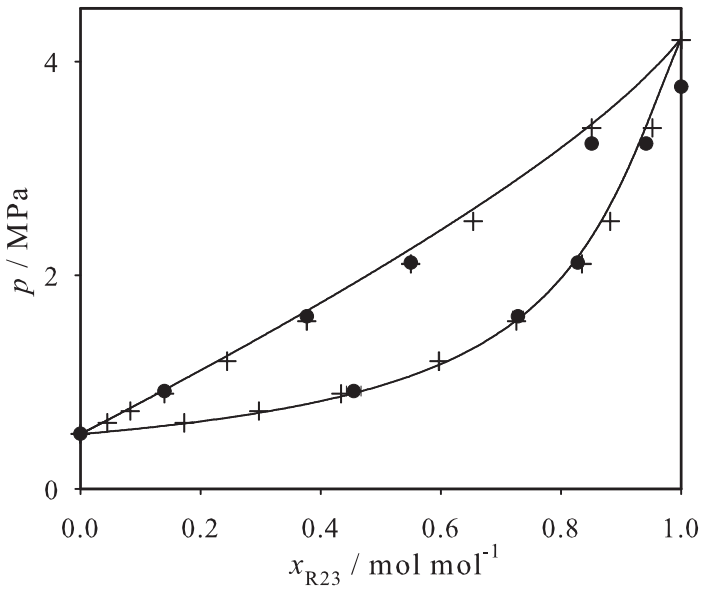

Figure 41: Binary vapor-liquid phase diagram of R23 + R152a at 293.15 K: + experimental data [328]; ● present simulation data with ξ=0.982; — Peng-Robinson EOS with k_{ij}=0.000.

By addressing the binaries, the lower boiling component is always mentioned first, i.e. in mixture A + B, A is lower boiling one. In all phase diagrams, also the pure substance vapor pressure of the molecular models is indicated. These were obtained via the vapor pressure correlations for polar 2CLJ fluids as given in [177, 178].

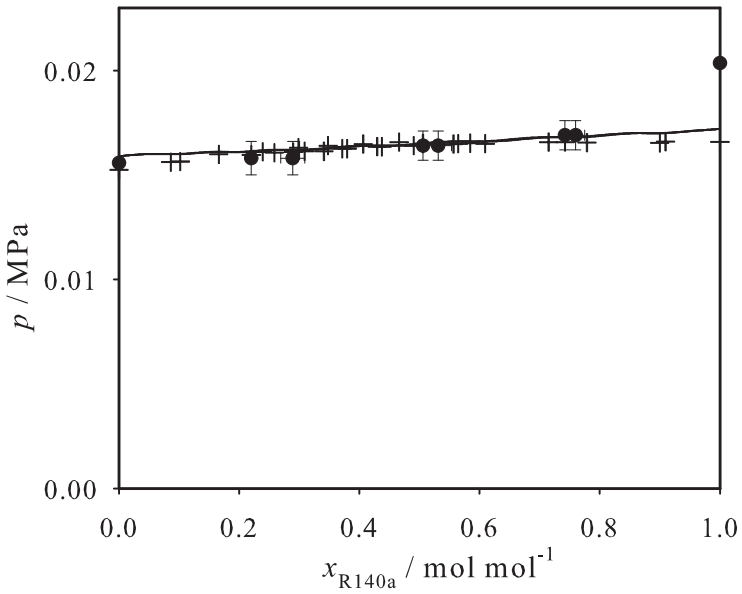

Figure 42: Binary vapor-liquid phase diagram of R140a + R10 at 298.15 K: + experimental data [361]; ● present simulation data with ξ=1.010; — Peng-Robinson EOS with k_{ij}=-0.001.

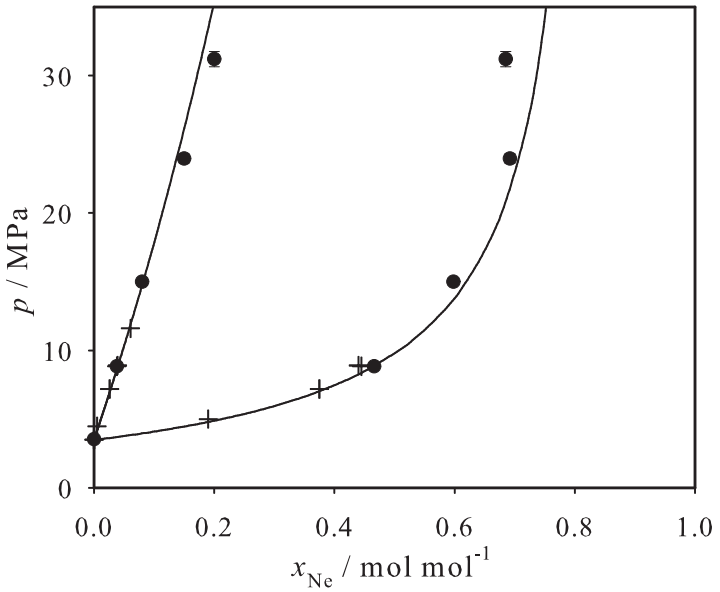

Figure 43: Binary vapor-liquid phase diagram of Ne + CO_2 at 273.15 K: + experimental data [192]; ● present simulation data with ξ=1.124; — Peng-Robinson EOS with k_{ij}=0.100.

To assess the quality of the mixture models, VLE calculations were made at other state points than those used for the adjustment of the binary interaction parameter ξ. Preferably, state points were chosen for which a direct comparison to experimental data is possible. The near-critical region was not covered to avoid difficulties in the simulations. The first criterion of the present assessment is the resulting slope of the bubble line which can directly be compared with experimental data in most cases. The second criterion is the resulting dew point composition as a function of pressure which is fully predictive here. These data may also directly be compared to experimental data in most cases. However, for 80 mixtures no experimental dew line data was published. A similar assessment was made in the Third Industrial Fluid Property Simulation Challenge 2007 [5] for molecular simulation data regarding the binary system R227ea + Ethanol.

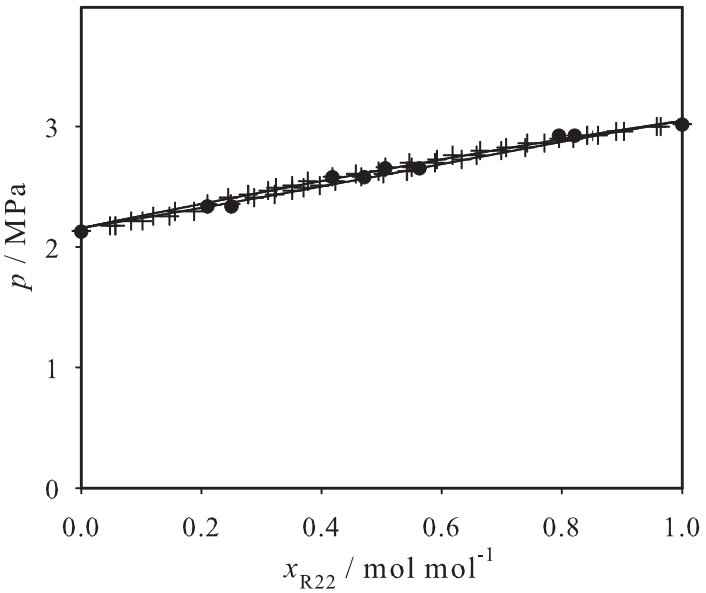

Figure 44: Binary vapor-liquid phase diagram of R22 + R134a at 343.81 K: + experimental data [320]; ● present simulation data with ξ=0.988; — Peng-Robinson EOS with k_{ij}=0.010.

The mixture models were rated according to the two criteria mentioned above: if the slope of the simulative bubble line was in agreement with the experiment roughly within the statistical uncertainty and the average deviation between simulation and experiment for the dew point mole fraction was below 0.05 mol/mol, it was assumed that the mixture model is *successful*. For a few pure fluids, e.g. R23 between around 260 to 300 K, the pure substance vapor pressure shows noticeable deviations when compared with experimental data, cf. Figure 41. Thus, the binary two-phase envelope must deviate in the region which is rich of this component. However, it was found that such deficiencies usually do

not translate into the remaining composition range. If the mixing behavior was generally predicted correctly in that sense, the mixture model was also rated as successful.

The successful cases are discussed here at a glance due to the large number of systems, however, they are all shown in the supplementary material of [390]. The regarded vapor pressure range, depending on the availability of experimental data, was extensive. It covers more than three orders of magnitude from around 0.016 MPa (R140a + R10, cf. Figure 42) to above 30 MPa (Ne + CO_2, cf. Figure 43).

For zeotropic mixtures, it can be seen that very different shapes of the two-phase envelope were predicted correctly. At sub-critical temperatures, there are very narrow envelopes (e.g. R22 + R134a, cf. Figure 44), wider envelopes (e.g. Propylene + R114, cf. Figure 45) and very wide envelopes (e.g. R14 + R152a, cf. Figure 46), where the vapor phase contains little of the high boiling component.

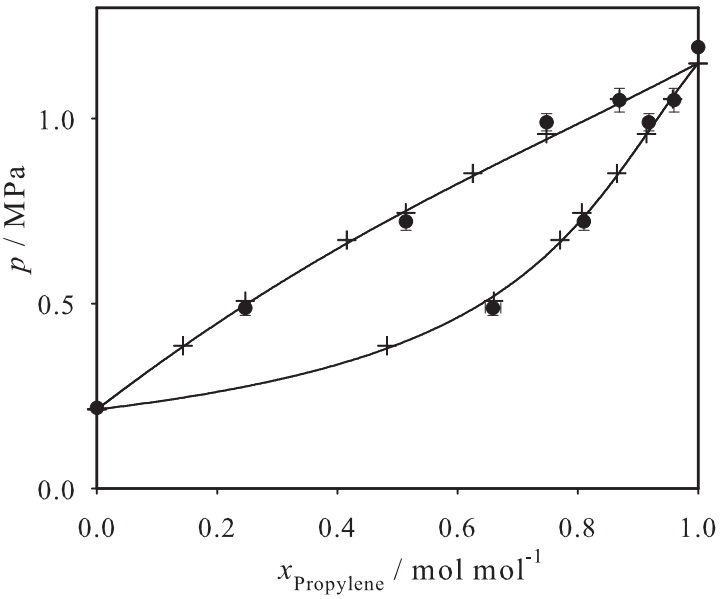

Figure 45: Binary vapor-liquid phase diagram of Propylene + R114 at 298 K: + experimental data [280]; ● present simulation data with ξ=0.966; — Peng-Robinson EOS with k_{ij}=0.050.

There are qualitatively different slopes of the bubble line: convex (e.g. Xe + R40, cf. Figure 47), straight (e.g. N_2 + Ar, cf. Figure 48), concave (e.g. R23 + R152a, cf. Figure 41) or S-shaped (e.g. R14 + Propylene, cf. Figure 49). Also qualitatively different slopes of the dew line were predicted correctly: convex (e.g. R22 + R12, cf. Figure 50), straight (e.g. R22 + R134a, cf. Figure 44), concave (e.g. CH_4 + C_2H_6, cf. Figure 51), or S-shaped (e.g. R22 + CS_2, cf. Figure 52).

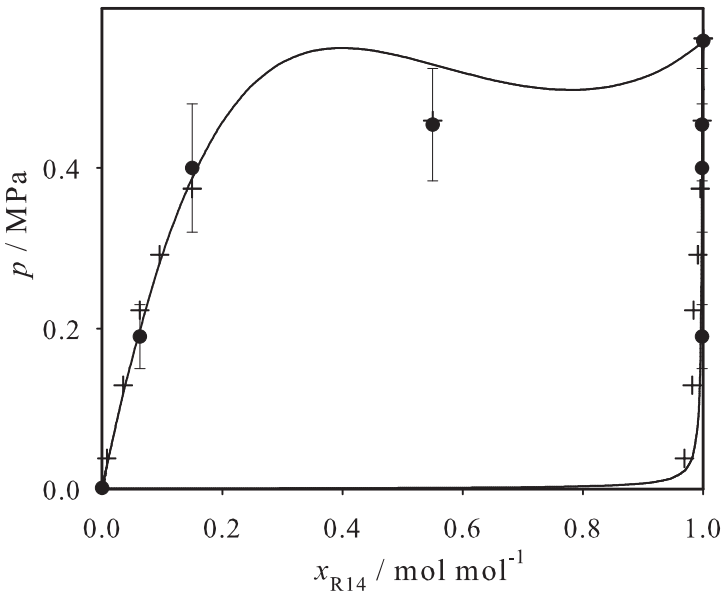

Figure 46: Binary vapor-liquid phase diagram of R14 + R152a at 174.91 K: + experimental data [306]; ● present simulation data with ξ=0.982; — Peng-Robinson EOS with k_{ij}=0.100.

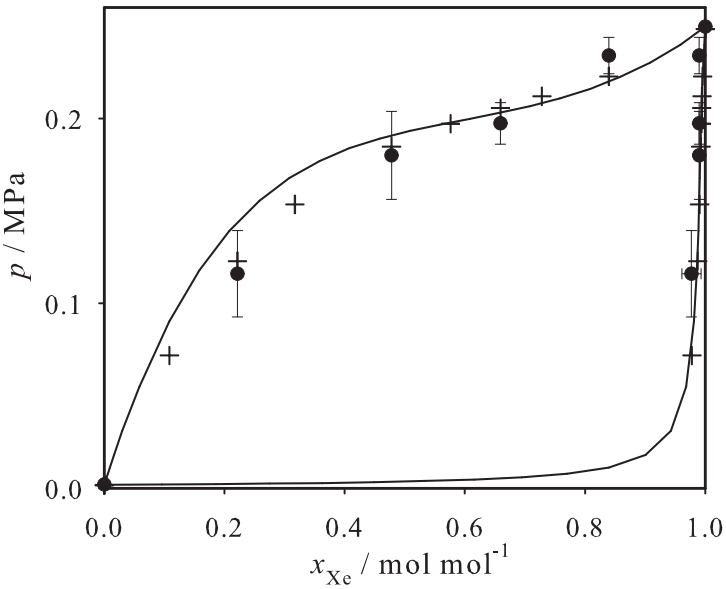

Figure 47: Binary vapor-liquid phase diagram of Xe + R40 at 182.32 K: + experimental data [206]; ● present simulation data with ξ=0.973; — Peng-Robinson EOS with k_{ij}=0.074.

Analyzing the VLE envelopes further, it was found that 36 binaries show an azeotropic behavior, thereof one exhibits a pressure minimum (R134 + R152a, cf. Figure 53). It should be noted that the location of the azeotropic point is a fully predictive property in the present work.

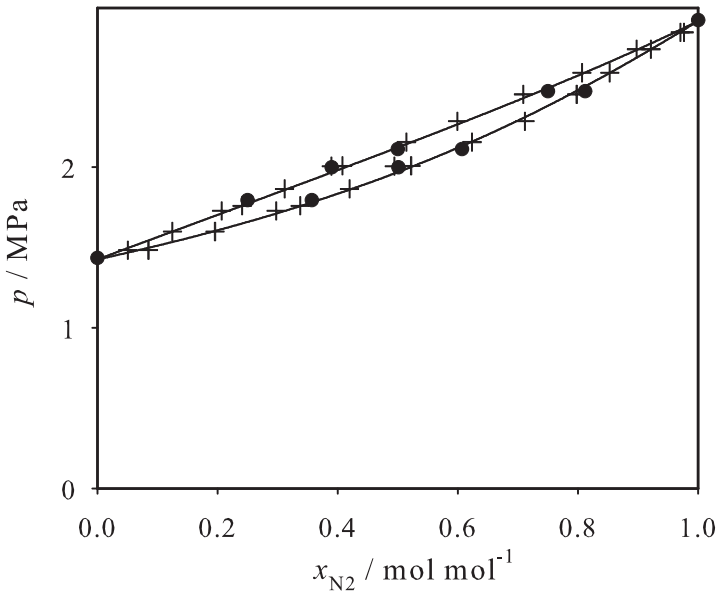

Figure 48: Binary vapor-liquid phase diagram of N_2 + Ar at 122.89 K: + experimental data [216]; ● present simulation data with ξ=1.010; — Peng-Robinson EOS with k_{ij}=-0.015.

To limit the computational effort, for most mixtures only one isotherm was simulated and, of course, it can be argued that the binary interaction parameter ξ and thus the mixture model might only be valid for the temperature where it was adjusted. This would significantly restrict the applicability of the present mixture models.

To counter this, a subset of 53 binaries was regarded for two to up to four different temperatures. A good example is CO + CH_4, cf. Figure 54, which is experimentally well explored. It can be seen there for four isotherms that the present mixture model is successful in a temperature range of 55 K in the entire composition range. Also larger temperature intervals were regarded, e.g. 100 K for R22 + CS_2, cf. Figure 52.

For 22 mixtures only isobaric experimental data is available, mostly at ambient pressure. Then, usually only these state points were simulated (e.g. R116 + R115, cf. Figure 55) and thus the predictive quality with respect to temperature and composition was assessed.

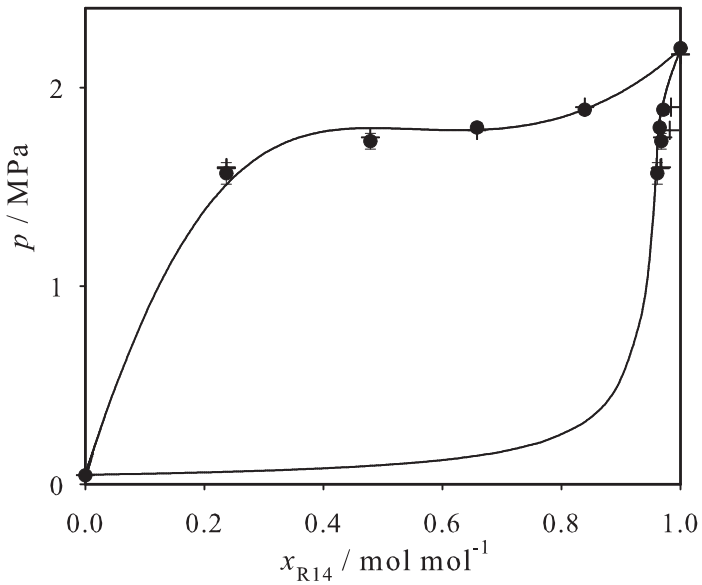

Figure 49: Binary vapor-liquid phase diagram of R14 + Propylene at 210 K: + experimental data [304]; ● present simulation data with ξ=0.872; — Peng-Robinson EOS with k_{ij}=0.050.

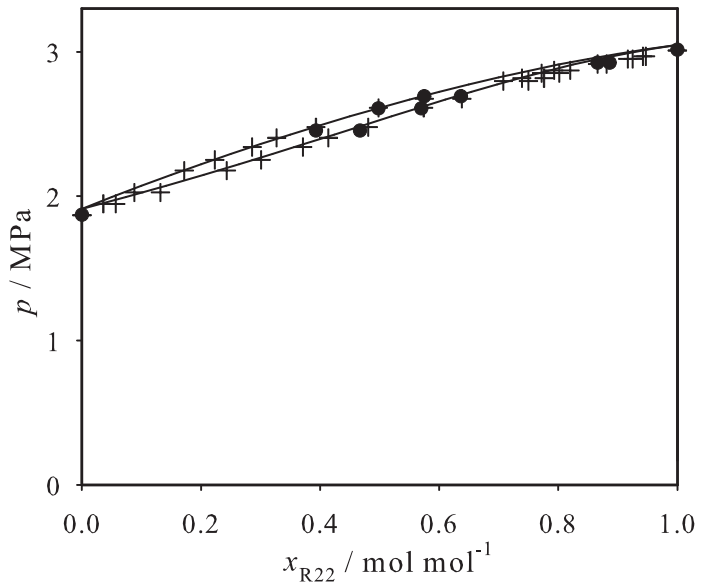

Figure 50: Binary vapor-liquid phase diagram of R22 + R12 at 343.81 K: + experimental data [315]; ● present simulation data with ξ=0.974; — Peng-Robinson EOS with k_{ij}=0.034.

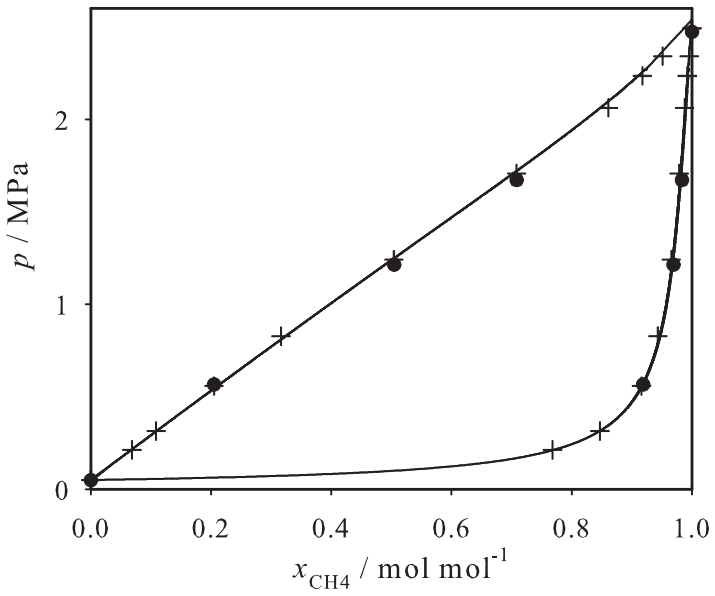

Figure 51: Binary vapor-liquid phase diagram of CH_4 + C_2H_6 at 172.04 K: + experimental data [212]; ● present simulation data with ξ=0.997; — Peng-Robinson EOS with k_{ij}=0.001.

In case of 12 binaries experimental data is only available for a fixed bubble point composition (e.g. SF_6 + R13B1, cf. Figure 56). There, the predictions regarding temperature and pressure were evaluated.

In summary, for a total of 267 binaries useful experimental VLE data were found. Based on the criteria mentioned above it has been rated the present modeling approach in 259 cases as successful, i.e. only for eight binaries, listed in Table 10, larger deviations were found. The quota of successful mixture models is hence 97 %.

Table 10: List of the 8 binary mixtures for which the present molecular mixture models show larger deviations.

Ne + Xe	[384]	Ne + R14	[385]	C_2H_2 + Propylene	[387]	Propylene + R30	[237]
Ne + R13	[385]	N_2 + R14	[386]	C_2H_2 + Propyne	[387]	R13 + R114	[388]

It is worthwhile to examine the unsatisfactory cases as well, which are listed in Table 10. Different deviation types can be distinguished: For five binaries, the agreement between simulation and experiment is good on the bubble line, however, the predicted dew point composition is off by more than 0.05 mol/mol on average.

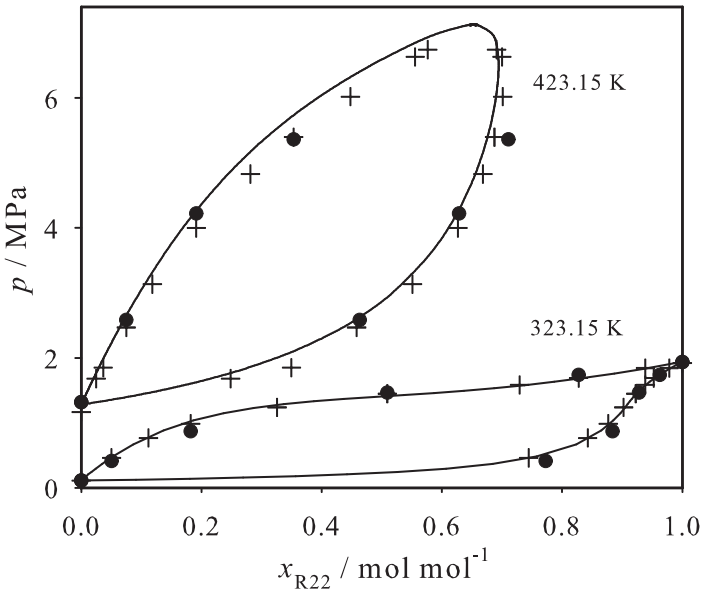

Figure 52: Binary vapor-liquid phase diagram of R22 + CS_2 at 323.15 and 423.15 K: + experimental data [245]; ● present simulation data with ξ=0.950; — Peng-Robinson EOS with k_{ij}=0.092.

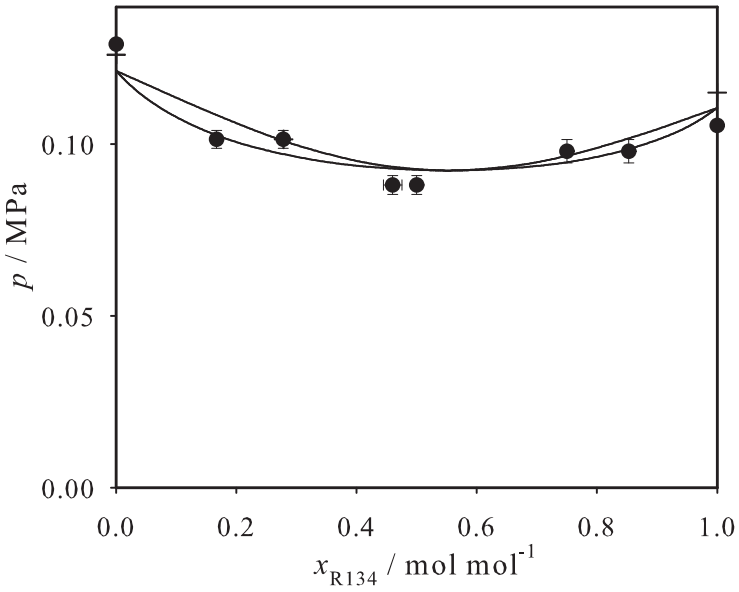

Figure 53: Binary vapor-liquid phase diagram of R134 + R152a at 253.45 K: + experimental data [355]; ● present simulation data with ξ=1.075; — Peng-Robinson EOS with k_{ij}=0.070.

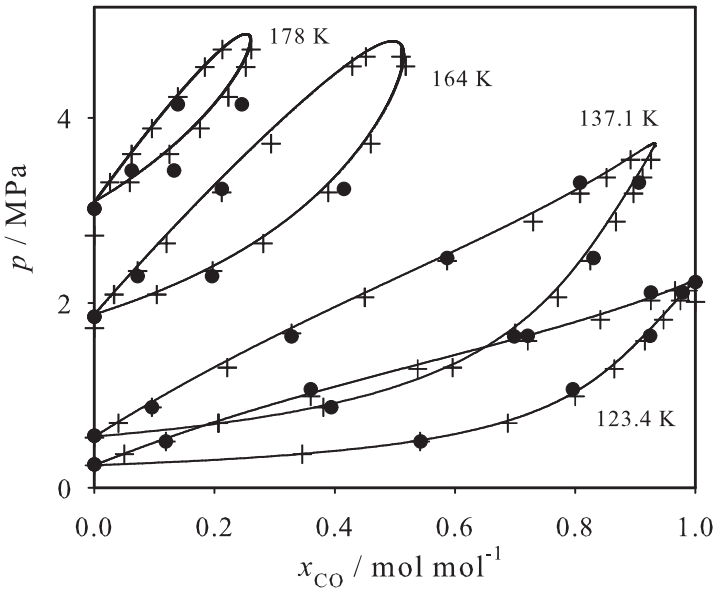

Figure 54: Binary vapor-liquid phase diagram of CO + CH_4 at 123.4, 137.1, 164 and 178 K: + experimental data [234]; ● present simulation data with ξ=1.003; — Peng-Robinson EOS with k_{ij}=0.026.

This is the case for Ne + Xe (Figure 57), Ne + R13, Ne + R14, N_2 + R14 and Propylene + R30. It should be noted that three of those mixtures contain Neon. In case of C_2H_2 + Propylene, cf. Figure 58, a modest temperature extrapolation over 21 K failed, where significant deviations in pressure were found. The simulated binary data for C_2H_2 + Propyne, cf. Figure 59, also shows deviations from experimental dew line data, however, the slope of the bubble line seems qualitatively wrong as well. Finally, a significant mismatch between experiment and simulation was found for R13 + R114. The experimental data for that system, taken from DDB, is from an anonymous author [388] and is the only available source. By inspection of Figure 60 it can be concluded the binary data from [388] seems doubtful as it does not correspond with the pure substance vapor pressure of the two components in the pure substance limit.

On the basis of such a large data set it is useful to examine the distribution of the optimized unlike interaction parameter ξ, cf. Figure 61. It can be seen that the modus of this distribution lies at $\xi = 1$ and that on average ξ is below unity. For 71 % of the binaries it is within 5 % of the Berthelot rule ($\xi = 1$). Six systems (Ne + Kr, Ne + CO_2, SF_6 + R32, R32 + R134a, R116 + R32, and R116 + R41) require binary parameters that significantly differ from unity, i.e $\xi < 0.8$ or $\xi > 1.1$. Among them two again contain Ne, which indicates together with the three unsatisfactory cases that the Lennard-Jones

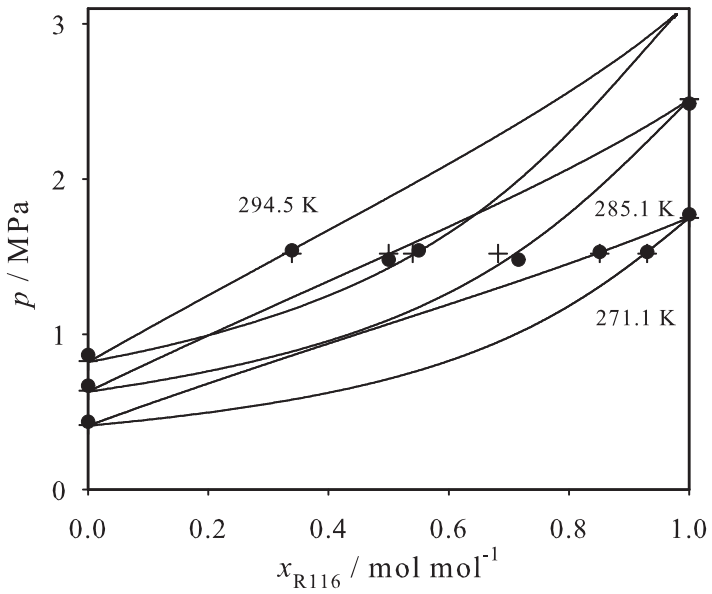

Figure 55: Binary vapor-liquid phase diagram of R116 + R115 at 271.1, 285.1 and 294.5 K: + experimental data [350]; ● present simulation data with ξ=1.000; — Peng-Robinson EOS with k_{ij}=0.020.

potential does not well represent the intermolecular interactions of Ne. Three of the remaining four binaries contain R32, which was modeled by the Stockmayer potential. It might be argued that the large deviation from unity is caused by this oversimplification of the molecular structure of R32.

For 263 systems, the results of the Peng-Robinson EOS with adjusted binary parameter k_{ij} are also shown. Due to the fact that this model is a reliable correlation tool, making it a workhorse in process engineering, it performs well in most cases too. Beside the fact that it sometimes overshoots in the critical region, which is a well known fact, only for few mixtures significant deviations were found. Examples are Ar + Propylene, CO_2 + CS_2 and R23 + CS_2 (all presented in the supplementary material of [390]) as well as R14 + R152a (Figure 46), Xe + R40 (Figure 47), C_2H_2 + Propylene (Figure 58) and R13 + R114 (Figure 60).

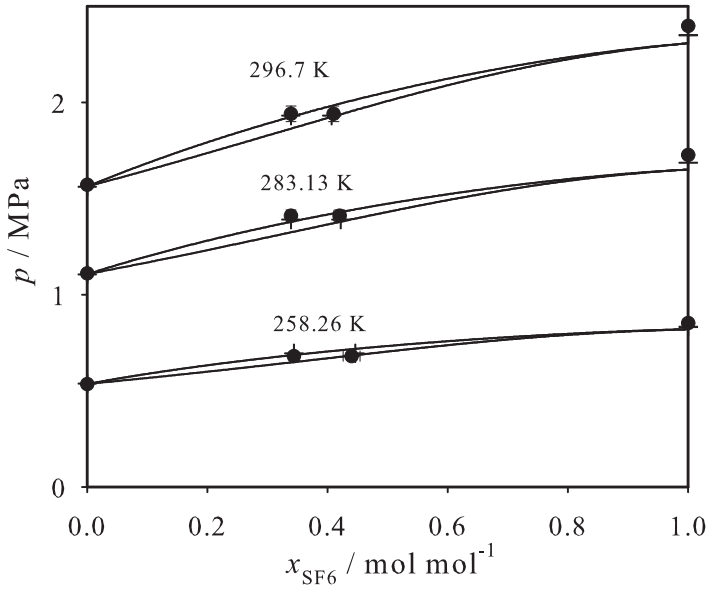

Figure 56: Binary vapor-liquid phase diagram of SF_6 + R13B1 at 258.26, 283.13 and 296.7 K: + experimental data [284]; ● present simulation data with ξ=0.999; — Peng-Robinson EOS with k_{ij}=0.035.

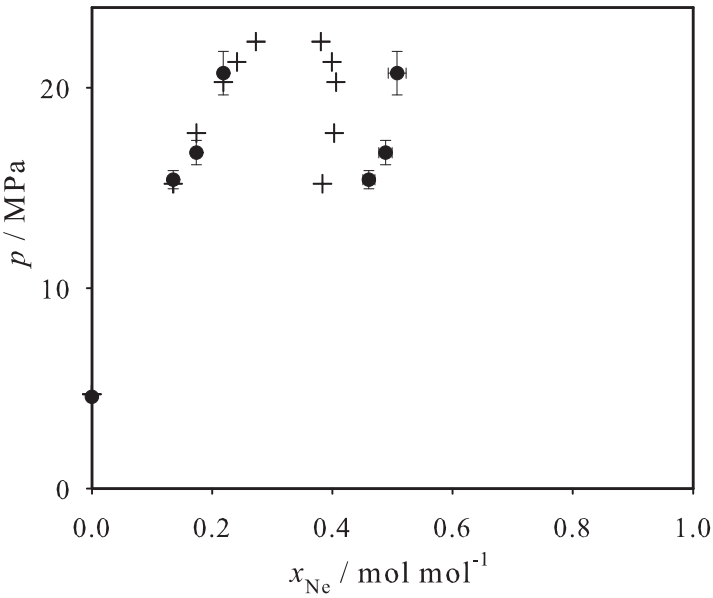

Figure 57: Binary vapor-liquid phase diagram of Ne + Xe at 279.14 K: + experimental data [384]; ● present simulation data.

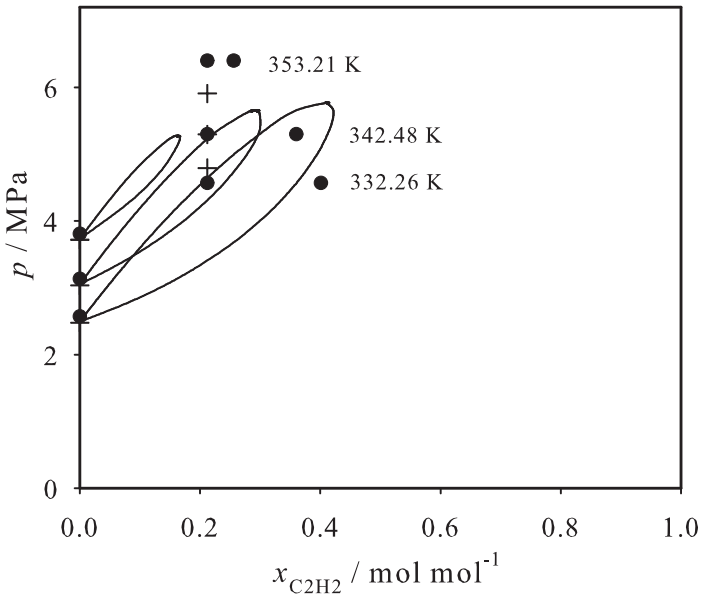

Figure 58: Binary vapor-liquid phase diagram of C_2H_2 + Propylene at 332.26, 342.48 and 353.21 K: + experimental data [387]; ● present simulation data; — Peng-Robinson EOS.

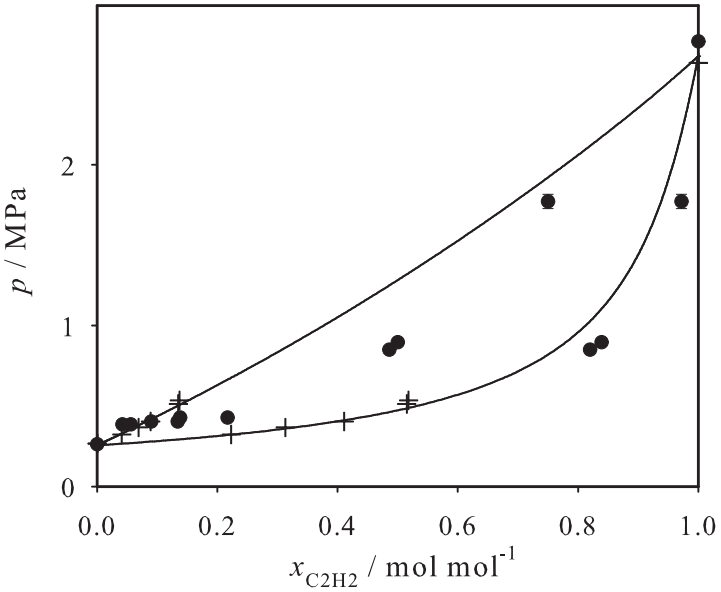

Figure 59: Binary vapor-liquid phase diagram of C_2H_2 + Propyne at 273.3 K: + experimental data [387]; ● present simulation data; — Peng-Robinson EOS.

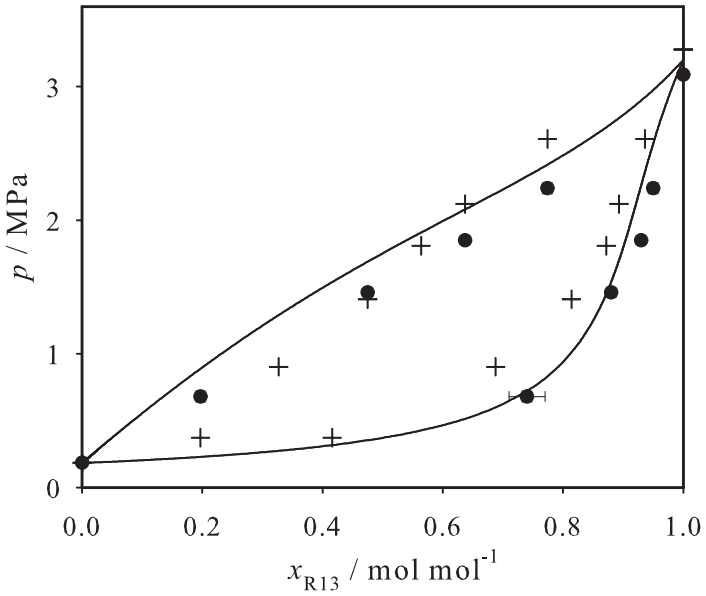

Figure 60: Binary vapor-liquid phase diagram of R13 + R114 at 293.15 K: + experimental data [388]; ● present simulation data; — Peng-Robinson EOS.

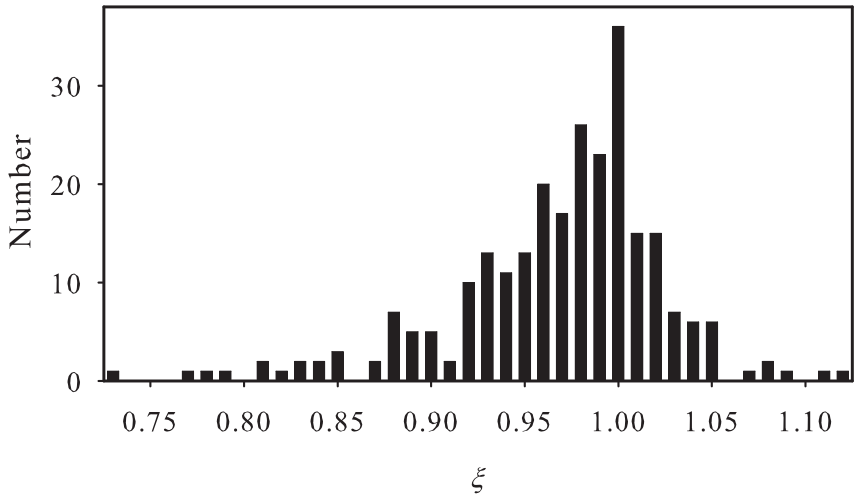

Figure 61: Distribution of the binary interaction parameter ξ for the 259 successful cases.

4.3 Ternary Vapor-Liquid Equilibria

The binary interaction parameters of 267 binary systems in Section 4.2 were applied here for all available ternary systems based on those 78 pure substance models.

To avoid an arbitrary selection of the studied systems, a combinatorial brute force approach was taken. Theoretically, out of the $N = 78$ components $N(N-1)(N-2)/6 =$ 76 076 ternary mixtures can be formed, but of course, by far not all of these systems have been studied experimentally. To our knowledge, VLE were measured only for a subset of 33 out of the 76 076 ternary systems, corresponding to 0.043%. In the present work, all these 33 ternary mixtures were studied. This is the largest set of ternary systems that was used so far to probe the application of molecular modeling and simulation to ternary mixtures.

It would have been attractive to investigate VLE of multi-component mixtures with more than three components too, however, to our knowledge no experimental data exist for any mixture consisting of four or more of those 78 components.

The simulation results from the present work are compared to experimental data and in most cases to the Peng-Robinson EOS [138] which was applied in the same predictive way, i.e. it was adjusted to the same binary data that were also used to adjust the molecular mixture models.

4.3.1 Experimental Database

Experimental data were predominately retrieved using Dortmunder Datenbank (DDB) [187]. According to DDB, for a subset of 33 of the potential 76 076 ternary mixtures experimental VLE data are available. They stem from 30 publications, cf. Table 11. These 33 ternary systems include 35 of the 78 pure components, cf. Section 4.1, Table 6.

The studied 33 ternary systems are listed in Table 11 together with a reference to the experimental VLE data. Of those 33 ternary mixtures, five have been modeled in previous work of our group [36, 37, 38], but the resulting VLE data were published only partly.

It can be argued that these 33 systems, being just 0.043% of the full combinatorial sample, were selected by the experimentalists due their technical or scientific importance. The majority of the 33 mixtures were measured for potential refrigeration applications, however, indiscriminately all ternary VLE out of the 78 components for which experimental data are available were studied here.

Table 11: List of the 33 studied ternary mixtures and reference to literature on experimental VLE. For systems indicated with †, only bubble line data is available from experiment.

Ar + CH_4 + N_2	[391]	N_2 + CO_2 + C_2H_6	[401]	R13 + R14 + R23	[407]
Ar + CH_4 + CO	[392]	N_2 + CO_2 + R12	[402]	R22 + R23 + R114 †	[406]
Ar + CH_4 + C_2H_6	[197]	N_2 + CO_2 + R22	[403]	R22 + R124 + R142b †	[408]
Ar + N_2 + O_2	[393]	N_2 + R13 + R14 †	[404]	R22 + R142b + R152a	[321]
CH_4 + N_2 + CO	[394]	CO_2 + R22 + R142b	[254]	R23 + R113 + R114 †	[325]
CH_4 + N_2 + CO_2	[395]	CO_2 + R142b + R152a	[254]	R30 + R30B1 + R30B2	[330]
CH_4 + N_2 + C_2H_6	[396]	C_2H_2 + C_2H_4 +C_2H_6	[274]	R32 + R125 + R134a	[409]
CH_4 + CO + CO_2	[397]	R10 + R20 + R30	[329]	R32 + R125 + R143a	[410]
CH_4 + CO_2 + C_2H_6	[398]	R10 + R1110 + R1120	[405]	R125 + R134a + R143a	[411]
CH_4 + C_2H_4 + C_2H_6	[399]	R11 + R22 + R23 †	[406]	R125 + R134a + R161 †	[411]
N_2 + O_2 + CO_2	[400]	R12 + R113 + R152a †	[324]	R140a + R141b + R142b	[334]

4.3.2 Molecular Mixture Models for Ternary Vapor-Liquid Equilibria

If a mixture A + B + C is modeled on the basis of Lennard-Jones potentials, the knowledge of three pairs of unlike Lennard-Jones parameters is required: σ_{AB}, ϵ_{AB} and σ_{AC}, ϵ_{AC} as well as σ_{BC}, ϵ_{BC}. For their determination, the broadly used Lorentz-Berthelot combining rule is a good starting point [75]. However, introducing a binary interaction parameter ξ to adjust the unlike energy parameter

For VLE, it was shown in [75] that ξ can be adjusted to a single experimental binary vapor pressure. Values for ξ are given in Section 4.2, Table 7 for 267 binary combinations. Note that the present 33 ternary systems comprise 65 different binary subsystems, whereof 62 were covered in Table 7. The three exceptions are N_2 + R14, R125 + R161 and R134a + R161. The binary interaction parameter for these three binary subsystems was not adjusted to ternary VLE data, thus $\xi = 1$ was specified instead. It was also refrained here from adjusting the binary interaction parameter k_{ij} of the Peng-Robinson EOS for those systems.

4.3.3 Results and Discussion

To assess the predictive quality of the mixture models, ternary VLE were determined by molecular simulation predominantly at state points for which a direct comparison to experimental data is possible. Simulation details are given in the Appendix B. The Grand Equilibrium method [96] was used for the VLE simulations, where temperature and liquid composition are the independently specified thermodynamic variables, while vapor pres-

sure, saturated vapor composition, saturated densities and enthalpy of vaporization are determined. In most cases, simulation results are presented that match exactly with the experimental bubble line composition. However, if it was found that there is a significant mismatch for the resulting vapor pressure with respect to the experiment, the simulative bubble line composition was altered so that both data sets are almost in the same temperature-pressure plane.

As experimental densities and enthalpies are rarely available in the literature, only vapor pressure and saturated vapor composition were used for this assessment. It should be noted that saturated vapor composition data are available for 26 of the investigated 33 ternary systems, for the remaining seven systems, only bubble line data are available, cf. Table 11.

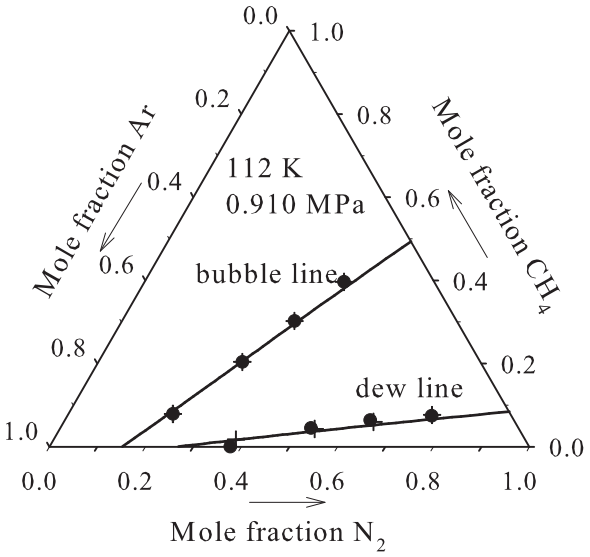

Figure 62: Ternary vapor-liquid equilibrium phase diagram of the mixture Ar + CH_4 + N_2 at 112 K and 0.91 MPa: + experimental data [391]; ● present simulation data; — Peng-Robinson EOS.

The results are presented here in ternary plots at constant temperature and pressure, cf. Figures 62 to 76, covering 15 of the 33 studied ternary mixtures. For the remaining 18 systems, the results are not presented in figures here, while the numerical comparison to experimental data can be found in the supplementary data of [412]. The full set of numerical VLE simulation results is given in the supplementary data of [412], which also contains saturated densities and heat of vaporization from simulation.

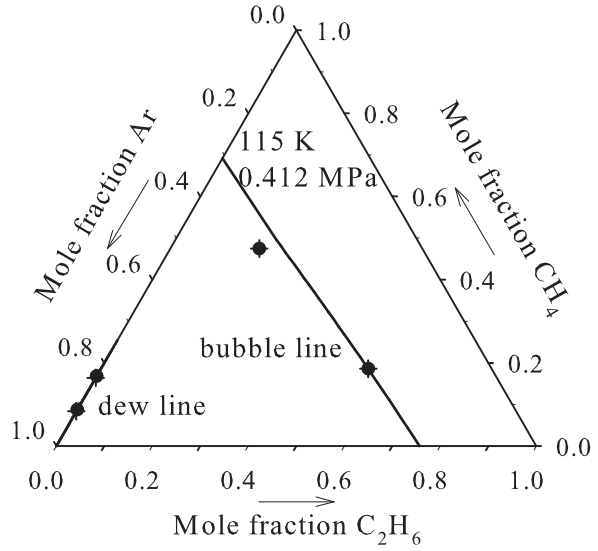

Figure 63: Ternary vapor-liquid equilibrium phase diagram of the mixture Ar + CH_4 + C_2H_6 at 115 K and 0.412 MPa: + experimental data [197]; ● present simulation data; — Peng-Robinson EOS.

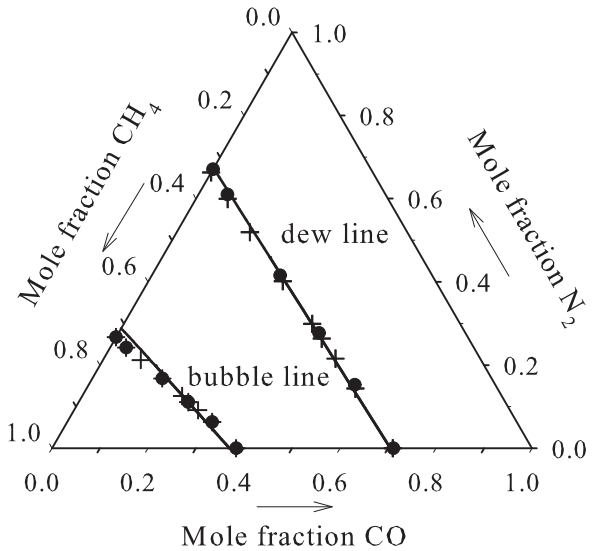

Figure 64: Ternary vapor-liquid equilibrium phase diagram of the mixture CH_4 + N_2 + CO at 140 K and 2 MPa: + experimental data [394]; ● present simulation data; — Peng-Robinson EOS.

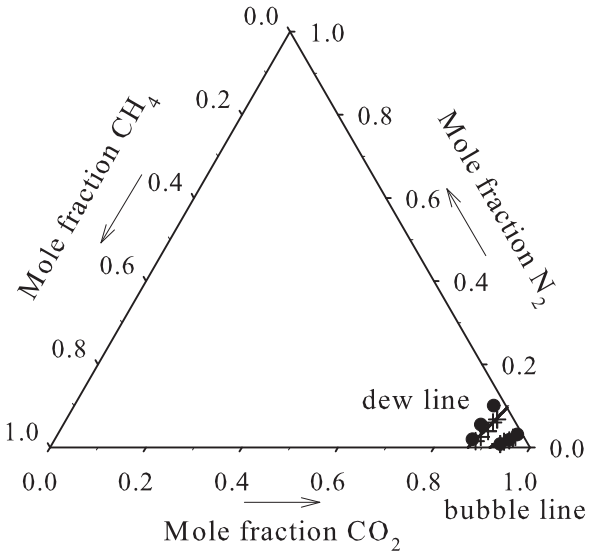

Figure 65: Ternary vapor-liquid equilibrium phase diagram of the mixture CH_4 + N_2 + CO_2 at 293.19 K and 7.15 MPa: + experimental data [395]; ● present simulation data; — Peng-Robinson EOS.

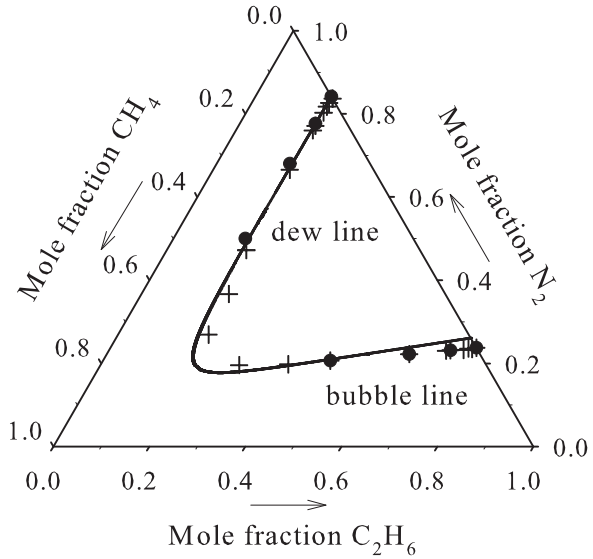

Figure 66: Ternary vapor-liquid equilibrium phase diagram of the mixture CH_4 + N_2 + C_2H_6 at 220 K and 8 MPa: + experimental data [396]; ● present simulation data; — Peng-Robinson EOS.

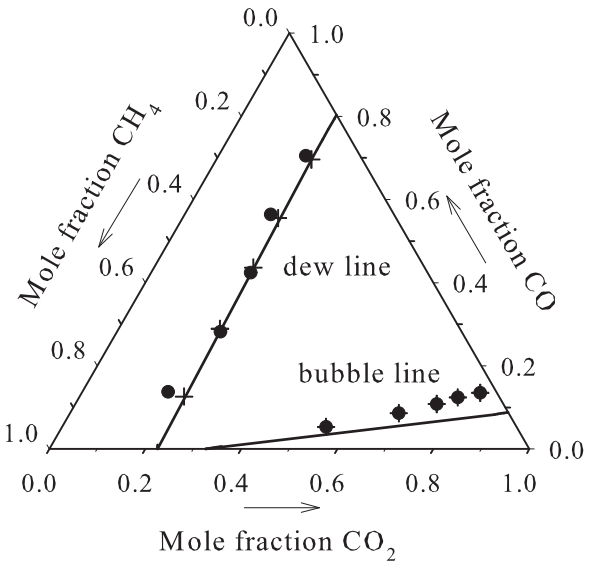

Figure 67: Ternary vapor-liquid equilibrium phase diagram of the mixture CH_4 + CO + CO_2 at 223.15 K and 6.7 MPa: + experimental data [397]; ● present simulation data; — Peng-Robinson EOS.

For all predicted VLE properties, an estimate of the statistical uncertainty is provided in the supplementary data of [412]. Due to the fact that the error bars are mostly within symbol size, they were omitted in the figures.

The present assessment was made on the basis of the resulting composition on the saturation lines which can directly be seen in comparison with the experimental data in the phase diagrams of this section. Note that the simulated vapor pressure in general does not match exactly with the presented pressure, but it is usually very close to it. The numerical data in the supplementary data of [412] allow for a direct comparison of the vapor pressure.

Not for all studied systems, the experimental data are sufficient to assess the topology of the saturation lines in the the isobaric-isothermal phase diagrams. Most of those, for which this is possible, show a simple topology where one straight bubble line and one straight corresponding dew line connect two binary subsystems, e.g. Ar + CH_4 + N_2, cf. Figure 62, CH_4 + N_2 + CO, cf. Figure 64, or N_2 + CO_2 + R22, cf. Figure 71.

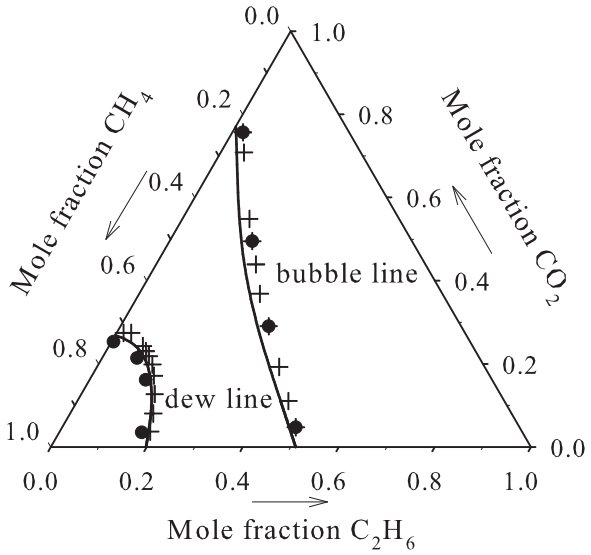

Figure 68: Ternary vapor-liquid equilibrium phase diagram of the mixture CH_4 + CO_2 + C_2H_6 at 230 K and 4.65 MPa: + experimental data [398]; ● present simulation data; — Peng-Robinson EOS.

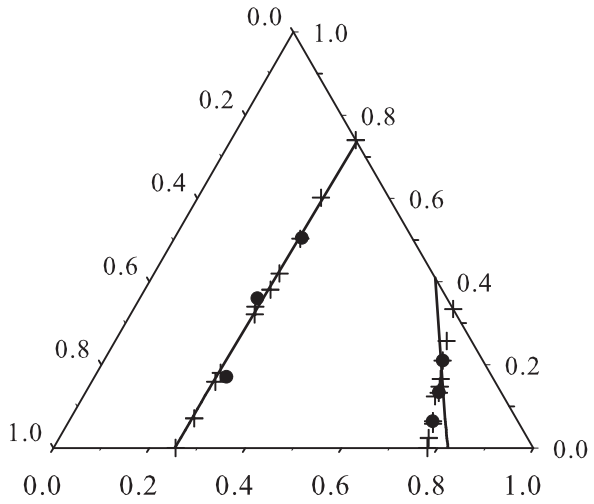

Figure 69: Ternary vapor-liquid equilibrium phase diagram of the mixture N_2 + O_2 + CO_2 at 232.85 K and 12.4 MPa: + experimental data [400]; ● present simulation data; — Peng-Robinson EOS.

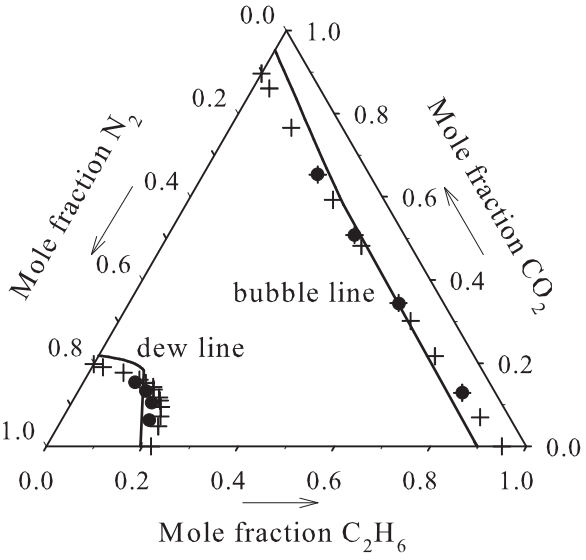

Figure 70: Ternary vapor-liquid equilibrium phase diagram of the mixture N_2 + CO_2 + C_2H_6 at 220 K and 4 MPa: + experimental data [401]; ● present simulation data; — Peng-Robinson EOS.

However, three mixtures have markedly curved phase envelopes, i.e. CH_4 + CO_2 + C_2H_6, cf. Figures 68, N_2 + CO_2 + C_2H_6, cf. Figure 70, and R13 + R14 + R23, cf. Figure 75. All three have one azeotropic subsystem, cf. Section 4.2, which however, cannot directly be seen from the figures for the ternary systems shown here. Please note that all respective subsystems are presented in Section 4.2. The phase envelope is also curved for the mixture CH_4 + N_2 + C_2H_6, cf. Figure 66, which has a ternary critical point. Finally, Figure 72 for the mixture C_2H_2 + C_2H_4 + C_2H_6, shows two pairs of straight saturation lines which also result from the azeotropic behavior of the subsystem C_2H_2 + C_2H_6.

The temperature range covered in the present study is quite large, i.e. from 112 K (Ar + CH_4 + N_2, cf. Figure 62) to 358.5 K (R10 + R1110 + R1120, cf. Figure 74). The same holds for the pressure range, i.e. from 0.07 MPa (R10 + R20 + R30, cf. Figure 73) to 12.4 MPa (N_2 + O_2 + CO_2, cf. Figure 69). For most mixtures, experimental data are available only for one pair of temperature and pressure values, however, for 11 ternary systems either two (10) or three (1) pairs of values were simulated. Thereby, the largest temperature interval was 50 K (N_2 + CO_2 + C_2H_6, cf. Figure 70 and supplementary data in [412]) and the largest pressure interval was 7.23 MPa (N_2 + O_2 + CO_2, cf. Figure 69 and supplementary data in [412]).

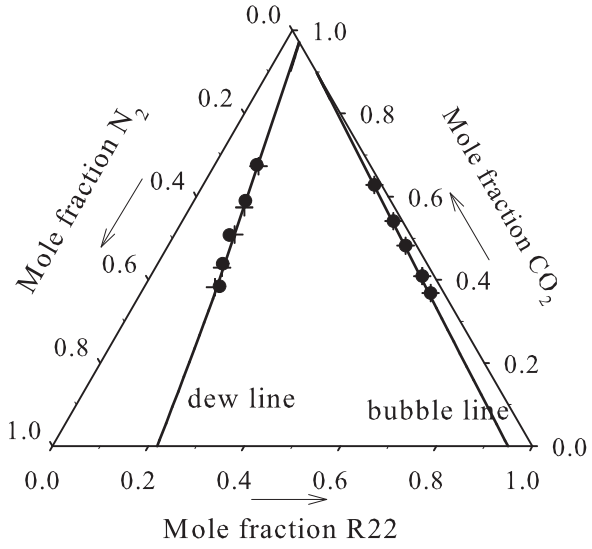

Figure 71: Ternary vapor-liquid equilibrium phase diagram of the mixture N_2 + CO_2 + R22 at 273.2 K and 3.083 MPa: + experimental data [403]; ● present simulation data; — Peng-Robinson EOS.

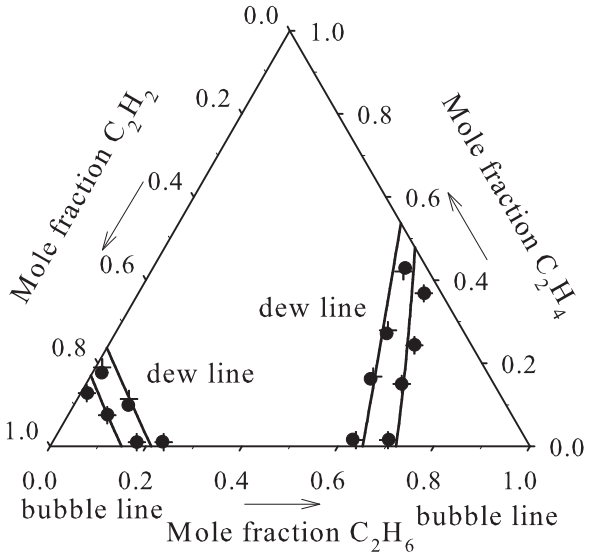

Figure 72: Ternary vapor-liquid equilibrium phase diagram of the mixture C_2H_2 + C_2H_4 + C_2H_6 at 277.6 K and 3.55 MPa: + experimental data [274]; ● present simulation data; — Peng-Robinson EOS.

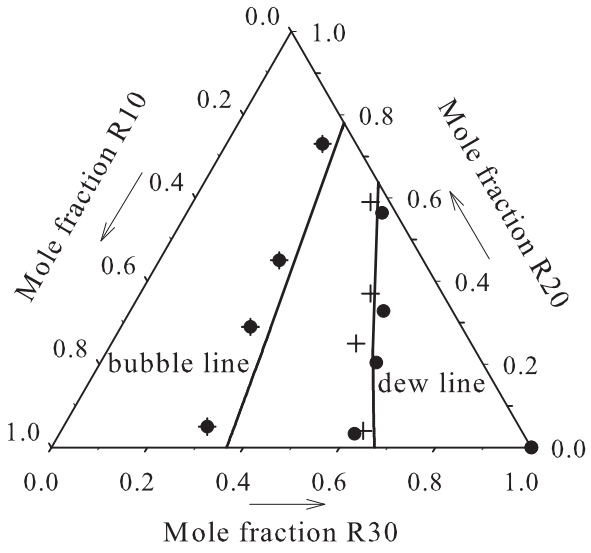

Figure 73: Ternary vapor-liquid equilibrium phase diagram of the mixture R10 + R20 + R30 at 318.15 K and 0.07 MPa: + experimental data [329]; ● present simulation data; — Peng-Robinson EOS.

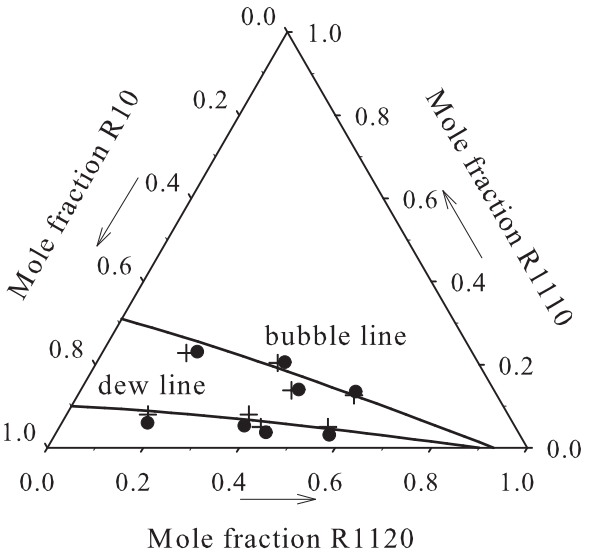

Figure 74: Ternary vapor-liquid equilibrium phase diagram of the mixture R10 + R1110 + R1120 at 358.5 K and 0.101 MPa: + experimental data [405]; ● present simulation data; — Peng-Robinson EOS.

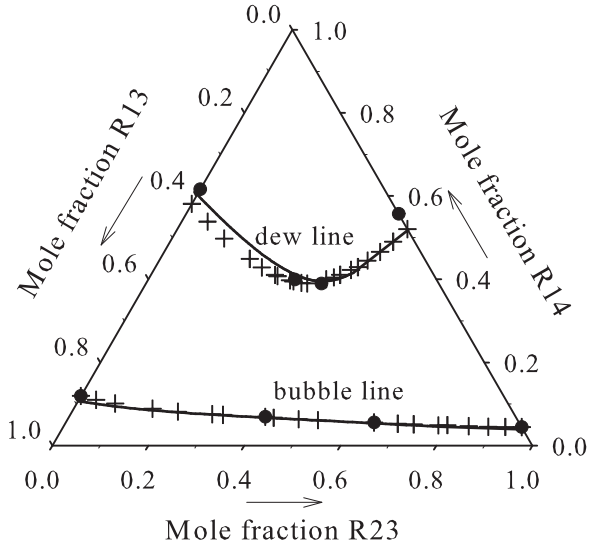

Figure 75: Ternary vapor-liquid equilibrium phase diagram of the mixture R13 + R14 + R23 at 199.8 K and 0.345 MPa: + experimental data [407]; ● present simulation data; — Peng-Robinson EOS.

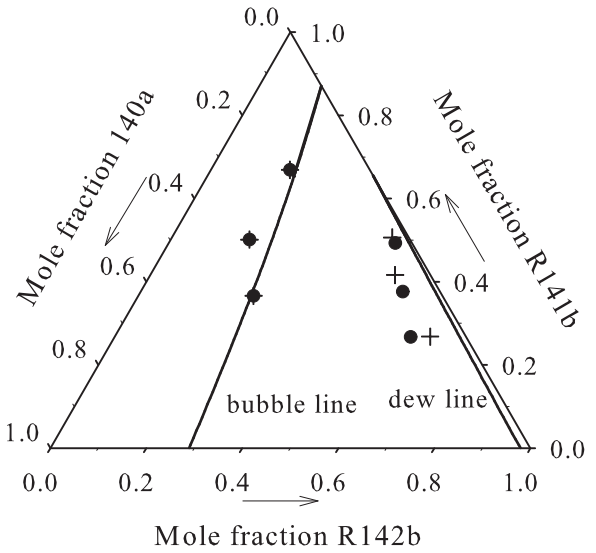

Figure 76: Ternary vapor-liquid equilibrium phase diagram of the mixture R140a + R141b + R142b at 323.25 K and 0.25 MPa: + experimental data [364]; ● present simulation data; — Peng-Robinson EOS.

In general, it can be stated that the agreement between simulation and experiment is very satisfactory. Both qualitatively and quantitatively, the data sets match in almost all cases.

Only for the mixture N_2 + R13 + R14, the VLE could not be simulated at the conditions for which experimental data [404] are available. Particularly the temperature of 77.8 K, which is well below the pure substance triple temperature of both R13 (92 K) and R14 (89.5 K), posed a problem during simulation as it is in immediate vicinity to solidification. It should be pointed out that the employed molecular models were neither optimized nor evaluated with respect to the triple line.

Also results from Peng-Robinson EOS with adjusted binary parameter k_{ij} are shown. Within the 15 examples presented here, three cases can be identified where significant deviations between the Peng-Robinson EOS and the remaining two data sets can be seen, i.e. N_2 + O_2 + CO_2, cf. Figure 69, R10 + R20 + R30, cf. Figure 73 and R140a + R141b + R142b, cf. Figure 76.

4.4 Gas Solubility in Pure Solvents

The aim of this work in this area is to predict the temperature dependence of the Henry's law constant in a systematic manner for a wide range of solutes and solvents by molecular modeling and simulation.

4.4.1 Experimental Database

Experimental data were predominately retrieved using the Dortmunder Datenbank (DDB) [187]. As pointed out in Section 4.2, theoretically, $N(N-1)/2 = 3003$ binary mixtures can be formed, but of course, by far not all of these systems have been studied experimentally. For 95 systems experimental Henry's law constant data were found in 72 publications, cf. Table 6, thereof for 29 binary mixtures also experimental VLE data are available, cf. Section 4.2.

The 95 binary systems studied here include 41 of the 78 pure components, cf. Table 6. Of the 41 components, 20 act as solutes, 15 as solvents and six as solutes and solvents, since they are studied in mixtures with less and more volatile components, cf. Table 6.

The studied 95 binary systems are listed in Table 12 together with a reference to the experimental H_i data, indicating the subgroup of 29 systems for which experimental VLE data are available as well.

For the 29 binary mixtures which were studied in Section 4.2 and also in this section, values for ξ were available. These were obtained by an adjustment to a single experimental vapor pressure p at some finite mole fraction of the binary mixture. Such values are indicated by ξ_p in the following. On the basis of that binary interaction parameter ξ_p, the temperature dependence of the Henry's law constant was predicted here for the subgroup of 29 mixtures. As discussed below, in some cases significant deviations were encountered so that the binary interaction parameter was then readjusted to the experimental Henry's law constant data here, being indicated by ξ_H. For the remaining 66 binary systems which were not studied with respect to binary VLE, ξ_H was adjusted here to H_i at some temperature, cf. Table 12.

Table 12: List of 92 binary mixtures. Binary interaction parameter ξ_H adjusted to the Henry's law constant, experimental data used for the adjustment with reference and simulation results with adjusted ξ_H. In cases where the experimental Henry's law constant is omitted, ξ_H was adjusted via temperature extrapolation. The number in parentheses denotes the statistical uncertainty in the last digit.

Mixture (i+S)	Category	ξ_H	T	H_i^{sim}	H_i^{exp}	Ref.
			K	MPa	MPa	
O_2 + Cl_2	3	0.993	298	66.5 (4)	66.3	[413]
CO_2 + Cl_2†	1	0.920	298.15	11.3 (1)	11.2	[413]
Xe + CO_2	1	0.904	283.15	8.7 (2)	8.7	[414]
O_2 + CO_2†	3	0.979	223.75	53.0 (5)	53.0	[415]
Ar + CS_2	1	0.901	298.15	208.9 (3)	209.2	[416, 417]
Kr + CS_2	3	0.966	298.15	57.2 (4)	57.7	[418]
Xe + CS_2	3	0.999	298	9.8 (2)	9.7	[418]
CH_4 + CS_2	1	0.984	298.15	78 (2)	80	[381, 418]
N_2 + CS_2	1	0.905	298.15	463 (6)	456	[381, 418, 419]
O_2 + CS_2	3	0.859	298.15	231 (2)	230	[420]
Cl_2 + CS_2	1	0.991	298	0.93 (3)	0.96	[421]
CO + CS_2	3	0.968	298	302 (4)	303	[420]
CO_2 + CS_2†	1	0.877	306.36	34.1 (5)	33.6	[381, 422]
C_2H_2 + CS_2	1	0.942	288.15	17.5 (6)	17.5	[423]
C_2H_4 + CS_2	3	0.995	298	15.7 (5)	15.7	[424]
C_2H_6 + CS_2	3	0.992	298.15	9.8 (4)	9.4	[416, 418]
Propylene + CS_2	3	0.870	298.15	20 (2)	19	[418]
SF_6 + CS_2	1	0.862	288.29	117 (6)	110	[381, 418]
R14 + CS_2	1	0.813	308	484 (14)	476	[425]
N_2 + Propylene†	4	0.959	180	52.1 (9)	-	[426]
N_2 + SF_6	3	1.400	300.15	8.34 (3)	8.33	[427]
Ar + R10†	2	0.964	348.15	77.9 (5)	74.1	[199, 417]
Kr + R10	5	1.049	350	31.2 (2)	-	[428, 429]
CH_4 + R10	5	1.068	350	38.3 (3)	-	[430]
N_2 + R10	5	0.899	340	134 (1)	-	[431, 432, 433]
O_2 + R10	5	0.888	350	77.9 (4)	-	[432, 433, 434, 435, 436, 437]
Cl_2 + R10	1	0.972	344.15	2.0 (2)	2.0	[438, 439, 440, 441, 442]
CO_2 + R10	4	0.808	340	18.2 (1)	-	[422, 434, 443, 444, 445, 446]
C_2H_2 + R10†	1	0.859	323.15	11.4 (1)	11.4	[423]

Table 12: continued.

Mixture (i+S)	Category	ξ_H	T K	H_i^{sim} MPa	H_i^{exp} MPa	Ref.
C_2H_4 + R10†	1	0.978	333.15	11.0 (4)	11.1	[279, 424, 447, 448]
C_2H_6 + R10	5	1.043	350	8.3 (1)	-	[448, 449]
Propylene + R10†	1	1.005	333.15	2.8 (9)	2.8	[279, 448]
SF_6 + R10	4	0.834	361	26.6 (7)	-	[425, 428]
R12 + R10†	4	0.991	330	1.9 (10)	-	[383]
R13 + R10	4	0.943	330	12.6 (3)	-	[383]
R14 + R10	4	0.794	350	82 (1)	-	[425]
R22 + R10†	5	0.929	350	4.07 (7)	-	[450]
R23 + R10	5	0.725	380	32.3 (3)	-	[451, 452]
R40 + R10	4	0.925	350	2.23 (2)	-	[453, 454, 455, 456]
R161 + R10	4	0.959	350	2.34 (4)	-	[457, 458]
R13 + R11†	1	0.975	273.15	2.56 (7)	3.42	[296]
R22 + R11†	1	0.956	273.15	0.68 (2)	0.92	[296]
R23 + R11†	1	0.802	303.15	14.0 (1)	14.3	[451, 459]
N_2 + R20	3	0.905	298.15	196.9 (3)	196.1	[460]
O_2 + R20	3	0.833	289.65	140.8 (2)	140.7	[461]
Cl_2 + R20	1	0.985	298.15	0.6 (8)	0.7	[438]
C_2H_4 + R20†	4	1.001	390	15.2 (2)	-	[279]
Propylene + R20†	4	0.975	390	6.79 (7)	-	[279]
R22 + R20	3	0.950	293.15	2 (2)	1.7	[450]
R40 + R20	3	0.991	298.15	0.4 (13)	0.5	[456]
R161 + R20	1	0.921	293.15	2 (2)	1.7	[457]
Kr + R20B3	3	0.956	295.15	61 (1)	61	[429]
CH_4 + R30	1	0.893	303.15	80.8 (8)	81.0	[462]
Cl_2 + R30	1	1.036	298.15	0.474(6)	0.483	[438]
CO_2 + R30†	1	0.868	310.93	10.38 (7)	10.38	[463]
CH_4 + R40	3	1.011	293.15	32.8 (3)	32.8	[464]
Ne + R113	2	0.928	298.15	116.9 (1)	116.9	[465]
Ar + R113†	1	1.027	298.06	32.7 (2)	32.7	[380]
Xe + R113	2	1.120	298.15	2.82 (3)	2.7	[465]
CH_4 + R113†	1	1.044	308.15	20.8 (1)	20.8	[380]
N_2 + R113	1	0.980	298.13	52.5 (4)	52.5	[380]
CO_2 + R113	1	0.870	308.50	6.4 (5)	6.49	[380]
C_2H_4 + R113	1	0.908	343.15	10.42 (6)	10.50	[466]
C_2H_6 + R113	1	1.020	298.08	3.64 (4)	3.76	[465, 467, 468]
SF_6 + R113†	1	0.894	319	6.6 (1)	5.6	[285, 380, 425]
R14 + R113	1	0.858	278.40	18.5 (5)	18.5	[425]
R116 + R113	2	0.998	300.73	3 (2)	3.6	[465, 468]
R1114 + R113	1	0.946	298.15	3.3 (9)	3.4	[469]
R1132 + R113	2	0.978	363.15	6.2 (2)	6.2	[469]
N_2 + R114	2	1.196	313.15	18.6 (1)	18.6	[470]
SF_6 + R114†	1	1.050	277	0.7 (5)	1.02	[285]

Table 12: continued.

Mixture (i+S)	Category	ξ_H	T K	H_i^{sim} MPa	H_i^{exp} MPa	Ref.
R23 + R114†	3	0.732	303.15	9.45 (7)	9.44	[451]
Cl_2 + R130a†	1	0.915	373	4.2 (1)	4.2	[230]
Cl_2 + R140†	4	0.948	450	8.45 (3)	-	[230]
C_2H_2 + R140	1	0.952	440	17.67 (8)	-	[471]
R1140 + R140†	4	0.980	450	5.25 (3)	-	[472]
Cl_2 + R140a†	1	0.930	281	0.7 (4)	0.5	[230]
CO_2 + R140a†	3	0.889	294.26	6.57 (6)	6.63	[445]
C_2H_2 + R140a	1	0.914	323.15	8.86 (7)	7.52	[471]
R1140 + R140a	1	0.928	323.15	1.23 (3)	1.24	[471]
Cl_2 + R150a†	4	0.967	360	2.8 (2)	-	[230]
C_2H_2 + R150a	4	0.965	360	9.18 (6)	-	[473]
Cl_2 + R150B2	3	0.994	313.15	0.8 (16)	0.9	[442]
CO + R150B2	3	0.909	298.15	369.1 (6)	370.7	[474]
O_2 + R1110	5	0.926	380	87.6 (2)	-	[436, 437]
Propylene + R1110†	4	1.011	380	5.4 (1)	-	[279]
R23 + R1110	5	0.664	380	60.0 (7)	-	[451, 452]
O_2 + R1120	5	0.961	340	88.3 (2)	-	[437]
CO_2 + R1120	5	0.829	310	16.3 (5)	-	[475]
C_2H_2 + R1120	5	0.847	314	13.1 (6)	-	[475]
Propylene + R1120†	1	0.983	303.15	2.0 (2)	1.9	[279, 282]
C_2H_2 + R1140	1	1.008	242.15	1.3 (11)	1.3	[473]

In all simulations 864 solvent molecules were used to evaluate the Henry's law constant. After an equilibration of 30 000 time steps, 200 000 production time steps of 1.5 fs were carried out inserting 3456 test molecules after each time step. The Lennard-Jones long range interactions beyond the cut-off radius were corrected employing angle averaging as proposed by Lustig [476]. The dipolar interactions were corrected using the reaction field method [72]. The cutoff radius was at least 17.5 Å. The quadrupolar and also the mixed dipolar-quadrupolar interactions need no long range corrections, as their contributions disappear by orientational averaging.

As discussed above, Widom's method has its limitations. Often, the solute molecules are smaller than the solvent molecules which is advantageous for the calculation of H_i. However, when the temperature is low and thus the saturated liquid solvent density is very high, the probability of successful test molecule insertions becomes very low. Then, the H_i calculation shows large statistical uncertainties or even a complete failure of that method. Nonetheless, exclusively molecular dynamics simulation in combination with Widom's method was used here because it does work at higher temperatures and simulation data over a larger temperature range allows for a reasonable temperature extrapolation.

4.4.2 Results and Discussion

For 95 binary mixtures, the Henry's law constant H_i was determined as a function of temperature. The results are presented in the supplementary material of [477] for each individual system in graphical form that contains the experimental data for comparison. There, it is distinguished graphically between the different experimental sources. The full numerical data set from simulation is provided in the supplementary material of [477] as well, together with an estimate of the statistical uncertainty. Error bars were calculated by a block averaging method [478] and the error propagation law. Due to the fact that the error bars are predominantly within symbol size, they were omitted in the figures to achieve a better visibility as the results for several binary mixtures are combined therein. In these figures, results for 37 of the 95 systems are exemplarily shown.

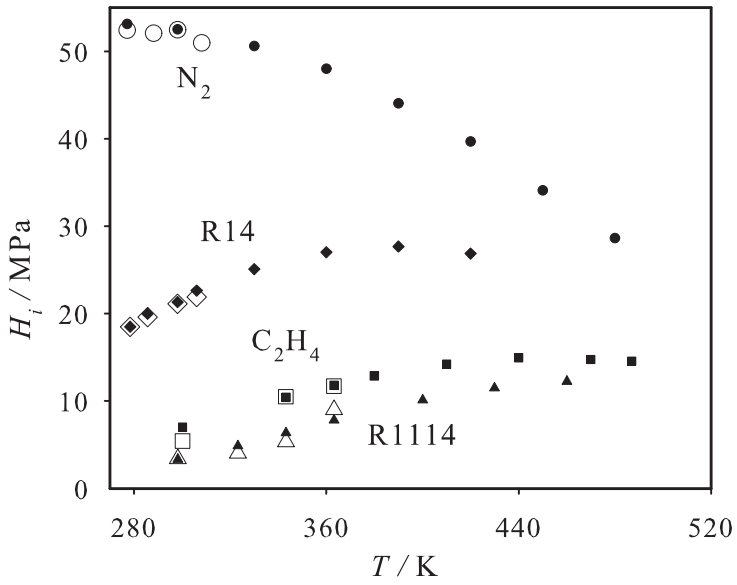

Figure 77: Henry's law constant of N_2 (●), C_2H_4 (■), R14 (⧫) and R1114 (▲) in liquid R113. Full symbols represent simulation results, empty symbols are experimental data [380, 425, 466, 469].

For this discussion, the 95 systems are grouped into six categories, cf. Table 12. The first category, containing 38 systems, is characterized by the presence of experimental data over a significant temperature range where a very good to excellent match with the simulation data was achieved. Eight such systems are shown Figures 77 and 78. The order of magnitude and also the temperature dependence of H_i vary. E.g., H_i ranges from around 4 MPa for R1114 in R113 that increases with temperature (Figure 77) to around 450 MPa for N_2 in CS_2 that decreases with temperature (Figure 78). In case of CH_4 in

CS_2 (Figure 78), H_i changes little with temperature in the regarded range.

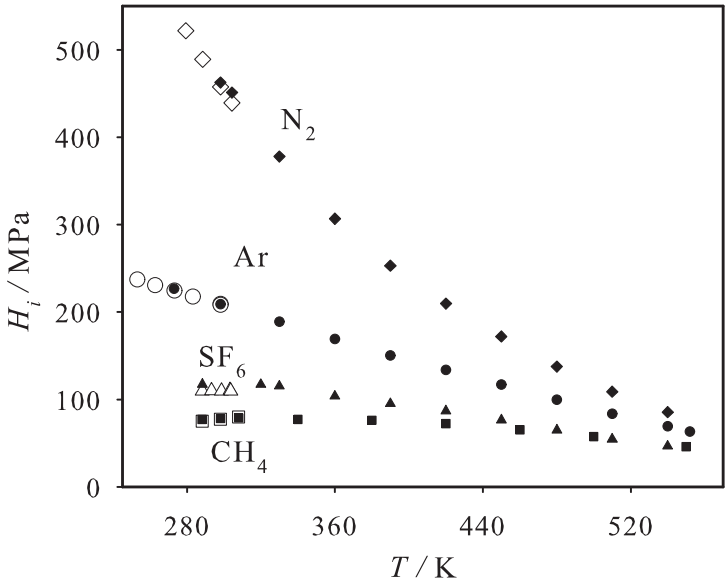

Figure 78: Henry's law constant of Ar (●), CH_4 (■), N_2 (♦) and SF_6 (▲) in liquid CS_2. Full symbols represent simulation results, empty symbols are experimental data [381, 416, 418].

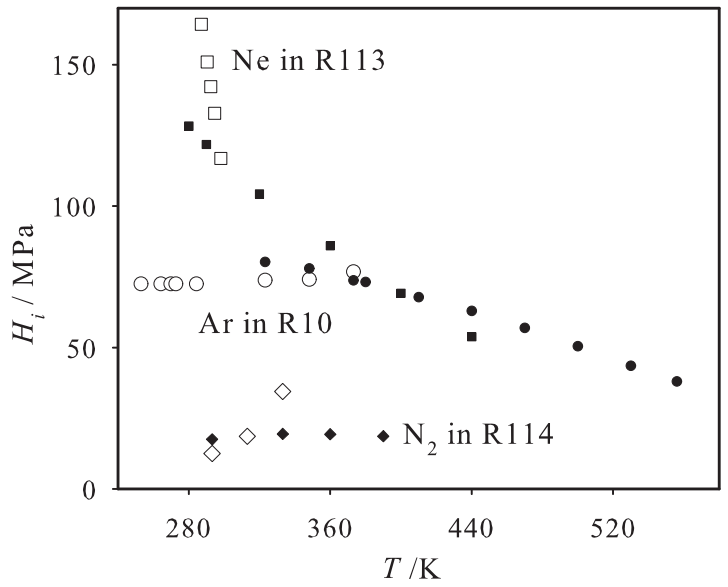

Figure 79: Henry's law constant of Ar in liquid R10 (●), of Ne in liquid R113 (■) and of N_2 in liquid R114 (♦). Full symbols represent simulation results, empty symbols are experimental data [417, 465, 470].

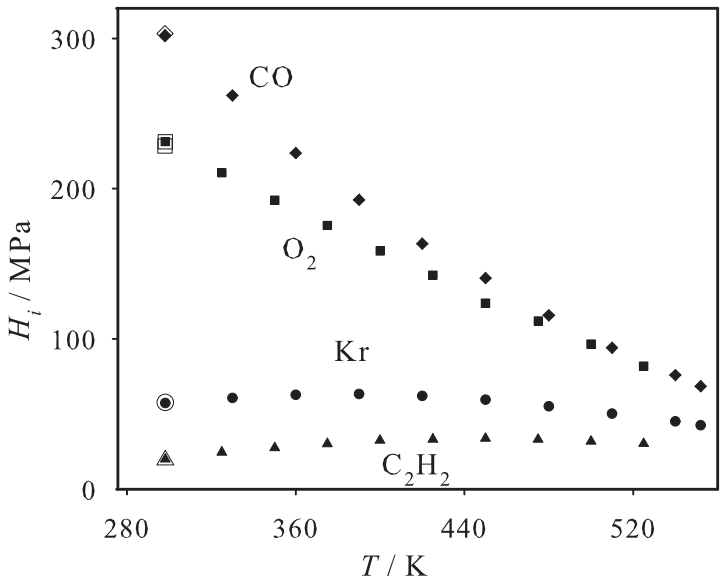

Figure 80: Henry's law constant of Kr (●), O_2 (■), CO (⧫) and C_2H_2 (▲) in liquid CS_2. Full symbols represent simulation results, empty symbols are experimental data [418, 420, 423].

For the second category, containing the six systems Ne in R113, Ar in R10, N_2 in R114, R1132 in R113, R116 in R113 and Xe in R113, the experimental data are also available over a significant temperature range, but the simulation results show a qualitatively different temperature dependence. Three typical systems are shown in Figure 79. Due to the fact that the binary interaction parameter was adjusted to experimental H_i data for five of the six systems, the data sets from simulation and experiment intersect. For the remaining system Ar in R10, cf. Figure 79, the binary interaction parameter was adjusted in Section 4.2 to experimental VLE data at 348.15 K. Around this temperature, the predicted H_i from simulation compares well with the experimental data, however, the temperature trend differs.

For the 44 mixtures in the first and second category a comparably broad experimental data base is available for the present assessment. As in 38 of the 44 cases the temperature dependence of H_i from simulation agrees well with the experiment, it can be stated that molecular modeling and simulations predominantly does yield good results.

The third category, containing 20 systems, is characterized by the presence of a single experimental H_i data point that is part of the temperature range where simulation was feasible. Due to the adjustment of ξ the simulation data coincides with the experiment, however, the presented temperature extrapolation cannot be assessed on the basis of experimental data. Figure 80 shows four typical systems.

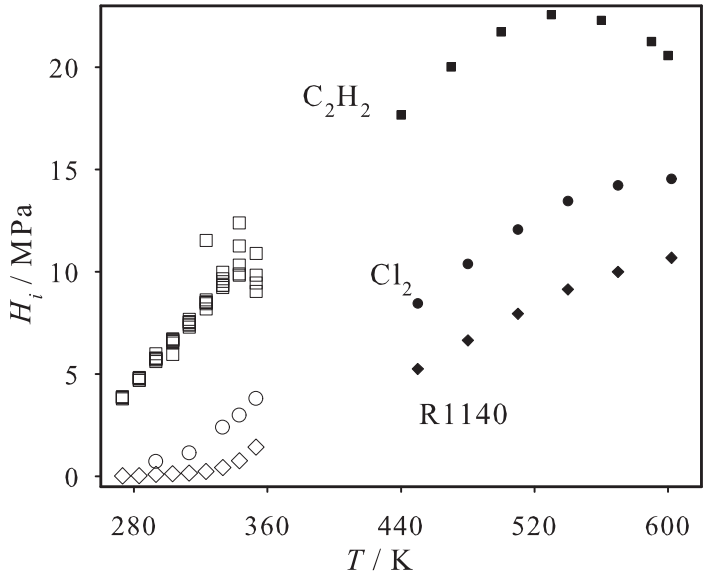

Figure 81: Henry's law constant of Cl_2 (●), C_2H_2 (■) and R1140 (⧫) in liquid R140. Full symbols represent simulation results, empty symbols are experimental data [230, 471, 472].

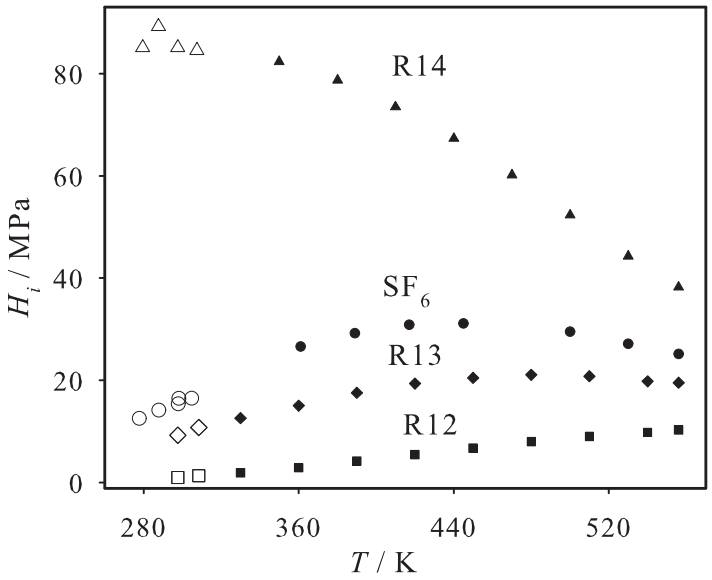

Figure 82: Henry's law constant of SF_6 (●), R12 (■), R13 (⧫) and R14 (▲) in liquid R10. Full symbols represent simulation results, empty symbols are experimental data [383, 425, 428].

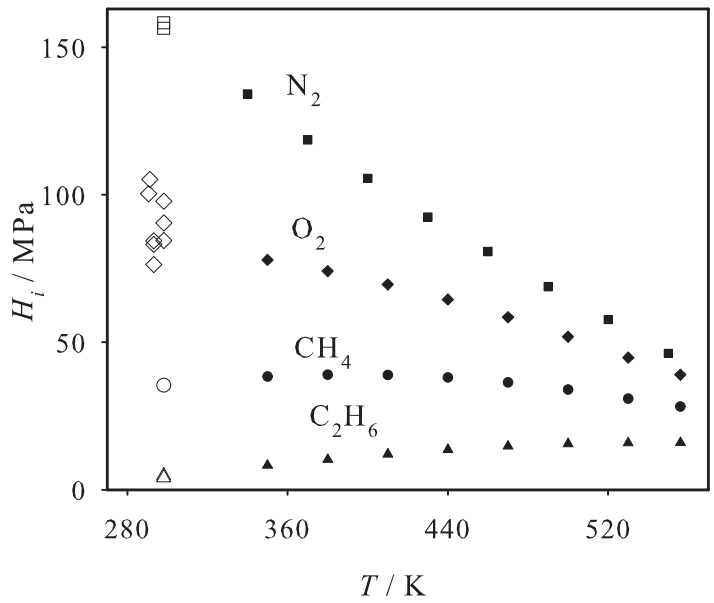

Figure 83: Henry's law constant of CH_4 (●), N_2 (■), O_2 (♦) and C_2H_6 (▲) in liquid R10. Full symbols represent simulation results, empty symbols are experimental data [430, 432, 434, 448].

For most mixtures, experimental H_i data are available only at low temperatures, typically below 360 K. Particularly for the studied polar solvents, the saturated liquid state is then highly dense so that the calculation of the chemical potential of the solute at infinite dilution by Widom's test particle method fails for low temperatures. This also depends on the nature of the solute; the larger and more polar the solute molecule is, the higher is the minimum temperature where such a calculation is feasible.

In 16 cases, H_i could not be determined in the temperature range where experimental data are present, which is the fourth category. However, as can be seen in Figures 81 and 82 for seven selected mixtures, both the experimental and simulation data allow for an overlapping extrapolation which can be regarded as satisfactory. Note that the binary interaction parameter for the three systems R12 in R10, Cl_2 in R140 and R1140 in R140 was adjusted in Section 4.2 to experimental VLE data at 297.75, 313 and 346.15 K, respectively, cf. Figures 81 and 82. Thus for these systems, it can be stated that the molecular mixture models yield correct and consistent H_i and VLE data. With respect to Widom's method, it can be seen in Figure 82 that the H_i calculation at 330 K was feasible for R13 in R10, while for R14 in the same solvent it was not.

Furthermore, the fifth category is also characterized by non-overlapping temperature ranges, but experimental data are present only for a single temperature or a very narrow temperature range. For the respective 12 systems only the simulation data allow for an extrapolation which was found to be in satisfactory agreement with the experiment. Four selected examples are shown in Figure 83.

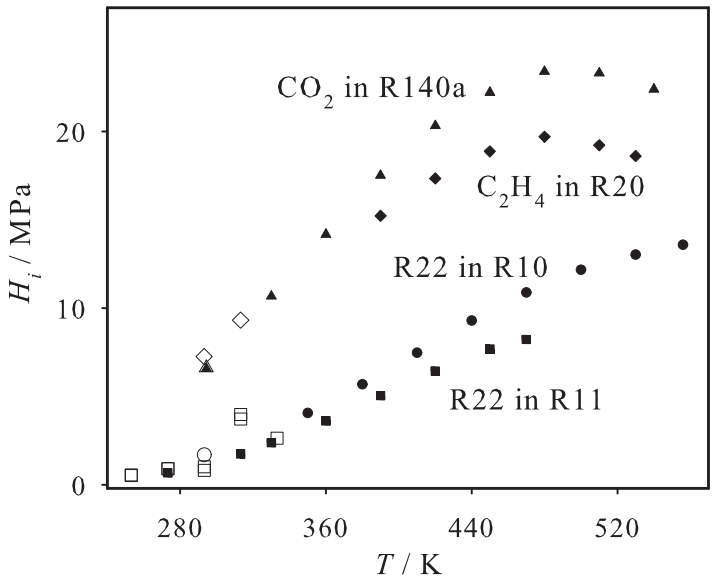

Figure 84: Henry's law constant of R22 in liquid R10 (●), R22 in liquid R11 (■), C_2H_4 in liquid R20 (♦) and CO_2 in liquid R140a (▲). Full symbols represent simulation results where the binary parameter ξ_p was adjusted to the vapor pressure in Section 4.2, empty symbols are experimental data [279, 296, 445, 450].

As indicated above, for 29 systems both experimental VLE and H_i data are available. For these systems, the binary interaction parameter has been adjusted to the vapor pressure at finite mole fractions in Section 4.2, being indicated by ξ_p, leading to an excellent match between experiment and simulation with respect to the VLE data. For a subgroup of 20 systems it was found here that these molecular mixture models are capable to yield correct and consistent H_i and VLE data. Exemplarily, four such systems are shown in Figure 84.

For the remaining nine systems, the predicted H_i data deviate from the experiment so that the binary interaction parameter was readjusted in these cases, labeled by ξ_H. This issue is illustrated in Figures 85 and 86 for six systems. E.g., in case of CO_2 in CS_2, cf. Figure 85, the H_i values predicted on the basis of ξ_p are too low by around 30%, but the temperature trend is satisfactory. Decreasing the binary interaction parameter by approximately 0.04 shifts H_i onto to the experimental data. For other systems, e.g. Ar in

R113, cf. Figure 86, the H_i values predicted on the basis on ξ_p are too high so that $\xi_H < \xi_p$. It was observed that the influence of the binary interaction parameter on H_i is weaker for higher temperatures.

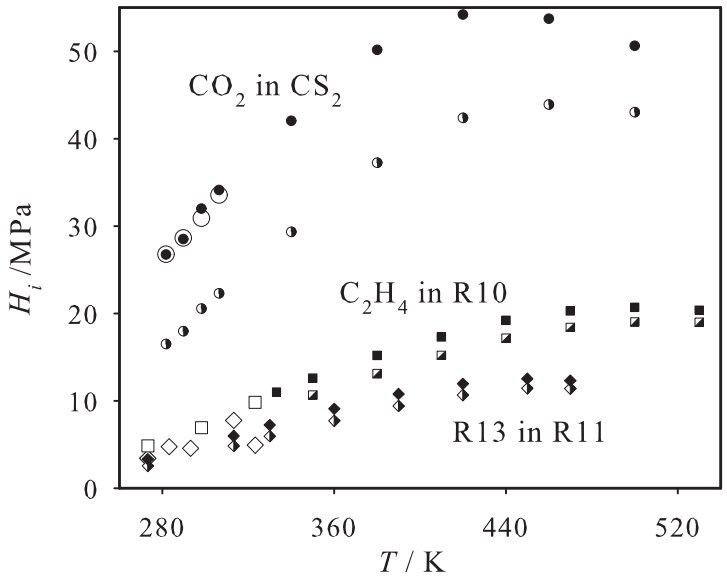

Figure 85: Henry's law constant for different binary systems. Full symbols represent simulation results where the binary parameter ξ_H was adjusted to the Henry's law constant in this this work, semi-filled symbols represent simulation results where the binary parameter ξ_p was adjusted to the vapor pressure in Section 4.2, empty symbols are experimental data: CO_2 in liquid CS_2 (●), $\xi_H = 0.877$, $\xi_p = 0.918$, [381, 416, 443]; C_2H_4 in liquid R10 (■), $\xi_H = 0.978$, $\xi_p = 1.003$, [279, 447]; R13 in liquid R11 (⧫), $\xi_H = 0.953$, $\xi_p = 0.975$, [296].

Figure 87 lists the 29 systems where both experimental VLE and H_i data are available, comparing their optimal binary interaction parameters ξ_p from Section 4.2 and ξ_H from this part. As can be seen, only in a few cases, e.g. C_2H_2 in R10 or R23 in R114, they strongly differ.

Finally, for the three mixtures Ne in R10, CO in R140a and CO_2 in R150B2, constituting the sixth category, the present modeling approach did not yield reasonable results. The simulation data according to the Berthelot rule, i.e. $\xi = 1$, were found to be very far off the experimental data which would require altering ξ by an unphysically large extent, e.g. $\xi > 2$ in case of CO in R140a. It should be noted that the 1CLJ model for Ne performs poorly with respect to VLE data, cf. Section 4.2. This is confirmed, as for both mixtures containing Ne studied here, i.e. Ne in R10 and Ne in R113 (wrong temperature dependence), unsatisfactory results were achieved.

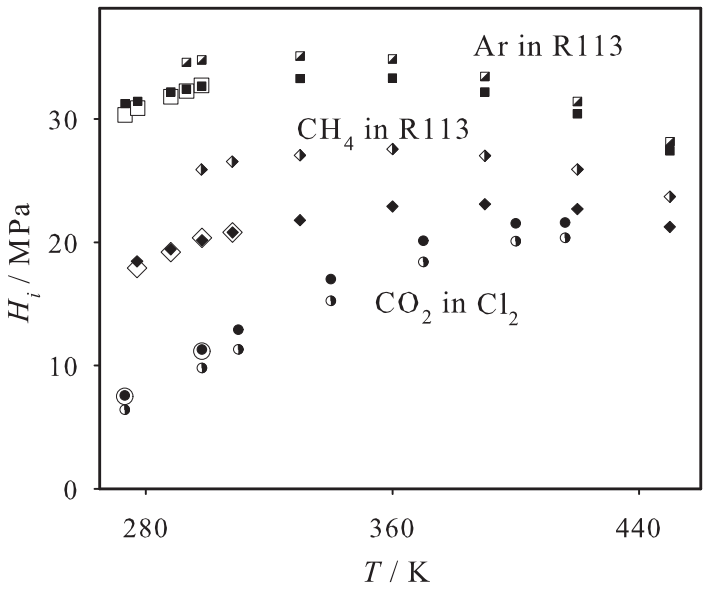

Figure 86: Henry's law constant for different binary systems. Full symbols represent simulation results where the binary parameter ξ_H was adjusted to the Henry's law constant in this work, semi-filled symbols represent simulation results where the binary parameter ξ_p was adjusted to the vapor pressure in Section 4.2, empty symbols are experimental data: CO_2 in liquid Cl_2 (●), $\xi_H = 0.920$, $\xi_p = 0.936$, [413]; Ar in liquid R113 (■), $\xi_H = 1.027$, $\xi_p = 1.012$, [380]; CH_4 in liquid R113 (♦), $\xi_H = 1.044$, $\xi_p = 0.997$, [380].

Another aspect that can be studied on the basis of the present simulation data is the general temperature trend of the Henry's law constant for different solutes in a given solvent. E.g., for the solvent R10 a total of 19 solutes were investigated. These simulation results are combined in Figure 88, showing that the H_i values at low temperatures cover a band of around 130 MPa. With increasing temperature the data sets for the different solutes converge, covering a band of around 35 MPa at the critical temperature of the solvent. For the solvent CS_2, where 15 solutes were investigated here, a similar behavior was found. Thus it can be concluded that the Henry's law constant at high temperatures is less influenced by the solute properties through the unlike interaction, but mainly by the like solute-solute interaction.

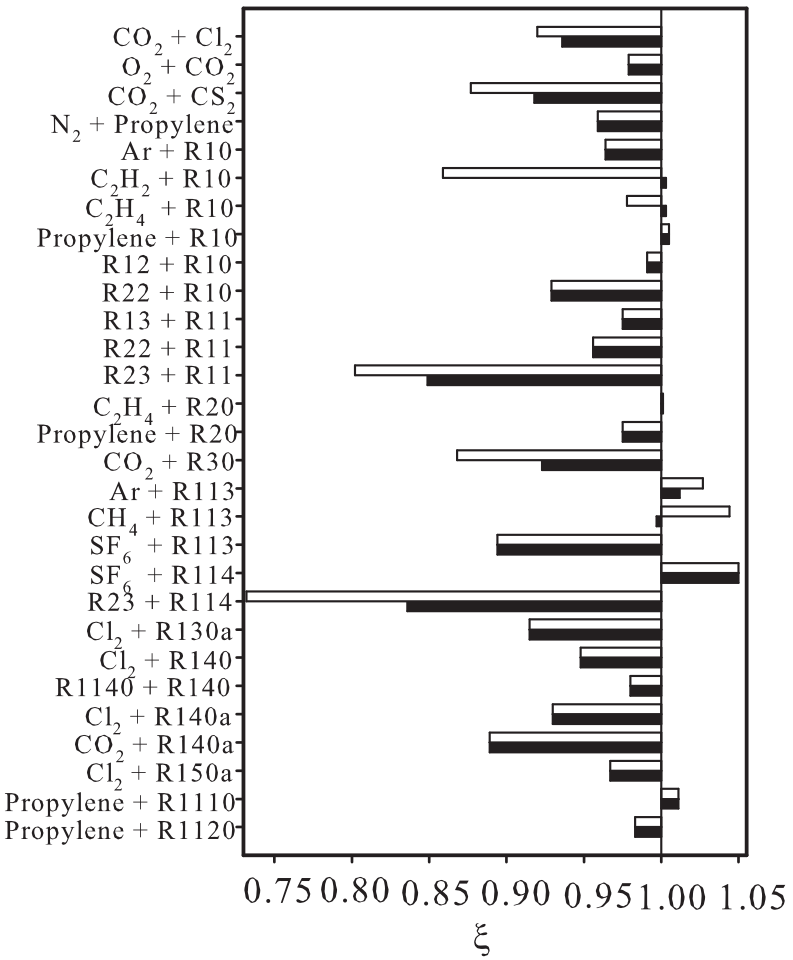

Figure 87: Comparison of the binary interaction parameter ξ_H that was adjusted to the Henry's law constant in this work (full bars) to the binary interaction parameter ξ_p that was adjusted to the vapor pressure in Section 4.2 (empty bars).

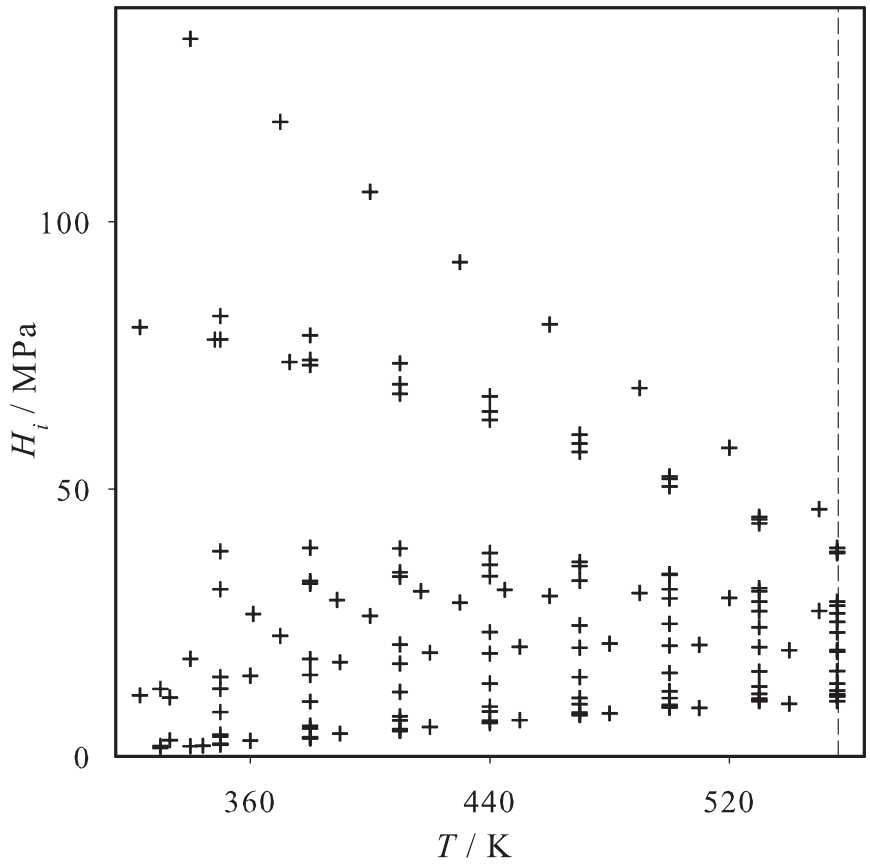

Figure 88: Henry's law constant of the 19 solutes Ar, Kr, CH_4, N_2, O_2, Cl_2, CO_2, C_2H_2, C_2H_4, C_2H_6, Propylene, SF_6, R12, R13, R14, R22, R23, R40 and R161 in liquid R10 from simulation (+). The dashed line indicates the critical temperature of the solvent.

5 Summary

This work was aimed to give both qualitative and quantitative evidence for the reliability of molecular modeling and simulation for VLE of industrial fluid mixtures. Eight new accurate molecular pure substance models were developed for experimentally inconvenient fluids. Furthermore, 377 binary and ternary mixtures were studied and 97 % of them were successfully described.

Molecular modeling and simulation was applied to predict VLE of binary mixtures containing Hydrogen chloride and Phosgene in combination with Benzene, Chlorobenzene, Ortho-Dichlorobenzene and Toluene. New molecular models were developed for these six components based on quantum chemical information on molecular geometry and electrostatics. Experimental data on the vapor pressure and the saturated liquid density were taken into account to optimize the pure substance models. These pure substance properties were accurately described by the molecular models from the triple point to the critical point. Average deviations to correlations of experimental data are typically less than 5 and 0.5 % for vapor pressure and saturated liquid density, respectively. Critical values of temperature, density and pressure from simulation agree with experimental data within the combined error bars.

The design of the models for the cyclic components allows for their compatibility with molecular Hydrogen chloride models by distributing the quadrupolar interaction sites among the methine groups. The second virial coefficient was predicted for Hydrogen chloride, Phosgene and Benzene and favorably compared to experimental data. The other three substances were not studied with respect to this property as there are no experimental data available for comparison.

For an optimized description of the binary VLE, the unlike dispersive interaction was adjusted for seven of the nine studied binary systems to a single experimental bubble point in the vicinity of ambient conditions. With these binary mixture models, VLE data, including dew point composition, saturated densities and enthalpy of vaporization, was predicted for a wide range of temperatures and compositions. The predictions show a good agreement with additional experimental binary VLE data that were not considered in the model development.

Analogous work was done for Ethylene oxide, Ethylene glycol and Water as well as their binary mixtures. Both Ethylene glycol and Water are strongly hydrogen bonding molecules so that they were modeled with point charges. For Ethylene oxide, a model from the literature was taken. Significant progress was achieved for these two fluids compared to previous works by other groups. Both their bubble density and vapor pressure were

well described. Furthermore, the Water model shows a good prediction of the second viral coefficient.

With respect to the binary VLE, the mixture Ethylene oxide + Water can not be described by the Peng-Robinson EOS, where excellent results were obtained with the present molecular model. In addition, the Henry's law constant of Ethylene oxide in Water was investigated. Models for the two binary mixtures Ethylene oxide + Ethylene glycol and Ethylene glycol + Water were presented.

A large scale simulation effort was made to cover 366 binary and ternary mixtures in a combinatorial way for another group of 78 components. The employed polar 2CLJ models in many cases oversimplify the molecular features of the substance that they represent. Unexpectedly, it was found that the molecular models are almost always able to compensate such oversimplifications and nonetheless adequately cover the effects of mixing.

To optimally represent the phase behavior of all regarded binary mixtures, the unlike dispersive energy parameter was adjusted to a single experimental vapor pressure of each mixture. It was found that the Berthelot rule is a good choice. In 71 % of all binaries, unlike dispersion was modified by 5 % or less. On average, unlike dispersion should by slightly weaker than the Berthelot rule suggests. Following that procedure, a large number of 259 molecular mixture models was presented that accurately cover the diverse fluid phase behavior of binary systems. Compared to the Peng-Robinson EOS, molecular modeling and simulation is superior, particularly in the critical region.

Next, 33 ternary mixtures were studied by molecular simulation with the Grand Equilibrium method. This method was found to be well suited for simulations of ternary VLE. Due to the fact that pairwise additive potentials were employed and no adjustment of binary parameters to ternary data was carried out, all results of that study on ternary systems are predictive. An excellent agreement between the predictions and the experimental data was observed throughout. Reliable predictions can also be expected for VLE of mixtures containing more than three components. Compared to the Peng-Robinson EOS, molecular modeling and simulation was found to yield superior predictions.

Finally, it was shown that molecular simulation is a reliable method for investigating the Henry's law constant of gases dissolved in liquid solvents. An extensive simulation effort, based on polar 2CLJ models, was made to cover 95 binary mixtures in a combinatorial way. It was found that molecular models are again predominantly able to compensate oversimplifications and adequately cover the gas solubility effects.

Based on these mixture models, the temperature dependence of the Henry's law con-

stant was predicted and compared to the available experimental data. For the large majority of systems that can be assessed in this sense, a good agreement was found. Moreover, it was shown that the models are predominantly capable to yield correct and consistent phase equilibrium data at infinite dilution and also at finite mole fractions. For high temperatures, it was found for a given solvent that the Henry's law constant of different solutes converges to a narrow band. This indicates that this thermophysical property is then mainly determined by the solute-solute interaction.

In summary, it was shown that molecular modeling and simulation can successfully be used to predict thermophyiscal data of industrially important pure substances and mixtures. It was applied here to properties that can often also be described well by phenomenological approaches like EOS. Nevertheless, even in such cases molecular modeling and simulation is valuable as it provides and independent approach where no experimental data are available. On the basis of this work, there are many possibilities how to progress into the future. Additional molecular models must be developed for various pure substances and mixtures that are both accurate and simple. And, of course, molecular modeling and simulation must further be applied to technical problems in process engineering, to establish the method for industrial use.

Appendix A: Numerical Simulation Results

Toxic Fluids for Process Engineering Applications

Table 13: Parameters of the new molecular models. Lennard-Jones interaction sites are denoted by the modeled atoms. Electrostatic interaction sites are denoted by point charge, dipole or quadrupole, respectively. Coordinates are given with respect to the center of mass in a principal axes system. Orientations of the electrostatic sites are defined in standard Euler angles, where φ is the azimuthal angle with respect to the $x-z$ plane and θ is the inclination angle with respect to the z axis.

interaction site	x Å	y Å	z Å	σ Å	ϵ/k_B Å	θ deg	φ deg	q e	μ D	Q DÅ
Hydrogen chloride										
HCl	0	0	-0.0378	3.520	179.00					
point charge(H)	0	0	1.2422					0.273		
point charge(Cl)	0	0	-0.0378					-0.273		
Phosgene										
C	0	0.5049	0	2.815	10.62					
O	0	1.7018	0	3.195	132.66					
Cl(1)	0	-0.4695	-1.4509	3.366	157.63					
Cl(2)	0	-0.4695	1.4509	3.366	157.63					
dipole	0	0.0845	0			90	90		1.002	
quadrupole	0	0	0			90	90			-3.627
Benzene										
CH(1)	0	1.5843	0.9147	3.243	91.82					
CH(2)	0	1.5843	-0.9147	3.243	91.82					
CH(3)	0	0	-1.8294	3.243	91.82					
CH(4)	0	-1.5843	-0.9147	3.243	91.82					
CH(5)	0	-1.5843	0.9147	3.243	91.82					
CH(6)	0	0	1.8294	3.243	91.82					
quadrupole(1)	0	1.5843	0.9147			90	0			-1.028
quadrupole(2)	0	1.5843	-0.9147			90	0			-1.028
quadrupole(3)	0	0	-1.8294			90	0			-1.028
quadrupole(4)	0	-1.5843	-0.9147			90	0			-1.028
quadrupole(5)	0	-1.5843	0.9147			90	0			-1.028
quadrupole(6)	0	0	1.8294			90	0			-1.028

Table 13: continued.

interaction site	x Å	y Å	z Å	σ Å	ϵ/k_B Å	θ deg	φ deg	q e	μ D	Q DÅ
Chlorobenzene										
CH(1)	0	0	2.7329	3.306	96.39					
CH(2)	0	-1.5723	1.8201	3.306	96.39					
CH(3)	0	1.5723	1.8201	3.306	96.39					
CH(4)	0	-1.5761	0.0025	3.306	96.39					
CH(5)	0	1.5761	0.0025	3.306	96.39					
C	0	0	-0.4563	2.787	11.66					
Cl	0	0	-2.1844	3.373	176.30					
dipole	0	0	-0.4563			0	-90		2.170	
quadrupole(1)	0	0	2.7329			90	0			-1.815
quadrupole(2)	0	-1.5723	1.8201			90	0			-1.815
quadrupole(3)	0	1.5723	1.8201			90	0			-1.815
quadrupole(4)	0	-1.5761	0.0025			90	0			-1.815
quadrupole(5)	0	1.5761	0.0025			90	0			-1.815
Ortho-Dichlorobenzene										
C(1)	0	0.6908	0.0051	2.771	11.46					
C(2)	0	-0.6908	0.0051	2.771	11.46					
CH(1)	0	0.9056	2.7612	3.413	102.32					
CH(2)	0	-0.9056	2.7612	3.413	102.32					
CH(3)	0	1.8027	1.1948	3.413	102.32					
CH(4)	0	-1.8027	1.1948	3.413	102.32					
Cl(1)	0	1.5813	-1.4524	3.354	173.25					
Cl(2)	0	-1.5813	-1.4524	3.354	173.25					
dipole	0	0	0.2400			0	-90		3.249	
quadrupole(1)	0	0.9056	2.7612			90	0			-2.196
quadrupole(2)	0	-0.9056	2.7612			90	0			-2.196
quadrupole(3)	0	1.8027	1.1948			90	0			-2.196
quadrupole(4)	0	-1.8027	1.1948			90	0			-2.196
Toluene										
CH_3	0	0	-2.7520	3.586	123.49					
C	0	0	-0.9597	2.794	10.94					
CH(1)	0	1.5720	-0.4615	3.276	100.52					
CH(2)	0	-1.5720	-0.4615	3.276	100.52					
CH(3)	0	1.5752	1.3557	3.276	100.52					
CH(4)	0	-1.5752	1.3557	3.276	100.52					
CH(5)	0	0	2.2729	3.276	100.52					
dipole	0	0	-0.9597			180	-90		0.440	
quadrupole(1)	0	1.5720	-0.4615			90	0			-1.688
quadrupole(2)	0	-1.5720	-0.4615			90	0			-1.688
quadrupole(3)	0	1.5752	1.3557			90	0			-1.688
quadrupole(4)	0	-1.5752	1.3557			90	0			-1.688
quadrupole(5)	0	0	2.2729			90	0			-1.688

Table 14: Vapor-liquid equilibrium simulation results of the pure substances on the basis of the new molecular models. The number in parentheses indicates the statistical uncertainty in the last digit.

T	p	ρ'	ρ''	Δh_v
K	MPa	mol/l	mol/l	kJ/mol
Hydrogen chloride				
180.00	0.061 (3)	33.19 (1)	0.040 (2)	16.527 (4)
210.00	0.308 (9)	30.92 (1)	0.129 (4)	15.246 (5)
240.00	0.95 (1)	28.42 (2)	0.530 (6)	13.743 (6)
270.00	2.37 (2)	25.45 (3)	1.39 (1)	11.586 (9)
300.00	4.99 (3)	21.50 (2)	3.30 (2)	8.38 (2)
305.00	5.47 (3)	20.66 (3)	3.67 (2)	7.78 (2)
310.00	5.98 (4)	19.70 (3)	4.10 (3)	7.08 (3)
Phosgene				
229.52	0.0081 (3)	15.390 (5)	0.0020 (1)	28.12 (1)
269.43	0.065 (3)	14.499 (6)	0.030 (1)	25.95 (1)
299.37	0.200 (8)	13.819 (6)	0.086 (3)	24.26 (1)
349.27	0.80 (1)	12.480 (8)	0.314 (4)	21.02 (1)
399.16	2.25 (2)	10.80 (2)	0.901 (8)	16.55 (3)
424.11	3.48 (2)	9.66 (2)	1.500 (9)	12.31 (5)
Benzene				
320.00	0.0310 (1)	10.833 (2)	0.00950 (3)	34.00 (1)
370.00	0.154 (3)	10.140 (3)	0.052 (1)	31.18 (1)
395.00	0.313 (1)	9.815 (2)	0.102 (9)	28.23 (8)
420.00	0.524 (8)	9.378 (4)	0.166 (3)	27.93 (2)
445.00	0.885 (4)	8.970 (6)	0.283 (4)	24.57 (8)
470.00	1.348 (9)	8.491 (6)	0.426 (3)	23.81 (2)
520.00	2.92 (2)	7.30 (2)	1.023 (7)	17.79 (6)
Chlorobenzene				
284.96	0.0007 (1)	9.994 (4)	0.00020 (3)	45.87 (2)
317.84	0.0042 (4)	9.664 (4)	0.0010 (1)	43.79 (3)
350.72	0.017 (1)	9.327 (4)	0.0050 (3)	41.71 (2)
394.56	0.079 (3)	8.870 (4)	0.0210 (7)	38.96 (2)
460.32	0.38 (2)	8.093 (7)	0.095 (5)	34.39 (3)
526.08	1.17 (2)	7.20 (3)	0.327 (6)	28.43 (5)
560.00	1.87 (2)	6.58 (1)	0.536 (6)	24.53 (7)
580.00	2.45 (2)	6.21 (2)	0.779 (6)	21.51 (9)
591.84	2.95 (2)	5.96 (1)	0.967 (7)	19.4 (2)
Ortho-Dichlorobenzene				
344.64	0.0022 (2)	8.515 (3)	0.00050 (5)	51.51 (3)
387.72	0.0138 (5)	8.150 (4)	0.0040 (1)	48.44 (3)
430.80	0.055 (2)	7.781 (4)	0.0140 (5)	45.41 (3)
506.19	0.311 (6)	7.066 (7)	0.080 (2)	39.51 (4)
560.04	0.800 (9)	6.48 (2)	0.202 (2)	34.51 (6)
613.89	1.66 (2)	5.79 (2)	0.489 (6)	27.75 (7)
Toluene				
277.51	0.00109 (4)	9.614 (4)	0.00040 (1)	42.85 (3)
349.45	0.03200 (5)	8.837 (2)	0.00160 (1)	38.23 (1)
411.12	0.2050 (5)	8.123 (2)	0.0604 (1)	33.95 (1)
472.79	0.766 (5)	7.311 (5)	0.229 (1)	28.78 (2)
534.46	1.96 (1)	6.23 (1)	0.659 (3)	21.52 (3)

Table 15: Vapor-liquid equilibrium simulation results of the binary mixtures on the basis of the new molecular models in partial comparison to experimental vapor pressure data. The number in parentheses indicates the statistical uncertainty in the last digit.

Mixture (A + B)	T K	x_A mol/mol	p MPa	p^{exp} MPa	y_A mol/mol	ρ' mol/l	ρ'' mol/l	Δh_v kJ/mol
Hydrogen chloride + Phosgene								
	266.15	0.09	0.20 (1)	0.24 [139]	0.75 (2)	15.435 (7)	0.092 (5)	25.72 (2)
	266.15	0.24	0.50 (4)	0.53 [139]	0.91 (1)	16.861 (7)	0.24 (2)	25.14 (2)
	266.15	0.39	0.84 (9)	0.84 [139]	0.95 (1)	18.55 (2)	0.42 (4)	24.07 (3)
	266.15	0.61	1.5 (3)	1.3 [139]	0.985 (3)	20.84 (2)	0.82 (16)	20.25 (2)
	423.15	0.06	5.04 (3)		0.228 (1)	9.74 (3)	2.15 (1)	12.26 (5)
	423.15	0.09	5.83 (3)		0.295 (2)	9.78 (2)	2.52 (1)	11.58 (5)
	423.15	0.13	6.75 (4)		0.353 (3)	9.77 (2)	2.98 (2)	10.68 (6)
	423.15	0.15	7.36 (4)		0.383 (3)	9.72 (3)	3.32 (2)	9.95 (8)
	423.15	0.18	8.25 (6)		0.404 (4)	9.78 (4)	3.95 (3)	8.9 (1)
Hydrogen chloride + Benzene								
	293.15	0.043	0.104 (2)	0.101 [140]	0.93 (1)	11.493 (5)	0.043 (1)	34.50 (2)
	293.15	0.401	1.04 (1)		0.999 (1)	14.770 (9)	0.460 (4)	26.76 (2)
	293.15	0.750	2.63 (3)		0.999 (1)	20.05 (2)	1.33 (2)	18.06 (2)
	393.15	0.108		1.51 [140]				
	393.15	0.112	1.39 (1)		0.787 (5)	10.463 (7)	0.453 (2)	27.56 (2)
	393.15	0.401	4.93 (2)		0.931 (2)	12.50 (1)	1.786 (7)	20.80 (3)
	393.15	0.700	10.72 (6)		0.953 (1)	14.97 (4)	4.95 (3)	11.95 (6)
Hydrogen chloride + Chlorobenzene								
	283.15	0.094	0.266 (9)	0.267 [140]	0.997 (3)	10.657 (5)	0.115 (4)	42.83 (3)
	283.15	0.300	0.95 (2)		0.998 (2)	12.471 (5)	0.434 (9)	35.86 (2)
	283.15	0.600	1.98 (3)		0.998 (2)	16.393 (2)	1.00 (2)	25.48 (2)
	283.15	0.800	2.65 (3)		0.999 (1)	20.37 (1)	1.45 (2)	18.32 (2)
	393.15	0.090	1.259 (8)		0.945 (3)	9.395 (5)	0.400 (3)	36.26 (2)
	393.15	0.117		1.61 [140]				
	393.15	0.300	4.43 (3)		0.980 (1)	10.850 (8)	1.53 (1)	29.10 (3)
	393.15	0.600	10.31 (5)		0.982 (1)	13.61 (1)	4.44 (2)	17.88 (4)
	423.15	0.095	1.73 (1)		0.902 (4)	9.053 (8)	0.577 (3)	34.25 (3)
	423.15	0.300	5.69 (2)		0.959 (1)	10.380 (3)	1.853 (7)	27.25 (2)
	423.15	0.600	12.90 (6)		0.964 (1)	12.74 (3)	5.12 (2)	15.90 (7)
Hydrogen chloride + Ortho-Dichlorobenzene								
	393.15	0.127		1.97 [140]				
	393.15	0.133	1.84 (2)		0.9920 (8)	8.897 (4)	0.588 (6)	42.74 (3)
	393.15	0.401	6.50 (5)		0.9990 (9)	11.008 (7)	2.36 (2)	31.24 (3)
	393.15	0.651	12.60 (8)		0.9921 (6)	13.84 (2)	5.79 (4)	19.06 (5)
Hydrogen chloride + Toluene								
	293.15	0.048	0.103 (2)	0.101 [140]	0.983 (4)	9.753 (3)	0.043 (1)	40.60 (2)
	293.15	0.401	1.21 (2)		0.998 (2)	12.883 (6)	0.541 (9)	30.81 (2)
	293.15	0.651	2.41 (3)		0.999 (1)	16.45 (1)	1.20 (1)	22.79 (2)
	393.15	0.124		1.42 [140]				
	393.15	0.143	1.749 (9)		0.921 (3)	9.176 (6)	0.568 (3)	31.58 (2)
	393.15	0.500	7.38 (4)		0.971 (1)	11.94 (3)	2.85 (2)	20.62 (4)
	393.15	0.750	13.13 (8)		0.960 (2)	14.2 (2)	6.85 (4)	10.39 (9)

Table 15: continued.

Mixture (A + B)	T K	x_A mol/mol	p MPa	p^{exp} MPa	y_A mol/mol	ρ' mol/l	ρ'' mol/l	Δh_v kJ/mol
Phosgene + Benzene								
	293.15	0.023	0.017 (1)	0.018 [141]	0.44 (3)	11.248 (5)	0.0070 (4)	35.11 (2)
	293.15	0.069	0.029 (2)	0.031 [141]	0.73 (2)	11.348 (5)	0.0120 (8)	34.50 (2)
	293.15	0.137	0.046 (2)	0.045 [141]	0.85 (2)	11.499 (4)	0.0190 (8)	33.63 (2)
	293.15	0.198	0.061 (2)	0.056 [141]	0.89 (1)	11.651 (7)	0.0250 (8)	32.88 (2)
	293.15	0.248	0.069 (3)	0.065 [141]	0.88 (2)	11.777 (6)	0.029 (1)	32.30 (2)
	293.15	0.332	0.084 (3)	0.081 [141]	0.923 (7)	11.973 (5)	0.035 (1)	31.26 (2)
	293.15	0.370	0.085 (3)	0.086 [141]	0.935 (7)	12.060 (6)	0.036 (1)	30.80 (2)
	293.15	0.461	0.098 (4)	0.098 [141]	0.942 (6)	12.300 (5)	0.041 (2)	29.79 (2)
	293.15	0.650	0.122 (4)		0.965 (5)	12.830 (6)	0.052 (2)	27.77 (2)
	293.15	0.800	0.133 (3)		0.980 (2)	13.294 (6)	0.056 (1)	26.36 (1)
Phosgene + Chlorobenzene								
	323.15	0.234	0.102 (4)	0.103 [140]	0.97 (1)	10.330 (5)	0.039 (2)	38.83 (3)
	323.15	0.600	0.254 (5)		0.99 (1)	11.641 (6)	0.099 (2)	31.33 (2)
	423.15	0.200	0.77 (1)		0.822 (6)	8.984 (5)	0.239 (3)	32.92 (2)
	423.15	0.431	1.47 (2)		0.918 (3)	9.451 (9)	0.485 (7)	27.77 (3)
	423.15	0.800	2.65 (3)		0.975 (1)	10.01 (1)	1.00 (1)	19.10 (3)
	448.15	0.200	1.08 (1)		0.760 (6)	8.63 (1)	0.324 (3)	31.07 (3)
	448.15	0.451	2.16 (2)		0.892 (2)	9.03 (1)	0.706 (7)	25.21 (4)
	448.15	0.800	3.86 (3)		0.959 (1)	9.20 (4)	1.54 (1)	16.04 (5)
Phosgene + Ortho-Dichlorobenzene								
	343.15	0.131	0.097 (8)		0.988 (9)	8.946 (5)	0.034 (3)	47.81 (3)
	343.15	0.401	0.32 (2)		0.998 (2)	9.965 (7)	0.119 (7)	39.74 (4)
	343.15	0.700	0.50 (2)		0.999 (1)	11.302 (9)	0.188 (8)	30.76 (3)
	363.15	0.080	0.105 (5)	0.103 [140]	0.97 (1)	8.611 (5)	0.035 (2)	47.96 (3)
	363.15	0.401	0.48 (1)		0.998 (2)	9.731 (4)	0.170 (2)	38.38 (2)
	363.15	0.700	0.81 (2)		0.999 (1)	10.958 (6)	0.301 (7)	29.30 (2)
Phosgene + Toluene								
	308.15	0.102	0.033 (2)	0.034 [140]	0.87 (1)	9.611 (5)	0.0129 (8)	39.10 (3)
	308.15	0.242	0.069 (3)		0.952 (5)	10.102 (5)	0.027 (1)	36.77 (2)
	308.15	0.700	0.190 (5)		0.9969 (7)	12.017 (6)	0.077 (2)	28.90 (2)
	423.15	0.200	0.81 (1)		0.698 (8)	8.433 (9)	0.258 (3)	29.60 (3)
	423.15	0.530	1.83 (2)		0.893 (3)	9.20 (1)	0.635 (7)	23.43 (3)
	423.15	0.750	2.48 (2)		0.948 (1)	9.62 (2)	0.926 (7)	19.11 (4)
	448.15	0.200	1.24 (2)		0.639 (8)	8.048 (9)	0.386 (6)	27.47 (4)
	448.15	0.426	2.12 (3)		0.812 (4)	8.46 (1)	0.71 (1)	23.15 (3)
	448.15	0.750	3.55 (5)		0.925 (1)	8.78 (4)	1.38 (2)	16.12 (6)

Table 16: Parameters of the new molecular model for Ethylene glycol based on Lennard-Jones interaction sites and point charges, cf. Figure 30. The coordinates are given with respect to the center of mass in a principal axes system.

interaction site	x Å	y Å	z Å	σ Å	ϵ/k_B Å	q e
OH(1)	1.6941	0.2400	0	3.18	89.31	
OH(2)	-1.6941	-0.2400	0	3.18	89.31	
CH_2(1)	-0.4831	0.8857	0	3.50	94.00	
CH_2(2)	0.4831	-0.8857	0	3.50	94.00	
point charge at CH_2(1)	-0.4831	0.8857	0			0.278
point charge at O(1)	1.6941	0.2400	0			-0.811
point charge at H(1)	-2.4793	0.2072	0			0.532
point charge at CH_2(2)	0.4831	-0.8857	0			0.278
point charge at O(2)	-1.6941	-0.2400	0			-0.811
point charge at H(2)	2.4793	-0.2072	0			0.532

Table 17: Vapor-liquid equilibrium simulation results for the pure substances on the basis of the new molecular models. The number in parentheses indicates the statistical uncertainty in the last digit.

T K	p MPa	ρ' mol/l	ρ'' mol/l	Δh_v kJ/mol
Ethylene glycol				
325.00	0.000092 (5)	17.45 (1)	0.000023 (1)	70.24 (7)
350.00	0.00051 (1)	17.18 (1)	0.000111 (2)	69.71 (6)
400.00	0.00722 (6)	16.626 (6)	0.002201 (1)	66.01 (6)
450.00	0.0514 (4)	15.973 (6)	0.02230 (1)	61.17 (4)
500.00	0.2245 (9)	15.218 (6)	0.04580 (3)	56.22 (3)
550.00	0.725 (1)	14.368 (8)	0.1841 (2)	50.09 (3)
600.00	1.78 (1)	13.32 (1)	0.4225 (9)	43.44 (4)
650.00	3.73 (2)	12.03 (3)	0.928 (3)	35.31 (6)
700.00	6.78 (3)	10.0 (1)	1.90 (1)	21.2 (2)
Water (TIP4P/2010)				
300.00	0.0040 (4)	56.35 (4)	0.001751 (1)	45.41 (1)
320.55	0.0120 (6)	55.23 (3)	0.004512 (2)	44.33 (1)
350.00	0.046 (2)	53.91 (3)	0.01690 (2)	42.86 (1)
373.97	0.109 (3)	52.64 (3)	0.03600 (2)	41.64 (2)
427.40	0.513 (9)	50.06 (4)	0.1541 (2)	38.63 (2)
450.00	0.89 (2)	48.85 (5)	0.2606 (7)	37.19 (1)
534.25	4.50 (5)	43.10 (5)	1.271 (4)	30.47 (4)
550.00	5.80 (6)	41.75 (7)	1.57 (1)	29.01 (1)
587.67	9.70 (8)	37.8 (2)	2.88 (2)	24.5 (1)
600.00	11.2 (1)	36.3 (2)	3.80 (2)	22.14 (3)

Table 18: Vapor-liquid equilibrium simulation results for binary mixtures in partial comparison to experimental vapor pressure data. The number in parentheses indicates the statistical uncertainty in the last digit.

Mixture (A + B)	T K	x_A mol/mol	p MPa	p^{exp} MPa	y_A mol/mol	ρ' mol/l	ρ'' mol/l	Δh_v kJ/mol
Ethylene oxide + Water								
	333.55	0.400	0.45 (2)	0.44 [171]	0.975 (1)	32.28 (2)	0.1778 (3)	34.80 (2)
	334.35	0.300	0.41 (2)	0.44 [171]	0.969 (2)	36.17 (2)	0.1608 (3)	37.01 (1)
	338.75	0.200	0.42 (2)	0.44 [171]	0.952 (5)	40.87 (2)	0.1596 (3)	39.05 (1)
	350.95	0.100	0.44 (1)	0.44 [171]	0.910 (5)	46.04 (1)	0.1621 (2)	40.52 (3)
	368.75	0.050	0.44 (2)	0.44 [171]	0.82 (2)	49.35 (1)	0.1687 (2)	40.59 (1)
	390.85	0.020	0.43 (3)	0.44 [171]	0.586 (7)	50.11 (3)	0.1191 (1)	40.36 (1)
	350.00	0.037	0.216 (7)	0.207 [171]	0.821 (8)	50.86 (2)	0.0769 (1)	42.12 (1)
	350.00	0.105	0.43 (3)	0.44 [171]	0.919 (5)	45.95 (2)	0.1601 (2)	40.48 (1)
	350.00	0.180	0.56 (2)	–	0.944 (3)	41.37 (2)	0.2176 (2)	38.66 (2)
	350.00	0.280	0.63 (3)	–	0.958 (3)	36.45 (2)	0.2441 (4)	36.40 (2)
	350.00	0.500	0.67 (2)	–	0.966 (1)	28.28 (2)	0.2569 (2)	31.46 (2)
	350.00	0.750	0.71 (1)	–	0.974 (1)	22.04 (1)	0.2772 (3)	26.11 (2)
	370.00	0.048	0.44 (3)	0.44 [171]	0.803 (9)	49.05 (2)	0.1658 (3)	40.65 (2)
	370.00	0.030	0.31 (3)	0.31 [171]	0.701 (8)	50.39 (3)	0.1084 (2)	41.17 (2)
	370.00	0.150	0.80 (2)	–	0.951 (2)	42.20 (3)	0.2647 (3)	38.22 (2)
	370.00	0.280	0.98 (3)	–	0.937 (4)	35.48 (3)	0.3581 (7)	35.00 (3)
	370.00	0.500	1.06 (2)	–	0.951 (2)	27.46 (2)	0.407 (1)	29.99 (2)
	370.00	0.800	1.16 (2)	–	0.967 (1)	20.24 (1)	0.446 (2)	23.62 (2)
	350.00	0.020	0.16 (4)	–	0.76 (1)	52.25 (2)	0.0615 (1)	42.49 (2)
	350.00	0.050	0.26 (3)	–	0.84 (2)	49.86 (2)	0.0886 (1)	41.83 (2)
	350.00	0.100	0.43 (3)	–	0.92 (1)	46.28 (2)	0.1580 (2)	40.57 (2)
	400.00	0.020	0.45 (2)	–	0.52 (3)	49.63 (3)	0.1426 (3)	39.86 (2)
	400.00	0.050	0.71 (2)	–	0.69 (1)	47.32 (3)	0.2297 (4)	39.01 (2)
	400.00	0.100	1.07 (1)	–	0.81 (1)	43.87 (3)	0.3598 (7)	37.60 (2)
	450.00	0.020	1.17 (2)	–	0.29 (1)	46.82 (3)	0.3469 (4)	36.77 (2)
	450.00	0.050	1.57 (2)	–	0.45 (1)	44.62 (3)	0.473 (1)	35.90 (3)
	450.00	0.100	2.12 (4)	–	0.61 (1)	41.18 (2)	0.668 (2)	34.36 (2)
	500.00	0.020	2.77 (4)	–	0.150 (7)	43.66 (5)	0.799 (1)	33.06 (3)
	500.00	0.050	3.23 (5)	–	0.296 (9)	41.35 (4)	0.946 (2)	32.17 (3)
	500.00	0.100	4.11 (7)	–	0.442 (9)	38.10 (4)	1.267 (3)	30.44 (3)

Table 18: continued.

Mixture (A + B)	T K	x_A mol/mol	p MPa	p^{exp} MPa	y_A mol/mol	ρ' mol/l	ρ'' mol/l	Δh_v kJ/mol
Ethylene oxide + Ethylene glycol								
	360.15	0.075	0.20 (1)	0.22 [172]	0.999 (1)	17.25 (1)	0.0523 (1)	64.85 (8)
	360.15	0.130	0.33 (2)	0.34 [172]	0.999 (1)	17.36 (1)	0.1119 (1)	62.13 (6)
	360.15	0.500	0.73 (3)	–	0.999 (1)	18.10 (1)	0.402 (1)	43.73 (4)
	360.15	0.800	0.96 (4)	–	0.999 (1)	17.94 (2)	0.3849 (9)	29.37 (3)
	360.15	0.300	0.98 (2)	–	0.999 (1)	17.72 (1)	0.2298 (6)	53.79 (8)
	378.15	0.051	0.21 (2)	0.21 [172]	0.999 (1)	16.98 (2)	0.0622 (1)	64.99 (9)
	378.15	0.100	0.38 (1)	0.38 [172]	0.999 (1)	17.15 (1)	0.1280 (2)	62.60 (9)
	378.15	0.300	1.05 (5)	–	0.999 (1)	17.50 (1)	0.380 (2)	52.01 (6)
	378.15	0.500	1.39 (5)	–	0.999 (1)	17.75 (1)	0.562 (1)	41.95 (3)
	378.15	0.800	1.44 (2)	–	0.999 (1)	17.40 (2)	0.559 (1)	27.91 (3)
Water + Ethylene glycol								
	383.15	0.200	0.0240 (7)	0.029 [173]	0.881 (3)	19.58 (2)	0.0039 (0)	63.75 (9)
	383.15	0.401	0.049 (1)	–	0.97 (1)	23.43 (4)	0.0106 (0)	60.01 (7)
	383.15	0.500	0.062 (2)	–	0.979 (3)	26.05 (3)	0.0163 (0)	57.75 (8)
	383.15	0.600	0.078 (3)	–	0.992 (3)	28.85 (5)	0.0230 (0)	54.70 (5)
	383.15	0.800	0.116 (4)	–	0.994 (3)	37.23 (3)	0.0372 (0)	48.10 (4)
	395.15	0.200	0.0360 (8)	–	0.872 (2)	19.40 (2)	0.0056 (0)	62.94 (8)
	395.15	0.401	0.072 (2)	–	0.945 (2)	23.25 (2)	0.0153 (0)	59.21 (4)
	395.15	0.466	0.082 (2)	0.084 [173]	0.965 (4)	24.84 (1)	0.0223 (0)	57.53 (4)
	395.15	0.600	0.110 (3)	–	0.971 (3)	28.55 (3)	0.0323 (0)	53.85 (4)
	395.15	0.800	0.162 (5)	–	0.990 (2)	36.79 (2)	0.0508 (1)	47.29 (3)

Appendix B: Simulation Details

B1. Toxic Fluids for Process Engineering Applications

In all cases Widom's insertion method yielded large statistical uncertainties for the chemical potential in the liquid, which is due to the high densities and the strongly interacting molecules. Instead, Monte Carlo simulations were performed in the NpT ensemble for the liquid. Thereby, the chemical potential was calculated by the gradual insertion method [98, 99]. The number of molecules was 500. Starting from a face centered cubic lattice, 15 000 Monte Carlo cycles were performed for equilibration and 50 000 for production, each cycle containing 500 translation moves, 500 rotation moves, and 1 volume move. Every 50 cycles, 5000 fluctuating state change moves, 5000 fluctuating particle translation/rotation moves, and 25000 biased particle translation/rotation moves were performed, to determine the chemical potential. These computationally demanding simulations yield the chemical potential in dense and strong interacting liquids with high accuracy, leading to reasonable uncertainties in the VLE.

For the corresponding vapor, Monte Carlo simulations in the pseudo-μVT ensemble were performed. The simulation volume was adjusted to lead to an average number of 500 molecules in the vapor phase. After 2 000 initial NVT Monte Carlo cycles, starting from a face centered cubic lattice, 10 000 equilibration cycles in the pseudo-μVT ensemble were performed. The length of the production run was 50 000 cycles. One cycle is defined here to be a number of attempts to displace and rotate molecules equal to the actual number of molecules plus three insertion and three deletion attempts.

The cut-off radius was set to 17.5 Å throughout and a center of mass cut-off scheme was employed. Lennard-Jones long-range interactions beyond the cut-off radius were corrected employing angle averaging as proposed by Lustig [476]. Electrostatic interactions were approximated by a resulting molecular dipole and corrected using the reaction field method [72]. Statistical uncertainties in the simulated values were estimated by a block averaging method [478].

B2. Large Systematic Study on Vapor-Liquid Equilibria of Mixtures

A center-center cut-off radius of 17.5 Å was used for the explicit evaluation of the intermolecular interactions. The Lennard-Jones tail corrections for internal energy, pressure, and chemical potential were calculated employing angle averaging as proposed by Lustig [476]. Long-range corrections for the dipolar part of the potential model were calculated

with the reaction field method [479, 480]. The quadrupolar interaction needs no long range correction as it disappears by orientational averaging. The same holds for the mixed polar interaction between dipoles and quadrupoles, cf. Weingerl et al. [481].

VLE was obtained with the Grand Equilibrium method [96]. Depend on Depending on thermodynamic conditions, different levels of computational effort were employed

Binary mixtures

(A) In simple cases (e.g. Ar + R22, Kr + Propylene and R116 + R134a) VLE can be obtained with small statistical uncertainties sampling $N = 500$ molecules for the liquid phase and about 200 molecules for the vapor phase. Liquid simulation runs were carried out using molecular dynamics with 100 000 time steps, vapor simulation runs were performed using the Monte Carlo technique with 100 000 cycles. Within one cycle, N attempts to translate or rotate, and two attempts to insert or delete molecules were performed. The chemical potentials were calculated by Widom's insertion technique [66] using 2000 test molecules each time step.

(B) In intermediate cases (e.g. R14 + R13, R116 + CO_2 and SF_6 + R13B1) where experimental data is present only for dense liquid phases, 864 molecules were used for liquid simulations and about 600 molecules for vapor simulations. Liquid runs were carried out using molecular dynamics with 300 000 time steps, vapor runs were performed by Monte Carlo with 200 000 cycles. The number of test molecules was 3456 every time step.

(C) In difficult cases (e.g. R134a + R114, R32 + R143a and R1120 + R1110) where experimental data is present only for highly dense strongly polar liquid phases where the vapor pressure is usually very low, the more elaborate gradual insertion scheme had to be employed to obtain the chemical potentials.

Ternary mixtures

(A) In simple cases (e.g. CH_4 + CO_2 + C_2H_6, CO_2 + R142b + R152a and R13 + R14 + R23) VLE can be obtained with small statistical uncertainties sampling $N = 864$ molecules for the liquid phase and about 500 molecules for the vapor phase. Liquid simulation runs were carried out using molecular dynamics with 200 000 time steps, vapor simulation runs were performed using the Monte Carlo technique with 200 000 cycles. Within one cycle, N attempts to translate or rotate, and two attempts to insert or delete molecules were sampled. The chemical potentials were calculated by Widom's insertion technique [66] using 3456 test molecules each time step.

(B) In difficult cases (e.g. Ar + N_2 + O_2, R10 + R20 + R30 and R30 + R30B1 + R30B2), where experimental data are present only for highly dense strongly polar liquid phases and the vapor pressure is usually low, the more elaborate gradual insertion scheme

had to be employed to obtain the chemical potentials in the liquid.

The gradual insertion method is an expanded ensemble method [97] based on the Monte Carlo technique. The version as proposed by Nezbeda and Kolafa [98], extended to the *NpT* ensemble [99], was used in Binary VLE mixture case *(C)* and Ternary mixture case *(B)*. It should be pointed out that the gradual insertion method was not employed for calculation of chemical potentials of binary system for gas solubility due to the simplicity of these binary systems. In comparison to Widom's insertion technique, where real molecules are inserted into the fluid, gradual insertion introduces one fluctuating molecule that undergoes changes in a predefined set of discrete states of coupling with all other real molecules of the fluid. Preferential sampling is done in the vicinity of the fluctuating molecule. This concept leads to considerably improved accuracy of the residual chemical potential. Gradual insertion simulations were performed with $N = 864$ molecules in the liquid phase. Starting from a face-centered cubic lattice arrangement, every simulation run was given 5 000 Monte Carlo cycles to equilibrate. Data production was performed over 100 000 Monte Carlo cycles. One Monte Carlo cycle is defined here as N trial translations, $(2/3)\,N$ trial rotations, and one trial volume change. Further simulation parameters for runs with the gradual insertion method were taken from Vrabec et al. [99].

References

[1] Schmidt M. W., Baldridge K. K., Boatz J. A., Elbert S. T., Gordon M. S., Jensen J. H., Koseki S., Matsunaga N., Nguyen K. A., Shujun S., Windus T. L., Dupuis M. and Montgomery A. M., "General atomic and molecular electronic structure system", J. Comput. Chem. **14**, 1347-1363 (1993).

[2] Lotfi A., Vrabec J. and Fischer J., "Vapour liquid equilibria of the Lennard-Jones fluid from the NpT plus test particle method", Mol. Phys. **76**, 1319-1333 (1992).

[3] Case F., Chaka A., Friend D. G., Frurip D., Golab J., Johnson R., Moore J., Mountain R. D., Olson J., Schiller M. and Storer J., "The first industrial fluid properties simulation challenge", Fluid Phase Equilib. **217**, 1-10 (2004).

[4] Case F., Chaka A., Friend D. G., Frurip D., Golab J., Gordon P., Johnson R., Kolar P., Moore J., Mountain R. D., Olson J., Ross R. and Schiller M., "The second industrial fluid properties simulation challenge", Fluid Phase Equilib. **236**, 1-14 (2005).

[5] Case F., Brennan J., Chaka A., Dobbs K. D., Friend D. G., Frurip D., Gordon P., Moore J., Mountain R. D., Olson J., Ross R., Schiller M. and Shen V. K., "The third industrial fluid properties simulation challenge", Fluid Phase Equilib. **260**, 153-163 (2007).

[6] Case F., Brennan J., Chaka A., Dobbs K. D., Friend D. G., Gordon P., Moore J., Mountain R. D., Olson J., Ross R., Schiller M., Shen V. K. and Stahlberg E. A., "The fourth industrial properties simulation challenge", Fluid Phase Equilib. **274**, 2-9 (2008).

[7] Case F., Chaka A., Moore J., Mountain R. D., Olson J., Ross R., Schiller M., Shen V. K. and Stahlberg E. A., "The fifth industrial fluid properties simulation challenge", Fluid Phase Equilib. **285**, 1-3 (2009).

[8] Vrabec J., Stoll J. and Hasse H., "A Set of Molecular Models for Symmetric Quadrupolar Fluids", J. Phys. Chem. B **105**, 12126-12133 (2001).

[9] Stoll J., Vrabec J. and Hasse H., "A set of molecular models for carbon monoxide and halogenated hydrocarbons", J. Chem. Phys. **119**, 11396-11407 (2003).

[10] Streett W. B. and Tildesley D. J., "Computer Simulations of Polyatomic Molecules. II. Molecular Dynamics Studies of Diatomic Liquids with Atom-Atom and Quadrupole-Quadrupole Potentials", Proc. Roy. Soc. Lond. A **355**, 239-266 (1977).

[11] Potoff J. J. and Siepmann J. I., "Vapor-liquid equilibria of mixtures containing alkanes, carbon dioxide, and nitrogen", AIChE J. **47**, 1676-1682 (2001).

[12] de Pablo J. J., Bonnin M. and Prausnitz J. M., "Vapor-Liquid equilibria for polyatomic fluids from site-site computer simulations: pure hydrocarbons and binary mixtures containing methane", Fluid Phase Equilib. **73**, 187-210 (1992).

[13] Gao G. T., Wang W. and Zeng X. C., "Gibbs ensemble simulation of HCFC/HFC mixtures by effective Stockmayer potential", Fluid Phase Equilib. **158-160**, 69-78 (1999).

[14] Kronome G., Szalai I., Wendland M. and Fischer J., "Extension of the NpT + test particle method for the calculation of phase equilibria of nitrogen + ethane", J. Mol. Liq. **85**, 237-247 (2000).

[15] Nath S. K., Escobedo F. A., de Pablo J. J. and Patramai I., "Simulation of Vapor-Liquid Equilibria for Alkane Mixtures", Ind. Eng. Chem. Res. **37**, 3195-3202 (1998).

[16] Cui S. T., Cochran H. D. and Cummings P. T., "Vapor-Liquid Phase Coexistence of Alkane-Carbon Dioxide and Perfluoroalkane-Carbon Dioxide Mixtures", J. Phys. Chem. B **103**, 4485-4491 (1999).

[17] Potoff J. J., Errington J. R. and Panagiotopoulos A. Z., "Molecular simulation of phase equilibria for mixtures of polar and non-polar components", Mol. Phys. **97**, 1073-1083 (1999).

[18] Delhommelle J. and Millié P., "Inadequacy of the Lorentz-Berthelot combining rules for accurate predictions of equilibrium properties by molecular simulation", Mol. Phys. **99**, 619-625 (2001).

[19] Liu A. and Beck T. L., "Vapor-Liquid Equilibria of Binary and Ternary Mixtures Containing Methane, Ethane, and Carbon Dioxide from Gibbs Ensemble Simulations", J. Phys. Chem. B **102**, 7627-7631 (1998).

[20] Vrabec J. and Fischer J., "Vapor-liquid equilibria of binary mixtures containing methane, ethane, and carbon dioxide from molecular simulation", Int. J. Thermophys. **17**, 889-908 (1996).

[21] Vrabec J. and Fischer J., "Vapor-liquid equilibria of the ternary mixture CH_4 + C_2H_6 + CO_2 from molecular simulation", AIChE J. **43**, 212-217 (1997).

[22] Boutard Y., Ungerer Ph., Teuler J. M., Ahunbay M. G., Sabater S. F., Pérez-Pellitero J., Mackie A. D. and Bourasseau E., "Extension of the anisotropic united atoms intermolecular potential to amines, amides and alkanols: Application to the problems of the 2004 Fluid Simulation Challenge", Fluid Phase Equilib. **236**, 25-41 (2005).

[23] Krishnamurthy M., Murad S. and Olson J., "Molecular dynamics simulation of Henry's constant of argon, nitrogen, methane and oxygen in ethylene oxide", Mol. Sim. **32**, 11-16 (2006).

[24] Shah J. K. and Maginn E. J., "Monte Carlo Simulations of Gas Solubility in the Ionic Liquid 1-n-Butyl-3-methylimidazolium Hexafluorophosphate", J. Phys. Chem. B **109**, 10395-10405 (2005).

[25] Grimm C., Kandratsenka A., Wagener P., Zerbs J. and Schroeder J., "Photoinduced Isomerization Kinetics of Diiodomethane in Supercritical Fluid Solution: Local Density Effects", J. Phys. Chem. A **110**, 3320-3329 (2006).

[26] Müller E. A., "Adsorption of Super Greenhouse Gases on Microporous Carbons", Environ. Sci. Technol. **39**, 8736-8741 (2005).

[27] Curbelo S. and Müller E. A., "Modelling of Ethane/Ethylene Separation Using Microporous Carbon", Adsorpt. Sci. Technol. **23**, 855-865 (2005).

[28] Jia W. and Murad S., "Molecular dynamics simulations of gas separations using faujasite-type zeolite membranes", J. Chem. Phys. **120**, 4877-4885 (2004).

[29] Jia W. and Murad S., "Separation of gas mixtures using a range of zeolite membranes: A molecular-dynamics study", J. Chem. Phys. **122**, 234708 (2005).

[30] Chialvo A. A. and Horita J., "Liquid-vapor isotopic fractionation factors of diatomic fluids: A direct comparison between molecular simulation and experiment", J. Chem. Phys. **125**, 034510 (2006).

[31] Schumacher C., Gonzalez J., Pérez-Mendoza M., Wright P. A. and Seaton N. A., "Design of Hybrid Organic/Inorganic Adsorbents Based on Periodic Mesoporous Silica", Ind. Eng. Chem. Res. **45**, 5586-5597 (2006).

[32] Carrero-Mantilla J. and Llano-Restrepo M., "Further Validation of a Set of Quadrupolar Potential Models for Ethylene and Propylene from the Prediction of some Binary Mixture Vapor-Liquid Equilibria by Gibbs-ensemble Molecular Simulation", Mol. Sim. **29**, 549-554 (2003).

[33] Carrero-Mantilla J. and Llano-Restrepo M., "Chemical equilibria of multiple-reaction systems from reaction ensemble Monte Carlo simulation and a predictive equation of state: Combined hydrogenation of ethylene and propylene", Fluid Phase Equilib. **242**, 189-203 (2006).

[34] Lísal M., Bendová M. and Smith W. R., "Monte Carlo adiabatic simulation of equilibrium reacting systems: The ammonia sythesis reaction", Fluid Phase Equilib. **235**, 50-57 (2005).

[35] Smith W. R. and Lísal M., "Direct Monte Carlo simulation methods for nonreacting and reacting systems at fixed total internal energy or enthalpy", Phys. Rev. E **66**, 011104-011106 (2002).

[36] Stoll J., Vrabec J. and Hasse H., "Vapor-Liquid Equilibria of Mixtures Containing Nitrogen, Oxygen, Carbon Dioxide, and Ethane", AIChE J. **49**, 2187-2198 (2003).

[37] Vrabec J., Stoll J. and Hasse H., "Molecular models of unlike interactions in fluid mixtures", Mol. Sim. **31**, 215-221 (2005).

[38] Stoll J., "Molecular Models for the Prediction of Thermalphysical Properties of Pure Fluids and Mixtures", Fortschritt-Berichte VDI, Reihe 3, Vol. 836, VDI-Verlag, Düsseldorf (2005).

[39] Galbraith A. L. and Hall C. K., "Vapor-liquid phase equilibria for mixtures containing diatomic Lennard-Jones molecules", Fluid Phase Equilib. **241**, 175-185 (2006).

[40] Carrero-Mantilla J. and Llano-Restrepo M., "Vapor liquid equilibria of the binary mixtures nitrogen + methane, nitrogen + ethane and nitrogen + carbon dioxide, and the ternary mixture nitrogen + methane + ethane from Gibbs-ensemble molecular simulation", Fluid Phase Equilib. **208**, 155-169 (2003).

[41] Kamath G. and Potoff J. J., "Monte Carlo Predictions for the phase behavior of H_2S + n-alkane, H_2S + CO_2, CO_2 + CH_4 and H_2S + CO_2 + CH_4 mixtures", Fluid Phase Equilib. **246**, 71-78 (2006).

[42] Hansen N., Agbor F. A. B. and Keil F. J., "New force fields for nitrous and oxygen and their application to phase equilibria simulations", Fluid Phase Equilib. **259**, 180-188 (2007).

[43] Nath S. K., Banaszak B. J. and de Pablo J. J., "Simulation of Ternary Mixtures of Ethylene, 1-Hexene, and Polyethylene", Macromolecules **34**, 7841-7848 (2001).

[44] Lisal M., Smith W. R. and Nezbeda I., "Molecular Simulation of Multicomponent Reaction and Phase Equilibria in MTBE Ternary System", AIChE J. **46**, 866-875 (2000).

[45] Van't Hof A., "Molecular Simulation of Binary and Ternary Vapor-Liquid Equilibria, An Advanced Gibbs-Duhem Integration Study", PhD thesis, TU Delft (2005).

[46] Tsang P. C., White O. N., Perigard B. Y., Vega L. F. and Panagiotopoulos A. Z., "Phase equilibria in ternary Lennard-Jones systems", Fluid Phase Equilib. **107**, 31-43 (1995).

[47] de Miguel E. and Telo da Gama M. M., "Phase equilibria of model ternary mixtures: Theory and computer Simulation", J. Chem. Phys. **107**, 6366-6378 (1997).

[48] Escobedeo F. A., "Tracing coexistence lines in multicomponent fluid mixtures by molecular simulation", J. Chem. Phys. **110**, 11999-12010 (1999).

[49] Sadus R. J., "Molecular simulation of the phase behaviour of ternary fluid mixtures: the effect of a third component on vapour-liquid and liquid-liquid coexistence", Fluid Phase Equilib. **157**, 169-180 (1999).

[50] Errington J. R. and Shen V. K., "Direct evaluation of multicomponent phase equilibria using flat-histogram methods", J. Chem. Phys. **123**, 164103 (2005).

[51] Attwood B. C. and Hall C. K., "Solid-Liquid Phase Behavior of Ternary Mixtures", AIChE J. **54**, 1886-1894 (2008).

[52] Shing K. S., Gubbins K. E. and Lucas K., "Henry constants in non-ideal fluid mixtures", Mol. Phys. **65**, 1235-1252 (1988).

[53] Stecki J., Samborski A. and Toxvaerd S., "Henry constant of large solutes by simulation", Mol. Phys. **70**, 985-990 (1990).

[54] Sadus R. J., "Molecular Simulation of Henry's Constant at Vaper-Liquid and Liquid-Liquid Phase boundaries", J. Phys. Chem. B **101**, 3834-3838 (1997).

[55] Murad S. and Gupta S., "A simple molecular dynamics simulation for calculating Henry's constant and solubility of gases in liquids", Chem. Phys. Lett. **319**, 60-64 (2000).

[56] Lotfi A. and Fischer J., "Chemical potentials of model and real dense fluid mixtures from perturbation theory and simulations", Mol. Phys. **66**, 199-219 (1989).

[57] Boulougouris G. C., Errington J. R., Economou I. G., Panagiotopoulos A. Z. and Theodorou D. N., "Molecular Simulation of Phase Equilibria for Water-n-Butane and Water-n-Hexane Mixtures", J. Phys. Chem. B **104**, 4958-4963 (2000).

[58] Boulougouris G. C., Voutsas E. C., Economou I. G., Theodorou D. N. and Tassios D. P., "Henry's Constant Analysis for Water and Nonpolar Solvents from Experimental Data, Macroscopic Models, and Molecular Simulation", J. Phys. Chem. B **105**, 7792-7798 (2001).

[59] Economou I. G., "Monte Carlo Simulation of Phase Equilibria of Aqueous Systems", Fluid Phase Equilib. **183-184**, 259-269 (2001).

[60] Lísal M., Smith W. R. and Aim K., "Analysis of Henry's constant for carbon dioxide in water via Monte Carlo Simulation", Fluid Phase Equilib. **228-229**, 345-356 (2005).

[61] Murad S. and Gupta S., "Molecular dynamics simulation for Henry's constant of oxygen in benzene", Fluid Phase Equilib. **187-188**, 29-37 (2001).

[62] Schnabel T., VrabecJ. and Hasse H., "Henry's Law Constants of Methane, Nitrogen, Oxygen and Carbon Dioxide in Ethanol from 273 to 498 K: Prediction from Molecular Simulation", Fluid Phase Equilib. **233**, 134-143 (2005).

[63] Cichowski E. C., Schmidt T. R. and Errington J. R., "Determination of Henry's law constants through transition matrix Monte Carlo Simulation", Fluid Phase Equilib. **236**, 58-65 (2005).

[64] Wu C., Li X., Dai J. and Sun H., "Prediction of Henry's law constants of small gas molecules in liquid ethylene oxide and ethanol using force field methods", Fluid Phase Equilib. **236**, 66-67 (2005).

[65] Zhang L. and Siepmann J. I., "Direct calculation of Henry's law constants from Gibbs ensemble Monte Carlo simulations: nitrogen, oxygen, carbon dioxide and methane in ethanol", Theor. Chem. Acc. **115**, 391-397 (2006).

[66] Widom B., "Some topics in the theory of fluids", J. Phys. Chem. **39**, 2808-2812 (1963).

[67] Letcher T. M., "Developments and applications in solubility", Cambridge, The Royal Society of Chemistry (2007).

[68] Lennard-Jones. J., "Condensed matter: structural, mechanical and thermal", Cohesion. Proc. Phys. Soc. **43**, 461-482 (1931).

[69] Gray C. G. and Gubbins K. E., "Theory of molecular fluids, 1. Fundamentals", Clarendon Press, Oxford (1984).

[70] Sadus R. J. and Prausnitz J. M., "Three-body interactions in fluids from molecular simulation: Vapor-liquid phase coexistence of argon", J. Chem. Phys. **104**, 4784-4787 (1996).

[71] Engin C., Vrabec J. and Hasse H., "On the difference between a point quadrupole and an equivalent arrangement of three point charges in force field models for vapor-liquid equilibria", Submitted (2010).

[72] Allen M. P. and Tildesley D. J., "Computer simulations of liquids", Clarendon Press, Oxford (1987).

[73] Lorentz H. A., "Über die Anwendung des Satzes vom Virial in der kinetischen Theorie der Gase", Ann. d. Phys. **12**, 127-136 (1881).

[74] Berthelot D., "Sur le Mélange des Gaz", Compt. Rend. Ac. Sc. **126**, 1703-1706 (1898).

[75] Schnabel T., Vrabec J. and Hasse H., "Unlike Lennard-Jones Parameters for Vapor-Liquid Equilibria", J. Mol. Liq. **135**, 170-178 (2007).

[76] Jones J. E., "On the Determination of Molecular Fields. I. From the Variation of the Viscosity of a Gas with Temperature", Proc. Roy. Soc. **106A**, 441-462 (1924).

[77] Jones J. E., "On the Determination of Molecular Fields. II. From the Equation of State of a Gas", Proc. Roy. Soc. **106A**, 463-477 (1924).

[78] Sandler S. I. and Castier M., "Computational quantum mechanics: An underutilized tool in thermodynamics", Pure Appl. Chem. **79**, 1345-1359 (2007).

[79] Ungerer P., Beauvais C., Delhommelle J., Boutin A., Rousseau B. and Fuchs A. H., "Optimization of the anisotropic united atoms intermolecular potential for n-alkanes", J. Chem. Phys. **112**, 5499-5510 (2000).

[80] Eggenberger R., Gerber S., Huber H. and Welker M., "A new ab initio potential for the neon dimer and its application in molecular dynamics simulations of the condensed phase", Mol. Phys. **82**, 689-699 (1994).

[81] Vogt P. S., Liapine R., Kirchner B., Dyson A. J., Huber H., Marcelli G. and Sadus R. J., "Molecular simulation of the vapour-liquid phase coexistence of neon and argon using ab initio potentials", PCCP **3**, 1297-1302 (2001).

[82] Garrison S. L. and Sandler S. I., "On the use of ab initio interaction energies for the accurate calculation of thermodynamic properties", J. Chem. Phys. **117**, 10571-10580 (2002).

[83] Nasrabad A. E., Laghaei R. and Deiters U. K., "Prediction of the thermophysical properties of pure neon, pure argon, and the binary mixtures neon-argon and argon-krypton by Monte Carlo simulation using ab initio potentials", J. Chem. Phys. **121**, 6423-6434 (2004).

[84] Ermakova E., Solca J., Huber H. and Welker M., "Argon in condensed phase: Quantitative calculations of structural, thermodynamic, and transport properties from pure theory", J. Chem. Phys. **102**, 4942-4951 (1995).

[85] Nasrabad A. E. and Deiters U. K., "Prediction of thermodynamic properties of krypton by Monte Carlo simulation using ab initio interaction potentials", J. Chem. Phys. **119**, 947-952 (2003).

[86] Leonhard K. and Deiters U. K., "Monte Carlo simulations of nitrogen using an ab initio potential", Mol. Phys. **100**, 2571-2585 (2002).

[87] Welker M., Steinebrunner G., Solca J. and Huber H., "Ab initio calculation of the intermolecular potential energy surface of $(CO_2)_2$ and first applications in simulations of fluid CO_2", Chem. Phys. **213**, 253-261 (1996).

[88] Naicker P. K., Sum A. K. and Sandler S. I., "Ab initio pair potential and phase equilibria predictions for Hydrogen chloride", J. Chem. Phys. **118**, 4086-4093 (2003).

[89] Hloucha M., Sum A. K. and Sandler S. I., "Computer simulation of acetonitrile and methanol with ab initio-based pair potentials", J. Chem. Phys. **113**, 5401–5406 (2000).

[90] Garrison S. L. and Sandler S. I., "An Accurate Acetylene Intermolecular Potential for Phase Behavior Predictions from Quantum Chemistry", J. Phys. Chem. **108**, 18972-18979 (2004).

[91] Garrison S. L. and Sandler S. I., "A potential from quantum chemistry for thermodynamic property predictions for methanethiol", J. Chem. Phys. **123**, 054506 (2005).

[92] Alder B. J. and Wainwright T. E., "Phase transition for a hard sphere system", J. Chem. Phys. **27**, 1208-1209 (1957).

[93] Stillinger F. and Rahman A., "Improved simulation of liquid water by molecular dynamics", J. Chem. Phys. **60**, 1545-1557 (1974).

[94] Frenkel D. and Smit B., "Understanding molecular simulation: From Algorithms to Applications", Academic Press, New York (1996).

[95] Metropolis N., Rosenbluth A., Rosenbluth M., Teller A. and Teller E., "Equation of state calculations by fast computing machines", J. Chem. Phys. **21**, 1087-1092 (1953).

[96] Vrabec J. and Hasse H., "Grand Equilibrium: vapour-liquid equilibria by a new molecular simulation method", Mol. Phys. **100**, 3375-3383 (2002).

[97] Shevkunov S. V., Martinovski A. A. and Vorontsov-Velyaminov P. N., "Calculation of the critical sizes and properties of microdrops using the Monte-Carlo method in a generalized ensemble", High Temp. Phys. (USSR) **26**, 246-254 (1988).

[98] Nezbeda I. and Kolafa J., "A New Version of the Insertion Particle Method for Determining the Chemical Potential by Monte Carlo Simulation", Mol. Sim. **5**, 391-403 (1991).

[99] Vrabec J., Kettler M. and Hasse H., "Chemical potential of quadrupolar two-centre Lennard-Jones fluids by gradual insertion", Chem. Phys. Lett. **356**, 431-436 (2002).

[100] Mayer J. E., "The statistical mechanics of condensing systems. I", J. Chem. Phys. **5**, 67-73 (1937).

[101] Mayer J. E., "Statistical mechanics of condensing systems. V. Two-component systems", J. Phys. Chem. **43**, 71-95 (1939).

[102] Mayer J. E. and Mayer M. G., "Statistical Mechanics", John Wiley and Sons, New York (1940).

[103] Mountain R. D., "A polarizable model for ethylene oxide", J. Phys. Chem. B **109**, 13352-13355 (2005).

[104] Eckl B., Vrabec J. and Hasse H., "A set of molecular models based on quantum mechanical ab initio calculations and thermodynamic data", J. Phys. Chem. B **112**, 12710-12721 (2008).

[105] Bourasseau E., Haboudou M., Boutin A., Fuchs A. H. and Ungerer P., "New optimization method for intermolecular potentials: Optimization of a new anisotropic united atoms potential for olefins: Prediction of equilibrium properties", J. Chem. Phys. **118**, 3020-3034 (2003).

[106] Rowley R. L., Wilding W. V., Oscarson J. L., Yang Y., Zundel N. A., Daubert T. E. and Danner R. P., DIPPR® Data Compilation of Pure Compound Properties, Design Institute for Physical Properties, AIChE, New York (2006).

[107] Mathews J. F., "The Critical Constants of Inorganic Substances", Chem. Rev. **72**, 71-100 (1972).

[108] Ambrose D., "Vapor-Liquid Critical Properties", National Physical Laboratory Report Chem. **107**, Middlesex, United Kingdom (1980).

[109] Ambrose D. and Tsonopoulos C., "Vapor-Liquid Critical Properties of Elements and Compounds. 3. Aromatic Hydrocarbons", J. Chem. Eng. Data **40**, 547-558 (1995).

[110] Alani G. H., Kudchadker A. P. and Zwolinski B. J., "The Critical Constants of Organic Substances", Chem. Rev. **68**, 659-735 (1968).

[111] Bunger W. B. and Riddick J. A., "Organic Solvents: Physical Properties and Methods of Purification, 3rd ed.", Wiley Interscience, New York (1970).

[112] Danner R. P., Tarakad, R. R., "An improved corresponding states method for polar fluids: correlation of second virial coefficients", AIChE J. **23**, 685-695 (1977).

[113] Nunes Da Ponte M., Staveley L. A. K., "The equation of state and thermodynamic properties of liquid hydrogen chloride", J. Chem. Thermodyn. **13**, 179-186 (1981).

[114] Tsonopoulos C., "Second virial coefficients of water pollutants", AIChE J. **24**, 1112-1115 (1978).

[115] Polt A., Platzer B. and Maurer G., "Parameter der thermischen Zustandsgleichung von Bender für 14 mehratomige reine Stoffe", Chem. Tech. (Leipzig), **44**, 216-224 (1992).

[116] de Leiuw F. H. and Dymanus A., "Magnetic Properties and Molecular Quadrupole Moment of HF and HCl by Molecular-Beam Electric-Resonance Spectroscopy", J. Mol. Spectrosc. **48**, 427-445 (1973).

[117] Buth C. and Paulus B., "Hydrogen bonding in infinite hydrogen fluoride and hydrogen chloride chains", Phys. Rev. B. **74**, 0450122 (2006).

[118] Meredith A. W., Liu M. and Nordholm S., "Quantum chemical exploration of the HCl dimer interaction", Chem. Phys. **220**, 63-68 (1997).

[119] Horvath A. L., "Physical Properties of Inorganic Compounds", Crane Russak, New York (1975).

[120] Howe J. A. and Flygare W. H., "Strong Field Stark Effect", J. Chem. Phys. **36**, 650-652 (1961).

[121] Wu L., Yang Q. Y. and Zhong C. L., "Molecular simulation of vapor-liquid equilibria of toxic gases", Fluid Phase Equilib. **220**, 1-6 (2004).

[122] Stull D. R., "Thermodynamic Functions of Gases", Butterworth Scientific Publications, London (1956).

[123] Bonnaud P., Nieto-Draghi C. and Ungerer P., "Anisotropic United Atom Model Including the Electrostatic Interactions of Benzene", J. Phys. Chem. B **111**, 3730-3741 (2007).

[124] Carrero-Mantilla J., "Simulation of the (vapor + liquid) equilibria of binary mixtures of benzene, cyclohexane, and hydrogen", J. Chem. Thermodyn. **40**, 271-283 (2008).

[125] Errington J. R. and Panagiotopoulos A. Z., "New intermolecular potential models for benzene and cyclohexane", J. Chem. Phys. **111**, 9731-9738 (1999).

[126] Contreras-Camacho R. O., Ungerer P., Boutin A. and Mackie A. D., "Optimized Intermolecular Potential for Aromatic Hydrocarbons Based on Anisotropic United Atoms. 1. Benzene", J. Phys. Chem. B. **108**, 14109-14114 (2004).

[127] Wick C. D., Martin M. G. and Siepmann J. I., "Transferable Potentials for Phase Equilibria. 4. United-Atom Description of Linear and Branched Alkenes and Alkylbenzenes", J. Phys. Chem. B. **104**, 8008-8016 (2000).

[128] Smith B. D., "Thermodynamic Data for Pure Compounds. Part A. Hydrocarbons and Ketones", Elsevier, Amsterdam (1986).

[129] American Petroleum Institute Research Project 44, "Selected Values of Properties of Hydrocarbons and Related Compounds", Thermodynamic Research Center, Texas A&M University, College Station, Texas (1980).

[130] Poynter R. L., "Microvawe Spectrum, Quadrpolar Constants, and Dipole Moment of Chlorobenzene", J. Chem. Phys. **39**, 1962-1966 (1963).

[131] Othmer D. F., "Concise Encyclopedia of Chemical Technology, 5th ed.", John Wiley&Sons, New York (2007).

[132] Srivastava R. and Smith B. D., "Total Pressure Vapor - Liquid Equilibrium Data for Binary Systems of Dichloromethane with Benzene, Toluene, Nitromethane, and Chlorobenzene", J. Chem. Eng. Data **30**, 313-318 (1985).

[133] Hurdis E. C. and Smyth C. P., "Dipole Moments in the Vapor State and Resonance Effects in Some Substituted Benzenes", J. Am. Chem. Soc. **64**, 2212-2216 (1942).

[134] Hu J., White D. and Johnston H. L., "Condensed Gas Calorimetry. V. Heat Capacities, Latent Heats and Entropies of Fluorine From 13 to 85 K; Heats of Transition, Fusion, Vaporization and Vapor Pressures of the Liquid", J. Am. Chem. Soc. **75**, 5642-5645 (1953).

[135] Kreiner W. A., Rudolph H. D. and Tan B. T., "Microwave Spectra of Several Molecular Isotopes of Toluene", J. Mol. Sectreosc. **48**, 86-99 (1973).

[136] Nieto-Draghi C., Bonnaud P. and Ungerer P., "Anisotropic United Atom Model Including the Electrostatic Interactions of Methylbenzenes. I. Thermodynamic and Structural Properties", J. Phys. Chem. C **111**, 15686-15699 (2007).

[137] Contreras-Camacho R. O., Ungerer P., Ahunbay M. G., Lachet V., Perez-Pellitero J., Mackie A. D., "Optimized Intermolecular Potential for Aromatic Hydrocarbons Based on Anisotropic United Atoms. 2. Alkylbenzenes and Styrene", J. Phys. Chem B. **108**, 14115-14123 (2004).

[138] Peng D. Y. and Robinson D. B., "A New Two-Constant Equation of State", Ind. Eng. Chem. Fundam. **15**, 59-64 (1976).

[139] Gillespie P. C., Cunningham J. R. and Wilson G. M., "Total pressure vapor-liquid equilibrium measurements for the Hydrogen chloride/vinyl chloride and Hydrogen chloride/phosgene systems", AIChE Symp. Ser. **81**, 49-56 (1985).

[140] Internal data, GCP/T, BASF SE, Ludwigshafen, Germany.

[141] Kireev V. A., Kaplan S. I. and Vasneva K. I., "Across the equilibrium of liquid mixtures and solutions: II. Phosgene vapor solubility in some solvents at pressures below atmospheric", Zh. Obshch. Khim. **6**, 799-805 (1936).

[142] Audette D. E., Giordano D. E. and Wedlich R. C., "Estimating VLE of binary liquid solutions by ARC and GC", J. Therm. Anal. **49**, 671-677 (1997).

[143] Eckl B., Vrabec J. and Hasse H., "On the Application of Force Fields for Predicting a Wide Variety of Properties: Ethylene Oxide as an Example", Fluid Phase Equilib. **274**, 16-26 (2008).

[144] Marchetti A., Preti C., Tagliazucchi M., Tassi L. and Tosi G., "The N,N-Dimethylformamide/Ethane-1,2-diol Solvent System. Density, Viscosity and Excess Molar Volume at Various Temperatures", J. Chem. Eng. Data **36**, 360-365 (1991).

[145] Ambrose D. and Hall D. J., "Thermodynamic Properties of Organic Oxygen Compounds. L. The Vapour Pressures of 1,2-Ethanediol (Ethylene Glycol) and bis(2-Hydroxyethyl) ether (Diethylene Glycol)", J. Chem. Thermo. **13**, 61-66 (1981).

[146] Salvi M. V. and Van Hook W. A., "Isotope Effects on PVT Properties of Ethylene Glycols $(C_2H_2OH)_2$ and $(CH_2OD)_2$. Pressure and Isotope Dependence of Liquid-liquid Phase Separation of $(CH_2OH)_2/CH_3NO_2$ and $(CH_2OD)_2/CH_3NO_2$ Solutions", J. Phys. Chem. **94**, 7812-7820 (1990).

[147] Curme G. O. and Johnson F., "Glycol: Physical Properties of Ethylene Glycol", Reinhold Publishing Corp., New York (1952).

[148] American Petroleum Institute Research Project 44., "Selected Values of Properties of Hydrocarbons and Related Compounds", Thermodynamic Research Center, Texas A&M University, College Station, Texas (1980).

[149] Haar L., Gallagher J. S. and Kell G. S., "NBS/NRC Steam Tables. Thermodynamic and Transport Properties and Computer Programs for Vapor and Liquid States of Water in SI Units", Hemisphere Publishing Corporation, Washington (1984).

[150] Keenan J. H., Kcyes F. G., Hill P. G. and Moore J. G., "Steam Tables. Thermodynamic Properties of Water Including Vapor, Liquid, and Solid Phases", John Wiley & Sons Inc., New York (1969).

[151] Kell G. S., McLaurin G. E. and Whalley E., "PVT Properties of Water. II. Virial Coefficients in the Range 150-450 °C Without Independent Measurement of Vapor Volumes", J. Chem. Phys. **48**, 3805-3812 (1968).

[152] Abusleme J. A. and Vera J. H., "A Group Contribution Method for Second Virial Coefficients", M. S. Thesis, The Pennsylvania State University, University Park, Pennsylvania (1982).

[153] Schnabel T., Vrabec J. and Hasse H., "Molecular Simulation Study of Hydrogen Bonding Mixtures and New Molecular Models for Mono- and Dimethylamine", Fluid Phase Equilib. **263**, 144-159 (2008).

[154] Ferrando N., Lachet V., Teuler J. and Boutin A., "Transferable Force Field for Alcohols and Polyalcohols", J. Phys. Chem. B **113**, 5985-5995 (2009).

[155] Guillot B., "A reappraisal of what we have learnt during three decades of computer simulations on water", J. Mol. Liq. **101**, 219-260 (2002).

[156] Brodsky A., "Is there predictive value in water computer simulations?", Chem. Phys. Lett. **261**, 563-568 (1996).

[157] Wallqvist A. and Mountain R. D., "Molecular models of water: Derivation and description", Rev. in Comp. Chem. **13**, 183-247 (1999).

[158] Finney J. L., "The water molecule and its interactions: the interaction between theory, modelling, and experiment", J. Mol. Liq. **90**, 303-312 (2001).

[159] Paricaud P., Předota M., Chialvo A. A. and Cummings P. T., "From dimer to condensed phases at extreme conditions: Accurate predictions of the properties of water by Gaussian charge polarizable model", J. Chem. Phys. **122**, 244511-244524 (2005).

[160] Buckingham R. A., "The classical equation of state of gaseous helium, neon and argon", Proc. Roy. Soc. **168A**, 264-283 (1938).

[161] Jorgensen W. L., Chandrasekhar J. D., Madura R. W., Impey R. W. and Klein M. L., "Comparison of simple potential functions for simulating liquid water", J. Chem. Phys. **79**, 926-935 (1983).

[162] Horn H. W., Swope W. C., Pitera J. W., Madura J. D., Dick T. J., Hura G. L. and Head-Gordon T., "Development of an improved four-site water model for biomolecular simulations: TIP4P-Ew", J. Chem. Phys. **120**, 9665-9678 (2004).

[163] Abascal J. L. F. and Vega C., "A general purpose model for the condensed phases of water: TIP4P/2005", J. Chem. Phys. **123**, 234505-234516 (2005).

[164] Abascal J. L. F., Sanz E., García Fernández R. and Vega C., "A potential model for the study of ices and amorphous water: TIP4P/Ice", J. Chem. Phys. **122**, 234511-234519 (2005).

[165] Guissani Y. and Guillot B., "A computer simulation study of the liquid-vapor coexistence curve of water", J. Chem. Phys. **98**, 8221-8235 (1993).

[166] Hasted J. B., "Liquid water: Dielectric properties, in Water A comprehensive treatise", Plenum Press, New York (1972).

[167] Lísal M., Smith, W. R. and Nezbeda I., "Accurate vapour-liquid equilibrium calculations for complex systems using the reaction Gibbs Ensemble Monte Carlo simulation method", Fluid Phase Equilib. **181**, 127-146 (2001).

[168] Vega C., Abascal J. L. F. and Nezbeda I., "Vapor-liquid equilibria from the triple point up to the critical point for the new generation of TIP4P-like models: TIP4P/Ew, TIP4P/2005, and TIP4P/ice", J. Chem. Phys. **125**, 034503 (2006).

[169] Baranyai A., Bartók A. and Chialvo A. A., "Testing the adequacy of simple water models at the opposite ends of the phase diagram", J. Mol. Liq. **134**, 94-98 (2007).

[170] Berendsen H. J. C., Grigera J. R. and Straatsma T. P., "The Missing Term in Effective Pair Potentials", J. Phys. Chem. **91**, 6269-6271 (1987).

[171] Schilk J. A. and Hurd C. O., Tech. Rep., Rep. No. SHELL 240-57, SUBJ. 1896, 11-13 (1957).

[172] Di Serio M., Tesser R., Dimiccoli A. and Santacesaria E., "Kinetics of Ethoxylation and Propoxylation of Ethylene Glycol Catalyzed by KOH", Ind. Eng. Chem. Res. **41**, 5196-5206 (2002).

[173] Lancia A., Musmarra D. and Pepe F., "Vapor-liquid equilibria for mixtures of ethylene glycol, propylene glycol, and water between 98°C and 122°C", J. Chem. Eng. Japan **29**, 449-455 (1996).

[174] Krichevsky I. R. and Kasarnovsky J. S., "Thermodynamical Calculations of Solubilities of Nitrogen and Hydrogen in Water at High Pressures", J. Am. Chem. Soc. **57**, 2168-2171 (1935).

[175] Schnabel T., Vrabec J. and Hasse H., "Henry's Law Constants of Methane, Nitrogen, Oxygen and Carbon Dioxide in Ethanol from 273 to 498 K: Prediction from Molecular Simulation", Fluid Phase Equilib. **233**, 134-143 (2005) and **239**, 125-126 (2006).

[176] Schnabel T., Srivastava A., Vrabec J. and Hasse H., "Hydrogen Bonding of Methanol in Supercritical CO_2: Comparison between 1H-NMR Spectroscopic Data and Molecular Simulation Results", J. Phys. Chem. B **11**, 9871-9878 (2007).

[177] Stoll J., Vrabec J., Hasse H. and Fischer J., "Comprehensive study of the vapour-liquid equilibria of the two-centre Lennard-Jones plus point quadrupole fluid", Fluid Phase Equilib. **179**, 339-362 (2001).

[178] Stoll J., Vrabec J. and Hasse H., "Comprehensive study of the vapour-liquid equilibria of the two-centre Lennard-Jones plus point dipole fluid", Fluid Phase Equilib. **209**, 29-53 (2003).

[179] Vrabec J., Kedia G. K. and Hasse H., "Prediction of Joule-Thomson inversion curves for pure fluids and one mixture by molecular simulation", Cryogenics **45**, 253-258 (2005).

[180] Vrabec J., Kumar A. and Hasse H., "Joule-Thomson inversion curves of mixtures by molecular simulation in comparison to advanced equations of state: natural gas as an example", Fluid Phase Equilib. **258**, 34-40 (2007).

[181] Fernández G. A., Vrabec J. and Hasse H., "Self-Diffusion and Binary Maxwell-Stefan Diffusion in Simple Fluids with the Green-Kubo Method", Int. J. Thermophys. **25**, 175-186 (2004).

[182] Fernández G. A., Vrabec J. and Hasse H., "A molecular simulation study of shear and bulk viscosity and thermal conductivity of simple real fluids", Fluid Phase Equilib. **221**, 157-163 (2004).

[183] Fernández G. A., Vrabec J. and Hasse H., "Self-Diffusion and Binary Maxwell-Stefan Diffusion Coefficients of Quadrupolar Real Fluids from Molecular Simulation", Int. J. Thermophys. **26**, 1389-1407 (2005).

[184] Fernández G. A., Vrabec J. and Hasse H., "Shear viscosity and thermal conductivity of quadrupolar real fluids from molecular simulation", Mol. Sim. **31**, 787-793 (2005).

[185] Fernández G. A., Vrabec J. and Hasse H., "Shear viscosity and thermal conductivity of dipolar real fluids", Cryogenics **46**, 711-717 (2006).

[186] Haslam A. J., Galindo A. and Jackson G., "Prediction of binary intermolecular potential parameters for use in modelling fluid mixtures", Fluid Phase Equilib. **266**, 105-128 (2008).

[187] Gmehling J., Rarey J. and Menke J., Dortmunder Datenbank, Mixture Properties, Version 1.3.0.211 (2004).

[188] Streett W. B., "Liquid-Vapor Phase Behavior and Liquid Phase Density in the System Neon-Argon at High Pressures", J. Chem. Phys. **46**, 3282-3286 (1967).

[189] Trappeniers N. J. and Schouten J. A., "Vapour-liquid and gas-gas equilibria in simple systems III. the system neon-krypton", Physica **73**, 546-555 (1974).

[190] Burch R. J., "Low Temperature Phase Equilibria of the Gas-Liquid System Helium-Neon-Nitrogen", J. Chem. Eng. Data **9**, 19-23 (1964).

[191] Streett W. B. and Jones C. H., "Liquid-vapor equilibrium in the system neon-oxygen from 63 to 152 K and at pressures to 5000 psi", Adv. Cryog. Eng. **11**, 356-366 (1966).

[192] Sasinovskii V., "Issledovanie rastvorimosti i ob'emnogo povedeniya sistemy dvuokis' ugleroda - neon na linii ravnovesiya gidkost' - gaz", Trudy Moskovskogo Energeticheskogo Instituta **364**, 13-18 (1979).

[193] Schmidt H., "Das thermodynamische Verhalten des flüssigen Systems Ar-Kr", Z. Phys. Chem. Neue Folge **24**, 265-274 (1960).

[194] Shatskaya L. V. and Zhirnova N. A., "Liquid-Vapour Phase Equilibria in Binary Systems at Low Temperatures. I. Argon-Methane System", Russ. J. Phys. Chem. **50**, 515 (1976).

[195] Clark A. M., Din F. and Robb J., "The Liquid-Vapour Equilibrium of the Binary System Argon-Oxygen", Proc. Roy. Soc. Lond. A **221**, 517-534 (1954).

[196] Kaminishi G. I., Arai Y., Saito S. and Maeda S., "Vapor-liquid equilibria for binary and ternary systems containing carbon dioxide", J. Chem. Eng. Jpn. **1**, 109-116 (1968).

[197] Elshayal I. M. and Lu B. C. Y., "Vapour-liquid equilibria in the argon-ethane and argon-methane-ethane systems at 155 K", Cryogenics **11**, 285-289 (1971).

[198] Orobinskii N. A., Blagoi Yu. P. and Semyannikova E. L., "Liquid-vapor phase equilibrium of the argon-propylene and krypton-propylene systems at high temperatures", Ukr. Fiz. Zh. (Russ. Ed.) **13**, 263-268 (1968).

[199] Graham E. B. and Weale K. E., "The Solubility of Compressed Gases in Non-Polar Liquids", Proc. Int. Res. Therm. Trans. Prop., 153-158 (1962).

[200] Baginskii V. A., Zakharov N. D. and Lapardin N. I., "Study and calculation of the liquid-vapor phase equilibrium of mixtures of refrigerants", Sb. Issled. Teplofiz. Svoistva Raboch. Veshch. Prots. Teploobm. Kholod. Tekh. **9**, 9-15 (1989).

[201] Nohka J., Sarashina E., Arai Y. and Saito S., "Correlation of vapor-liquid equilibria for systems containing a polar component by the BWR equation", J. Chem. Eng. Jpn. **6**, 10-17 (1973).

[202] Calado J. C. G., Chang E. and Streett W. B., "Vapour-liquid equilibrium in the krypton-xenon system", Physica A **117**, 127-138 (1983).

[203] Calado J. C. G., Nunes Da Ponte M., Soares V. A. M. and Staveley L. A. K., "The thermodynamic excess functions of krypton+ethene liquid mixtures", J. Chem. Thermodyn. **10**, 35-44 (1978).

[204] Holcomb C. D. and Zollweg J. A., "Comparison of interfacial tension and capillary constant for argon + krypton, CH_4 + krypton, and C_2H_6 + krypton using two independent methods of measurement", Fluid Phase Equilib. **75**, 213-224 (1992).

[205] Nunes Da Ponte M., Chokappa D., Calado J. C. G., Clancy P. and Streett W. B., "Vapor-liquid equilibrium in the xenon + ethane system", J. Phys. Chem. **89**, 2746-2751 (1985).

[206] Calado J. C. G., Gomes de Azevedo E. J. S., Soares V. A. M., Lucas K. and Shukla K. P., "Thermodynamics of the xenon + methyl chloride system", Fluid Phase Equilib. **16**, 171-183 (1984).

[207] Fonsecax I. M. A. and Lobo L. Q., "VLE for cryogenic methyl fluoride + nitrous oxide + xenon at 182.33 K", Fluid Phase Equilib. **113**, 127-138 (1995).

[208] Aldersley S. C., Lobo L. Q. and Staveley L. A. K., "Thermodynamics of liquid mixtures of xenon + hexafluoroethane", J. Chem. Thermodyn. **11**, 597-604 (1979).

[209] Calado J. C. G. and Staveley L. A. K., "Thermodynamics of liquid mixtures of krypton and methane", Trans. Faraday Soc. **67**, 1261-1269 (1971).

[210] Davalos J., Anderson W. R., Phelps R. E. and Kidnay A. J., "Liquid-vapor equilibria at 250.00 K for systems containing methane, ethane and carbon dioxide", J. Chem. Eng. Data **21**, 81-84 (1976).

[211] Miller R. C., Kidnay A. J. and Hiza M. J., "Liquid + vapor equilibria in methane + ethene and in methane + ethane from 150.00 to 190.00 K", J. Chem. Thermodyn. **9**, 167-178 (1977).

[212] Wichterle I. and Kobayashi R., "Vapor-liquid equilibrium of methane-ethane system at low temperatures and high pressures", J. Chem. Eng. Data **17**, 9-12 (1972).

[213] Steckel F., "Vapor-liquid equilibria under pressure of some binary hydrogen sulfide-containing systems", Swensk. Kem. Tidskr. **57**, 209-216 (1945).

[214] Yorizane M., Yoshimura S., Masuoka H., Miyano Y. and Kakimoto Y., "New procedure for vapor-liquid equilibria. Nitrogen + carbon dioxide, methane + Freon 22 and methane + Freon 12", J. Chem. Eng. Data **30**, 174-176 (1985).

[215] Simon M. and Knobler C. M., "The excess Gibbs energy of liquid CH_4 + CF_4 at 98 K", J. Chem. Thermodyn. **3**, 657-662 (1971).

[216] Lewis K. L. and Staveley L. A. K., "Excess enthalpies of the liquid mixtures nitrogen + oxygen, nitrogen + argon, argon + ethane and methane + carbon tetrafluoride", J. Chem. Thermodyn. **7**, 855-864 (1975).

[217] Mastera S. G. J., "Dampf-Flüssig-Gleichgewichtsdaten der Systeme Ar-N_2, Kr-Ar, Kr-N_2 und Xe-Kr sowie Löslichkeitsgrenzen des festen Xenons und des festen Kryptons in flüssigen Luftkomponenten", Thesis, Technical University Aachen, (1976).

[218] Kidnay A. J., Miller R. C., Parrish W. R. and Hiza M. J., "Liquid-vapour phase equilibria in the N_2 + CH_4 system from 130 to 180 K", Cryogenics **15**, 531-540 (1975).

[219] Dodge B. F., "Isotherms and Isobars for Air Separation Studies", Chem. Metall. Eng. **10**, 622 (1927).

[220] Sprow F. B. and Prausnitz J. M., "Vapor-Liquid equilibria for five cryogenic mixtures", AIChE J. **12**, 780-784 (1966).

[221] Somait F. A. and Kidnay A. J., "Liquid-vapor equilibriums at 270.00 K for systems containing nitrogen, methane and carbon dioxide", J. Chem. Eng. Data **23**, 301-305 (1978).

[222] Grausø L., Fredenslund A. and Mollerup J., "Vapor-liquid equilibrium data for the systems C_2H_6+N_2, C_2H_4+N_2, C_3H_8+N_2 and C_3H_6+N_2", Fluid Phase Equilib. **1**, 13-26 (1977).

[223] Maslennikova V. Ya., Goryunova N. P. and Tsiklis D. S., "Phase equilibria in the systems nitrogen-freon-12 and nitrogen-freon-22", Russ. J. Phys. Chem. **41**, 735-737 (1967).

[224] Lim J. S. and Kim J. D., "Vapor-Liquid Equilibria of the Binary Systems Nitrogen + Bromotrifluoromethane, + Bromochlorodifluoromethane, + 1,1,1,2,3,3,3-Heptafluoropropane, and + Trifluoroiodomethane from 293.2 to 313.2 K and 30 to 100 bar", J. Chem. Eng. Data **42**, 112-115 (1997).

[225] Laitinen A. and Jäntti M., "Solubility of 6-Caprolactam in Supercritical Carbon Dioxide", J. Chem. Eng. Data **41**, 1418-1420 (1996).

[226] Kulka J. and Schneider G. M., "Low-temperature high-pressure crystallization and fluid-phase equilibria of the binary systems nitrogen + trifluoromethane and argon + trifluoromethane between 110 and 230 K and at pressure up to 200 MPa", Fluid Phase Equilib. **63**, 111-128 (1991).

[227] Fastowskij W. G. and Petrowskij Ju. W., "Investigation of Vapor-Liquid Equilibria in the System O_2-Kr", Russ. J. Phys. Chem. **30**, 589-592 (1956).

[228] Fredenslund A. and Sather G. A., "Gas-liquid equilibrium of the oxygen-carbon dioxide system", J. Chem. Eng. Data **15**, 17-22 (1970).

[229] Komarova E. G., Sosoreva G. F., Petrova T. V. and Finyakina E. D., "Untersuchung des Dampf-Flüssig-Gleichgewichtes im System Chlor-Difluorchlormethan bei isothermischen Bedingungen", Sb. Issled. Appar. Tekhnol. Oforml. Avtomatiz. Khim. Protses. (Leningrad), 60-61 (1983).

[230] Efstigneev O. V., Santimova M. B., Dunaev S. G. and Levanova S. B., "Solubility of chlorine in polychloroalkanes", Khim. Prom. **6**, 342-343 (1985).

[231] Spicer W. M. and Kruger J., "Azeotrope in the Bromine-Carbon Tetrachloride System", J. Am. Chem. Soc. **72**, 1855-1856 (1950).

[232] Spicer W. M. and Meyer L. H., "Some Azeotropes of Bromine", J. Am. Chem. Soc. **73**, 934-938 (1951).

[233] Duncan A. G. and Staveley L. A. K., "Thermodynamic functions for the liquid systems argon + carbon monoxide, oxygen + nitrogen and carbon monoxide + nitrogen", Trans. Faraday Soc. **62**, 548-552 (1966).

[234] Christiansen L. J., Fredenslund A. and Mollerup J., "Vapor-liquid equilibrium of the CH_4-Ar, CH_4-CO and Ar-CO systems at elevated pressures", Cryogenics **13**, 405-413 (1973).

[235] Christiansen L. J., Fredenslund A. and Gardner N., "Gas-liquid equilibria of the CO_2-CO and CO_2-CH_4-CO systems", Adv. Cryog. Eng. **19**, 309-319 (1974).

[236] Trust D. B. and Kurata F., "Vapor-Liquid and Liquid-Liquid Vapor Phase Behavior of the Carbon Monoxide-Propane and the Carbon Monoxide-Ethane Systems", AIChE J. **17**, 415-419 (1971).

[237] Jónasson A., Persson O., Rasmussen P. and Astrath D. U., "Vapor-Liquid Equilibria of Systems Containing Dichloromethane and Gaseous Components", J. Chem. Eng. Data **45**, 642-646 (2000).

[238] Kimura E. and Fukushima S., "Vapor-Liquid Equilibria in the Cl_2-CO_2 System", J. Jpn. Inst. Metals **43**, 223-229 (1979).

[239] Reiff W. E., Roth H. and Lucas K., "Phase equilibria in the binary system carbon disulfide-carbon dioxide", Fluid Phase Equilib. **73**, 323-338 (1992).

[240] Kuenen J. P., "Condensation and critical phenomena of some substances and mixtures", Philos. Mag. **44**, 174-199 (1897).

[241] Fredenslund A. and Mollerup J., "Measurement and prediction of equilibrium ratios for the C_2H_6+CO_2 system", J. Chem. Soc. Faraday Trans. I **70**, 1653-1660 (1974).

[242] Nagahama K., Konishi H., Hashino D. and Hirata M., "Binary vapor-liquid equilibria of carbon dioxide-light hydrocarbons at low temperature", J. Chem. Eng. Jpn. **7**, 323-328 (1974).

[243] Lavrenchenko G. K., Nikolovsky V. A. and Baklai O. V., "Thermodynamic properties of a new refrigerant for household refrigerators", Kholod. Tekh. **6**, 41-45 (1983).

[244] Scurto A. M., Lubbers C. M., Xu G. and Brennecke J. F., "Experimental measurement and modeling of the vapor-liquid equilibrium of carbon dioxide + chloroform", Fluid Phase Equilib. **190**, 135-147 (2001).

[245] Roth H., Peters-Gerth P. and Lucas K., "Experimental vapor-liquid equilibria in the systems R22-R23, R22-CO_2, CS_2-R22, R23-CO_2, CS_2-R23 and their correlations by equations of state", Fluid Phase Equilib. **73**, 147-166 (1992).

[246] Gonzalez A. V., Tufeu R. and Subra P., "High-Pressure Vapor-Liquid Equilibrium for the Binary Systems Carbon Dioxide + Dimethyl Sulfoxide and Carbon Dioxide + Dichloromethane", J. Chem. Eng. Data **47**, 492-495 (2002).

[247] Diefenbacher A. and Türk M., "(Vapour + liquid) Equilibria of binary mixtures of CO_2, CH_2F_2, CHF_3, and SF_6", J. Chem. Thermodyn. **34**, 1361-1375 (2002).

[248] Hartman C. M. A., "Metingen omtrent de dwarsploi van het psi-vlak van Van der Waals bij mengsels van chloormethyl en koolzuur", Thesis, (1899).

[249] Holcomb C. D., Magee J. W., Scott J. L., Outcalt S. L. and Haynes W. M., "Design of a vapor-liquid-equilibrium, surface tension, and density apparatus", Proceedings of the 15th Symposium on Energy Engineering Sciences, National Technical Information Service Report, A1-A87 (1997).

[250] Di Nicola G., Pacetti M., Polonara F. and Stryjek R., "Isochoric Measurements for CO_2 + R125 and CO_2 + R32 Binary Systems", J. Chem. Eng. Data **47**, 1145-1153 (2002).

[251] Silva-Oliver G. and Galicia-Luna L. A., "Vapor-liquid equilibria for carbon dioxide + 1,1,1,2-tetrafluoroethane (R134a) systems at temperatures from 329 to 354 K and pressures upto 7.37 MPa", Fluid Phase Equilib. **199**, 213-222 (2002).

[252] Sengupta S., Gupta S., Dooley K. M. and Knopf F. C., "Measurement and modeling of extraction of chlorinated hydrocarbons from water with supercritical carbon dioxide", J. Supercrit. Fluids **7**, 201-209 (1994).

[253] Fink S. D. and Hershey H. C., "Modeling the vapor-liquid equilibria of 1,1,1-trichloroethane + carbon dioxide and toluene + carbon dioxide at 308, 323 and 353 K", Ind. Eng. Chem. Res. **29**, 295-306 (1990).

[254] Bian B., "Measurement of Phase Equilibria in the Critical Region and Study of Equation of State", Thesis, (1992).

[255] Hlavaty K., "Vapour-Liquid Equilibrium in the Systems CS_2-CCl_4 at 25, 35 and 45 °C", Collect. Czech. Chem. Commun. **35**, 2878-2884 (1970).

[256] Schmidt G. C., "Binäre Gemische", Z. Phys. Chem. (Leipzig) **121**, 221-253 (1926).

[257] Prochazka K. and Boublik T., "Excess Thermodynamic Functions in the Carbon Disulphide-Tetrachloroethylene System", Collect. Czech. Chem. Commun. **40**, 497-506 (1975).

[258] Gaziev G. A., Zelvenskii Ya. D. and Shalygin V. A., "Liquid-Vapor Equilibrium in the Binary Mixtures Ethyl Alcohol Isopropyl Alcohol and Carbon Disulfide-Methyl Iodide", Zh. Prikl. Khim. (Leningrad) **31**, 1220 (1958).

[259] Moelwyn-Hughes E. A. and Missen R. W., "Thermodynamic properties of methyl iodide + chloromethane solutions", Trans. Faraday Soc. **53**, 607-615 (1957).

[260] Litvinov N. D., "Dampfdruck der Flüssigkeiten und binären flüssigen Mischungen", Zh. Fiz. Khim. **14**, 782-788 (1940).

[261] Khodeeva S. M. and Kukina R. P., "Phase and Volume Relations in the System Acetylene-Carbon Tetrachloride", Russ. J. Phys. Chem. **42**, 2444-2449 (1968).

[262] Lim J. S., Lee Y. W., Kim J. D. and Lee Y. Y., "Vapor-Liquid Equilibria for 1,1-Difluoroethane + Acetylene and 1,1-Difluoroethane + 1,1-Dichloroethane at 303.2 K and 323.2 K", J. Chem. Eng. Data **41**, 1168-1170 (1996).

[263] Nunes Da Ponte M., Chokappa D., Calado J. C. G., Zollweg J. and Streett W. B., "Vapor-liquid equilibrium in the xenon + ethene system", J. Phys. Chem. **90**, 1147-1152 (1986).

[264] Mollerup J., "Vapor-liquid equilibrium in ethylene + carbon dioxide", J. Chem. Soc. Faraday. Trans. I **71**, 2351-2360 (1975).

[265] Hogan R. J., Nelson W. T., Hanson G. H. and Cines M. R., "Ethane-Ethylene-Acetylene System–Vapor-Liquid-Equilibrium Data at -35°, 0° and 40° F", Ind. Eng. Chem. **47**, 2210-2215 (1955).

[266] Karakhorin F. F., "Phase Relations in Systems of Liquefied Gases. Equilibrium of Co-Existent Liquid and Vapor Phases in the System Ethane - Ethylene", Foreign Petr. Techn. **9**, 411-422 (1941).

[267] Haselden G. G., Holland F. A., King M. B. and Strickland-Constable R. F., "Two Phase Equilibrium in Binary and Ternary Systems. X. Phase Equilibria and Compressibility of the Systems Carbon Dioxdie-Propylene, Carbon Dioxide-Ethylene and Ethylene-Propylene and an Account of the Thermodynamic Functions of the System Carbon Dioxide-Propylene", Proc. Roy. Soc. Lond. A **240**, 1-28 (1957).

[268] Efremova G. D. and Leonteva G. G., "Phase Equilibria in the Ethylene - Tetrachloromethane System", Tr. Gosudarst. Nauch. Issled. I Proekt. Inst. Azot. Prom. **3**, 5-12 (1954).

[269] Shim J. and Kohn J. P., "Vapor-Liquid Equilibrium Relations in Binary Systems. Ethylene-Chloroform Systems", J. Chem. Eng. Data **9**, 1-2 (1964).

[270] Yang X., "Beitrag zur experimentellen Untersuchung und Berechnung von Dampf-Flüssigkeits-Phasengleichgewichten", Thesis, (1991).

[271] Lebedeva E. S. and Khodeeva S. M., "Phase equilibrium and volume relations in the system methylene chloride-ethylene", Tr. Gosudarst. Nauch. Issled. I Proekt. Inst. Azot. Prom. **13**, 79-90 (1963).

[272] Lebedeva E .S., Kashirina A. S. and Grokholskaya V. P., "Phase equilibriums and volume relations in the bromochloromethane-ethylene system", Tr. Gosudarst. Nauch. Issled. I Proekt. Inst. Azot. Prom. **12**, 92-100 (1971).

[273] Zernov V. S., Kogan V. B., Lyubetski S. G. and Kobyakov V. M., "Phase and volumetric relations in the ethylene-vinyl chloride system", Viniti, Code no. 1479-78 dep. Leningrad, 1-11 (1978).

[274] McCurdy J. L. and Katz D. L., "Phase Equilibria in the System Ethane-Ethylene-Acetylene", Ind. Eng. Chem. **36**, 674-680 (1944).

[275] Sage B. H. and Lacey W. N., "Some Properties of the Lighter Hydrocarbons, Hydrogen Sulfide and Carbon Dioxide", American Petroleum Institute, New York, (1955).

[276] Takahashi R. and Nagahama K., Thesis, Tokyo Metropolitan Univ., (1989).

[277] Hakuta T., Nagahama K. and Hirata M., "Binary vapor-liquid equilibra for C3 hydrocarbons", Bull. Jap. Petrol. Inst. **11**, 10-15 (1969).

[278] Doering K. E. and Preuss H., "Vapor pressures of mixtures propene-propadiene and propene-propyne", FIZ Report, 6191 (1967).

[279] Konobeev B. I. and Lyapin V. V., "Solubility of ethylene and propylene in organic solvent", Khim. Prom. **43**, 114-116 (1967).

[280] Kleiber M., "Vapor-liquid equilibria of binary refrigerant mixtures containing propylene or R134a", Fluid Phase Equilib. **92**, 149-194 (1994).

[281] Ohgaki K., Kageyama M. and Katayama T., "P-Vm-x,y Relations for Azeotropic Mixture of 1,1-Difluoroethane and Propylene", J. Chem. Eng. Jpn. **23**, 763-764 (1990).

[282] Guzechak O. Y., Sarancha V. N., Romanyuk I. M., Yavorskaya O. M. and Churik G. P., "Solubility of propylene in organic solvents", Russ. J. Appl. Chem. **57**, 1662-1665 (1984).

[283] Kovac A. and Dykyj J., Petrochemia **11**, 91-93 (1971).

[284] Bayer A., "Untersuchungen zum Blasensieden von binären Stoffgemischen in einem grossen Druckbereich", Thesis, TH Karlsruhe, (1988).

[285] Jaster H. and Kosky P. G., "Solubility of sulfur hexafluoride in fluorocarbon liquids", J. Chem. Eng. Data **21**, 66-71 (1976).

[286] Kissell F. N. and Manning F. S., "Vapor-Liquid Equilibrium Data for the Binary Mixtures Carbon Tetrachloride-1,1,2-Trichloroethane and 1,2-Dichloroethane-1,1,2-Trichloroethane", J. Chem. Eng. Data **7**, 205-206 (1962).

[287] Perez P., Valero J. and Gracia M., "Isothermal Vapor-Liquid Equilibrium of 1,2-Dibromoethane + Tetrachloromethane at Temperatures between 283.15 and 323.15 K", J. Chem. Eng. Data **39**, 789-792 (1994).

[288] Fried V., Franceschetti D. R. and Gallanter A. S., "Thermodynamic Properties of the System Carbon Tetrachloride-Tetrachloroethylene", J. Phys. Chem. **73**, 1476-1479 (1969).

[289] Xie R., Liu Y., Yu P., He C., Qin H., Dong B. and Shiyou H., "Phase Equilibria for Binary and Ternary Systems of CCl_4, C_2HCl_3 and C_2Cl_4", Petrochem. Tech. **17**, 155-161 (1988).

[290] Loi N. D., "Flüssigkeit-Dampf-Gleichgewicht Versuchsanlage und Messwerte am Gemisch R12-R11", Luft- und Kältetech. **19**, 37-40 (1983).

[291] Hackstein G., "Ein Beitrag zur experimentellen Bestimmung thermodynamischer Stoffwerte an halogenierten Kohlenwasserstoffen, deren Gemische sowie deren Gemische mit Kältemaschinenöl", Thesis, (1975).

[292] Kubota H., Ikawa T., Tanaka Y., Makita T. and Miyoshi K., "Vapor-Liquid Equilibria of Non-Azeotropic Halogenated Hydrocarbon Mixtures under High Pressure", J. Chem. Eng. Jpn. **23**, 155-159 (1990).

[293] Lee J., Lee J. and Kim H., "Vapor-Liquid Equilibria for 1,1,1,2-Tetrafluoroethane + 1-Chloro-1,2,2,2-tetrafluoroethane and 1-Chloro-1,2,2,2-tetrafluoroethane + 1-Chloro-1,1-difluoroethane Systems", J. Chem. Eng. Data **41**, 745-747 (1996).

[294] Wang K., Shi Y., Liu H., Fu J. and Hu Y., "Study on isothermal vapor-liquid equilibrium for dichorodifloromethane - 1,1-difluoroethane binary system", J. East China Inst. Chem. Techn. **19**, 653-659 (1993).

[295] Fedorova A. A., Kruglova L. V. and Danishevskii L. P., "Die Phasengleichgewichte in bromhaltigen Kältemittel-Systemen", Sb. Teor. Osn. Khim. Tekhnol. (Leningrad), 14-18 (1980).

[296] Kriebel M. and Löffler H. J., "Experimentelle Bestimmung einiger thermodynamischer Eigenschaften der Gemische aus R13 (CF_3Cl) und R11 ($CFCl_3$)", Kältetechnik **18**, 34-36 (1966).

[297] Mollerup J. and Fredenslund A., "Vapor-liquid equilibriums in the Freon 12–Freon 13 system", J. Chem. Eng. Data **21**, 299-301 (1976).

[298] Kleiber M., Thesis, (1994).

[299] Meskel-Lesavre M., Richon D. and Renon H., "Bubble pressures and liquid molar volumes of the system chlorotrifluoromethane-1,1,2-trichlorotrifluoroethane", J. Chem. Eng. Data **27**, 160-165 (1982).

[300] Takaishi Y. and Oguchi K., "Dew- and bubble-point measurements for the mixtures of dichlordifluoromethane and bromotrifluoromethane", Int. J. Thermophys. **7**, 721-730 (1986).

[301] Hongo M., Kusunoki M., Matsuyama H., Takagi T., Mishima K. and Arai Y., "Bubble point pressures for binary mixtures of bromotrifluoromethane (R13B1) and chloropentafluoroethane (R115) with chlorodifluoromethane (R22)", J. Chem. Eng. Data **35**, 414-417 (1990).

[302] Mishima K., Hongo M., Takagi T. and Arai Y., "Bubble point pressures for chlorodifluoromethane + 1,2-dichloro-1,1,2,2-tetrafluoroethane, bromotrifluoromethane + 1,2-dichloro-1,1,2,2-tetrafluoroethane and bromotrifluoromethane + chloropentafluoro-ethane", J. Chem. Eng. Data **38**, 49-52 (1993).

[303] Utrobina L. V., Komarova E. G. and Petrova T. V., "Study of phase equilibriums in mixtures formed by products of the synthesis of bromine-containing Freons", Sb. Teor. Osn. Khim. Tekhnol. (Leningrad), 37-41 (1980).

[304] Orobinskii N. A., Blagoi Y. P., Semyannikova E. L. and Vyunnik L. N., "Liquid-vapor equilibrium of methane-propylene and carbon tetrachloride-propylene systems at high temperatures", Fiz. Khim. Rastvorov, 233-238 (1972).

[305] Altunin V. V., Skopintsev E. V. and Zhekshenbaev M. O., "Complex study of thermodynamic properties of binary mixtures of sulfur hexafluoride with low-boiling substances", Tr. Mosk. Energ. Inst. **206**, 59-64 (1989).

[306] Storm J., "Anwendung der UNIFAC-Methode zur Vorausberechnung der Verdampfungsgleichgewichte von Kaeltemittelgemischen", Thesis, TU Braunschweig, (1989).

[307] Kubic W. L. and Stein F. P., "An experimental and correlative study of the vapor-liquid equilibria of the tetrafluoromethane-chlorotrifluoromethane system", Fluid Phase Equilib. **5**, 289-304 (1981).

[308] Piacentini A. and Stein F. P., "An Experimental and Correlative Study of the Vapor-Liquid Equilibria of the Tetrafluoromethane-Trifluoroethane System", Chem. Eng. Progr. Symp. Ser. **63**, 28-36 (1967).

[309] Fonseca I. M. A., Sardinha G. G. and Lobo L. Q., "(Vapour + liquid) equilibria of (fluoromethane + tetrafluoromethane) at the temperature 130.46 K", J. Chem. Thermodyn. **30**, 1271-1274 (1998).

[310] McGlashan M. L., Prue J. E. and Sainsbury I. E. J., "Equilibrium properties of mixtures of carbon tetrachloride and chloroform", Trans. Faraday Soc. **50**, 1284-1292 (1954).

[311] Dakshinamurty P. and Rao C. V., "Vapor-Liquid Equilibria. Systems: Acetone-Tetrachloroethylene, Chloroform-Tetrachloroethylene", Metals Miner. Rev., (1955).

[312] Kang Y. W., Cho S. Y. and Nah I. W., "Isothermal Vapor-Liquid Equilibria for the Binary Systems of Chlorine with Difluoromethane, Chlorodifluoromethane, and Dichlorodifluoromethane at 10 °C", J. Chem. Eng. Data **43**, 611-613 (1998).

[313] Xu N., Yao J., Wang Y., Shi J. and Lu B. C. Y., "Vapor-liquid equilibria of five binary systems containing R22", Fluid Phase Equilib. **69**, 261-270 (1991).

[314] Meskel-Lesavre M., Richon D. and Renon H., "Bubble pressures and saturated liquid molar volumes of trichlorofluoromethane-chlorodifluoromethane mixtures. Representation of refrigerant-mixtures vapor-liquid equilibrium data by a modified form of the Peng-Robinson equation of state", Fluid Phase Equilib. **8**, 37-53 (1982).

[315] Nishiumi H., Kohmatsu S., Yokoyama T. and Konda A., "Phase behavior of the binary refrigerant mixtures HCFC22-CFC12 and HCFC22-HCFC123", Fluid Phase Equilib. **104**, 131-143 (1995).

[316] Feng Y., Wu G., Li C., Chen J., Gu J. and Wang Z., "Vapor-Liquid Equilibrium for the System Chlorodifluoromethane and Dichlorofluoromethane", J. Chem. Ind. Eng. (China) **36**, 93-99 (1985).

[317] Valtz A., Laugier S. and Richon D., "Bubble pressures and saturated liquid molar volumes of difluoromonochloromethane–fluorochloroethane binary mixtures: experimental data and modelling", Int. J. Refrig. **9**, 282-289 (1986).

[318] Togo J. and Nagahama K., Thesis, Tokyo Metropolitan Univ., (1972).

[319] Blinova G. V., Kovaleva A. B. and Danyushevskii L. P., "Study of liquid-vapor equilibrium in systems of fluorohydrocarbons", Teor. Osn. Khim. Tekhnol. **6**, 19-24 (1980).

[320] Nishiumi H., Komatsu M., Yokoyama T. and Kohmatsu S., "Two- and three-phase equilibria and critical locus for the system of HCFC22-HFC134a", Fluid Phase Equilib. **83**, 109-117 (1993).

[321] Cao W., Yu H. and Wang W., "Vapor-Liquid Equilibria for CFC Alternatives", J. Chem. Ind. Eng. (China) **48**, 136-142 (1997).

[322] Geller E. I., Chaikovskii V. F. and Egorov A. V., "Phase equilibriums of refrigerant mixtures", Kholod. Tekh. Tekhnol. **15**, 70-75 (1972).

[323] Stein F. P. and Proust P. C., "Vapor-liquid equilibriums of the trifluoromethane-trifluorochloromethane system", J. Chem. Eng. Data **16**, 389-393 (1971).

[324] Valtz A., Laugier S. and Richon D., "Bubble pressures and saturated liquid molar volumes of trifluorotrichloroethane-fluorochlorohydrocarbon mixtures. Experimental data and modelization", J. Chem. Eng. Data **32**, 397-400 (1987).

[325] Laugier S., Richon D. and Renon H., "Bubble pressures and saturated liquid molar volumes of binary and ternary mixtures of chlorofluorocarbons and hydrochlorofluorocarbons", Fluid Phase Equilib. **93**, 297-316 (1994).

[326] Semenyuk Y. V., Zheleznyi V. P. and Aftenev Y. M., "The investigation of phase equilibria and critical line of mixture R23–R116", Kholod. Tekh. Tekhnol. **51**, 79-81 (1990).

[327] Lim J. S., Park K. H., Lee B. G. and Kim J. D., "Phase Equilibria of CFC Alternative Refrigerant Mixtures. Binary Systems of Trifluoromethane (HFC23) + 1,1,1,2-Tetrafluoroethane (HFC134a) and Trifluoromethane (HFC23) + 1,1,1,2,3,3,3-Heptafluoropropane (HFC227ea) at 283.15 and 293.15 K", J. Chem. Eng. Data **46**, 1580-1583 (2001).

[328] Lim J. S., Park K. H. and Lee B. G., "Phase Equilibria of HFC Mixtures: Binary Mixtures of Trifluoromethane + 1,1-Difluoroethane and Trifluoromethane + 1,1,1-Trifluoroethane at 283.15 and 293.15 K", J. Chem. Eng. Data **47**, 582-586 (2002).

[329] Rulewicz G., Schuberth H. and Leibnitz E., "Untersuchungen über das Dampf-Flüssigkeits-Phasengleichgewicht des Systems Methylenchlorid-Chloroform-Tetrachlorkohlenstoff bei 45 °C unter einer gaschromatographischen Analysenmethode", J. Prakt. Chem. **37**, 122-136 (1968).

[330] Apelblat A., Wisniak J. and Tamir A., "Vapor-liquid equilibriums in the dichloromethane-chlorobromomethane-dibromomethane system and its binaries", J. Chem. Eng. Data **26**, 144-147 (1981).

[331] Rowley R. L. and Powell R. H., "Vapor-liquid equilibrium measurements on mixtures important to industrial design", Dippr Data Series **2**, 116-142 (1994).

[332] Golubkov Yu. V., Kotenkova N. V., Repneva T. G., Markovich V. E. and Papsueva V. P., "Dampf-Flüssig-Gleichgewicht im System Methylenchlorid-Tetrachlorethylen", Zh. Prikl. Khim. (Leningrad) **53**, 1666-1667 (1980).

[333] Artal M., Embid J. M., Otin S. and Velasco I., "Isothermal vapor-liquid equilibria of bromochloromethane or 1-bromo-2-chloroethane+tetrachloromethane or benzene. Experimental measurements and analysis in terms of group contributions", Fluid Phase Equilib. **154**, 223-239 (1999).

[334] Kang Y. W. and Lee Y. Y., "Vapor-Liquid Equilibria for the Systems Composed of 1-Chloro-1,1-difluoroethane, 1,1-Dichloro-1-fluoroethane and 1,1,1-Trichloroethane at 50.1 °C", J. Chem. Eng. Data **41**, 303-305 (1996).

[335] Lim J. S., Lee Y. W. and Lee Y. Y., "Vapor-Liquid Equilibria for Difluoromethane + Dichloromethane at 303.2 and 323.2 K and 1,1-Difluoroethane + Vinyl Chloride at 303.2 and 323.2 K", J. Chem. Eng. Data **42**, 566-569 (1997).

[336] Mears W. H., Sinka J. V., Malbrunot P. F., Meunier P. A., Dedit A. G. and Scatena G. M., "Pressure-volume-temperature behavior of a mixture of difluoromethane and pentafluoromonochloroethane", J. Chem. Eng. Data **13**, 344-347 (1968).

[337] Lee J., Lee J. and Kim H., "Vapor-liquid equilibria for HFC-32 containing systems", Fluid Phase Equilib. **150**, 297-302 (1998).

[338] Jung M. Y., Kim C. N., Park Y. M. and Yoo J. S., "Vapor-Liquid Equilibria for the Difluoromethane (HFC-32) + Pentafluoroethane (HFC-125) System", J. Chem. Eng. Data **46**, 750-753 (2001).

[339] Widiatmo J. V., Fujimine T., Sato H. and Watanabe K., "Liquid Densities of Alternative Refrigerants Blended with Difluoromethane, Pentafluoroethane and 1,1,1,2-Tetrafluoroethane", J. Chem. Eng. Data **42**, 270-277 (1997).

[340] Kim C. N. and Park Y. M., "Vapor-Liquid Equilibria for the Difluoromethane (HFC32) + 1,1,1-Trifluoroethane (HFC143a) System", J. Chem. Eng. Data **45**, 34-37 (2000).

[341] Lee B. G., Park J. Y., Lim J. S., Cho S. Y. and Park K. Y., "Phase Equilibria of Chlorofluorocarbon Alternative Refrigerant Mixtures", J. Chem. Eng. Data **44**, 190-192 (1999).

[342] Serna A. M. P., Fonseca I. M. A. and Lobo L. Q., "(Vapour + liquid) equilibria of $\{x\mathrm{CH_3Cl} + (1\text{-}x)\mathrm{CH_3F}\}$ at temperatures of 159.01 K and 182.33 K", J. Chem. Thermodyn. **35**, 1051-1057 (2003).

[343] Hnědkovský L., Dohnal V. and Cibulka I., "(Vapour+liquid) equilibria and limiting activity coefficients and excess molar volumes of 1-bromo-1-chloro-2,2,2-trifluoroethane (halothane) + tetrachloromethane or trichloromethane or 1,1,1-trichloroethane", J. Chem. Thermodyn. **19**, 1145-1154 (1987).

[344] Hinrichsen H., "Azeotrope Kältmittelgemische", Kältetechnik Klimatisierung **21**, 290-293 (1969).

[345] Lee Y. Y., Kang Y. W., Hong W. H. and Lee H., "Isobaric vapor-liquid equilibria for the systems dichlorotetrafluoroethane-trichlorotrifluoroethane, dichlorotetrafluoroethane-tetrachlorodifluoroethane and trichlorotrifluoroethane-tetrachlorodifluoroethane", J. Chem. Eng. Data **33**, 155-157 (1988).

[346] Yada N., Uematsu M. and Watanabe K., "Analysis of PVTξ measurements for binary mixtures of R115 and R114", Int. J. Thermophys. **10**, 639-647 (1989).

[347] Shiflett M. B. and Sandler S. I., "Modeling fluorocarbon vapor-liquid equilibria using the Wong-Sandler model", Fluid Phase Equilib. **147**, 145-162 (1998).

[348] Leu A. D., Chen C. J. and Robinson D. B., "Vapor-liquid equilibria in selected binary systems", AIChE Symp. Ser. **85**, 11-16 (1989).

[349] Shiflett M. B., Yokozeki A. and Minor B., "Azeotropic Compositions of Perfluoroethane and Trifluoromethane or Oxide or Nitrous Oxide or Carbon Dioxide or Fluoromethane", WO-Patent 001512, (1994).

[350] Zenkevich N. G., Komarova E. G. and Petrova T. V., "Study of liquid-vapor equilibrium in systems formed by Freons of the ethane series", Osnovy Khim. Tekhnol. L, 3-6 (1980).

[351] Mahler B. A., Nappa M. J., Casey M. A. and Miller R. N., "Distillation Processes for Removing CFC-115 and Hydrofluoric Acid from HFC-125", WO-Patent 003936, (1997).

[352] Nagel M. and Bier K., "Vapor-liquid equilibrium of ternary mixtures of the refrigerants R32, R125 and R134a", Int. J. Refrig. **18**, 534-543 (1995).

[353] Nagel M. and Bier K., "Vapor-liquid equilibrium of ternary mixtures of the refrigerants R125, R143a and R134a", Int. J. Refrig. **19**, 264-271 (1996).

[354] Nishiumi H., Akita H. and Akiyama S., "High Pressure Vapor-Liquid Equlibria for the HFC125-HFC152a System", Korean J. Chem. Eng. **14**, 359-364 (1997).

[355] Bartlett P. L., Bivens D. B., Lunger B. S. and Yokozeki A., "Azeotropic and Azeotrope-Like Compositions of 1,1,2,2-Tetrafluoroethane", US-Patent 5968406, (1992).

[356] Kubota H., Zheng Q., Zheng X. Y. and Makita T., "High Pressure Vapor-Liquid Equilibria of the HFC134a + HCFC123 System", J. Chem. Eng. Jpn. **24**, 659-661 (1991).

[357] Zheng X. Y., Kubota H., Zheng Q. and Makita T., "High-pressure vapor-liquid equilibrium data of the HFC134a + HCFC141b system", J. Chem. Eng. Data **35**, 441-444 (1990).

[358] Shi Y., Wang K., Liu H. and Hu Y., "Measurement of VLE for 1,1,1,2-tetrafluoreoethane-1,1-Difluoroethane binary system", J. East China Univ. Sci. Technol. **21**, 613-618 (1995).

[359] Kovac A., Svoboda J. M. and Ondrus I., "Vapor-liquid equilibrium of some binary systems containing 1,1,2-trichloroethane", Chemical Papers **39**, 737-742 (1985).

[360] Rathbone P., "Vapor Liquid Equilibrium Data on Binary Chlorinated Hydrocarbon Systems", Conf. Int. Thermodyn. Chim., 64-74 (1975).

[361] Meijer E. L., Brouwer N. and Van Miltenburg J. C., "Vapor Pressures and excess Gibbs energy of the liquid mixture carbon tetrachloride + 1,1,1-trichloroethane", J. Chem. Thermodyn. **8**, 703-708 (1976).

[362] Weber L. A. and Silva A. M., "Design of a high-pressure ebulliometer, with vapor-liquid equilibrium results for the systems CHF_2Cl + CF_3CH_3 and CF_3CH_2F + CH_2F_2", Int. J. Thermophys. **17**, 873-888 (1996).

[363] Lim J. S., Park J. Y., Lee B. G. and Lee Y. W., "Phase equilibria of 1,1,1-trifluoroethane (HFC143a) + 1,1,1,2-tetrafluoroethane (HFC134a), and + 1,1-difluoroethane (HFC152a) at 273.15, 293.15, 303.15 and 313.15 K", Fluid Phase Equilib. **193**, 29-39 (2002).

[364] Kaplan S. I. and Monakhova Z. D., "Über das Gleichgewicht in Lösungen. IY. Siedetemperaturen bei atmosphärischem Druck und Dampfzusammensetzung der binären Mischungen aus Chlorderivaten von Methan und Ethan", Zh. Obshch. Khim. **7**, 2499-2512 (1937).

[365] Gölles F., Wolfbauer O. and Still F., "Dampf-Flüssigkeits-Gleichgewichte und Stoffwerte des Systems 1,1-Dichloräthan-Chloroform-1,2-Dichloräthan", Monatsh. Chem. **106**, 1437-1447 (1975).

[366] Kuznetsov A. P., Volobuev I. V. and Khmelnyuk M. G., "Thermodynamic analysis of the phase equilibria of refrigerant mixture R12B1–R152a", Kholod. Tekh. Tekhnol. **30**, 54-56 (1980).

[367] Yada N., Uematsu M. and Watanabe K., "Study of the PVTx Properties for Binary R152a + R114 System", Trans. JAR **5**, 107-115 (1988).

[368] Bian B. G., Xu N. P., Dong J. H., Wang Y. R. and Shi J., "Determination of vapor-liquid equilibra for the mixtures R22-R142b and R152a-R142b", J. Eng. Thermophys. **14**, 238-240 (1993).

[369] Guglielmo G., "Sulle tensioni parziali e sulle pressioni osmotiche delle miscele di due liquidi volatili", Acad. Naz. Lincei, Cl. Sci. Fis. Mat. Natur., Rend **1**, 242-249 (1892).

[370] Anonymous, "Vapor-Liquid Equilibria of the System Difluoromethane (F32) - Tetrafluoroethylene (TFE)", Confident. Comp. Res. Rep., (1978); cf. [187].

[371] Sagnes M. and Sanchez V., "Vapor-liquid equilibriums for fourteen systems consisting of chlorinated hydrocarbons and alcohols", J. Chem. Eng. Data **16**, 351-354 (1971).

[372] Owens J. L., Brady C. J., Freeman J. R., Wilding W. V. and Wilson G. M., "Vapor-liquid equilibrium measurements", AIChE Symp. Ser. **83**, 18-41 (1987).

[373] Azbel I. Ya., Panfilov A. A., Vdovets A. V. and Gavrilchuk N. M., "Liquid-Vapor Equilibrium in Vinyl Chloride-Impurities Solutions", Khim. Prom. **44**, 269-273 (1968).

[374] Hiza M. J. and Duncan A. G., "Azmultipurpose phase equilibrium apparatus to study mixtures of cryogenic fluids: Application to argon–methane", Adv. Cryog. Eng. **15**, 42-45 (1969).

[375] Destaillats H. and Fernández Prini R., "Solubility of I_2(s) and equilibrium concentration of the (I_2 + C_6H_6) charge transfer complex in supercritical xenon with added C_6H_6", J. Chem. Thermodyn. **29**, 1209-1221 (1997).

[376] Fang R. B., Zhang S. H. and Zhang W. H., "Determination of solubilities of iodine and sulfur in supercritical CO_2 using the chromatographic retention method", Chem. J. Chin. Univ. (Changchun) **18**, 869-872 (1997).

[377] Prausnitz J. M. and Benson P. R., "Solubility of liquids in compressed hydrogen, nitrogen, and carbon dioxide", AIChE J. **5**, 161-164 (1959).

[378] Kuskova N. V., Kukarin V. F., Martynets V .G. and Matizen E. V., "Study of the phase equilibrium of (1 - x) CO_2 + x Kr for $x < 0.032$ near the critical point of CO_2", J. Chem. Thermodyn. **23**, 523-530 (1991).

[379] Volobuev I. V., Los V. I., Los L. V. and Khmelnyuk M. G., "Phase equilibrium in a mixture of the refrigerants R12B1 and R143", Kholod. Tekh. Tekhnol. **39**, 65-67 (1984).

[380] Hiraoka H. and Hildebrand J. H., "The solubility and entropy of the solution of certain gases in $(C_4H_9)_3N$, CCl_2F-CCl_2F_2 and $2,2,4$-$(CH_3)_3C_5H_9$", J. Phys. Chem. **68**, 213-218 (1964).

[381] Kobatake Y. and Hildebrand J. H., "Solubility and entropy of solution of He, N_2, Ar, O_2, CH_4, C_2H_6, CO_2 and SF_6 in various solvents", J. Phys. Chem. **65**, 331-334 (1961).

[382] Makarevich L. A. and Sokolova E. S., "P-V-T-N relations in weak solutions near the critical point of a pure solvent. II. Carbon dioxide-sulfur hexafluoride system near the critical point of sulfur hexafluoride", Termodin. Termokhim. Konstanty, 120-124 (1970).

[383] Wilhelm E. and Battino R., "The solubility of gases in liquids I. The solubility of a series of fluorine-containing gases in several non-polar solvents", J. Chem. Thermodyn. **3**, 379-392 (1971).

[384] Deerenberg A., Schouten J. A. and Trappeniers N. J., "Vapour-liquid and gas-gas equilibria in simple systems : V. The system neon-xenon", Physica A **101**, 459-476 (1980).

[385] Zakharov N. D., Semenov V. G. and Domnina E. V., Zh. Fiz. Khim. **56**, 2575 (1982).

[386] Chaikovskii V. F., Zakharov N. D., Grezin A. K. and Matyash Yu. I., "Experimental investigation of thermodynamic properties of refrigient agents – solutions", Kholod. Tekh. Tekhnol. **22**, 51-55 (1976).

[387] Burch R. J. and Leeds M. W., "Phase Equilibria Molecular Transport Thermodynamics. Vapor-Liquid Equilibria in the Acetylene-Propyne System", Ind. Eng. Chem., Chem. Eng. Data Series **2**, 3-7 (1957).

[388] Anonymous, "Flüssigkeits-Dampf-Gleichgewicht des Systems Frigen 13 - Frigen 114", Confident. Comp. Res. Rep., (1970); cf. [187].

[389] Deiters U. K., "Some remarks on the nomenclature of refrigerants" Fluid Phase Equilib. **132**, 265-270 (1997).

[390] Vrabec J., Huang Y. L. and Hasse H., "Molecular models for 267 binary mixtures validated by vapor-liquid equilibr.: A systematic approach", Fluid Phase Equilib. **279**, 120-135 (2009).

[391] Miller R. C., Kidnay A. J. and Hiza M. J., "Liquid-vapor equilibria at 112.00 K for systems containing nitrogen, argon, and methane", AIChE J. **19**, 145-151 (1973).

[392] Christiansen L. J. and Fredenslund Aa., "Vapour-liquid equilibria of the CH_4-Ar-CO system", Cryogenics **14**, 10-14 (1974).

[393] Fastovsky W. G. and Petrovsky Yu. W., "A Study of the Vapor-Liquid Equilibrium in the System Oxygen-Argon-Nitrogen", Zh. Fiz. Khim. **31**, 836-841 (1957).

[394] Kremer H. and Knapp H., "Vapor-liquid equilibria in ternary mixtures of H_2, N_2, CO and CH_4", Fluid Phase Equilib. **11**, 289-310 (1983).

[395] Xu N., Dong J., Wang Y. and Shi J., "High pressure vapor liquid equilibria at 293 K for systems containing nitrogen, methane and carbon dioxide", Fluid Phase Equilib. **81**, 175-186 (1992).

[396] Trappehl G. and Knapp H., "Vapour-liquid equilibria in the ternary mixtures N_2-CH_4-C_2H_6 and N_2-C_2H_6-C_3H_8", Cryogenics **27**, 696-716 (1987).

[397] Okambawa R., St-Arnaud J. M., Bose T. K. and Le Noe O., "Virial coefficients and compression factors of nine ternary gaseous mixtures obtained by the dielectric constant method", Fluid Phase Equilib. **134**, 225-237 (1997).

[398] Knapp H., Yang X. and Zhang Z., "Vapor-liquid equilibria in ternary mixtures containing nitrogen, methane, ethane and carbondioxide at low temperatures and high pressures", Fluid Phase Equilib. **54**, 1-18 (1990).

[399] Hsi C. and Lu B. C. Y., "Vapor-Liquid Equilibria in the Methane-Ethylene-Ethane System", Can. J. Chem. Eng. **49**, 140-143 (1971).

[400] Zenner G. H. and Dana L. I., "Liquid-Vapor Equilibrium Compositions of Carbon Dioxide-Oxygen-Nitrogen Mixtures", Chem. Eng. Progr. Symp. Ser. **59**, 36-41 (1963).

[401] Zhang Z., Guo L., Yang X. and Knapp H., "Vapor and liquid equilibrium for nitrogen-ethane-carbon dioxide ternary system", J. Chem. Ind. Eng. (China) **50**, 392-398 (1999).

[402] Al Wakeel I. M., "Experimentelle und analytische Bestimmung von binären und ternären Dampf-Flüssig-Gleichgewichtsdaten der Stoffe Difluordichlormethan-Kohlendioxyd-Stickstoff im Bereich hoher Drücke und tiefer Temperaturen", PhD thesis, Technische Universität Berlin, (1976).

[403] Wang X., Wang Y., Shi J. and Lu B. C. Y., "Isothermal vapor-liquid equilibria at elevated pressures for the systems containing nitrogen, carbon dioxide, and chlorodifluoromethane", J. Chem. Eng. Data. **36**, 436-439 (1991).

[404] Zaharov N. D., Litvinov A. S., Grezin A. K. and Gromov E. A., "Thermodynamic properties of nitrogen-freon solutions", Zh. Fiz. Khim. **9**, 162-167 (1976).

[405] Xie R., Liu Y., Yu P., He C., Qin H. and Dong B., "Phase Equilibria for Binary and Ternary Systems of CCl_4, C_2HCl_3 and C_2Cl_4", Petrochem. Tech. **26**, 144-147 (1981).

[406] Chareton A., Valtz A., Laugier S., Richon D. and Renon H., "Bubble pressures and saturated liquid molar volumes of binary and ternary refrigerant mixtures", J. Chem. Eng. Data. **35**, 162-165 (1990).

[407] Proust P. C. and Stein F. P., "Vapor-liquid equilibria of the ternary system CF_4-CHF_3-$CClF_3$ at 199.80 K and 3.447 and 6.895 bars", Fluid Phase Equilib. **3**, 313-322 (1979).

[408] Bouchot C. and Richon D., "Direct Pressure-Volume-Temperature and Vapor-Liquid Equilibrium Measurements with a Single Equipment Using a Vibrating Tube Densimeter up to 393 K and 40 MPa: Description of the Original Apparatus and New Data", Ind. Eng. Chem. Res. **37**, 3295-3304 (1998).

[409] Kobayashi M. and Nishiumi H., "Vapor-liquid equilibria for the pure, binary and ternary systems containing HFC32, HFC125 and HFC134a", Fluid Phase Equilib. **144**, 191-202 (1998).

[410] Kruse H., Chen J., Koester R., Herres G., Buschmeiner M. and Gorenflo D., "Kältemittelgemische als Substitute für R22, R502 und R13B1: Literaturübersicht und neue Messungen zu thermodynamischen Eigenschaften technisch relevanter Zwei- und Dreistoffgemische", DKV-Tagungsberichte **23**, 67-84 (1996).

[411] Kul I., DesMarteau D. D. and Beyerlein L. A., "Vapor-liquid equilibria of novel chemicals and their mixtures as R22 alternatives", Fluid Phase Equilib. **173**, 263-276 (2000).

[412] Huang Y. L., Vrabec J. and Hasse H., "Prediction of ternary vapor-liquid equilibria for 33 systems by molecular simulation", Fluid Phase Equilib. **287**, 62-69 (2009).

[413] Krieve W. F. and Mason D. M., "The soulubility of chlorine in titanium tetrachlorine and of carbon dioxine and oxygen in chlorine", J. Phys. Chem. **60**, 374 (1956).

[414] Ackley R. D. and Notz K. J., "Distribution of xenon between gaseous and liquid CO_2", Technical Report ORNL-5122, Oak Ridge National Lab. TN (USA), 1-35 (1976).

[415] Fredenslund A., Mollerup J. and Persson O., "Gas-Liquid Equilibrium of Oxygen-Carbon Dioxide System", J. Chem. Eng. Data **17**, 440-443 (1972).

[416] Gjaldbaek J. C. and Niemann H., "The Solubitity of Nitrogen, Argon and Ethane in Alcohols and Water", Acta Chem. Scand. **12**, 611-614 (1958).

[417] Reeves L. W. and Hildebrand J. H., "The Solubility and Entropy of Solution of Argon in Five Selected Non-polar Solvents", J. Am. Chem. Soc. **79**, 1313-1314 (1957).

[418] Powell R. J., "Solubility of 16 gases in $(C_4H_9)_3N$ and CS_2", J. Chem. Eng. Data **17**, 302-304 (1972).

[419] Gjaldbaek J. C. and Hildebrand J. H., "The Solubility of Nitrogen in Carbon Disulfide, Benzene, Normal- and Cyclo-hexane and in Three Fluorocarbons", J. Am. Chem. Soc. **71**, 3147-3150 (1949).

[420] Gjaldbaek J. C., "The solubility of hydrogen, oxygen and carbon monoxide in some non-polar solvents", Acta Chem. Scand. **6**, 623-633 (1952).

[421] Raskina A. D., Zetkin V. I., Zakharov E. V., Kolesnikov I. M. and Kosorotov V. I., "Solubility of chlorine in carbon disulfide and products of its chlorination", J. Appl. Chem. (USSR) **45**, 1374-1375 (1972).

[422] Gjaldbaek J. C., "The Solubility of Carbon Dioxide in Perfluoro-n-heptane, Normal Heptane, Cyclohexane, Carbon Tetrachloride, Benzene, Carbon Disulphide and Aqueous Solution of Aerosol", Acta Chem. Scand. **7**, 537-544 (1953).

[423] Miyano Y. and Hayduk W., "Solubility of acetylene in several polar and non-polar solvents and solvent mixtures", Can. J. Chem. Eng. **59**, 746-751 (1981).

[424] Sahgal A., La H. M. and Hayduk W., "Solubility of ethylene in several polar and non-polar solvents", J. Chem. Eng. **56**, 354-357 (1978).

[425] Archer G. and Hildebrand J. H., "The soulbility and entropy of solution of carbon tetrafluorine and sulfur hexaflourine in nonpolar solvents", J. Phys. Chem. **67**, 1830-1833 (1963).

[426] Blagoi Yu. P. and Orobinskii N. A., "Liquid-vapor phase equilibrium in the propylene-nitrogen system", Russ. J. Phys. Chem. **39**, 1073-1074 (1965).

[427] Miller H. C., Verdelli L. S. and Gall J. F., "Some Physical Properties of Sulfur Hexafluoride", Ind. Eng. Chem. **43**, 1126-1129 (1951).

[428] Tominaga T., Battino R., Gorowara H. K., Dixon R. D. and Wilhelm E., "Solubility of gases in liquids. 17. The solubility of helium, neon, argon, krypton, hydrogen, nitrogen, oxygen, carbon monoxide, methane, carbon tetrafluoride, and sulfur hexafluoride in tetrachloromethane at 283 to 318 K", J. Chem. Eng. Data **31**, 175-180 (1986).

[429] Körösy F., "Two rules concerning solubility of gases and crude data on solubility of krypton", Trans. Faraday Soc. **33**, 416-425 (1937).

[430] Lannung A. and Gjaldbaek J. C., "Solubility of methane in hydrocarbons, alcohols, water and other solvents", Acta Chem. Scand. **14**, 1124-1128 (1960).

[431] Akimoto T., Nitta T. and Katayama T., "Nitrogen solubility and vapor pressure of binary mixed solvents containing benzene, carbon tetrachloride, cyclohexane and 1-hexane", J. Chem. Eng. (Japan) **17**, 637-641 (1984).

[432] Gorbachev V. M. and Tretyakov T. V., "Determination of the Solubility of Oxygen and Nitrogen in CH_3SiCl_3, $SiCl_4$ and $GeCl_4$ using Gas-Liquid Chromatography", Zavod. Lab. (USSR) **32**, 796-798 (1966).

[433] Wolfe J. K., "Solubility of Air in Freon-12 and Freon-22", Refrig. Eng. **59**, 704-706 (1951).

[434] Luehring P. and Schumpe A., "Gas Solubilities in organic liquids at 293.2 K", J. Chem. Eng. Data **34**, 250-252 (1989).

[435] Naumenko N. K., "Investigation on the Solubility of Oxygen in Organic Solvents", Thesis, 3-11 (1970).

[436] Schlaepfer P., Audykowski T. and Bukowiecki A., "Über die Lösungsgeschwindigkeit des Sauerstoffs in verschiedenen Flüssigkeiten", Schweizer Archiv für Wiss. u. Technik **15**, 299-307 (1949).

[437] Sinn E., Matthes K. and Naumann E., "Experimentelle Untersuchungen über die Löslichkeit von Sauerstoff in flüssigen organischen Substanzen", Wiss. Z. Friedrich-Schiller-Univ. Jena, Math.-Naturwiss. R. **16**, 523-529 (1967).

[438] Vdovichenko V. T. and Kondratenko V. I., "Solubilities of chlorine and hydrogen chloride in chloromethanes and of methyl chloride in anisole", Khim. Prom. (USSR) **43**, 290-291 (1967).

[439] Kogan L. M., Koltsov N. S. and Litvinov N. D., "Apparatus for Determining Solubility of Chlorine and other Gas in Liquids", Russ. J. Phys. Chem. **37**, 1040-1042 (1963).

[440] Smith T. L., "The Solubility of Chlorine in Carbon Tetrachloride", J. Phys. Chem. **59**, 188-189 (1955).

[441] Blair C. M. and Yost D. M., "The Thermodynamic Constants of Iodine Monochloride, Iodine Monobromide and Bromine Monochloride in Carbon Tetrachloride", J. Am. Chem. Soc. **55**, 4489-4496 (1933).

[442] Taylor N. W. and Hildebrand J. H., "Solubility. VIII. Solubility Relations of Certain Gases", J. Am. Chem. Soc. **45**, 682-694 (1923).

[443] Just G., "Löslichkeit von Gasen in organischen Lösungsmitteln", Z. Phys. Chem. (Leipzig) **37**, 342-367 (1901).

[444] Takahashi M., Kobayashi Y. and Takeuchi H., "Diffusion coefficients and solubilities of carbon dioxide in binary mixed solvents", J. Chem. Eng. Data **27**, 328-331 (1982).

[445] Hsu H. and Campbell D., "Formulations With Soluble Gas Propellants", Aerosol Age **9**, 34-139 (1964).

[446] Takeuchi H., Fujine M., Sato T. and Onda K., "Simultaneous Determination of Diffusion Coefficient and Solubility of Gas in Liquid by a Diaphragm Cell", J. Chem. Eng. (Japan) **8**, 252-253 (1975).

[447] Brueckl N. and Kim J. I., "Gibbs free energies of solute-solvent interactions for He, Ne, Ar, Kr, Xe, H_2, O_2, N_2, CH_4, SF_6, C_2H_4", Z. Phys. Chem., Neue Folge **126**, 133-150 (1981).

[448] Jadot R., "Determination of Henry constants by chromatography", J. Chim. Phys. Phys.-Chim. Biol. **6**, 1036-1040 (1972).

[449] Hayduk W. and Cheng S. C., "Solubilities of ethane and other gases in normal paraffin solvents", Can. J. Chem. Eng. **48**, 93-99 (1970).

[450] Makitra R. G., Pirig Ya. N., Politanskaya T. I. and Moin F. B., "Effect of properties of solvents on solubility of Freon 22", Russ. J. Phys. Chem. **55**, 424-426 (1981).

[451] Anonymous, "Löslichkeit von F23 und HCl in verschiedenen Lösungsmitteln", Confident. Comp. Res. Rep., Rep. No. LC4912 (1970); cf. [187].

[452] Anonymous, "Löslichkeit von HCl und F23 in verschiedenen Lösungsmitteln", Confident. Comp. Res. Rep., Rep. No. LC4914 (1970); cf. [187].

[453] Sies P. and Krafczyk J., Unpublished Data, (1992); cf. [187].

[454] Krafczyk J., Unpublished Data, (1991); cf. [187].

[455] Mamedaliev Yu. G. and Musakhanly S., "The solubility of chloromethane in some solvents", Zh. Prikl. Khim. (USSR) **13**, 735-737 (1940).

[456] Horiuti J., "The Solubility of Gas and Coefficient of Dilation by Absorption", Sci. Pap. Inst. Phys. Chem. Res. (Japan) **17**, 125-256 (1931).

[457] Makitra R. G., Politanskaya T. I., Moin F. B., Pirig Y. N. and Politanskaya T. S., "Solubility of ethyl fluoride in organic solvents", J. Appl. Chem. (USSR) **56**, 2048-2051 (1984).

[458] Makitra R. G., Moin F. B. and Politanskaya T. I., "Solubility of Fluoroethane in Toluene, Tetrachloromethane and N-Methylpyrrolidone", J. Phys. Chem. (USSR) **53**, 572-573 (1979).

[459] Anonymous, "Löslichkeit von gasförmigem F13, F22 und F23 in flüssigem F11", Confident. Comp. Res. Rep., Rep. No. LC4994 (1969); cf. [187].

[460] Nitta T., Nakamura Y., Ariyasu H. and Katayama T., "Solubilities of nitrogen in binary solutions of acetone with cyclohexane, benzene, chloroform and 2-propanol", J. Chem. Eng. (Japan) **13**, 97-103 (1980).

[461] Fischer F. and Pfleiderer G., "Über die Löslichkeit von Sauerstoff in verschiedenen organischen Lösungsmitteln", Z. Anorg. Chem. **124**, 61-69 (1922).

[462] Giles N. F., Wilson L. C., Wilson G. M. and Wilding W. V., "Phase equilibria on eight binary mixtures", J. Chem. Eng. Data **42**, 1067-1074 (1997).

[463] Vonderheiden F. H. and Eldridge J. W., "The system carbon dioxide - methylene chloride", J. Chem. Eng. Data **8**, 20-21 (1963).

[464] Doering K. E., "Solubility of methane in methyl chloride", FIZ Report, 1201 (1965).

[465] Linford R. G. and Hildebrand J. H., "Solubility and entropy of solution of gases in CCl_2F-$CClF_2$", Trans. Faraday Soc. **66**, 577-581 (1970).

[466] Sokolov Y. P. and Konshin A. I., "Study of solubility of ethylene and tetrafluoroethylene in perhalogenated solvents under pressure", J. Appl. Chem. (USSR) **62**, 1310-1312 (1989).

[467] Armitage D. A., Linford R. G. and Thornhill D. G. T., "Appratus for accurately and rapidly measuring the solubility of gases in liquid mixtures", Ind. Eng. Chem. Fundam. **17**, 362-364 (1978).

[468] Linford R. G. and Hildebrand J. H., "Solubility of gases in mixtures of nonpolar liquids", J. Phys. Chem. **73**, 4410-4411 (1969).

[469] Sokolov Yu. A., Konshin A. I. and Sokolov S. V., "Study of solubility of tetrafluoroethylene and vinylidene fluoride in Freon 113 under pressure", J. Appl. Chem. (USSR) **60**, 2523-2525 (1988).

[470] Williams V. D., "Solubility of Nitrogen in Freon144", J. Chem. Eng. Data **4**, 92-93 (1959).

[471] Makitra R. G., Moin F. B., Pirig Ya. N. and Politanskaya T. I., "Solubility of acetylene in some haloethanes", J. Appl. Chem. (USSR) **60**, 663-665 (1987).

[472] Makitra R. G., Moin F. B., Pirig Ya. N. and Politanskaya T. I., "Solubility of vinyl chloride in tri- and tetrachloroethanes", J. Appl. Chem. (USSR) **62**, 2567-2571 (1990).

[473] Danov S. M. and Golubev Yu. D., "Solubility of acetylene and hydrogen chloride in vinyl chloride, 1,1-dichloroethane and trans-1,2-dichloroethylene", Khim. Prom. (USSR) **44**, 116-120 (1968).

[474] Gjaldbaek J. C. and Anderson E. K., "The solubility of carbon dioxide, oxygen, carbon monoxide and nitrogen in polar solvents", Acta Chem. Scand. **8**, 1398-1413 (1954).

[475] Otsuka E. and Takada M., "Purification of acetyls formed in combustion gases by partial oxidation of methane. I. Investigation of the solubility of acetylene and carbon dioxide in methanol and selectivity for carbon dioxide", Nenryo-Kyokai-shi **42**, 229-237 (1963).

[476] Lustig R., "Angle-average for the powers of the distance between two separated vectors", Mol. Phys. **65**, 175-179 (1988).

[477] Huang Y. L., Miroshnichenko S., Hasse H. and Vrabec J., "Henrys law constant from molecular simulation: a systematic study of 95 systems", Int. J. Thermophys. **30**, 1791-1810 (2009).

[478] Flyvbjerg H. and Petersen H. G., "Error estimates on averages of correlated data", J. Chem. Phys. **91**, 461-466 (1989).

[479] Barker J. A. and Watts R. O., "Monte Carlo studies of the dielectric properties of water-like models", Mol. Phys. **26**, 789-792 (1973).

[480] Saager B., Fischer J. and Neumann M., "Reaction Field Simulations of Monatomic and Diatomic Dipolar Fluids", Mol. Sim. **6**, 27-49 (1991).

[481] Weingerl U. and Fischer J., "Consideration of dipole-quadrupole interactions in molecular based equations of state", Fluid Phase Equilib. **202**, 49-66 (2002).